THE MECHANICAL PROPERTIES OF FIBRE REINFORCED COMPOSITE PLATES

OCTOBER 1975

R.S.ANDERSON

This thesis is submitted for the degree of Doctor of Philosophy

at The University of Aston.

CONTENTS

SYNOPSIS

The manufacture of composites reinforced with strong, stiff fibres is now a well established practice. The use of glass fibres allowed the theory developed for plywood and similar materials to be used directly as it was assumed that glass fibres were elastically isotropic. Carbon fibres are now used in increasing quantities and the same theory is often used to calculate the mechanical behaviour of carbon composites. It is now known that carbon fibre is highly anisotropic and thus may preclude the use of conventional theory suited to isotropic fibres. This thesis is a study of the effects of fibre anisotropy on the elastic properties of composites.

The introduction covers the development of carbon fibres leading to the production of anisotropic fibres, with particular interest in the attempts to calculate the properties of the fibres. The question of the isotropy or otherwise of glass fibres is considered, and it is concluded that glass fibres are isotropic.

The properties of composite constituents are determined and used to calculate the properties of unidirectional composites. The properties of the unidirectional composites are measured, compared with the calculated values, and used to predict the properties of laminated composites. The calculated and experimental values of the laminate properties are compared. It is concluded that the properties of laminates may be predicted reasonably accurately from the unidirectional composite properties, but only some of the unidirectional composite properties can be predicted with reasonable accuracy from the constituent properties.

NOTATION

A_{ij} Component of matrix $[A]$ defined by equation 3.35

B_{ij} Component of matrix $[B]$ defined by equation 3.36

C_{ij} Component of matrix $[C]$ defined by equation 3.2

D_{ij} Component of matrix $[D]$ defined by equation 3.38

A'_{ij} Component of matrix $[A']$ defined by equation 3.42

B'_{ij} Component of matrix $[B']$ defined by equation 3.42

C'_{ij} Component of matrix $[C']$ defined by equation 3.42

D'_{ij} Component of matrix $[D']$ defined by equation 3.42

A^*_{ij} Component of matrix $[A^*]$ defined by equation 3.43

B^*_{ij} Component of matrix $[B^*]$ defined by equation 3.43

C^*_{ij} Component of matrix $[C^*]$ defined by equation 3.43

D^*_{ij} Component of matrix $[D^*]$ defined by equation 3.43

C Constant in equation 20 table 6

E_{11} Young's modulus of a unidirectional composite in direction 1
(longitudinal modulus)

E_{22} Young's modulus of a unidirectional composite in direction 2
(transverse modulus)

E_f Young's modulus of an isotropic fibre

E_{f1} Axial Young's modulus of an anisotropic fibre

E_{f2} Transverse Young's modulus of an anisotropic fibre

E_m Young's modulus of the matrix

E_x Young's modulus of a composite in direction X

E_y Young's modulus of a composite in direction Y

G_f Shear modulus of an isotropic fibre

G_{f1} Axial shear modulus of an anisotropic fibre

G_{f2} Transverse shear modulus of an anisotropic fibre

G_{12} Shear modulus of a unidirectional composite in the 1-2 plane

G_{23} Shear modulus of a unidirectional composite in the 2-3 plane

G_m Shear modulus of the matrix

G_{xy} Shear modulus of a composite in the X-Y plane

K Constant in equation 3 table 6

K_f Bulk modulus of a fibre

K_m Bulk modulus of the matrix

K_{23} Transverse plane strain bulk modulus of a unidirectional composite

L_1 Invariant property of a composite

L_2 Invariant property of a composite

M_x Bending resultant in direction X defined by equation 3.28

M_y Bending resultant in direction Y defined by equation 3.28

M_{xy} Twisting resultant in direction X-Y defined by equation 3.28

N_x Normal stress resultant in direction X defined by equation 3.27

N_y Normal stress resultant in direction Y defined by equation 3.27

N_{xy} Shear stress resultant in direction X-Y defined by equation 3.27

Q_{ij} Component of matrix $[Q]$ defined by 3.13

R_{ij} Component of matrix $[R]$ defined by 3.15

S_{ij} Component of compliance matrix $[S]$

U Airy stress function defined by equations 3.50-3.52

U_i Elastic properties of a composite defined by 3.45

V_f Fibre volume fraction of a composite

V_m Matrix volume fraction of a composite

V_{xy} Shear stress in the X-Y plane

V_{yz} Shear stress in the Y-Z plane

V_{xz} Shear stress in the X-Z plane

X Cartesian coordinate direction

Y Cartesian coordinate direction

Z Cartesian coordinate direction

a Constant in equation 1 appendix D

b Constant in equation 1 appendix D

c Constant in equation 1 appendix D

f Subscript to denote fibre

i Subscript to denote direction

j Subscript to denote direction

k Subscript to denote direction

l Subscript to denote direction

k_x Lamina curvature in the X direction

k_y Lamina curvature in the Y direction

k_{xy} Lamina curvature in the X-Y direction

u Lamina displacement in direction X

v Lamina displacement in direction Y

w Lamina displacement in direction Z

x Distance along X axis

y Distance along Y axis

z Distance along Z axis

$\left.\begin{array}{l}\alpha \\ \beta_m \\ \beta_f \\ \gamma\end{array}\right\}$ Constants in equation 34 table 6

γ_{ij} Engineering shear strain component

ε_{ij} Normal strain component

ζ Reinforcement factor

ν_f Poisson's ratio of an isotropic fibre

ν_m Poisson's ratio of matrix

ν_{f1} Major Poisson's ratio of anisotropic fibre

ν_{f2} Minor Poisson's ratio of anisotropic fibre

ν_{12} Major Poisson's ratio of a unidirectional composite in the 1-2 plane

ν_{21} Minor Poisson's ratio of a unidirectional composite in the 1-2 plane

ν_{xy} Major Poisson's ratio of a composite in the X-Y plane

ρ Constant in equation 34 table 6

σ_{ij} Normal stress component

τ_{ij} Shear stress component

1 INTRODUCTION

1.1 Carbon

The element carbon has two basically different structures, that of diamond and graphite. Diamond has a face centred cubic structure with the atoms 1.54 $\overset{o}{A}$ apart. Pure graphite has a layered structure (figure 1), each layer being composed of carbon atoms arranged in a regular hexagonal network. The spacing of the atoms in the layers or planes is 1.42 $\overset{o}{A}$ and the spacing between planes is 3.40 $\overset{o}{A}$. In the diamond structure all the carbon-carbon bonds are covalent giving a hard, strong material. In the layers of graphite each carbon atom is surrounded by three carbon atoms thus. The Sigma bond between the carbon atoms are sp^2 hybrid bonds with inter-bond angles of 120°. Each carbon atom uses three electrons for these bonds. The fourth electron is an unhybridised p orbital. These electrons are delocalised and form a cloud above and below the Sigma bonds, thus giving pi bonding in addition to Sigma bonding, hence the internuclear distance in graphite (1.415 $\overset{o}{A}$) is shorter than that of diamond. The electrons are able to move throughout all the branches of the network resembling the electrons in a metallic structure in this respect, but in two dimensions only. The layers are 3.3539$\pm$ 0.0001 $\overset{o}{A}$ apart, held together by weak Van der Waal's forces. The layers are stacked in an ABAB sequence (figure 1), but Van der Waal's forces make it fairly easy to shift the layer planes with respect to each other. 'Bulk carbon' is generally considered to be 'amorphous' and is formed from small graphite crystallites randomly arranged. A typical bulk carbon has a strength of 5 MPa, a modulus of 10 GPa, density of 2200kg/m^3 and is isotropic unless some preferred orientation is imposed by the manufacturing process.

Using a D.C. arc, Bacon (1) produced 'graphite' whiskers with diameters of a fraction of a micron to greater than 5 microns with recoverable lengths up to 30mm. The whiskers appeared to be in the form of concentric tubes in a scroll-like manner. The modulus was estimated to be at least 700 GPa and the strength about 200MPa. The electrical

resistivity of the whiskers was 650Ωmm compared with 400Ωmm for a single crystal of graphite in the basal plane direction. Eartherly calculated the theoretical modulus of graphite in the basal plane to be 1000GPa $\pm$ 20%. Examination of the whiskers by X-ray diffraction suggested that the a-axis of the graphite crystallites were parallel to the whisker axis, and that the c-axis was perpendicular to the axis. This early experiment clearly demonstrated the potential of carbon as a strucutral material.

Brenner (2) modified the Von Polyani model (3) of the sodium chloride structure to calculate the theoretical strength of perfect whiskers. Taking into account the theoretical shear strength necessary to initiate plastic flow, Brenner showed that the maximum tensile strength lay in the range 3/100 to 17/100 of the modulus. The average value of 1/10 of the modulus is normally quoted as the theoretical strength of materials, giving a value of about 100 GPa for the basal plane of graphite.

1.2 Carbon Fibres

The terms carbon fibre and graphite fibre are not clearly defined, although Bacon(4) suggested that carbon should refer to a fibre heat-treated to 1273-1773°K with a composition of 80-95% carbon, and graphite should refer to fibres heat-treated to temperatures in excess of 1773°K with a composition of at least 99% carbon. As graphite is a particular form of the element carbon, in this thesis the term carbon will be applied to any fibre heat-treated above 1273°K.

Carbon fibres and fabrics have been made for several years by carbonising various forms of cellulose (cotton for carbon fabric, bamboo for early electric light filaments), but all have a low strength and modulus. Carbon fibres made explicitly for reinforcement purposes are normally made from viscose cellulose fibre (Rayon) in the United States of America and from polyacrylonitrile (PAN) fibre in the United Kingdom.

In 1964 Phillips, Watt and Johnson (5,6) started to develop carbon fibres with properties approaching those of graphite whiskers. The dramatic increase in the fibre modulus and strength was the result of stretching the fibre during processing thus tending to preferentially

align the carbon structure. The directional structure of Grafil A type fibre is clearly shown in figure 2. In recent years in an effort to reduce the high cost of carbon fibre, attempts to use other materials as a base (precursor) have been made with varying degrees of success. Kumura and Jenkins (7) produced glassy carbon fibres from phenolic resin with a maximum modulus of 69GPa. Hawthorne and Baker (8) used pitch as a precursor and produced fibres with strengths up to 2.6 GPa and moduli up to 440 GPa.

The process of converting the precursor to carbon fibre takes place in stages under closely controlled steps which vary according to the type of precursor and manufacturer. Watt and Johnson (9) have proposed that the conversion of PAN to carbon fibre takes place in a manner similar to the following decomposition path.

Chain molecule of PAN   + heat under tension →   Ladder polymer- more stable structure.   + further heat → Carbon
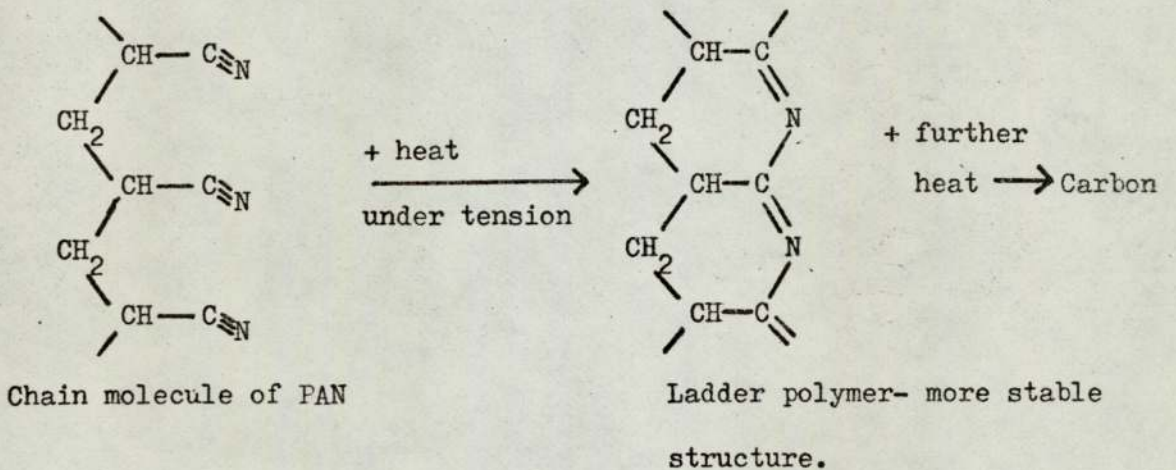
Figure 3 Decomposition of PAN fibre.

By keeping the fibres under tension, shrinkage is prevented and the carbon molecules tend to 'straighten out'. The active C-N groups cause the chain molecules to form aggregates calles fibrils. Further heating and controlled oxidation leads to oxygen bonds between molecular chains. Since the C-N groups can be orientated at different angles several molecular chains can be tied together by oxygen bonding. Oxygen links in three dimensions can produce a fairly rigid structure and prevent the chains from bending and distorting on further heating.

Bacon and Tang (10) proposed a mechanism for the conversion of cellulose fibre into carbon fibre through various stages. By use of X-ray

diffraction and electron microscopy techniques and by measuring the
physical changes which take place in the carbonisation process, Bacon and
Tang showed a structural similarity between cellulose molecular orientation
and preferred orientation of the carbon fibre. The shrinkage in the fibre
length which takes place with carbonisation decreased with increasing
cellulose molecular orientation and Bacon and Tang suggested that the
building of the carbon chain structure probably begins along the paths
of the original cellulose structure, thus preserving a 'replica' of the
original fibre structure. The idea of longitudinal and transverse poly-
merisation was introduced to account for the dimensional changes in the
fibre. Longitudinal polymerisation of the cellulose to carbon leads to a
reduction of 8.3% for perfect molecular orientation, whereas with
transverse polymerisation the carbonised fibres would be only 48% of the
length of the original fibre. See figure 4.

Figure 4   Tranverse polymerisation
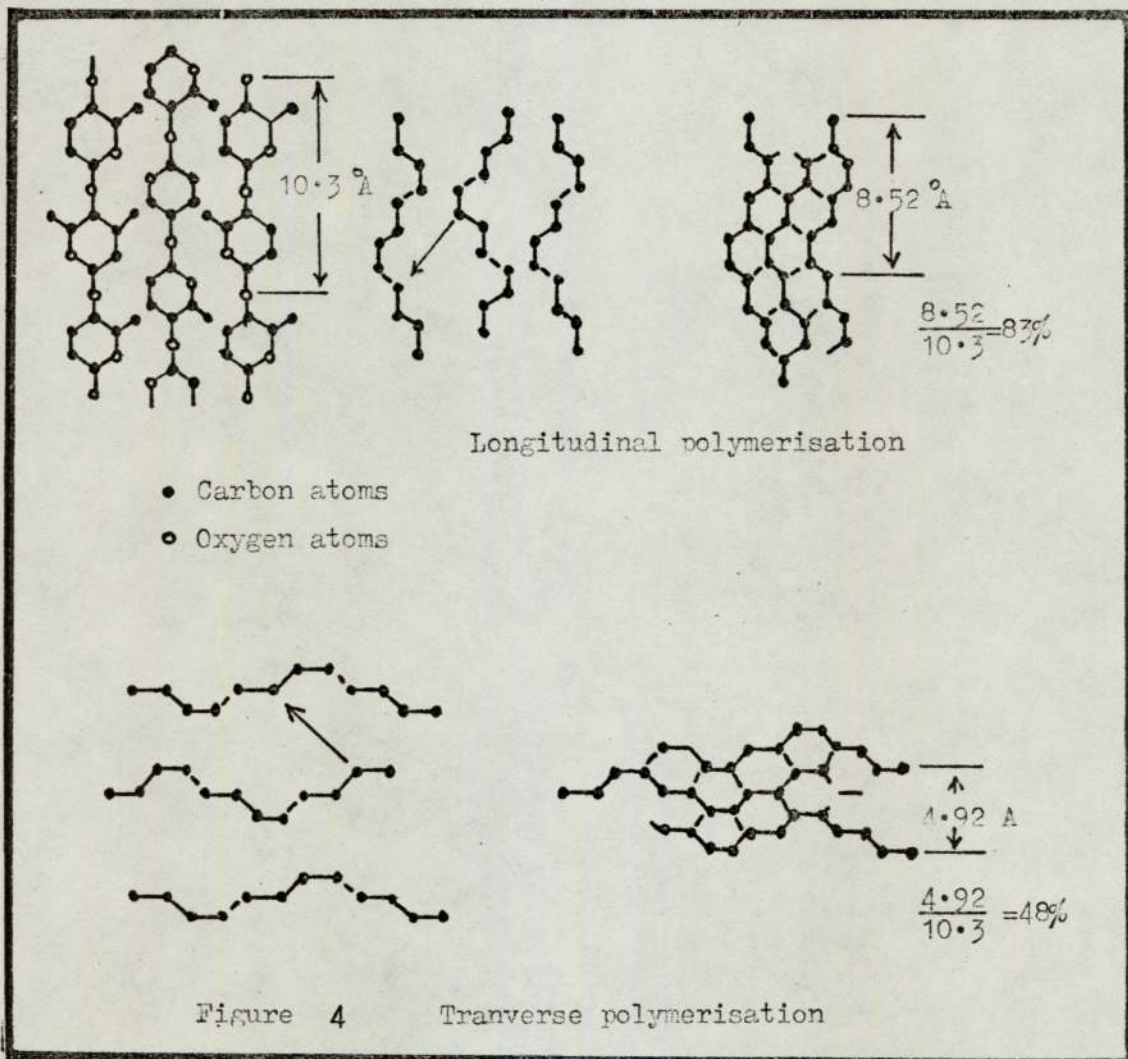
The final properties of the carbon fibre depend on (a) the precursor, (b) the precursor treatment, (c) the maximum heat treatment temperature, (d) the percentage elongation during heat treatment.

Consider (a) first, the type of precursor used. The highest published values of fibre modulus and strength for stress graphitised carbon fibres (that the author is aware of) are those for fibres made from a PAN precursor by RAE. (Watt and Johnson (15) modulus 690 GPa).The difference in carbon fibre moduli produced from various precursors is a reflection of the orientation of the molecules rather than being a special property of the precursor. Any process which increases the perfection and alignment of the carbon structure in the carbon fibre may be expected to increase the modulus in the direction of the fibre axis.

Some types of precursors lend themselves to stretching more readily than others and can thus achieve a higher degree of orientation. Rayon and PAN fibre are both made by drawing through a die or bushing and possess some preferred orientation before the carbonisation process starts, but many are completely amorphous. e.g. pitch. Moreton (11) has shown that carbon fibre made from PAN fibre which had been stretched in glycerol at 423 $^\circ$K prior to heat treatment, has a higher modulus and strength than PAN fibres stretched in steam by the same amount. The increases recorded were 1.32 to 1.71 GPa for the strength and 427 to 455 GPa for the modulus. Examination of the PAN fibres stretched in steam showed evidence of pores, possibly due entrapped water, (12) which could cause a weakening of the fibres.

The heat treatment process which converts the base material to carbon controls the amount of 'graphitisation' that occurs in the fibre, although other factors such as the type of atmosphere also have an effect. Moreton, Watt and Johnson (13) found the relationship between maximum heat treatment temperature, strength and modulus for PAN based (RAE) fibres to be as shown in figure 5. The strength of carbon fibre apparently reaches a peak value with a heat treatment temperature of about 1873°K .This
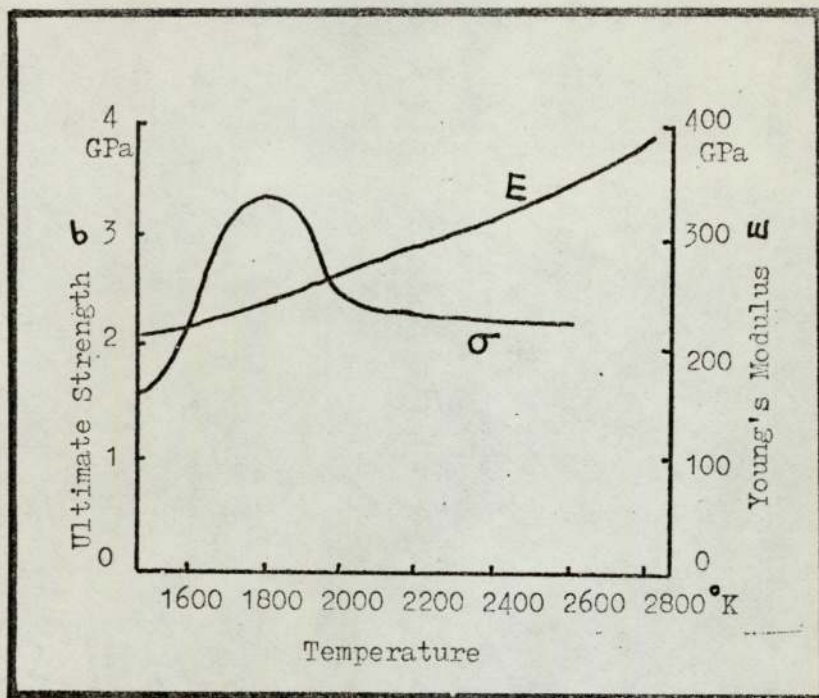
Figure 5   Effect of heat treatment temperature.

discovery results in two types of carbon produced commercially, 'high

modulus' or type 1 and 'high strength' or type 2. The reason for the

decrease in strength of fibres heat treated to temperatures higher

than 1873°K is thought to be due to the growth of 'pure' three dimensional

graphite crystallites which have weak bonding with the rest of the structure.

The percentage elongation produced during the stretching and heat

treatment of a fibre can have a dramatic affect on the modulus and

strength. Hawthorne (14) produced glassy carbon fibres with a modulus of

40 GPa and strength of 1.75 GPa by heat treating asphalt pitch at 1273°K.

X-ray diffraction showed the fibres to have no preferred orientation and

were probalbly amorphous with Lc=10 $\overset{\circ}{A}$ and La=17 $\overset{\circ}{A}$. After subjecting the

fibres to stress graphitisation the modulus increased to 440 GPa and the

strength to 2.60 GPa. In a further study Hawthorne (14) examined the effect

of elongation on carbon fibres from several precursors. Although from

different sources many of the properties were the same after similar

treatments. The effect of elongation on orientation, Young's modulus,

shear modulus and electrical resistivity are shown in figures 6,7,8,9.

The relationship between Young's modulus and elongation had a limited

amount of scatter and the results of the shear modulus relationship had

considerable scatter, but an overall trend was demonstrated.

-6-
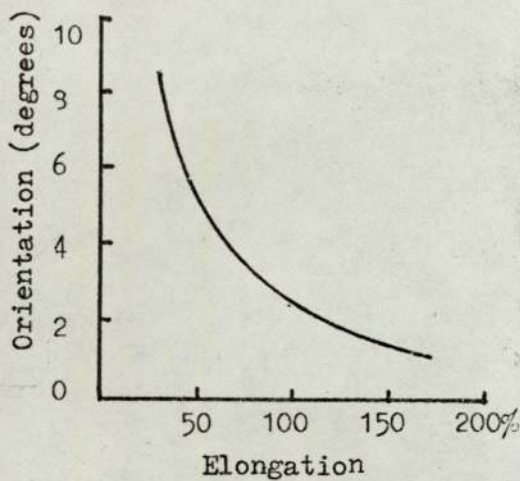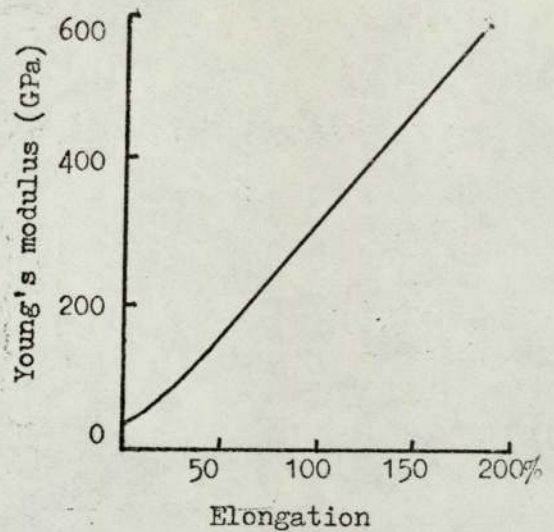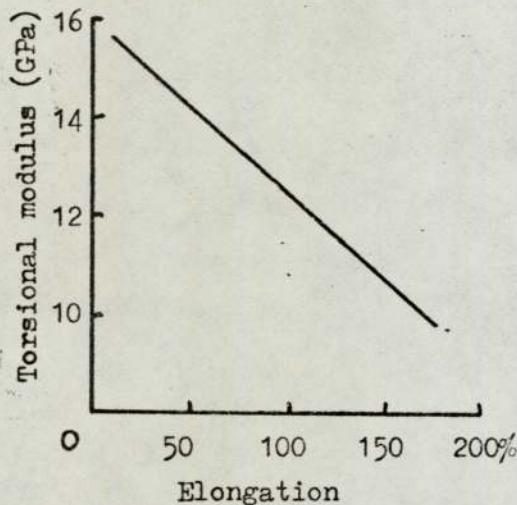
Figure 6

Figure 7

Figure 8
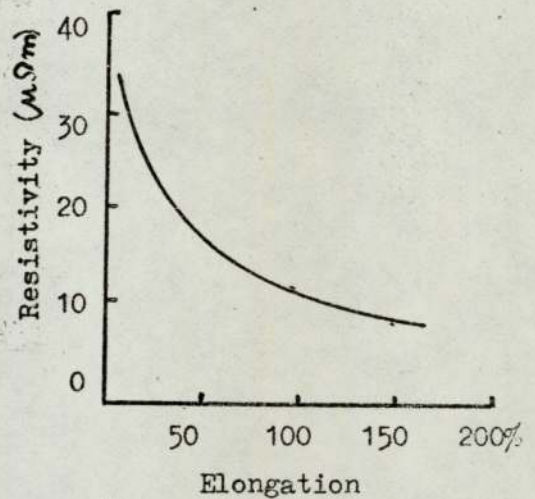
Figure 9

Allen, Cooper and Meyer (16) demonstrated that it is possible to affect the modulus and strength of a carbon fibre by introducing other elements into the graphite lattice. By heating carbon fibres in a Boron doped crucible the modulus of RAE carbon fibres were increased from 410 to 550 GPa. No boron carbide was detected and it was estimated that only about 1 atom in 10000 was displaced by the boron. No explanation for the phenomena was given, but it is well known that the modulus of reactor grade graphite increases after neutron radiation due to the pinning of dislocations. (Kelly 17). It is thought that the distortion of the carbon lattice by the boron atoms could have a similar effect.

The modulus and strength of any material are ultimately limited by the strength of the interatomic bonds. The theoretical strengths and moduli of many materials have been established and found to be in excess of experimental values by factors of up to 1000. The experimental values found by testing bulk materials do not reflect the strength of the interatomic bonds of the material so much as the weakness of the material due to various types of 'faults' such as intercrystalline boundaries. Carbon fibre has a structure far closer to a 'perfect' structure than most materials used for engineering purposes.

The structure of perfect graphite is shown in figure 1 , and in a perfect carbon fibre the planes would be continuous, correctly stacked and perfectly aligned with the fibre axis. The bond energy of carbon atoms in the basal plane is estimated to be 600 kJ/g atom and the interfacial bond energy between planes is estimated to be 5.1 kJ/g atom. Hence the perfect carbon fibre would be stiff and strong in two directions parallel to the graphite planes and weak and 'soft' in the direction normal to the planes.

The structure of carbon fibre is responsible for all the physical properties and is a centre of considerable study. Electron microscopy and X-ray diffraction have provided most of the information on the inner structure of fibres , and by taking into account the macro-properties of the fibre, attempts have been made to provide a model structure which satisfies all the experimental observations.

Bacon[18] provided an experimental X-ray technique for measuring the degree of preferred orientation in reactor graphites in which the width of the 002 line was measured at varying angles with a microdensitometer. When the intensity of the reflected beam is plotted against the angle $\emptyset$, a Gaussian shaped curve is formed. Half the width at half the peak height of the graph is taken as a measurement of the average preferred orientation angle. Ruland [19] adopted a similar principle to Bacon for measuring the preferred orientation in carbon fibres. He measured the preferred orientation in terms of a factor q , where q=1 signifies

perfect orientation of the planes parallel to the fibre axis, q=-1 signifies perfect orientation of the planes normal to the axis, and q=0 signifies completely random orientation. Other information available from X-ray and electron microscopy is La, the average size of the hexagonal plane of the graphite crystallites, Lc, the depth or stacking height of the crystallites and information on the size, shape and internal surface area of any pores in the fibres. La and Lc can be calculated from line broadening using the Sherrer equation $L=K\lambda/B \cos\Theta$. The sudden change in density at the interface of a pore/solid causes diffuse scattering of X-rays which can yield information on the diameter and length of pores. Direct observation of individual features with an electron microscope has provided further information and confirmation of some of the data obtained by X-ray work.

Ruland (19) studied the structural changes during the carbonisation of cellulose fibre (Fortisan 36) and found that the preferred orientation of the cellulose structure was almost completely destroyed between 513-553°K. From 553°K to 1173°K a small but significant orientation existed. An increase in the preferred orientation started at about 1273°K and continued gradually to higher temperatures, and under special conditions could exceed the original orientation. (See figure 10).A direct relationship between the preferred orientation in the rayon and carbon fibres was not found, and in fact ''highly orientated fibres as starting materials did not necessarily produce well orientated carbon fibres''. Further work by Ruland (20) revealed periodic density fluctuations of small angle scattering along the fibre. This was thought to be due to differences in the decomposition process resulting in domains of amorphous and crystalline material. This inhomogeneity was found to persist in carbonised fibres. The recovery of the preferred orientation at about 1273°K also resulted in the formation of needle-like pores about 10-30 Å in diameter with lengths in excess of 200 Å.

Pores are not uncommon in textile fibres, and using X-ray diffraction techniques, Statton (21) demonstrated the existence of microvoids in

PAN fibres by diffuse scattering patterns. Discrete scattering patterns also indicated the existence of a long periodic order commonly found in drawn fibres. Sharp and Burnay(22) examined defects in carbon fibres heat treated up to 2873°K and observed elongated cavities in the surface up to 3μm in diameter, some containing inclusions, which suggested that the defects were formed by a gouging action during processing.

Watt, Phillips and Johnson (6) examined RAE PAN based fibres and concluded that they were of a polycrystalline nature with a preferred orientation of the c-axis of the graphite crystallites normal to the fibre axis. The degree of orientation was calculated from the half width of the 002 line and plotted against the average fibre modulus. (Figure 11).
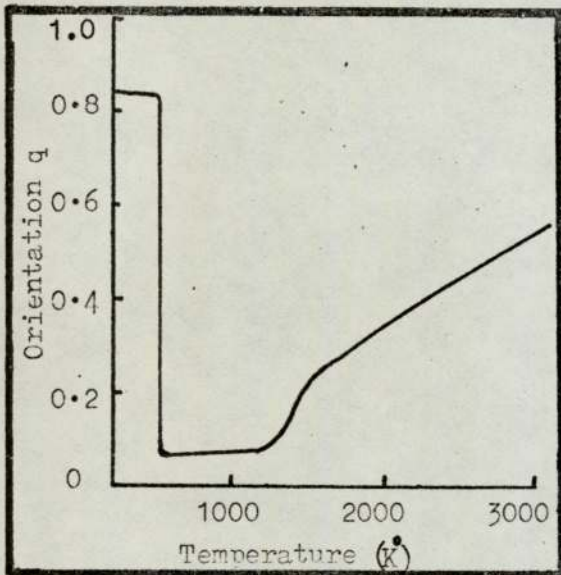
Figure 10 Orientation/temperature   Figure 11 Orientation/modulus
         for Fortisan 36 fibre.   for RAE carbon fibre.
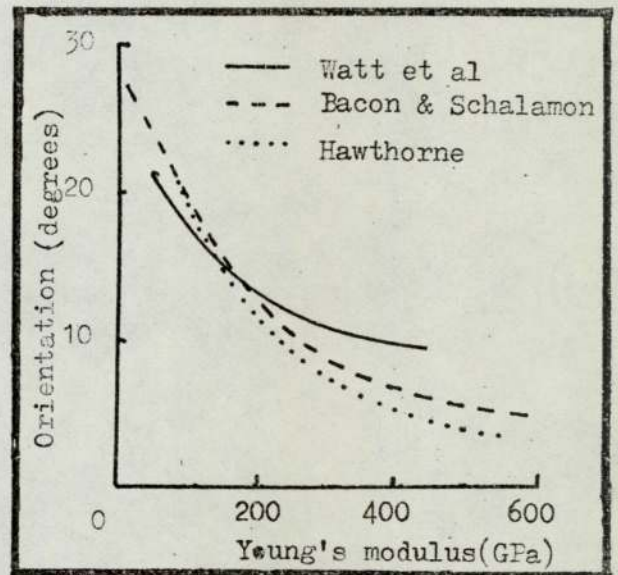
Bacon and Schalamon (23) examined rayon based fibres and found a similar relationship between orientation and modulus. Watt et al also studied the relationship between Young's modulus and strength, (figure 12) electrical conductivity and density and found similar results to Hawthorne.
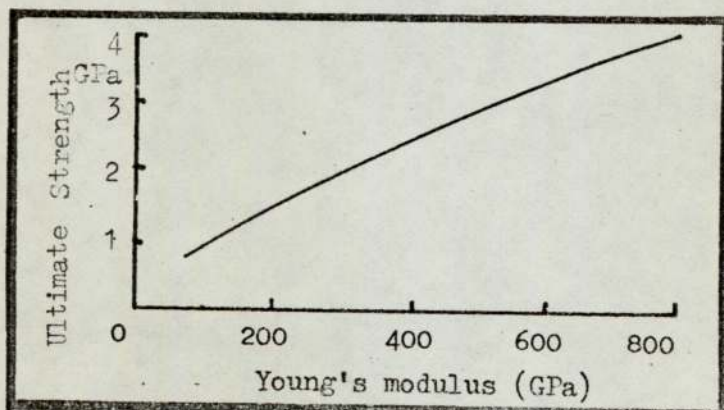
Figure 12 Strength/modulus relatioship of RAE fibre

It is interesting to note that the apparently linear relationship between modulus and strength is not in agreement with the results of Moreton, Watt and Johnson (figure 5), but is in agreement with the results of Johnson, Marjoram and Rose for the case of stress graphitised fibres. Johnson, Marjoram and Rose (24) studied the effect of stretching PAN based carbon fibres at high temperatures.(Stress graphitisation) Although there was considerable scatter in the results it appears that stress graphitisation (up to 30% stretch) produces an increase in the modulus, strength and orientation. See figures 13 and 14.

Johnson and Watt (25) examined RAE fibres heat treated at $2773^{\circ}K$ with a modulus of 410 GPa , and found a fibre structure consisting of long narrow units parallel to the fibre axis with a width of about 100 $\overset{o}{A}$. X-ray analysis showed a high degree of preferred orientation with the planes parallel to the axis. The crystallites appeared to be turbostratic with Lc at least 12 layers thick and La in the range 60-120 $\overset{o}{A}$. Sections from fibres heat treated to $1273^{\circ}K$ ruptured while being cut to reveal a net-like structure. Fibrils in the network were about 800-1000 $\overset{o}{A}$ across and ran the full length of the section. La in this structure was about 30 $\overset{o}{A}$. It was concluded that the modulus of the fibre was controlled by the orientation and the strength by interfibrillar bonding. For a further check on the size of the crystallites the thermal conductivity of the fibre was calculated from the Debye equation, $K=\frac{1}{3}\rho cvl$. The mean free path,l,of the electrons was assumed to be equal to 100 $\overset{o}{A}$, the width of the fibril. The calculated value ,0.0596 $Wm^{-1}K^{-1}$ was in reasonable agreement with the experimental value calculated from a composite bar.

Johnson and Tyson (26) studied the intimate structure of a fibre carbonised at $1273^{\circ}K$ then graphitised at $2923^{\circ}K$. From the 002 reflections and the fact that there were no h k l reflections observed with l > 0 they concluded that the fibre had a turbostratic structure with the c-axis normal to the fibre axis. The interlayer spacing was estimated to be 3.42 $\overset{o}{A}$, Lc approximately 60-70 $\overset{o}{A}$ and La about 70 $\overset{o}{A}$. They presented a model of the carbon fibre structure shown in figure 15, in which crystallites with basal

plane dimensions of about 60×60 Å and stacking heights of about 60 Å are positioned such that the basal planes are parallel to the fibre axis within ± 8°. To help confirm the conclusions drawn from the X-ray data a section of the precursor was stained with phosphotungstic acid and examined with an electron microscope. It showed fibrils about 75 Å wide and longitudinal sections of the carbonised fibre gave the impression of a fibrillar system with crystalline regions parallel to the axis separated by voids to give intercrystalline repeats of about 50-100 Å. Extinction bands gave a measure of the crystalline width which was about 65 Å. They concluded that the extinction bands were caused by sub-grain boundaries with predominating twist components. In a later study Johnson and Tyson (27) used low angle X-ray diffraction to evaluate lp, Porod's distance of heterogeneity, and Sv, the internal surface area of carbon fibres. Good correlation between low angle parameters and fibre strength were reported, but with a discontinuity at 2173 K. The discontinuity was related to a change from a highly cross-linked structure with many small pores and crystallites to a graphite structure with fewer cross-links, lower internal surface area and larger pores and crystallites. The results showed a sudden increase in lp and Lc with a decrease in Sv, but with little change in the strength or modulus. It was concluded that in stress graphitised fibres the pores were more uniform and had less sharp boundaries than in non-stress graphitised fibres.

Ruland (28) made a comprehensive study of rayon based carbon fibres and proposed a 'wrinkled ribbon' model for the structure of the fibre. The basic unit of the model is a ribbon-like structure (figure 16) about 60 Å wide and thousands of angstroms long, made up from the hexagonal rings of the basal planes. The ribbons contain 'holes' where numbers of carbon atoms are missing; there is no correlation between the general direction of the borders and the direction of the a-axis of the hexagonal rings. Numbers of the ribbons run parallel to form microfibrils, (Figure 17) with a preferred orientation parallel to the axis. The microfibrils are 'wrinkled' with voids between them, typically 200-300 Å long and 10-20 Å wide. Dark field micrographs revealed light and dark domains which were

attributed to Moiré effects from the superposition of two microfibrils with layer planes in the reflection position for 002 but tilted with respect to each other. Measurement of the angle between the layers confirmed this observation. The variation in spacings of the Moiré patterns along a given microfibril was taken to indicate smoothly curved regions in the model with no sharp tilt boundaries. Dark field pictures of the 103 reflection indicated small areas of regular stacking (ABABAB) but only for 3-7 layers with lengths of about 100-400 A. Ruland considered this observation in keeping with the 'wrinkled ribbon' model in that it would only be possible to maintain the correct stacking sequence in the straight sections of the fibrils. In wide angle scattering the variation of the 002 line with angle for both PAN and rayon based fibres indicated a correlation between size and/or perfection of the stacking of the layers and the orientation of the layer normals with respect to the fibre axis. As the width of the first interface maximum is more sensitive to variations in the size of the scattering domains than to variations in the perfection, these results are incorporated in the model as shown in figure 18. The branched microfibrilar structure with sharp ended pores is somewhat similar to the branched structures in textile fibres.

Ruland's results of La and Lc are shown in table 1. The increase in La /Lc with preferred orientation for a given type of fibre was interpreted as an increase of the average length of the ribbons straightened out by thermal or mechanical means.

Fibre type	La	Lc	q	H.T.Temp.
Type 1 (PAN based)	119 Å	64 Å	0.902	2973 K
Type 2 (PAN based)	35 Å	34 Å	0.787	1523 K
Rayon based	59 Å	50 Å	0.230	3073 K
''	81 Å	54 Å	0.820	3073 K
''	91 Å	65 Å	0.980	3173 K
''	130 Å	65 Å	0.982	3173 K

Table 1 Ruland's X-ray results.

The stereochemical reactions of Bacon (10) and Watt (9) implied a preferred orientation of the a-axis of the hexagonal lattice, but Ruland found no evidence to support this supposition. Low angle scattering due to voids was essentially the same for fibres made from PAN or rayon, and was similar to that found in textile fibres. It was shown that the angular distribution of voids and graphite layers was almost identical, proving that the voids are parallel to the layer planes. In type 1 PAN based fibre 75% of the voids were within 12° of the fibre axis, but in type 2 only about 25% are within 12°. The length of voids increased at an increasing rate with heat treatment temperature and was independent of the base material. The microporosity also increased with heat treatment temperature but was also dependent on chemical and mechanical treatment. A plot of the average distance between voids and the stacking height showed that the voids increased in width as the fibril stacking height increased. Variations in the intensity of the reflections from the values predicted by Porod's law at wide angles were thought to be due to density fluctuations in the parallel stacking of the layers. Ruland suggested that the small angle scattering reported by Johnson and Tyson (27) as amorphous carbon was probably due to this effect. Increasing the heat treatment temperature generally reduced density fluctuations while mechanical stretching tended to increase them. Using the ribbon model, Ruland suggested that an increase in heat treatment temperature caused the atoms at the edges of the ribbons to diffuse and 'smooth out' the ribbon, whereas stretching caused the ribbons to move parallel to each other and disturb the smoothing process. See figure 19.

1.3. Theoretical calculation of the fibre modulus

Hill (29) showed theoretically that the upper and lower bounds of the modulus of a multicrystalline anisotropic material were given by models where homogeneous strain and homogeneous stress were assumed respectively. Ward (30) developed expressions for calculating the optical birefringence and moduli of an idealized semicrystalline polymer in terms of molecular orientation. For the case of uniform stress the elastic properties of the polymer were found in terms of the orientation parameters and compliance constants (S_{ij}') of a single transversely isotropic unit ; for the case of uniform strain the elastic properties were found in terms of the stiffness constants (C_{ij}').

Price (31) derived expressions to express the Young's modulus of an aggregate of hexagonal crystallites while taking into account the preferred orientation of the sample. For the uniform strain model he derived that the modulus in direction OZ is given by:-

$$E_{oz} = \frac{\int_{o}^{2\pi} \int_{o}^{\frac{\pi}{2}} E(\phi) I(\phi,\theta) \sin\phi \, d\phi \, d\theta}{\int_{o}^{2\pi} \int_{o}^{\frac{\pi}{2}} I(\phi,\theta) \sin\phi \, d\phi \, d\theta} \qquad \text{(See appendix A)}$$

where ϕ = angle between c-axis of crystallites and direction OZ

θ = other coordinate angle (polar coordinates)

$I(\phi,\theta)$ = density of crystallites in direction (ϕ,θ)

$E(\phi)$ = modulus of single crystal at angle ϕ to c-axis

Note $E(\phi) = 1 / (S_{11} \sin^4\phi + S_{33} \cos^4\phi + (2S_{13} + S_{44}) \cos^2\phi \sin^2\phi)$

S_{ij} = elastic compliances of crystallites

For the uniform stress model he derived:-

$$1/E_{oz} = \frac{\int_{o}^{2\pi} \int_{o}^{\frac{\pi}{2}} \frac{1}{E(\phi)} I(\phi,\theta) \sin\phi \, d\phi \, d\theta}{\int_{o}^{2\pi} \int_{o}^{\frac{\pi}{2}} I(\phi,\theta) \sin\phi \, d\phi \, d\theta}$$

Price used elastic constant values supplied by Spence (32) and experimental orientation values for cylindrically symmetric and completely anisotropic

-15-

pyrolytic graphites to calculate the moduli of the graphite. The results were in best agreement with the experimental values when the constant stress model was assumed, but all the calculated values were too large. The values of the compliances used were as follows; $S_{11}=1.11*10^{-12}$,

$S_{22}=-0.04*10^{-12}$, $S_{13}=-2.5*10^{-12}$, $S_{33}=33.2*10^{-12}$, $S_{44}=435*10^{-12}$ units Pa^{-1} All $\pm25\%$

Goggins and Reynolds (33) noted that Price's treatment for the case of the uniform strain model was incorrect. In order to calculate the elastic properties of the graphite assuming uniform strain it is first necessary to calculate the general stiffness components C_{ij}' from the basic crystalline stiffnesses C_{ij}, then invert the C_{ij}' matrix to obtain the elastic compliances from which the graphite properties may be deduced. Ruland (34) made a similar observation on Ward's treatment of the uniform strain case. Goggin and Reynolds used the same relationship for the uniform stress model as Price but they assumed transverse isotropy (which eliminates dependence on Θ). Experimental/theoretical comparisons for the values of S_{11}, S_{33}, S_{13}, S_{12} and S_{44} of Pile Grade A reactor graphite showed that the theoretical values were much lower than the experimental values. The main reasons for the discrepancy were thought to lie with the effects of porosity, cracks and possibly inaccurate values of the crystalline constants.

Brydges, Badami,Joiner and Jones (35) calculated the values of the elastic compliances of type 1 carbon fibre from X-ray data using the uniform stress and strain models with Goggin and Reynolds relationships and elastic constant values of pyrolytic graphite supplied by Spence (private communication). The limits of the two models were very wide and the experimental values of Young's modulus for both the type 1 fibre and an experimental high modulus fibre were just above the lower (uniform stress) limit. See figure 20.The experimental value of the shear modulus was also just above the lower limit. They concluded that the results indicated that the modulus of the fibre can be quantitatively accounted for by the assumption of a fibre composed of orientated distributed crystallites with the elastic constants of perfect graphite crystals.

Ruland (34) investigated the application of the uniform stress and strain models to the case of anisotropic carbon fibres. The structure of the carbon fibres was assumed to be in the form of crystallites composed of turbostratically stacked graphite layers about 5-10 layers high ,separated by needle-like pores, but with no information regarding any cross-links. The uniform stress model assumes that the stacks of layers are strongly linked in the longitudinal direction and weakly in the transverse direction and that a stress applied in the longitudinal direction affects all stacks uniformly regardless of orientation. Ruland argues that this model is reasonable to a point, but" it is difficult to assume that the transmission of stresses between two consecutive stacks of layers which are tilted with respect to each other can be at a non-zero angle to the layer planes".
In the uniform strain model strong lateral (transverse) bonds between individual crystallites are assumed so that the neighbouring crystallites have identical dimensional changes in the direction of the applied force. Although this assumption seems unreasonable in view of the nature of the graphite structure, the model cannot be excluded because of a lack of information on any cross-links. Ruland proposed that the 'elastic unwrinkling' model is a closer approximation to the 'true' carbon fibre structure than either the uniform stress or uniform strain model. In the unwrinkling model the graphite layers are assumed to be linked together to form long wrinkled ribbons along the fibre axis. Applied stress in the longitudinal direction causes the ribbons to 'unwrinkle' and increase the preferred orientation of individual layers. The surrounding environment of the layers produces resistance to tilting of the layers and the components of stress cause elongation of the layer planes. The resultant longitudinal Young's modulus is given by:-

$$S_{33} = 1/E_c = \ell_3 S_{11} + m_3 k \qquad \qquad ①$$

ℓ_3 and m_3 are given by
$$\ell_3 = \frac{\int Sin^2\phi \; g(\phi) d\phi}{\int Sin\phi \; g(\phi) d\phi} = \frac{\pi (q)^{\frac{1}{2}}}{4 \, arth \, (q)^{\frac{1}{2}}} \qquad ②$$

$$m_3 = \frac{\int \cos^2 \phi \, g(\phi) \, d\phi}{\int \sin \phi \, g(\phi) \, d\phi} = \frac{\pi}{4} \frac{1+q}{1-q} \frac{q^{\frac{1}{2}}}{arth(q)^{\frac{1}{2}}} \quad (3)$$

See appendix A

$g(\phi)$ = Angular distribution of layer normals

The elastic constant k (same dimensions as S_{11}) takes into account the resistance of the enviroment but has no physical basis and is derived from equations 4 or 5 using experimental data.

The unwrinkling model has the advantage over the models in that it more closely represents the real situation (as seen by Ruland) and is considerably more simple. However, the elastic constant k is difficult to interpret physically and the model does not provide any means of calculating the fibre modulus from single crystal data.

Ruland determined the distribution of layer normals $g(\phi)$, from X-ray techniques and calculated the orientation parameters from the Fourier coefficient, Pn for 9 carbon fibres with different degrees of preferred orientation. The porosity of the fibres was determined from the difference between macroscopic density and X-ray density (calculated from the layer spacings),and the modulus of the fibres corrected by $Ec = \frac{\rho_x}{\rho_m} E$.

where   E= observed modulus

ρ_x = X-ray density

ρ_m = macrodensity

The theoretical fibre moduli were calculated from the orientation parameters and the values of S_{11},S_{13} and S_{33} which were assumed to be those of a single graphite crystallite; $S_{11}=0.985*10^{-12}$, $S_{13}=-0.63*10^{-12}$, $S_{33}=27.8*10^{-12}$ units Pa^{-1} from a private communication from Blackslee. The variation of shear modulus with q for the uniform stress and uniform strain models is shown in figure 21. Also shown in figure 21 is the calculated value of k which is based on the linear relationship of equation 1. Assuming a linear relationship Ruland obtained the relationship between shear modulus and q by a least squares method, equations 4 and 5. Figure 22 is a plot of the experimental and theoretical values of Young's modulus calculated from the unwrinkling model using the average value of k from

-18-

figure 21. Also shown are the theoretical values predicted by the uniform stress and strain models. The results in figure 22 do not indicate which model is closest to reality but clearly demonstrate the large increase in the modulus for $|q| > 0.9$.

The values of S_{44} obtained for the uniform strain model are in the range of values so far observed for a moderately to highly imperfect graphite structure. The values of S_{44} from the uniform stress model are considerably less but this could be due to a stiffening effect of transverse cross-links. The fact that both series of S_{44} with increasing preferred orientation is explained by Ruland as a change in the manner of transmission of stress between individual particles but with no apparent effect on layer size or stacking height.

1.4 Discussion on carbon fibres

The relationship between plastic straining and the mechanical proper-
ties of carbon fibres during or before the carbonising process has been
clearly demonstrated with experimental results published. Further invest-
igations with X-ray diffraction and electron microscopy have shown that
various degrees of preferred orientation are induced in the structure of
the fibres by plastic straining and that some of the physical properties
of the fibre are related to the degree of preferred orientation . The
relationship between some properties and orientation are less obvious.
(consider figure 14) and are probably also influenced by other details of
the fibre microstructure.The microstructure of the fibre at any one time
depends on the type of precursor, percentage of plastic straining and the
heat treatment temperature , and hence it is not easy to define any general
structure for "carbon fibre".

It is apparent that the structure of a fibre changes considerably
as it is converted from a low modulus textile fibre to a high modulus
carbon fibre. A successful model for carbon fibres must be capable of
explaining the properties at each stage of the process. Two models have
been proposed for the structure of carbon fibre of similar modulus but of
different origin. Ruland's 'wrinkled ribbon' model is based on a rayon
based fibre and Johnson and Tyson's model on a PAN based fibre. The two
models differ mainly in the length of unbroken graphite layers and the
shape and position of voids . It is tempting to assume that Johnson and
Tyson's model is the result of stretching Ruland's model sufficently to
break the ribbons into shorter lengths but not to fracture the fibre as a
whole. Intrinsically one would expect fibres with a Ruland structure to be
stronger and have a higher electrical and thermal conductivity than fibres
with a Johnson and Tyson structure, but comparative figures are not given.
Neither model provides any information about the fibre structure perpen-
dicular to the fibre axis. Ruland suggested that although it is premature
to form any definite ideas on a model for transverse structure, there is

evidence for short range order in the packing of adjacent stacks of ribbons in the sense that there is a higher probability for the lateral ribbon boundaries to be in contact with the same, than with the surface of the graphite layer plane. The same argument could equally well apply to the Johnson and Tyson model, and taken to the limit would result in a flat sided fibre whose axis of symmetry was perpendicular to the fibre axis. The evidence that Ruland bases his assertion on is from the probability of the occurence of Moiré patterns in 002 dark field microscopy and some optical anisotropy reported by Butler and Diefendorf (36). This type of packing would result in rectangular section voids bounded on opposite sides by ribbon surfaces and lateral ribbons respectively for the Ruland model. (see figure 19).The case for a Johson and Tyson model would be similar but more complicated.

Brydges et al calculated theoretical limits of Young's modulus of a carbon fibre given by the Reuss and Voigt models using the graphite crystal constants of Spence and experimental orientation data for a type 1 fibre. A similar calculation for a high modulus experimental fibre was carried out using simulated orientation data based on the type 1 fibre results. Both results are shown in table 2 and in figure 20.

Experimental modulus	Orientation	Theoretical moduli	
		Reuss	Voigt
Fibre 1 385 GPa	7.7°	189 GPa	985 GPa
Fibre 2 736 GPa	6.4°	281 GPa	1000 GPa

Table 2   Orientation/modulus results of Brydges et al.

The average experimental results of Hawthorne, Bacon and Schalamon and Watt et al, are shown in figure 20 for comparative purposes. It should be noted that the graphs shown only represent the best fit curves for experimental results which showed a considerable scatter. If we assume that the experimental errors are approximately equal for each case,it appears that as the orientation of the crystallites decrease (and also the modulus) the spread between the various results also tends to decrease.

This is to be expected with an exponential type of relationship as variations in the orientation of fibres with a low degree of orientation will have a small effect on the modulus. All the experimental results lie within the bounds of the Reuss and Voigt limits as expected, and generally the Reuss model offers a closer approximation to the experimental values than the Voigt model.

Ruland corrected his experimental values of the fibre moduli for porosity (analogous with fibre volume fraction in a composite) and plotted a relationship between modulus and orientation (q) with very little scatter (figure 22) and with a maximum 'fibre modulus' of 870 GPa for q=0.98. It is only possible to compare Ruland's q factor with the 'half-width at half peak height' measure of orientation at q=1 (perfect orientation) and q=0 (random orientation) because they represent measures of different quantities.

According to Ruland's results there was very little difference in the predicted fibre modulus values whether the uniform stress, uniform strain or unwrinkling model was assumed. No explanation can be found for the similarity of the results.

The elastic constants of a single graphite crystal which are the basis of all the theoretical predictions for the fibre modulus vary some-what depending on which set of figures you take. The values quoted by Spence and Bowman and Krumhansl are shown in table 3.

Elastic constant	Spence 1961	Spence revised	Bowman & Krumhansl
S_{11}	$1.11*10^{-12}$ m N	$0.98*10^{-12}$ m N	—
S_{12}	-0.04 "	-0.16 "	—
S_{13}	-2.5 "	-0.33 "	—
S_{33}	33.2 "	27.4 "	—
S_{44}	435 "	250 "	—
C_{11}	$1160*10^9$ Nm^{-2}	$1130*10^9$ Nm^{-2}	$1130*10^9$ Nm^{-2}
C_{12}	290 "	180 "	282 "
C_{13}	109 "	15 "	— "
C_{33}	46.6 "	36.5 "	$\geqslant$18 "
C_{44}	0.23 "	4.4 "	2.3 "

Table 3   Elasic constants of a graphite crystal

Spence's earlier figures were used by Price and Goggin and Reynolds to calculate the elastic constants of various types of pyrolytic graphite . Spence later revised his results and Brydges et al and Ruland used the new figures in their calculation. If it is assumed that the values of the elastic compliances of a single graphite crystal derived by Spence and Bowman and Krumhansle are of the correct order of magnitude, then the majority of the experimental work carried out to date on experimental/ theoretical comparisons of carbon fibre elastic constants suggest that a uniform stress model gives the better . description of the longitudinal elastic properties of a carbon fibre. The exception to this observation is the work of Goggin and Reynolds on Pile Grade A reactor graphite, where the experimental values lay outside the theoretical limits. However this type of graphite is far removed from the aligned structures encountered in carbon fibres, and there are many faults in reactor graphites to account for the apparent disagreement. The structure of carbon fibre as pictured by Ruland would tend to suggest comparison with a fibre reinforced composite where the fibres are replaced by the microfibrils. However if the fibrils are assumed to be wrinkled normally, under stress the ribbons will straighten out and not necessarily be equally stressed. If a fibre structure based on the Johnson and Tyson model is assumed there is no continuity of structure and the individual crystallites are not likely to be strained equally. Hence unless there is a structure in carbon fibres which is analogous to the straight,continuous fibres of a unidirectional composite there is no basis for assuming that the fibre behaviour can be predicted using a Voigt model.

In attempting to produce fibres with greater strengths and moduli in the longitudinal direction , little attention has been paid to the properties in other directions. This is partially due to the fact that it is difficult to measure the fibre properties in any direction not parallel to the fibre axis with any accuracy due to the small non-circular cross-section. Some measurements of the torsional modulus of sigle fibres have

-23-

been reported by Hawthorne and Brydges. Hawthorne's results (figure 8) were typical in that the scatter was large, but an overall decrease in the torsional modulus with increasing crystallite orientation was indicated. Brydges et al compared the theoretical and experimental values of torsional modulus for type 1 fibre, and found best agreement with the lower limit.

Experimental Young's Modulus	Experimental Shear (Torsional) Modulus	Reuss shear Modulus	Voigt shear Modulus
385 GPa	24.1 GPa	8.27.GPa	226 GPa

Table 4   Experimental/theoretical shear modulus values

Ruland calculated the value of fibre shear modulus on the basis of uniform stress and strain models using experimental values of q. The results were fairly scattered but Ruland assumed a linear relationship in both cases and showed that the fibre torsional modulus increased with an increase in orientation. No experimental measurements of shear modulus were made but a comparison of Ruland's predicted values of shear modulus based on the constant stress model agrees reasonably well with Brydges' experimental value for type 1 carbon fibre. The shear modulus value of a fibre with a Young's modulus of 385 GPa from Hawthorne's results is about 12 GPa. Unfortunately there has been very little data published on the experimental values of the torional modulus of carbon fibres, but one would expect the torsional modulus of a fibre to decrease as the longitudinal orientation increased, as Hawthorne's results show. Ruland has suggested that the explanation for the increase in shear modulus with orientation predicted from his results may be due to a change in the transmission of stress between individual crystallites.

As far as the author is aware no-one has yet made any direct measurement of the fibre transverse modulus or major Poisson's ratio and little attention has been given to the theoretical values of the same. The small diameter of the fibre makes any experimental work very difficult and the unknown 'cross-links' in the microstructure make any theoretical work open to challenge. The value of the transverse modulus and Poisson's ratio

should lie between the limits set by the Reuss and Voigt models whatever the details of the structure. As it is difficult/impossible to measure the transverse modulus and Poisson's ratio directly, they can be estimated from the properties of a composite, if the relationships between composite and composite component properties are known to be accurate.

The theoretical values of the transverse modulus and Poisson's ratios of a single crystal are given by $1/S_{33}$, S_{12}/S_{11} and S_{13}/S_{33} respectively. using Spence's data the following values are obtained:- transverse modulus =36.5 GPa, major Poisson's ratio=0.163, minor Poisson's ratio=0.012. It should be noted that although the transverse modulus of the graphite crystal is theoretically 36 GPa, it is possible for a graphite fibre to have transverse modulus of less than 36 GPa due to the porosity of the fibre structure. The porosity would similarly affect the Poisson's ratios, tending to increase the major Poisson's ratio and reduce the minor Poisson's ratio.

To sum up, the structure of carbon fibre has been partially described by Ruland and Johnson and Tyson but without sufficent detail to use as a base for theoretical calculations of the fibre properties. Theoretical predictions of the fibre properties based on the elastic properties of a single graphite crystal have produced very wide bounds. Only the longitudinal modulus has been studied experimentally to any extent and comparison with the theoretical values suggests that a uniform stress model gives a closer approximation than a uniform strain model. The shear and transverse moduli and the Poisson's ratio are probably affected to a far greater extent than the longitudinal modulus by cross-links in the fibre structure and may be difficult to relate to the orientation alone.

1.5. Glass fibres

In 1924 Griffith (37) first demonstrated that the strength of glass in the form of a very thin fibre could exceed the strength of bulk glass by a factor of up to 20.

The theoretical strength of glass is 7.57 GPa when calculated as 1/10 of the modulus, but the strength of bulk glass is about 0.172 GPa due to the formation of microcracks. (37)

The strength of freshly drawn glass fibre (virgin fibre) can be reduced by a factor of 2 by mechanical handling and exposure to the environment. This is due to defects or damage in the surface of the glass in the form of cracks or etch pits. However the elastic properties of the fibres are similar to those of the bulk glass and are not affected by mechanical handling or the environment to any degree.

There are many formulations of glass giving some variation in properties, but E (electrical) glass originally developed for electrical insulation purposes is the type of glass most commonly used for reinforcement purposes. Other glasses used for reinforcement are A (alkali) glass and S (high strength) glass. The composition of E glass varies slightly but is within the following limits.(39)

Silicon dioxide	52-56%	by weight
Aluminium oxide	12-16%	"
Calcium oxide	16-25%	"
Magnesium oxide	0-6%	"
Boron oxide	8-13%	"
Sodium and potassium oxide	0-3%	"
Ferric oxide	0.05-0.4%	"
Titanium oxide	0-0.4%	"
Iron	0-0.5%	"

Glass fibres are produced by re-melting glass 'marbles' in a temperature controlled bushing and drawing the glass through orifices of 1-3mm diameter at a high rate, causing the fibre diameter to be reduced to

about 12μm. The drawn fibres are coated with a size to prevent inter-fibre abrasion and wound into a cheese.This method of production results in an extremely fast cooling rate of the glass.(Typically 1373 K° to room temperature in 0.1 second.)
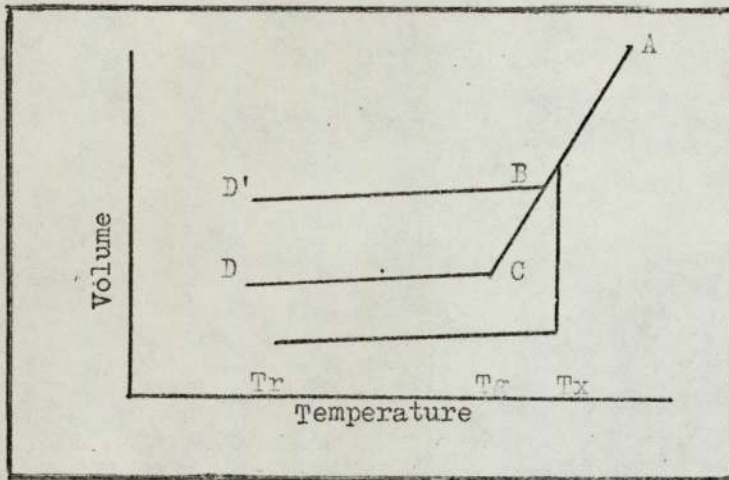
Figure 23 Cooling curve for glass fibre

The normal cooling curve for bulk glass is ABCD (figure 23), but because of the rapid cooling, the fibre cooling curve is modified to ABD'. Hence although chemically the bulk glass and virgin fibre are of the same composition, physically they have different structures. Typical physical differences of bulk and fibrous glass are shown in table 5.

Property	Units	Fibre	Bulk
Density	kgm^{-3}	2540±30	2580±30
Strength (virgin) @ 293 K°	GPa	3.64	0.172
Young's modulus	GPa	75.8	84.5
Torsional modulus	GPa	32.0	35.2
Refractive index	–	1.548	1.552
Thermal conductivity	$Wm^{-1}K^{-1}$	1.04	1.11
Thermal coefficient of expansion	K^{-1}	$4.9*10^{-6}$	$5.05*10^{-6}$

Table 5 Glass bulk and fibre properties.

The important features of the retention of the 'open' structure in the fibre resulting from the rapid cooling is a decrease in density, modulus, refractive index, specific heat and thermal conductivity. The

structure differs from the equilibrium structure of bulk glass both in interatomic spacing (lower density) and in atomic arrangement (stabilized expanded structure). However by reheating the fibre above about 900 K for 1 hour (less at a higher temperature) the structure reverts to normal— this process being referred to as thermal compaction.

Otto (40) measured the fractional change in fibre length with thermal compaction and found it to be approximately $\frac{1}{3}$ of the change in density and hence concluded that the thermal compaction effect is isotropic.

Griffith (37) found that the fibre strength increased with decreasing diameter of fibre and proposed that at the surface of the fibre the most stable orientation of the molecules is that in which their maxima of molecular attraction lie along the surface. This would lead to a similar effect in the next molecular layer but the effect decreasing with distance. This tempered layer hypothesis would give the fibre anisotropic properties.

Bartenev and Izmailova (41) worked with specially made alumino-borosilicate glass fibres and found that the strength/diameter relationship was only very slight for virgin fibres but more pronounced on industrial grade fibres. (Figure 24) On testing numerous fibres they produced the graph shown in figure 25. The explanation of the results incorporates the concept of a fibre with an orientated outer layer and an 'inner core'. Associated with these three 'components' are three strengths. σ_3 is the strength of the outer layer, σ_2 is the strength of the inner core and σ_1 is the strength of the of the fibre containing macrocracks. By etching the fibres for various times the fibre strength was improved. This was assumed to be due to the removal of an outer damaged layer, which they estimated to be about 100 $\overset{o}{A}$ thick.

Metcalfe and Schmidtz (42) found a strength/length relationship with a sudden decrease in strength at about 100mm. The results were interpreted in terms of 3 types of flaws, A, B, C, but without reference to a quenched surface layer. Type A are severe surface flaws generated during handling and occuring on average every 20mm and controlling fibre strength below

3.3 GPa. Type B are rounded surface flaws (possibly etch pits) about 0.1mm apart and controlling the strength in the range 4.8-3.3 GPa. Type C flaws occur in sections about 10^{-14} to 10^{-3} mm and control strengths above 4.8 GPa. Type C flaws were thought to be due to internal structural defects arising from ionic heterogeneity.

Cameron (43) showed that by refining glass at 1723 K or above, it was possible to obtain fibres with strengths of 3.8 GPa with only a 2% variation. Although some fibres contained long thin bubbles they did not appear to act as stress raisers.

In most investigations of the strength/diameter relationship of fibres, the production of smaller diameter fibres necessitated an increase in the bushing temperature. Otto (44) used a lime alumina borosilicate glass (used for textiles) and varied the fibre diameter by using different sizes of orifice and by varying the winding speed but keeping the bushing temperature constant. The fibres produced did not show any clear relationship between diameter and strength. A further study of strength variation with bushing temperature for constant diameter fibres produced the results shown in figure 26. Thomas (45) carried out a similar investigation and confirmed that no strength/diameter relationship could be detected for fibres with diameters between 5μm to 15μm.

Warren(46) studied the structure of glass using information from the laws of chemistry, X-ray diffraction data, physical properties and by comparison with other glass-like materials. The X-ray diffraction showed the predominant bonding to be tetrahedral in silicate glasses. Secondary structures such as those which change with annealing do not show up in X-ray diffraction. Warren's model of the two dimensional structure of glass is shown in figure 27 and shows no orientation effects. Work on vitreous silicate fibres (Na_2O MgO $3SiO_2$) by Stratton and Hoffman (47) with X-ray diffraction showed only diffuse scattering which was interpreted as evidence of voids.

The small diameter of glass fibres used in composites (12μm) makes it difficult to make any direct measurement of the physical properties

-29-

in any direction other than parallel to the fibre axis or even to measure the diameter accurately. Brannan (48) partially overcame this difficulty in his measurement of the Poisson's ratio of glass fibres by measuring the torsional modulus and flexural modulus. The torsional modulus was measured by use of a torsional pendulum and the flexural modulus by three point bending, on the same sample of fibre. The two moduli are given by the following formulae:-

Torsional modulus, $G = \dfrac{128 \pi L I}{T^2 d^4}$ (1.6)   Flexural modulus, $E = \dfrac{4Fl}{3 \pi d^4 \delta}$ (1.7)

where L=length of fibre   F=applied load

I=moment of inertia   l=span

T=period of oscillation δ=deflection at centre

d=fibre diameter   d=fibre diameter

Brannan argued that for any material to be considered isotropic its Poisson's ratio must lie between 0 and 0.5. If the glass fibre is assumed to be isotropic, the Poisson's ratio, ν, is related to the two moduli by

$$\nu = \frac{E}{2G} - 1 \qquad (1.8)$$

The major source of error in any direct measurement of the two moduli is the measurement of the fibre diameter. Brannan combined equations 1.6 and 1.7 to derive an expression for the Poisson's ratio which did not include the diameter of the fibre. The average value of Poisson's ratio was 0.18 ±0.02. After the fibres had been heat treated at 783 $\overset{o}{K}$ for $2\frac{1}{2}$ hours (sufficient to anneal out any preferred orientation), a drop in strength of about 50% was recorded, but no significant change in Poisson's ratio was detected.

Thomas (45) suggested that surface devitrification could reduce the strength of a glass fibre on heating.

Kroenke (49) calculated the value of Poisson's ratio from a measurement of tensile and torsional moduli and obtained a value of 0.34 ± 0.07, but the calculations called for an accurate measurement of the fibre diameter with a microscope, and thus the accuracy is uncertain.

In 1966 DeWys (50) published the results of an examination of spod-umene fibres,(Li Al Si$_2$O$_6$) with a transmission electron microscope, and claimed that a chain structure up to 1000 $\overset{\circ}{A}$ long exixted. In an attempt to create inorganic fibres with an improved modulus, Kroenke produced spodumene fibres which he subjected to an isotropy test (51,52) based on measuring the tensile and torsional strengths. This test proved negative and X-ray diffraction measurement did not show up any features which could be attributed to fibre anisotropy, although flaws and crystallites were detected.

1.6 Discussion on glass fibres

From the evidence published it is evident that the strength of glass fibre is probably controlled by the surface condition and by production parameters. The existence of a surface layer or aligned arrangement of atoms on or near the surface has not been proved. The lack of any definite structure demonstrated by X-ray diffraction, and the similarity in the modulus of the fibre with that of bulk glass and the value of Poisson's ratio of the fibres would strongly suggest that glass fibres are isotropic. For the purpose of calculating the properties of composites made from glass fibres, it will be assumed that glass fibre is isotropic.

1.7 Boron fibre

Boron fibres are produced by the vapour plating of a tungsten wire 0.5mm in diameter. The finished boron fibres have diameters of about 4mm, strength of 2.75 GPa, tensile modulus of 414 GPa and a torsional modulus of 168 GPa. From the method of manufacturing it is obvious that the fibre is not homogeneous and optical examination of the cross-section reveals growth cones and radial cracks (due to built in stress). Calculation of Poisson's ratio from the tensile and torsional moduli gives a value of 0.23, which is typical for an isotropic solid. X-ray diffraction shows diffuse rings corresponding to d-spacings of 4.4, 2.5 and 1.4 $\overset{\circ}{A}$ which Galasso et al (53) interpreted as an amorphous structure. Otte and Lipsitt (54) examined crushed boron fibre with an electron microscope and found that selected areas showed diffuse rings which could be indexed as face centred cubic. When samples were heated in the electron beam until the diffuse rings disappeared a pattern of spots remained. This could be interpreted in terms of a layer structure with extensive faults in stacking sequence. They concluded that boron fibres exhibited features characteristic of layer type structures, and many of the observed X-ray results could be interpreted as stacking faults. The 'amorphous boron can be regarded as heavily faulted f.c.c. which when heated re-crystallises to rhombohedral form, annealing out faults.

Despite the uncertainty of the boron fibre structure, it is normally assumed to be isotropic when calculating the properties of composite structures made from boron fibres.

1.8 Kevlar fibre PRD49

DuPont have recently marketed a new type of fibre for reinforcement purposes. Full details of the chemical composition and structure of the fibre have not been disclosed by the manufacturer, but it is based on an aromatic polyamide. The properties of the fibre are as follows:-
Tensile modulus 127.5 GPa, tensile strength 2.65 GPa, maximum elongation 2% specific gravity 1.45.

It is not known whether the fibre is isotropic or anisotropic, but the high modulus and strength combined with a relatively low elongation suggest that the fibre has been subject to considerable stretching during processing and probably has a highly aligned structure.

If the fibre proves to be a success it is anticipated that other organic fibres with similar properties will become available in the future. To obtain the high longitudinal properties required it is almost inevitable that highly aligned, highly anisotropic structures of the fibres will be used.

1.9 Whiskers

Whiskers are the next step from orientated fibres towards 'perfect' materials with fully realised strength and modulus. The whiskers are necessarily anisotropic as the are nearly perfect crystals. To calculate the properties of a composite containing aligned whiskers the number of elastic constants of the whiskers that will be required will depend on the symmetry of the whisker structure, but the situation could be more complicated than for carbon fibre.

1.10   Fibre/matrix interface

In the prediction of glass reinforced composite properties from the knowledge of the separate properties of the fibre and matrix it is normally assumed that there is a good bond between the fibre and matrix with no interfacial layer. The production of glass fibre necessitates the use of a size to prevent fibre/fibre abrasion. If the glass is to be used for reinforcement purposes the size is somtimes combined with a coupling agent (compatible size) to improve the bond between the fibre and matrix. Alternatively the size is removed and replaced by a coupling agent. Various compounds are used depending on the matrix and enviromental considerations, but it has been shown that the effectiveness of the coupling agent depends on how the fibres are cleaned and the method of application.[Eakins (55).] The optimum thickness of the coupling agent is 1 or 2 monolayers, although in practice it is found that sufficient coupling agent for several mono-layers gives the highest composite strength due to the uneven coating. The main purpose of the coupling agent is to increase the strength of a composite particularly the wet strength. In the case of composites stressed in a direction normal to the fibres, fibre debonding is one of the principal causes of failure.Hence at low strains the coupling agent and interfacial bond may not affect the composite transverse modulus but at high strains the interfacial bond will play a major role in limiting the maximum transverse strain.

Carbon fibres are sometimes coated with a size or they can be surface treated, usually by a controlled oxidation. This results in a 'roughened' surface which enables the matrix to 'key in' and also possibly form a chemical link which gives a stronger fibre/matrix bond.Published photographs of fractures in composites with and without treated fibres clearly show that there is little fibre pull-out with treated fibres. Even before treatment carbon fibres have a fluted appearance (figure 2) which may help in providing a strong bond. Generally rayon based fibres have coarsor fluting than Pan based fibres, but this is probably dependent on the precursor.

The same argument regarding interfacial bond/composite transverse modulus relationship applies to carbon fibres as much as glass, although generally there is a better bond between carbon and the matrix than glass and the matrix. The surface treatment of carbon fibres increases the inter-laminar shear strength considerably, but as far as the author is aware no data has been published which shows that an improved fibre/matrix bond affects the elastic properties of the composite.

1.11 Isotropic and anisotropic fibres

We have seen that carbon fibre has a highly aligned structure approaching that of graphite which gives it anisotropic properties, although accurate measurement of the transverse properties presents certain physical difficulties. In glass fibres there has been no real evidence of any alignment of the structure so that they may be assumed to be isotropic, although again it is difficult to measure the transverse properties to provide absolute confirmation. An indirect method of assessing the transverse properties of the fibres is from measurement of the mechanical properties of composites made from the fibres. In order to evaluate the fibre properties from the composite properties the relationships linking the two must be understood. Section 2 is a study of the attempts to calculate the elastic properties of a unidirectional fibre reinforced composite from the knowledge of the properties of the composite constituents.

2 THE PROPERTIES OF UNIDIRECTIONAL COMPOSITES

2.1 The relationship between component and composite properties

In order to predict the properties and behaviour of a multilayered structure laminated from single sheets of orthotropic material, it is neccessary to have knowledge of (a) the forces applied to the structure, (b) the constraints on the structure, (c) the geometry of the structure, (d) the properties of the single sheet of orthotropic material. This section is concerned only with (d), the properties of a single sheet of orthotropic material.

The sheets of orthotropic material considered in this study consist of a thin layer of matrix material reinforced with unidirectional continuous fibres. Further details on the theory of unidirectional composites are given in section3, where it is shown that the stiffness of an orthotropic lamina can be characterized by four independent parameters:-

E_{11} The composite modulus parallel to the fibre direction.

E_{22} The composite modulus normal to the fibre direction.

G_{12} The shear modulus in the plane of the lamina.

ν_{12} The Poisson's ratio defined as transverse strain/longitudinal strain
and is also known as the Major Poisson's ratio.

A fifth parameter ν_{21} sometimes referred to as the Minor Poisson's ratio is related to E_{11}, E_{22} and ν_{12} by $\nu_{21} = (\nu_{12} * E_{22})/E_{11}$

In order to derive any relationships between fibre and matrix properties and the properties of the unidirectional reinforced lamina , it is necessary to make certain assumptions and simplifications. They are as follows:-

1) The fibres are linearly elastic and homogeneous.

2) The matrix is linearly elastic and homogeneous.

3) The fibres and matrix are void free.

4) There is complete bonding between fibre and matrix with no transition region at the interface.

5) The lamina is macroscopically homogeneous, linearly elastic and orthotropic.

6) The fibres are regularly spaced, straight and aligned.

7) The lamina is initially in a stress-free condition.

Although these assumptions apparently apply considerable restrictions and are not likely to be all met, deviations from them result in varying degrees of 'inaccuracy' in the predicted results. Some of the more likely sources of error connected with each assumption are listed below.

Assumption	Comment and possible sources of error
1	It is generally accepted that glass, carbon and boron fibres are linearly elastic up to at least half their maximum strain, and usually to fracture at room temperature. At higher temperatures the modulus is reduced in all the fibres but they are still reasonably linearly elastic. At temperatures near the transition point of glass, marked plasticity is observed in glass fibre, but as this sort of temperature would be sufficient to destroy most resin matrices it is only of academic interest.
	Neither carbon or boron fibres are microscopically homogeneous but can be considered as such on a macroscopic scale.
2	The properties of the resin matrix can vary from a soft plasticaly deforming material to a hard elastic material. Most resin matrices are linearly elastic at room temperature up to a limiting strain, but tend to undergo plastic deformation before failure. However the maximum strain reached in a composite can be limited by the fibre and the non-linear elastic or plastic strain level of the matrix may not be reached. Hence whether assumption 2 is justified or not depends on the relative properties of the matrix and fibre, temperature and geometry of the composite.

3 Any voids present in the fibres (as in carbon) are taken into account by the measured value of fibre modulus. For most resin/fibre composites it is possible to make a substantially void free lamina (according to density measurements), although some composites can have long thin voids between fibres. If this is the case there is not only a reduction of cross-sectional area but a stress concentration , and often an unbonded fibre. Hence it is essential to use void-free lamina for experimental comparison with theoretical work.

4 The bond strength in a composite depends on the type of fibre and matrix and fibre surface treatment. In some composites with a thermoplastic matrix the bond is little better than a frictional bond relying on the high shrinkage of the matrix phase change, whereas in a composite made from an epoxy resin with treated carbon fibre the bond strength approaches the tensile strength of the matrix. The use of coupling agents on glass fibres has improved the bond strength of glass fibre composites but their mode of action and the possibility of an interfacial region is uncertain.

5 The degree of homogeneity of a composite is very dependent upon the method of manufacture. For most fibre/resin composites it is possible to produce reasonable homogeneity but 'bunching'of fibres can occur at low fibre volume fractions unless care is taken.If a unidirectional composite made with isotropic or orthotropic fibres is homogeneous, then it will also be orthotropic.

The linearity or otherwise of a composite depends on the fibre and matrix properties and the angle between the fibres and the applied stress. Most composites made with continuous fibres are linearly elastic over at least part

of the stress/strain response when stressed in the fibre direction, but not necessarily at other angles.

6   Most carbon and glass fibre composites have a random array of fibres which become slightly more uniform at higher fibre volume fractions. Boron fibres, being much larger can be arranged in a specified geometric pattern if required.The straightness and alignment of the fibres is again dependent on the method of manufacture and can be controlled for boron fibres but not carbon or glass. If a composite is made from roving there are bound to be some non-straight fibres and misalignment where the fibres cross each other. The degree of both can be controlled to a limited extent by the size of the roving used, the smaller sizes being slightly better.

7   In producing any type of composite the matrix undergoes a phase change from a liquid to a solid with which there is normally an associated shrinkage. In addition to this,if a hot curing resin is involved there is the thermal expansion and contraction of the resin and fibre to be considered. In practice the effect of the shrinkage from both causes is reduced by the fact that until the resin has cured there is no bond between fibre and matrix. Any strain that is 'built in' to the composite due differential thermal expansions is often reduced over a period of time due to stress relaxation in the resin.

Throughout the past ten years of so there has been a continuous output of micromechanical theories for predicting the physical properties of unidirectional fibrous composites. Two major areas of work have been on the strength and stiffness of composites while thermal expansion and conductivity have also attracted some attention. The complexity of the models used and the mathematics involved has tended to increase with time from simple netting theory to complicated statistical relationships. In simplif-

ing the theory it has sometimes been necessary to make assumptions which are not justified in reality ,with the result that many of the predicted results do not agree with experimental ones. To overcome these problems some investigators have introduced 'correction factors' or even imaginary structural features.

Some of the relationships published are reviewed here and experimental evidence quoted where applicable and available.The sources from which the relationships are derived can be broadly classified as follows; netting analysis, mechanics of materials, self consistent models, variational, exact(within the context of classical elasticity), statistical, discrete elements and semi-empirical methods.

2.2 Methods of predicting the properties of a unidirectional composite

Many different approaches have been used in attempts to provide a method of calculating the properties (mechanical, electrical and thermal) of composites made from a variety of materials with varying geometries. In this section, only methods which are related to the calculation of the elastic properties of the composite will be mentioned.

Netting analysis

Methods of predicting composite properties based on netting analysis techniques assume that the fibre and matrix are free to act independently, that is the bond between the fibre and matrix is non-existant. For the longitudinal case (parallel to the fibre) the fibre is assumed to provide the entire composite stiffness ,and in the transverse direction (normal to the fibres) the matrix is assumed to provide the entire composite stiffness. In the early days of glass/polyester composites before the use of coupling agents, this assumption may have been near the truth under some conditions, but generally it cannot be assumed that the fibre and matrix act independently. In the longitudinal case if the fibre is much stiffer than the matrix as is the normal situation, then the majority of the stress is carried by the fibres and the assumption of a good or bad bond makes little difference to the modulus.

Mechanics of materials

The mechanics of materials is the next step from netting analysis and can provide simple relationships for predicting the composite properties which are in reasonable agreement with experimental values. The geometry of the composites is simplified to a specific geometry (square, rectangular or hexagonal arrays of fibres) and the composite stress-strain response expressed in terms of stress-strain response of the constituents. This method provides solutions based on the classical Voigt and Reuss models (see sketch) which are generally known as 'rule of mixture equations'.

<u>Voigt or uniform strain model</u>   <u>Reuss or uniform stress model</u>

(used for longitudinal response)   (used for transverse response)

$$P = \sum_{i=1}^{n} v_i P_i$$
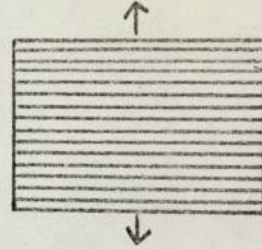
$$\frac{1}{P} = \sum_{i=1}^{n} \frac{v_i}{P_i}$$

Self consistent model

In this approach the phase geometry of the composite is approximated
to a basic element which is subjected to applied stresses. The simplified
strain fields which result from the loading are used to determine the
elastic constants. This method of calculating the elastic constants has
been used by several authors but the basic elements chosen and the
associated assumptions vary from case to case.

Exact methods

This method involves an assumption of a model for the composite in
which the fibres are arranged in an exact periodic array. The periodicity
of the arrangements enables the system to be expressed in terms of a series.
The elastic fields thus derived are then used to obtain expressions for
the elastic constants.

Variational methods

Bounds for the elastic properties of the composite are determined from
consideration of the internal energy. The minimum potential energy provides
the basis for the upper bound and the minimum complementary energy provides
the lower bound. Depending on the property being considered and the
assumptions made, the bounds may be far apart, close, or coincide.

Semi-empirical methods

As a more immediately practically applicable solution, semi-empirical
methods are frequently used to 'predict' composite properties. The main
argument in defence of this approach is that the assumptions and simplif-
ications which are required even in the most rigorous theories are not

necessary with an empirical approach.

Discrete elements

Discrete element methods which are frequently used to study the stress-strain behaviour of large scale structures have been employed on a micro-scale to predict the elastic behaviour of composites. Both regular and random fibre arrays have been assumed in different approaches. In common with exact methods the resulting complexity of the solutions necessitates the use of a digital computer.

Other methods

In an attempt to account more accurately for the true arrangement of fibres rather than assume a definite pattern, statistical methods have been employed. The composite is assumed to be homogeneous but have elastic prop-erties which vary throughout its volume. This is expressed mathematiclly as a series of partial differential equations with variable coefficients. The elastic fields are given in terms of an average value (derived from the rule of mixtures) and a varying term so that the field equations are satisfied by the dervied fluctuations. These equations are then multiplied by the variation in the elastic constants and the statistical average taken, from which the expressions for the composite constants are derived. As it is necessary to include all statistical moments in statistical averaging the process involved is extremely complicated and leads to computational problems.

Methods based on the mechanics of materials

Ekvall (56) used a model with a square array of fibres and assumed a plane stress state to derive equations for E_{11}, E_{22}, G_{12} and ν_{12}. The expression for E_{11} was the rule of mixtures with a modified value of the matrix modulus Em' given by $Em/(1-2\nu_m^2)$ to account for the restraint imposed on the matrix by the fibre. The predicted values of E_{22} and G_{12} were in poor agreement with experimental values, although the modified value of the matrix modulus increased the value of E_{22} to bring it closer to the experimental values.

Greszczuk (57) used the same model as Ekvall and derived similar equations but included the strain concentration effects of voids in the matrix. The theoretical predictions were in reasonable agreement with the experimental results. Later work extended the theory to derive equations for the coefficients of thermal expansion.

Shaffer (58) used a model with a hexagonal array of fibres to derive equations for E_{11} and E_{22} . The equation for E_{11} was the standard law of mixtures, and the equation for E_{22} based on the inverse law of mixtures is only applicable for volume fractions up to 68% when the fibres start to intermesh. The theoretical values of E_{22} were lower than experimental values.

Rabinovich (59) used a model consisting of two plates in parallel, one representing an orthotropic fibre , the other a highly elastic matrix. This resulted in a modified law of mixtures relationship for E_{11}, E_{22} and G_{12}. In later work the model was changed to two plates in series and the new expressions for the elastic constants included the inverse law of mixtures for G_{12}. As neither the first or second equation for G_{12} predicted results which agreed with experimental values, Rabinovich took the geometric average of the two equations as the relationship for calculating G_{12}.

Abolinish (60) assumed a square array of fibres with the extra condition that the Poisson's ratio effect normal to the fibres under longitudinal loading is ignored. Only his equation for E_{22} was unique but

no comparison was made with experimental work, although it compares favourably with the values predicted by the lower limit of Hashin and Rosen's work.(61)

Nosarev (62) modified the normal assumptions that fibres are regularly spaced and aligned to assuming that a) the fibres were curved in one plane only, b) the fibre diameters are small compared with their curvature, c) the character of the misalignment is uniform over the extent of the composite and symmetric with respect to the longitudinal axis. The composite was replaced by a fictitious medium consisting of homogeneous layers containing aligned fibres. The elastic constants of the layered medium were then calculated and taken as the properties of the composite. Reasonable agreement between theoretical and experimental results were claimed.

Self consistent models

Hill (63) used a method to derive expressions for the composite elastic constants based on earlier work by Hershey (64) for the elastic properties of an isotropic aggregate of anisotropic crystals. His model fulfilled the normal assumptions with the exception of number 6, in that the model consisted of a single fibre embedded in a unbounded homogeneous medium which is macroscopically indistinguishable from the composite. A uniform force at infinity induced a uniform strain in the fibre. The elastic constants were calculated from the strain field. The expressions derived by this method gave reasonable values at low fibre volume fractions but became unreliable at higher volume fractions.

Kilchinski(65) modified a model originally used by Fröhlich and Sach (66) for predicting the viscosity of a Newtonian fluid containing a dispersion of equal elastic spheres. Kilchinski's model consisted of three concentric cylinders, the outer one being unbounded and having the properties of the composite. The middle cylinder had the properties of the matrix and the innermost cylinder the properties of the fibre. The cylinder radii were such that the cross-sectional areas of the fibre and matrix cylinders were in the same ratio as the fibre and matrix volume fractions. Homogeneous stresses at infinity produced strains in the cylinders and the

-46-

strain fields were used to determine the elastic constants. Further to this
Kilchinski imposed an additional restriction by assuming that the fibres
were arranged in a regular hexagonal array. The outer radius of the matrix
cylinder was governed by the requirement that the cross-sectional area of
the basic hexagon and matrix cylinder be the same. His equations for E_{11},
ν_{12} and G_{12} were the same as those derived by Hashin and Rosen(61).

Whitney and Riley (67) used a model consisting of a single fibre
surrounded by a matrix cylinder of finite radius. Airy stress functions
were applied to both fibre and matrix with the boundary conditions requir-
ing continuity of displacement and stress at the fibre interface. The
stresses in the cylinders were found for various surface loadings and the
results used in an energy balance. Expressions for E_{11}, E_{22} and ν_{12} were
derived and compared with experimental values for a boron/epoxy composite.
The calculated values for E_{22} were slightly higher than the experimental
values and the shear modulus was lower than the experimental values.
For the case of transversely isotropic fibre Whitney (68) concluded that
the present expressions for E_{11} and ν_{12} (law of mixtures) were not affected
by fibre anisotropy, but expressions for G_{12} and E_{22} required modifications,
in that the values of the fibre longitudinal shear and Young's modulus
should be replaced by the transverse modulus. Whitney (69) adjusted his
own theory to allow for anisotropic fibres and showed that only E_{22} is
affected by the use of transversely isotropic fibres, and the expression
for G_{12} is the same as for isotropic fibres.

Variational methods

Paul (70) derived upper and lower bounds for a macroscopically
isotropic material ($E_{11}=E_{22}=E$) constructed from isotropic linearly elastic
paricles embedded in an isotropic linearly elastic matrix. He demonstrated
that the upper bound for the Young's modulus is given by the law of mixtures
for the case of a transversely isotropic material under plane strain cond-
itions when the Poisson's ratios of the two phases are equal. The lower
bound was given by the inverse law of mixtures and hence for typical fibre/
resin composites the bounds are widely spaced at intermediate values of

fibre volume fraction.

Hashin and Rosen (61) considered models with both hexagonal and random arrays but assumed transverse isotropy in the composite. A hexagonal prism containing one fibre and a cylinder containing many fibres were the two models considered for the two arrays respectively. Using the principle of minimum potential energy and minimum complementary energy, bounds for all five elastic constants were derived. For G_{12} with a random array the bounds coincide but comparison with experimental data showed poor correlation. The work was extended (71) to obtain bounds on the bulk moduli of material with arbitrary phase geometry but no comparison was made with experimental work.

Hill (72) derived upper and lower bounds for transversely isotropic material and showed by rigorous mathematical arguments that the rule of mixtures is the lower bound for E_{11} and that the bounds presented were the best possible that can be obtained without taking the detailed phase geometry into account.

Exact methods

Filshtinskii (73) originally developed a method involving a set of infinite algebraic equations for predicting the moduli of a plate weakened by a doubly periodic array of equal circular holes. He later extended the method to the calculation of elastic moduli of a plate containing a periodic array of circular elastic inclusions.

Van Fo Fy (74) applied Filshtinskii's analysis to the case of an unbounded matrix containing a doubly periodic array of circular fibres and mathematically expressed the problem as a set of infinite series. The resulting elastic boundary value problem was solved using complex variable techniques and the elastic moduli derived by averaging the elastic fields. As the series expressions were difficult to use, Van Fo Fy developed approximate ones which he claims were accurate to within 10% of the exact ones. Equations for predicting the moduli of a matrix reinforced with hollow fibres were also derived.

Chen and Cheng (75) used a basic triangular unit in a hexagonal array

of fibres. Using an infinite series solution of the differential equations they satisfied the boundary conditions at both the fibre/matrix interface and the sides of the triangular unit by a modified least square method. They later modified the work to include the case of transversely isotropic fibres. Comparison with Whitney's work for anisotropic fibres showed that the shear moduli were very similar.

Adams and Doner (76) adopted a doubly periodic array and used a finite difference technique to calculate the shear and transverse moduli of a unidirectional composite. Figures given were not compared with experimental work but demonstrated that a square array should give a higher modulus than a hexagonal array at higher volume fractions.

Sendeckyj developed an exact analytical solution for the longitudinal shear modulus in a fibre reinforced composite which takes account of random spacing, random variations of the fibre radii and variations in shear moduli from fibre to fibre. The infinite series involved are simplified for the case of a regular array with fibres of identical moduli and comparison with the work of Chen(75) showed good agreement.

Semi-empirical methods

Tsai's approach (78) to the prediction of elastic properties of a unidirectional composite could be considered to be semi-empirical because there is no analytical method of allocating values to the factors $K^{\dagger}$ and $C^{\dagger}$ The range of K is given as 0.9 to 1.0 for composites with a reasonable alignment, but values of K can only be determined by extrapolation from experimental values of the modulus. The contiguity factor which has a value of 0 to 1 is involved with ν_{12}, E_{22} and G_{12} and can have a large effect on the predicted values. The value of C will be partially dependent on the fibre volume fraction but no attempt has been made to correlate the two. When C=0 (corresponding to isolated fibres) Tsai's relationships for ν_{12} and G_{12} are reduced to ones very similar to those obtained by Hashin and Rosen.

Bishop(79) developed the netting analysis approach by the addition

† See pages 52 and 53 for explanation

-49-

of imaginary transverse fibre to account for the transverse modulus of a composite. The properties of the imaginary fibres are selected such that the theoretical and experimental results agree. In this way any effect of voids, fibre/matrix bonding etc are taken into account.

Halpin and Tsai (80) showed that Hill's self-consistent model could be reduced to approximate forms incorporating a factor, zeta, which is a 'measure of reinforcement and depends on the boundary conditions'. The value of zeta is determined by comparison of the appropriate equations with numerical micromechanics solutions employing formal elasticity theory or by extrapolation from experimental results. The value of zeta is not necessarily the same for G_{12} and E_{22} for the same set of conditions.

Discrete elements

Foye (81) used a discrete element technique for the prediction of E_{22}, G_{12}, V_{12} and V_{23} of a fibrous composite. The elements employed were triangular in shape and constant strain was assumed. The cross-sectional area of the fibre and the type of array pattern was varied and the results for circular fibres in a square array agree reasonably well with those of Ekvall.

Adams and Tsai introduced the idea of a randomisation factor in an attempt to give a more realistic fibre distribution. In calculating the value of the transverse modulus the cross-section of the composite was divided into a number of elements, a random distribution of which contained fibres and the remainder only matrix material. Several random patterns (from a random number generator) were used, and the transverse modulus calculated by a finite element technique assuming plane strain conditions. Results indicated that using the randomisation technique, a hexagonal array gave results closer to experimental values than a randomised square. This is directly contrary to evidence produced by a number of other non-randomized analyses.

2.4 Discussion on the prediction of unidirectional composite properties

Notation

A list of the expressions developed by various authors for the prediction of the elastic properties of a unidirectional composite is shown in table 6 It is unfortunate that there is no standard notation used in the formulation of equations related to the analyses of composite materials so in many cases the formulae are not reproduced in the original form or notation in which they were published, but they have not been altered mathematically. The four basic elastic properties E_{11}, E_{22}, G_{12} and V_{12} of a thin lamina will be dicussed separately.

The longitudinal Young's modulus E_{11}

The longitudinal modulus is normally measured as a tensile or flexural modulus because it is usually simpler than measurement of the compressive modulus. In a unidirectional composite the longitudinal modulus is dependent on the fibre modulus to a very large degree (see figure 28)and hence whether the compressive and tensile moduli are equal at low strains will depend principally on the fibre properties. At higher strains the possibility of fibre buckling occurring under compressive loads will depend on the composite phase geometry, fibre volume fraction, interfacial bonding and matrix properties.At high strains under tension some of the fibres may break(depending on the relative maximum strains of fibre and matrix) and the composite will no longer consist of continuous fibres, causing the composite modulus to decrease. The theories contained in this thesis were not designed to predict the stress-strain behaviour of a composite near the limit of maximum strain ,although it is assumed that the fibre and matrix are linearly elastic with equal tensile and compressive moduli.

The bounds on E_{11} without taking the fibre and matrix geometry into account are given by Hill as:-

$$E_f V_f + E_m V_m + \frac{4(\nu_f - \nu_m)^2 V_f V_m}{\frac{V_f}{K_m} + \frac{V_m}{K_f} + \frac{1}{G_f}} \geqslant E_{11} \geqslant E_f V_f + E_m V_m + \frac{4(\nu_f - \nu_m)^2 V_f V_m}{\frac{V_f}{K_m} + \frac{V_m}{K_f} + \frac{1}{G_m}}$$

If the matrix and fibre Poisson's ratios are identical the bounds coincide
and the formulation is simplified to the rule of mixtures relationship.
Even if there is a small difference between the two Poisson's ratios the
law of mixtures still gives a very good approximation because the difference
in the Poisson's ratios is raised to the power 2 in the equation.See table 7
and figure 29.The rule of mixtures derived from simple mechanics of
materials is now generally accepted as giving good agreement with experi-
mental data provided that the fibre alignment is good. Ekvall's modification
to the matrix modulus only has any appreciable affect at low fibre volume
fractions or when the fibre and matrix moduli are similar in magnitude.
Tsai's K factor to account for the non-alignment or non-straight fibres
should not be necessary if the assumptions regarding the composite construc-
tion are kept, but in most composites there is a degree of imperfection
and the value of K could be linked to the type of production technique used.
A strictly more correct procedure would be to treat a 'unidirectional'
composite as a three dimensional $\pm \Theta$ composite (see section 3) where Θ is
the average angle between the fibre and composite axis, or to utilize
Cook's work.

Cook (79) calculated the reduction in composite modulus due to
non-perfect alignment of fibres in terms of a factor K and the angular
scatter. K is given by $K=(Vf*Ef)/(Vm*Em)$. For the case of glass or carbon
fibre composites with a fibre volume fraction of 60%, a scatter of 5°in
the direction of the fibre will reduce the longitudinal modulus by about
4%.

For the case of a composite made from transversely isotropic fibres
such as carbon, Rabinovich derived a modified form of the rule of mixtures
equation. Similarly Whitney modified his equations to take account of the
anisotropy of some fibres. However when the relevant data is used with
either of the anisotropic equations it can be seen the assumption of fibre
anisotropy makes very little difference. See tables 25-32.

The major Poisson's ratio ν_{12}

For an orthotropic composite there are three Poisson's ratios (see section 3) whether the composite is made from isotropic or orthotropic fibres. In most cases where a thin fibre reinforced plate is considered the Poisson's ratio concerned with strains normal to the plate surface, ν_{23} or ν_{31}, is disregarded. Of the other two Poisson's ratios ν_{12} is the most commonly quoted and known as the major Poisson's ratio.

Hill calculated the bounds on ν_{12} to be

$$\nu_f V_f + \nu_m V_m + \frac{(\nu_m - \nu_f) V_m V_f \left(\frac{1}{k_f} - \frac{1}{k_m}\right)}{\frac{V_m}{K_f} + \frac{V_f}{K_m} + \frac{1}{G_f}} \geqslant \nu_{12} \geqslant \nu_f V_f + \nu_m V_m + \frac{(\nu_m - \nu_f) V_f V_m \left(\frac{1}{k_f} - \frac{1}{k_m}\right)}{\frac{V_m}{K_f} + \frac{V_f}{K_m} + \frac{1}{G_m}}$$

These bounds are expressed in similar terms to the bounds for the modulus E_{11} but are not as close as the modulus bounds because the term $(\nu_m - \nu_f)$ is not raised to the power 2. The upper bound of Hill's expression was also derived by Kilchinski, Whitney, Hashin and Rosen and Van Fo Fy as the expression for ν_{12}. In the bounds for E_{11} the much simpler law of mixtures was the result of assuming that the Poisson's ratios of the fibre and matrix were the same. In order to reduce the bounds on ν_{12} to a law of mixtures the bulk moduli of the fibre and matrix would have to be equal. As they are functions of the Young's moduli this is not likely to happen in practice. However when suitable figures are substituted into the equations for the bounds ,the bounds are very close and approximate to the law of mixtures.See table 8 and figure 30.

The mechanics of materials approach to the prediction of ν_{12} results in the rule of mixtures, and this is given by Ekvall, Rabinovich,Abolinsh and Halpin and Tsai despite different initial assumptions. Tsai's expression for ν_{12} is made up of two parts, one part assuming that the fibres are in contact with each other (contiguous case)and the other part assuming that the fibres are isolated. The real composite will lie somewhere between the two cases and the coefficient of proportionality C is referred to as the contiguity factor.When C=0 Tsai's expression is very similar to Hill's upper bound, although the definition of K in terms of other

elastic constants is different. Hill defines K as the bulk modulus and is given by $K=E/(2(1-\gamma-2\gamma^L))$ whereas Tsai does not call K the bulk modulus and defines it as $K=E/(2(1-\gamma))$. The two values of K do not vary much with the result that γ_{12} is similar for the two cases.

Whitney's equation for the Poisson's ratio of a composite made with transversely isotropic fibre is similar to his equation for isotropic fibres, and the difference in γ_{12} for the isotropic and anisotropic case is small.

The transverse Young's modulus E_{22}

The transverse modulus of a composite is defined as the transverse stress divided by the transverse strain. The transverse strain is dependent on the fibre array and hence in any calculation of E_{22} the fibre array must be specified. The normal 'array' in a real composite is random unless specially made, but tends towards a hexagonal array at very high fibre volume fractions. In many of the theories published for the prediction of E_{22} both square and hexagonal arrays have been assumed in turn and it is usually found that the square array gives better agreement with experimental results. The exception to this is Tsai's randomisation technique. However the array generated by this method is not genuinely random and the procedure is semi-empirical in nature.

Hashin and Rosen expressed E_{22} in terms of K_{23} and G_{23}, the bulk and shear moduli respectively, governing plane strain deformation in the 2-3 plane. Bounds were established for hexagonal fibre arrays but for a random array the bounds on K_{23} coincide and K_{23} is given by:—

$$K_{23} = \frac{Km*Kf+Gm(Vm*Km+Vf*Kf)}{Vm*Kf+Vf*Km+Gm}$$

The bounds on G_{23} require the solution of a system of eight simultaneous equations representing the boundary conditions. In a later publication Rosen found that the upper bound of G_{23} provided reasonable agreement with experimental results and a simplified expression for G_{23} was given.

$$G_{23} = \frac{G_m\left[(\alpha + \beta_m V_f)(1 + \rho V_f^3) - 3V_f V_m^2 \beta_m^2\right]}{(\alpha - V_f)(1 + \rho V_f^3) - 3V_f V_m^2 \beta_m^2}$$

where $\quad \alpha = \dfrac{\gamma + \beta_m}{\gamma - 1} \qquad \beta = \dfrac{1}{3 - 4\gamma} \qquad \rho = \dfrac{\beta_m - \gamma \beta_f}{1 + \gamma \beta_f} \qquad \gamma = \dfrac{G_f}{G_m}$

Whitney and Riley found E_{22} in terms of K_{23} and ν_{23} but when re-arranged is the same expression as that of Hashin and Rosen. However in place of the complicated relationship for G_{23}, Whitney and Riley assumed $\nu_{23} = \nu_f V_f + \nu_m V_m$ In a later publication Whitney derived the same relationship for a composite with orthotropic fibres. When Whitney and Riley's isotropic fibre expression was compared with experimental work the values predicted were higher than the experimental ones for a boron composite, and Hashin and Rosen's predictions were too low.

The mechanics of materials approach has produced a number of variations in expressions for calculating the value of E_{22}. The simplest expression, the inverse law of mixtures, was given as a first attempt by Schaffer who later modified it to suit an assumed hexagonal array with a maximum fibre volume fraction of 68 %. (The fibres in an assumed hexagonal array start to intermesh at a fibre volume fraction of 68 %). Most of the expressions based on the inverse law of mixtures tend to produce values of E_{22} which are lower than the experimental values, but the modified versions of Rabinovich and Ekvall give values that are closer to the experimental ones.

Tsai's contiguity factor C can change the value of E_{22} by a factor of up to 2, so it is difficult to make any comparison with other predictions or experimental data without first deciding upon a value for C. Similarly the equation of Hashin and Rosen incorporates a reinforcement factor, zeta. It has been suggested that zeta=2 gives reasonable agreement between the predicted and experimental values so this value is used in table 9. Also see figure 33.

Longitudinal shear modulus G_{12}

For a transversely isotropic or orthotropic fibre reinforced composite there are two shear moduli, the longitudinal shear modulus G_{12} or G_{13} and the transverse shear modulus G_{23} or G_{32}. In the case of thin

plates G_{23} is not considered to be of much importance from an engineering point of view and few attempts have been made to derive expressions for G_{23}.

Hashin and Rosen established bounds for both G_{12} and G_{23} for hexagonal arrays and found that for a random array the bounds for G_{12} coincide but not for G_{23}. The same expression for G_{12} was also derived by Abolinish, Kilchinski, Van Fo, Fy and Whitney. Tsai's expression for G_{12} again incorporates a contiguity factor C, which when zero makes Tsai's expression the same as that of Hashin and Rosen. Similarly in the Halpin-Tsai expression for G_{12} substitution of zeta=1 gives an expression identical with that of Hashin and Rosen. The Hashin and Rosen expression generates values that are lower than the experimental ones, particularly at higher volume fractions. As an improvement to the Halpin-Tsai expression Hewitt and de Malherbe (84) suggested that a completely empirical value of $1+40Vf^{10}$ for zeta gives better agreement between theory and experiment. See table 10 and figure 32.

The final expression for G_{12} presented by Rabinovich based on the geometric mean of his two previous expressions could be considered to be almost empirical ,but gives better agreement with experimental results.

The modified equations of Whitney and Rabinovich for predicting the properties of composites made from orthotropic fibres are shown plotted in figures 35-38. Only the transverse modulus and the shear modulus are affected by the assumption of anisotropic fibres. The equations give similar predictions for anisotropic fibres, but Rabinovich's figures are very much higher when the expressions are used for isotropic fibres.

2.5 Theoretical values of composite elastic properties

Table 6 contains all the relationships used in generating the data shown in tables 7-10 and in figures 29-32. To generate the data, constituent properties representing those used in an average glass fibre/epoxy resin composite were employed. They are as follows: Fibre modulus=75.8 GPa, fibre Poisson's ratio= 0.21, matrix modulus= 3.32 GPa and matrix Poisson's ratio=0.37. The fibre and matrix were assumed to be isotropic, and it is assumed that $G=E/2(1+\nu)$. In addition to plotting the normal property/ fibre volume fraction relationships, the effect of varying the constituent properties is shown in tables 11-24 and figures 39-49 . The composite properties displayed are based on an assumed fibre volume fraction of 50% with a void content of zero. The constituent properties used were those above and the shear moduli were assumed to be a function of the Young's modulus and Poisson's ratio for both the fibre and the matrix.

The comparison of composite properties calculated on the basis of the assumption of fibre isotropy and anisotropy is shown in figures 35-38 . The fibre and matrix properties assumed for the graphs is as follows:- Fibre longitudinal modulus (E_{f1}) =200 GPa, fibre major Poisson's ratio (ν_{f1})=0.35, matrix modulus=3.32 GPa and matrix Poisson's ratio=0.37. Four values were used for the fibre transverse modulus (E_{f2}) and the transverse fibre Poisson's ratio (ν_{f2}) calculated from E_{f1}/E_{f2} =1,10,20,40 and $\nu_{f2}=\dfrac{E_{f2}*\nu_{f1}}{E_{f1}}$.

3 COMPOSITE THEORY

3.1 Notation

The theory of the elastic behaviour of anisotropic materials presented here is a condensed version of the elastic theory which specifically applies to the types of considered in this thesis. Unfortunately there is no universally accepted system of notation and some confusion can result when comparing references. In compiling this section the main sources of reference were Lekhnitskii (85), Calcote(86) and Ashton(87). The notation used does not follow any one author entirely but the system is clearly stated to avoid any confusion.

3.2 The elastic behaviour of anisotropic materials

The relationship between stress and strain for any material which is considered to behave elastically can be expressed using Hooke's law. For anisotropic materials the arithmetic expressions are normally written in matrix form for convenience and Hooke's law is expressed as $\sigma_{ij} = C_{ijkl} \varepsilon_{kl}$ where σ_{ij} are the stress components, ε_{kl} are the strain components C_{ijkl} are the stiffness components. Since stress and strain are second order tensors the stiffness matrix is a fourth order tensor with 81 components. However by consideration of the strain energy it can be shown that a completely anisotropic material with no axes of symmetry has only 21 different elements in the stiffness matrix. Hooke's law may also be written in terms of the strains using the compliance matrix S_{ijkl} where

$$\varepsilon_{ij} = S_{ijkl} \sigma_{kl}$$

In this thesis in order to simplify the mathematical expressions the subscripts will be modified according to the following rules:-

11 becomes 1, 22 becomes 2, 33 becomes 3, 12 becomes 4, 23 becomes 5 and 13 becomes 6.

Hence for the stresses we have:-

$$\left.\begin{array}{l} \sigma_{11} = \sigma_1 \\ \sigma_{22} = \sigma_2 \\ \sigma_{33} = \sigma_3 \end{array}\right\} \text{ Normal stresses} \qquad \left.\begin{array}{l} \sigma_{12} = \sigma_4 = \tau_{12} \\ \sigma_{23} = \sigma_5 = \tau_{23} \\ \sigma_{13} = \sigma_6 = \tau_{13} \end{array}\right\} \text{ Shear stresses}$$

-58-

and for the strains we have:-

$$\left.\begin{array}{l} \varepsilon_{11} = \varepsilon_1 \\ \varepsilon_{22} = \varepsilon_2 \\ \varepsilon_{33} = \varepsilon_3 \end{array}\right\} \text{ Normal strains} \qquad \left.\begin{array}{l} 2\varepsilon_{12} = \varepsilon_4 = \gamma_{12} \\ 2\varepsilon_{23} = \varepsilon_5 = \gamma_{23} \\ 2\varepsilon_{13} = \varepsilon_6 = \gamma_{13} \end{array}\right\} \text{ Shear strains}$$

The factor 2 is introduced for the shear strains because γ_{23}, γ_{13}, γ_{12} are engineering shear strains which have twice the value of tensorial shear strains.

The full stiffness matrix for a completely anisotropic material (in retracted form) is then:-

$$\begin{bmatrix} \sigma_1 \\ \sigma_2 \\ \sigma_3 \\ \tau_{12} \\ \tau_{23} \\ \tau_{13} \end{bmatrix} = \begin{bmatrix} C_{11} & C_{12} & C_{13} & C_{14} & C_{15} & C_{16} \\ C_{12} & C_{22} & C_{23} & C_{24} & C_{25} & C_{26} \\ C_{13} & C_{23} & C_{33} & C_{34} & C_{35} & C_{36} \\ C_{14} & C_{24} & C_{34} & C_{44} & C_{45} & C_{46} \\ C_{15} & C_{25} & C_{35} & C_{45} & C_{55} & C_{56} \\ C_{16} & C_{26} & C_{36} & C_{46} & C_{56} & C_{66} \end{bmatrix} \begin{bmatrix} \varepsilon_1 \\ \varepsilon_2 \\ \varepsilon_3 \\ \gamma_{12} \\ \gamma_{23} \\ \gamma_{13} \end{bmatrix} \qquad 3.1$$

The stiffness matrix is symmetric with 21 different elements.

3.3 Fibre reinforced plastic

A matrix reinforced with equally spaced, continuous, straight fibres has three mutually orthogonal axes of symmetry and is generally referred to as an orthotropic material. The stiffness matrix for such a material is simplified considerably and has only 9 different elements.

$$\begin{bmatrix} \sigma_1 \\ \sigma_2 \\ \sigma_3 \\ \tau_{12} \\ \tau_{23} \\ \tau_{13} \end{bmatrix} = \begin{bmatrix} C_{11} & C_{12} & C_{13} & 0 & 0 & 0 \\ C_{12} & C_{22} & C_{23} & 0 & 0 & 0 \\ C_{13} & C_{23} & C_{33} & 0 & 0 & 0 \\ 0 & 0 & 0 & C_{44} & 0 & 0 \\ 0 & 0 & 0 & 0 & C_{55} & 0 \\ 0 & 0 & 0 & 0 & 0 & C_{66} \end{bmatrix} \begin{bmatrix} \varepsilon_1 \\ \varepsilon_2 \\ \varepsilon_3 \\ \gamma_{12} \\ \gamma_{23} \\ \gamma_{13} \end{bmatrix} \qquad 3.2$$

For the case of a thin plate of fibre reinforced plastic with the fibres in the plane of the plate (and parallel to one edge) the stresses normal to the plate can usually be assumed to be negligible in comparison with the in-plane forces.

Material axes.   Plate axes.
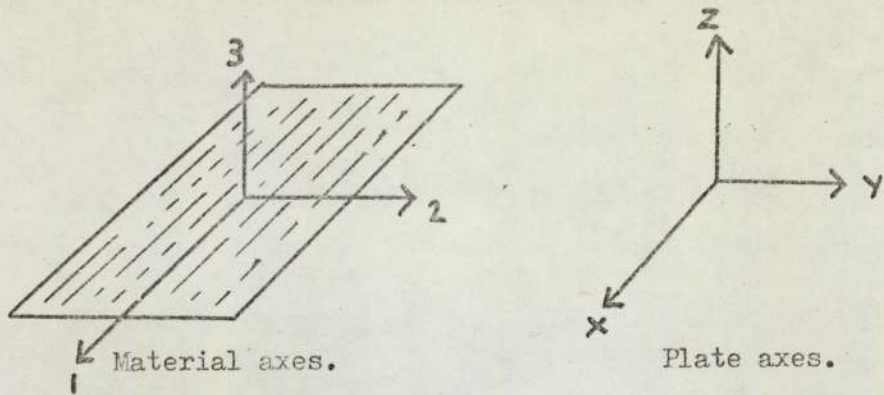
Assume $\sigma_3 = \tau_{23} = \tau_{13} = 0$. From equation 3.2 we see that $\gamma_{23} = \gamma_{13} = 0$ and

$\varepsilon_3 C_{33} = -(\varepsilon_1 C_{13} + \varepsilon_2 C_{23})$ As ε_3 is a function of ε_1 and ε_2 and not independent, it

is not necessary to include it in the matrix equation. The elastic stiffness

equation for a thin orthotropic material with its natural axes 1,2 parallel

to the plate axes X,Y is then given by:-

$$\begin{bmatrix} \sigma_1 \\ \sigma_2 \\ \tau_{12} \end{bmatrix} = \begin{bmatrix} C_{11} & C_{12} & 0 \\ C_{82} & C_{22} & 0 \\ 0 & 0 & C_{66} \end{bmatrix} \begin{bmatrix} \varepsilon_1 \\ \varepsilon_2 \\ \gamma_{12} \end{bmatrix} \qquad 3.3$$

Similarly the equation can be expressed in terms of elastic compliances as:-

$$\begin{bmatrix} \varepsilon_1 \\ \varepsilon_2 \\ \gamma_{12} \end{bmatrix} = \begin{bmatrix} S_{11} & S_{12} & 0 \\ S_{12} & S_{22} & 0 \\ 0 & 0 & S_{66} \end{bmatrix} \begin{bmatrix} \sigma_1 \\ \sigma_2 \\ \tau_{12} \end{bmatrix} \qquad 3.4$$

Thus we see that C_{ij} and S_{ij} are related by the following expressions:-

$$C_{11} = \frac{S_{22}}{S_{11}S_{22}-S_{12}^2} \qquad C_{22} = \frac{S_{11}}{S_{11}S_{22}-S_{12}^2} \qquad C_{12} = \frac{S_{12}}{S_{11}S_{22}-S_{12}^2} \qquad C_{66} = \frac{1}{S_{66}}$$

$$3.5$$

3.4 Relationship between matrix elements and engineering elastic constants

It has been shown that the elastic behaviour of a thin orthotropic

plate can be expressed in terms of four independent constants S_{11}, S_{12}, S_{22} and S_{26}

or C_{11}, C_{12}, C_{22} and C_{66}. The relationship between these elements and the

normal engineering constants can be found by consideration of the definit-

ions of Young's modulus, shear modulus and Poisson's ratio.Mathematically

these definitions may be expressed as:-

Longitudinal Young's modulus $E_{11} = \sigma_1/\varepsilon_1$

Transverse Young's modulus $E_{22} = \sigma_2/\varepsilon_2$

In-plane shear modulus $G_{12} = \tau_{12}/\gamma_{12}$

Major Poisson's ratio $\nu_{12} = -\varepsilon_2/\varepsilon_1$

Minor Poisson's ratio $\nu_{21} = -\varepsilon_1/\varepsilon_2$

Based on these definitions we see that:-

$$C_{11} = \frac{E_{11}}{1 - \nu_{12}\nu_{21}} \qquad C_{22} = \frac{E_{22}}{1 - \nu_{12}\nu_{21}} \qquad C_{12} = \frac{\nu_{21}E_{11}}{1 - \nu_{12}\nu_{21}} \qquad C_{66} = G_{12} \qquad 3.6$$

$$S_{11} = \frac{1}{E_{11}} \qquad S_{22} = \frac{1}{E_{22}} \qquad S_{12} = \frac{-\nu_{12}}{E_{11}} \qquad S_{66} = \frac{1}{G_{12}} \qquad 3.7$$

As $\frac{\nu_{12}}{E_{11}} = \frac{\nu_{21}}{E_{22}}$ there are only four independent engineering constants required

for the characterisation of a thin orthotropic material.

3.4 Thin orthotropic materials

Consider the case of a thin anistropic material where direction 3

is perpendicular to the plane, equation 3.1 is simplified to:-

$$\begin{bmatrix} \sigma_x \\ \sigma_y \\ \tau_{xy} \end{bmatrix} = \begin{bmatrix} C_{11} & C_{12} & C_{16} \\ C_{12} & C_{22} & C_{26} \\ C_{16} & C_{26} & C_{66} \end{bmatrix} \begin{bmatrix} \varepsilon_x \\ \varepsilon_y \\ \gamma_{xy} \end{bmatrix} \qquad\qquad 3.8$$

The subscripts have been changed to x and y to show that the stresses

and strains are not necessarily parallel to any natural axes of the plate

and thus represent the general case. When the elastic properties of a thin

orthotropic material are considered in any direction not parallel to the

natural axes, the orthotropic material behaves with the characteristics

of an anisotropic material. Thus it is possible to derive expressions for

the elastic properties of an orthotropic composite at any angle in terms

of C_{ij} and the angle Θ .

3.5 Elastic properties of a thin orthotropic lamina at an angle Θ to the natural axes

— Natural (material) axes

Y — Lamina axes
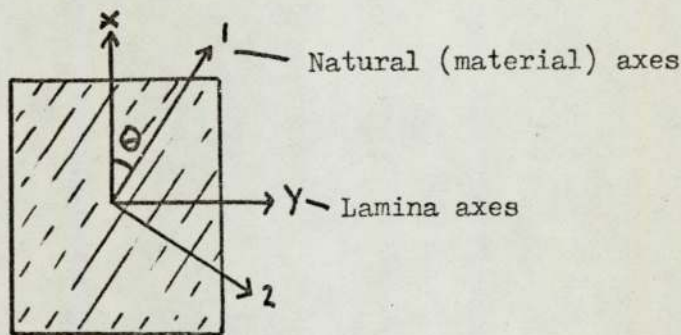
— In order to determine the elastic properties in directions other than

parallel and perpendicular to the natural axes of an orthotropic lamina, it

is necessary to transpose the stresses and strains according to the rules

for second order tensors. i.e. $T_{ij} = a_{ik}a_{jl}T_{kl}$ where a_{ik} and a_{jl} are direction

cosines. The strains are transposed according to:-

$$\begin{bmatrix} \varepsilon_1 \\ \varepsilon_2 \\ \frac{1}{2}\gamma_{12} \end{bmatrix} = [T] \begin{bmatrix} \varepsilon_x \\ \varepsilon_y \\ \frac{1}{2}\gamma_{xy} \end{bmatrix} \qquad\qquad 3.9$$

and the stresses as:-

$$\begin{bmatrix} \sigma_1 \\ \sigma_2 \\ \tau_{12} \end{bmatrix} = [T] \begin{bmatrix} \sigma_x \\ \sigma_y \\ \tau_{xy} \end{bmatrix}$$

3.10

where $[T] = \begin{bmatrix} Cos^2\theta & Sin^2\theta & 2Sin\theta\,Cos\theta \\ Sin^2\theta & Cos^2\theta & -2Sin\theta\,Cos\theta \\ -Sin\theta\,Cos\theta & Sin\theta\,Cos\theta & Cos^2\theta - Sin^2\theta \end{bmatrix}$

3.11

Substitution for the strains ε_1, ε_2 and δ_{12} and the stresses σ_1, σ_2 and τ_{12}

from equations 3.9 and 3.10 into equation 3.3 yields

$$[T]\begin{bmatrix} \sigma_x \\ \sigma_y \\ \tau_{xy} \end{bmatrix} = \begin{bmatrix} C_{11} & C_{12} & 0 \\ C_{12} & C_{22} & 0 \\ 0 & 0 & 2C_{66} \end{bmatrix} [T] \begin{bmatrix} \varepsilon_x \\ \varepsilon_y \\ \frac{1}{2}\delta_{xy} \end{bmatrix}$$

$$\therefore \begin{bmatrix} \sigma_x \\ \sigma_y \\ \tau_{xy} \end{bmatrix} = [T]^{-1}[C][T]\begin{bmatrix} \varepsilon_x \\ \varepsilon_y \\ \frac{1}{2}\delta_{xy} \end{bmatrix}$$

3.12

Hence the matrix represented by $[T]^{-1}[C][T]$ is the required stiffness

matrix relating the stresses and strains of the X,Y coordinates. The elements

of this matrix are often denoted by a dash to signify that they are

functions of C_{ij} and the angle θ. However it is easy to overlook the dash, or

it may be accidentally omitted, so in this thesis $[Q] = [T]^{-1}[C][T]$.

From equations 3.11 and 3.12 we have:-

$Q_{11} = C_{11} Cos^4\theta + 2C_{12} Sin^2\theta\,Cos^2\theta + C_{22} Sin^4\theta + 4C_{66} Sin^2\theta\,Cos^2\theta$

$Q_{12} = C_{11} Sin^2\theta\,Cos^2\theta + C_{12}(Sin^4\theta + Cos^4\theta) + C_{22} Sin^2\theta\,Cos^2\theta - 4C_{66} Sin^2\theta\,Cos^2\theta$

$Q_{16} = C_{11} Sin\theta\,Cos^3\theta + C_{12}(Sin^3\theta\,Cos\theta - Sin\theta\,Cos^3\theta) - C_{22} Sin^3\theta\,Cos\theta + 2C_{66}(Sin^3\theta\,Cos\theta - Sin\theta\,Cos^3\theta)$

$Q_{22} = C_{11} Sin^4\theta + 2C_{12} Sin^2\theta\,Cos^2\theta + C_{22} Cos^4\theta + 4C_{66} Sin^2\theta\,Cos^2\theta$

3.13

$Q_{26} = C_{11} Sin^3\theta\,Cos\theta + C_{12}(Sin\theta\,Cos^3\theta - Sin^3\theta\,Cos\theta) - C_{22} Sin\theta\,Cos^3\theta + 2C_{66}(Sin\theta\,Cos^3\theta - Sin^3\theta\,Cos\theta)$

$Q_{66} = C_{11} Sin^2\theta\,Cos^2\theta - 2C_{12} Sin^2\theta\,Cos^2\theta + C_{22} Sin^2\theta\,Cos^2\theta + C_{66}(Sin^4\theta + Cos^4\theta - 2Sin^2\theta\,Cos^2\theta)$

The relationship between the angular stresses and strains in terms of the

compliances is given by:-

$$\begin{bmatrix} \varepsilon_x \\ \varepsilon_y \\ \frac{1}{2}\delta_{xy} \end{bmatrix} = \begin{bmatrix} R_{11} & R_{12} & \frac{1}{2}R_{16} \\ R_{12} & R_{22} & \frac{1}{2}R_{26} \\ R_{16} & R_{26} & \frac{1}{2}R_{66} \end{bmatrix} \begin{bmatrix} \sigma_x \\ \sigma_y \\ \tau_{xy} \end{bmatrix}$$

3.14

where $[R] = [T]^{-1}[S][T]$

3.15

In a similar manner to that used for the stiffness matrices $[C_{ij}]$ and $[Q_{ij}]$, it can be shown that the following relationships hold:-

$$R_{11} = S_{11}\cos^4\theta + 2S_{12}\sin^2\theta\cos^2\theta + S_{22}\sin^4\theta + S_{66}\sin^2\theta\cos^2\theta$$

$$R_{12} = S_{11}\sin^2\theta\cos^2\theta + S_{12}(\sin^4\theta+\cos^4\theta) + S_{22}\sin^2\theta\cos^2\theta - S_{66}\sin^2\theta\cos^2\theta$$

$$R_{16} = 4S_{11}\sin\theta\cos^3\theta + 4S_{12}(\sin^3\theta\cos\theta - \sin\theta\cos^3\theta) - 4S_{22}\sin^3\theta\cos\theta + 2S_{66}(\sin^3\theta\cos\theta - \sin\theta\cos^3\theta)$$

$$R_{22} = S_{11}\sin^4\theta + 2S_{12}\sin^2\theta\cos^2\theta + S_{22}\cos^4\theta + S_{66}\sin^4\theta\cos^2\theta$$

$$R_{26} = 4S_{11}\sin^3\theta\cos\theta + 4S_{12}(\sin\theta\cos^3\theta - \sin^3\theta\cos\theta) - 4S_{22}\sin\theta\cos^3\theta + 2S_{66}(\sin\theta\cos^3\theta - \sin^3\theta\cos\theta)$$

$$R_{66} = 4S_{11}\sin^2\theta\cos^2\theta - 8S_{12}(\sin^2\theta\cos^2\theta) + 4S_{22}\sin^2\theta\cos^2\theta + S_{44}(\sin^4\theta + \cos^4\theta - 2\sin^2\theta\cos^2\theta)$$

3.16

From equations 3.7 and 3.16 the relationships between the basic engineering constants of the orthotropic material E_{11}, E_{22}, G_{12}, V_{12} and V_{21} and general lamina engineering constants E_x, E_y, G_{xy}, V_{xy} and V_{yx} are as follows:-

$$\frac{1}{E_x} = \frac{\cos^4\theta}{E_{11}} + \left(\frac{1}{G_{12}} - \frac{2V_{12}}{E_{11}}\right)\sin^2\theta\cos^2\theta + \frac{\sin^4\theta}{E_{22}}$$

$$\frac{1}{E_y} = \frac{\sin^4\theta}{E_{11}} + \left(\frac{1}{G_{12}} - \frac{2V_{12}}{E_{11}}\right)\sin^2\theta\cos^2\theta + \frac{\cos^4\theta}{E_{22}}$$

$$\frac{1}{G_{xy}} = \frac{\cos^2 2\theta}{G_{12}} + \left(\frac{1+V_{12}}{E_{11}} + \frac{1+V_{21}}{E_{22}}\right)\sin^2 2\theta$$

$$\frac{V_{xy}}{E_x} = \frac{V_{yx}}{E_y} = \frac{V_{12}}{E_{11}} - \frac{1}{4}\left(\frac{1+V_{12}}{E_{11}} + \frac{1+V_{21}}{E_{22}} - \frac{1}{G_{12}}\right)\sin^2 2\theta$$

3.17

In addition to these relationships two commonly used others are for the 'cross coefficients' m_1 and m_2. These are defined as follows:

$$m_1 = -\frac{E_{11}}{\tau_{12}}\varepsilon_1 \qquad\qquad m_2 = -\frac{E_{11}}{\tau_{12}}\varepsilon_2$$

m_1 and m_2 are related to the basic engineering constants by

$$m_1 = \sin 2\theta\left[V_{12} + \frac{E_{11}}{E_{22}} - \frac{E_{11}}{2G_{12}} - \cos^2\theta\left(1 + 2V_{12} + \frac{E_{11}}{E_{22}} - \frac{E_{11}}{G_{12}}\right)\right]$$

3.18

$$m_2 = \sin\theta\left[V_{12} + \frac{E_{11}}{E_{22}} - \frac{E_{11}}{2G_{12}} - \sin^2\theta\left(1 + 2V_{12} + \frac{E_{11}}{E_{22}} - \frac{E_{11}}{G_{12}}\right)\right]$$

The importance of m_1 and m_2 is that they relate the normal strain ε_1 to the shear stress τ_{12}, or conversely the normal stress σ_1 to the shear strain β_{12}.

Relationship of strain, curvature and dispacement

    Consider a thin layer where the X and Y axes lie in the plane of the plate and the Z axis is normal to the plate.
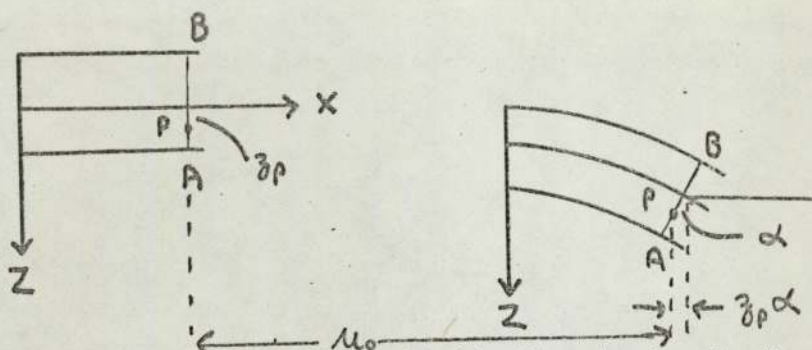
From the classical theory of elasticity the strains in the X,Y and Z directions for small deflections are given by:-

$$\mathcal{E}_x = \frac{\partial u}{\partial x} \qquad \mathcal{E}_y = \frac{\partial v}{\partial y} \qquad \mathcal{E}_z = \frac{\partial w}{\partial z} \qquad\qquad 3.19$$

where u,v and w are the displacements in the X,Y and Z directions respectively. If the plate is subject to bending in the X-Z plane the strain at any point in the material can be expressed in terms of the displacement in the Z direction (w) and the displacement of the midplane ($u_o v_o$). The displacement of the line AB in the X direction is and the line is assumed to remain perpendicular to the midplane (Kirchoff-Love hypothesis, this is equivalent to effectively ignoring the effect of shearing deformations γ_{xz} and γ_{yz}). The displacement of point P an the line AB is u_p and is given by $u_o - z_p \alpha$ where α is the angle between the line AB and its previous direction, and z_p is the distance of point P in the Z direction. For small angles measured in radians we can assume that

$$\alpha = Tan\alpha = Sin\,\alpha \quad , \text{ and hence } \quad \alpha = \frac{\partial w}{\partial x}$$

$$u_p = u_o - z_p\,\alpha = \quad u_o - z_p \frac{\partial w}{\partial x} \qquad\qquad 3.20$$

Similarly it can be shown that $\qquad v_p = v_o - z\frac{\partial w}{\partial y} \qquad\qquad 3.21$

Substituting for u of equation 3.20 and v of equation 3.21 into equation 3.19 we obtain

$$\mathcal{E}_x = \frac{\partial u_o}{\partial x} - z\frac{\partial^2 w}{\partial x^2} \qquad\qquad 3.22$$

$$\mathcal{E}_y = \frac{\partial v_o}{\partial y} - z\frac{\partial^2 w}{\partial y^2} \qquad\qquad 3.23$$

The shear strain in the X-Y plane is defined from the theory of elasticity (for small deflections) as $\qquad \gamma_{xy} = \frac{\partial u}{\partial y} + \frac{\partial v}{\partial x}$

$$\therefore \ \gamma_{xy} = \frac{\partial u_0}{\partial y} + \frac{\partial v_0}{\partial x} - 2z \frac{\partial^2 w}{\partial x \partial y} \qquad 3.24$$

Equations 3.22, 3.23 and 3.24 can be written in matrix form as

$$\begin{bmatrix} \varepsilon_x \\ \varepsilon_y \\ \gamma_{xy} \end{bmatrix} = \begin{bmatrix} \varepsilon_x^0 \\ \varepsilon_y^0 \\ \gamma_{xy}^0 \end{bmatrix} + z \begin{bmatrix} k_x \\ k_y \\ k_{xy} \end{bmatrix} \quad \text{or} \ [\varepsilon] = [\varepsilon^0] + z[k] \qquad 3.25$$

where $\varepsilon_x^0, \varepsilon_y^0, \gamma_{xy}^0$ are the mid-plane strains and k_x, k_y, k_z are the curvatures.

$$\varepsilon_x^0 = \frac{\partial u_0}{\partial x} \qquad \varepsilon_y^0 = \frac{\partial v_0}{\partial y} \qquad \gamma_{xy}^0 = \frac{\partial u_0}{\partial y} + \frac{\partial v_0}{\partial x}$$

$$k_x = -\frac{\partial^2 w}{\partial x^2} \qquad k_y = -\frac{\partial^2 w}{\partial y^2} \qquad k_{xy} = -2\frac{\partial^2 w}{\partial x \partial y}$$

Substituting into equation 3.12 we have for a single layer

$$\begin{bmatrix} \sigma_x \\ \sigma_y \\ \tau_{xy} \end{bmatrix} = \begin{bmatrix} Q_{11} & Q_{12} & Q_{16} \\ Q_{12} & Q_{22} & Q_{26} \\ Q_{16} & Q_{26} & Q_{66} \end{bmatrix} \begin{bmatrix} \varepsilon_x^0 \\ \varepsilon_y^0 \\ \gamma_{xy}^0 \end{bmatrix} + z \begin{bmatrix} Q_{11} & Q_{12} & Q_{16} \\ Q_{12} & Q_{22} & Q_{26} \\ Q_{16} & Q_{26} & Q_{66} \end{bmatrix} \begin{bmatrix} k_x \\ k_y \\ k_{xy} \end{bmatrix} \qquad 3.26$$

where Q_{ij} are the general elastic constants for the single layer.

3.7 Forces acting on an elemental portion of a laminate
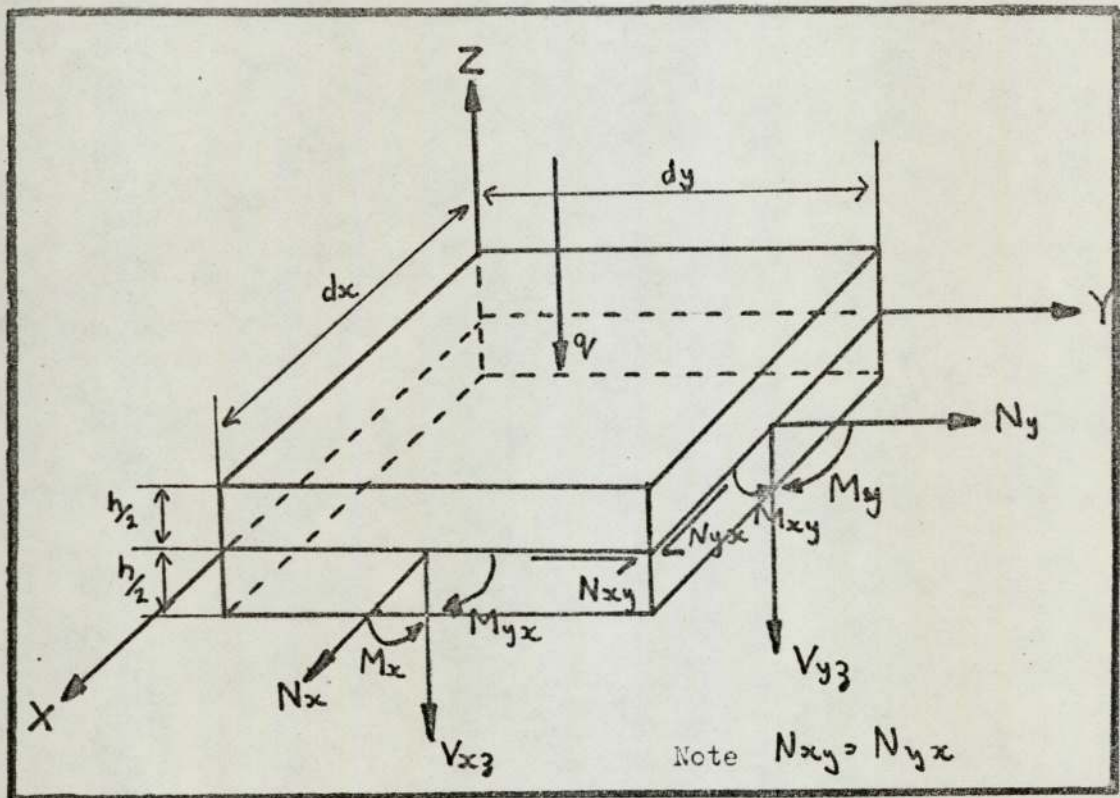
The forces acting on an elemental portion of a lamina may be separated into three main types, Normal forces $\sigma_x, \sigma_y, \sigma_z$ Shear forces $\tau_{xy}, \tau_{yz}, \tau_z$ and Bending couples M_x, M_y, M_{xy}. In addition there may be a pressure acting on the surface of the plate. As the stresses in a multilayered laminate vary from layer to layer, it is convenient to introduce a system of stress resultants and moment resultants which when applied to the geometric mid-plane produce

a system which is statically equivalent to the original. The stress resultants have units of force per length and the moment resultants have units of moment per unit length. The stresses in the Z direction are considered to be negligible compared with the in-plane stresses and are thus disregarded. The remaining resultants are defined as follows:-

$$\underline{\text{Stress resultants}}$$

$$N_x = \int_{-\frac{h}{2}}^{\frac{h}{2}} \sigma_x \, dz \qquad N_y = \int_{-\frac{h}{2}}^{\frac{h}{2}} \sigma_y \, dz$$

$$N_{xy} = \int_{-\frac{h}{2}}^{\frac{h}{2}} \tau_{xy} \, dz \qquad 3.27$$

$$\underline{\text{Moment resultants}}$$

$$M_x = \int_{-\frac{h}{2}}^{\frac{h}{2}} \sigma_x z \, dz \qquad M_y = \int_{-\frac{h}{2}}^{\frac{h}{2}} \sigma_y z \, dz$$

$$M_{xy} = \int_{-\frac{h}{2}}^{\frac{h}{2}} \tau_{xy} z \, dz \qquad 3.28$$

or

$$\begin{bmatrix} N_x \\ N_y \\ N_{xy} \end{bmatrix} = \int_{-\frac{h}{2}}^{\frac{h}{2}} \begin{bmatrix} \sigma_x \\ \sigma_y \\ \tau_{xy} \end{bmatrix} dz \qquad 3.29 \qquad \begin{bmatrix} M_x \\ M_y \\ M_{xy} \end{bmatrix} = \int_{-\frac{h}{2}}^{\frac{h}{2}} \begin{bmatrix} \sigma_x \\ \sigma_y \\ \tau_{xy} \end{bmatrix} z \, dz \qquad 3.30$$

By combining equations 3.26, 3.29 and 3.30 we can express the stress resultants and moment resultants in terms of the mid-plane strains and curvatures.

$$\begin{matrix} N_x \\ N_y \\ N_{xy} \end{matrix} = \int_{-\frac{h}{2}}^{\frac{h}{2}} \left(\begin{bmatrix} Q_{11} & Q_{12} & Q_{16} \\ Q_{12} & Q_{22} & Q_{26} \\ Q_{16} & Q_{26} & Q_{66} \end{bmatrix} \begin{bmatrix} \varepsilon_x^o \\ \varepsilon_y^o \\ \gamma_{xy}^o \end{bmatrix} + \begin{bmatrix} Q_{11} & Q_{12} & Q_{16} \\ Q_{12} & Q_{22} & Q_{26} \\ Q_{16} & Q_{26} & Q_{66} \end{bmatrix} \begin{bmatrix} k_x \\ k_y \\ k_{xy} \end{bmatrix} z \right) dz \qquad 3.31$$

$$\begin{matrix} M_x \\ M_y \\ M_{xy} \end{matrix} = \int_{-\frac{h}{2}}^{\frac{h}{2}} \left(\begin{bmatrix} Q_{11} & Q_{12} & Q_{16} \\ Q_{12} & Q_{22} & Q_{26} \\ Q_{16} & Q_{26} & Q_{66} \end{bmatrix} \begin{bmatrix} \varepsilon_x^o \\ \varepsilon_y^o \\ \gamma_{xy}^o \end{bmatrix} z + \begin{bmatrix} Q_{11} & Q_{12} & Q_{16} \\ Q_{12} & Q_{22} & Q_{26} \\ Q_{16} & Q_{26} & Q_{66} \end{bmatrix} \begin{bmatrix} k_x \\ k_y \\ k_{xy} \end{bmatrix} z^2 \right) dz \qquad 3.32$$

3.8 Multilayered laminate analysis

Mid-plane (reference plane)
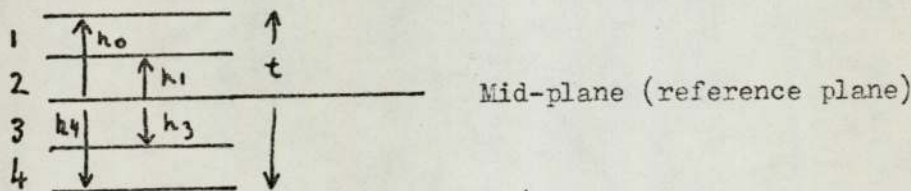
If we have a multilayered plate of n layers of different properties and different thicknesses as the most general case, the stress resultants can be determined by summing over all the individual layers.

$$\begin{bmatrix} N_x \\ N_y \\ N_{xy} \end{bmatrix} = \sum_{k=1}^{n} \int_{h_{k-1}}^{h_k} \begin{bmatrix} \sigma_x \\ \sigma_y \\ \tau_{xy} \end{bmatrix}_k dz$$

where k is the subscript identifying each layer.

Hence

$$\begin{bmatrix} N_x \\ N_y \\ N_{xy} \end{bmatrix} = \sum_{k=1}^{n} \int_{h_{k-1}}^{h_k} \left(\begin{bmatrix} Q_{11} & Q_{12} & Q_{16} \\ Q_{12} & Q_{22} & Q_{26} \\ Q_{16} & Q_{26} & Q_{66} \end{bmatrix} \begin{bmatrix} \varepsilon_x^0 \\ \varepsilon_y^0 \\ \gamma_{xy}^0 \end{bmatrix} dz + \begin{bmatrix} Q_{11} & Q_{12} & Q_{16} \\ Q_{12} & Q_{22} & Q_{26} \\ Q_{16} & Q_{26} & Q_{66} \end{bmatrix} \begin{bmatrix} k_x \\ k_y \\ k_{xy} \end{bmatrix} z \, dz \right) \qquad 3.33$$

If the elastic properties of each layer do not vary throughout its thickness Q_{ij} are not functions of z. As $[\varepsilon^0]$ and $[k]$ refer to the midplane there are also not functions of z or k. Hence equation 3.33 may be written as

$$\begin{bmatrix} N_x \\ N_y \\ N_{xy} \end{bmatrix} = \begin{bmatrix} A_{11} & A_{12} & A_{16} \\ A_{12} & A_{22} & A_{26} \\ A_{16} & A_{26} & A_{66} \end{bmatrix} \begin{bmatrix} \varepsilon_x^0 \\ \varepsilon_y^0 \\ \gamma_{xy}^0 \end{bmatrix} + \begin{bmatrix} B_{11} & B_{12} & B_{16} \\ B_{12} & B_{22} & B_{26} \\ B_{16} & B_{26} & B_{66} \end{bmatrix} \begin{bmatrix} k_x \\ k_y \\ k_{xy} \end{bmatrix} \quad \text{or} \quad [N] = [A][\varepsilon^0] + [B][k] \qquad 3.34$$

where $\qquad\qquad\qquad\qquad\qquad\qquad\qquad\qquad\qquad\qquad\qquad\qquad\qquad 3.35$

$$A_{ij} = \sum_{k=1}^{n} (Q_{ij})_k (h_k - h_{k-1})$$

$$\qquad\qquad\qquad\qquad\qquad\qquad\qquad\qquad\qquad\qquad 3.36$$

$$B_{ij} = \frac{1}{2} \sum_{k=1}^{n} (Q_{ij})_k (h_k^2 - h_{k-1}^2)$$

Equation 3.34 is of great importance in general laminate plate theory as it shows that there is a link between mid-plane stress resultants , normal and shear strains and curvature. Similarly the moment resultants of the multilayered plate can be expressed by summing the product of the stress vector and distance z over the thickness of the plate.

$$\begin{bmatrix} M_x \\ M_y \\ M_{xy} \end{bmatrix} = \sum_{k=1}^{n} \int_{h_{k-1}}^{h_k} \left(\begin{bmatrix} Q_{11} & Q_{12} & Q_{16} \\ Q_{12} & Q_{22} & Q_{26} \\ Q_{16} & Q_{26} & Q_{66} \end{bmatrix} \begin{bmatrix} \varepsilon_x^0 \\ \varepsilon_y^0 \\ \gamma_{xy}^0 \end{bmatrix} z + \begin{bmatrix} Q_{11} & Q_{12} & Q_{16} \\ Q_{12} & Q_{22} & Q_{26} \\ Q_{16} & Q_{26} & Q_{66} \end{bmatrix} \begin{bmatrix} k_x \\ k_y \\ k_{xy} \end{bmatrix} z^2 \right) dz$$

As $Q_{ij}, [\varepsilon^0]$ and $[k]$ are not functions of z we can write

$$\begin{bmatrix} M_x \\ M_y \\ M_{xy} \end{bmatrix} = \begin{bmatrix} B_{11} & B_{12} & B_{16} \\ B_{12} & B_{22} & B_{26} \\ B_{16} & B_{26} & B_{66} \end{bmatrix} \begin{bmatrix} \varepsilon_x^0 \\ \varepsilon_y^0 \\ \gamma_{xy}^0 \end{bmatrix} + \begin{bmatrix} D_{11} & D_{12} & D_{16} \\ D_{12} & D_{22} & D_{26} \\ D_{16} & D_{26} & D_{66} \end{bmatrix} \begin{bmatrix} k_x \\ k_y \\ k_{xy} \end{bmatrix} \qquad 3.37$$

or $\quad [M] = [B][\varepsilon^0] + [D][k]$

where

$$[B] = \frac{1}{2} \sum_{k=1}^{n} (Q_{ij})_k (h_k^2 - h_{k-1}^2)$$

$$[D] = \frac{1}{3} \sum_{k=1}^{n} (Q_{ij})_k (h_k^3 - h_{k-1}^3) \qquad\qquad 3.38$$

Equation 3.37 is also of great importance in understanding the mechanical behaviour of laminated materials ,as it shows that for the general case there is a relationship between the moment resultant and mid-plane strains and curvature. Equations 3.34 and 3.37 can be combined to form the joint laminate constitutive equation.

$$\begin{bmatrix} N \\ \hline M \end{bmatrix} = \begin{bmatrix} A & | & B \\ \hline B & | & D \end{bmatrix} \begin{bmatrix} \varepsilon^0 \\ \hline k \end{bmatrix} \qquad\qquad 3.39$$

For convenience equation 3.39 is sometimes partially inverted to give

$$\begin{bmatrix} \varepsilon^0 \\ \hline M \end{bmatrix} = \begin{bmatrix} A^* & \vdots & B^* \\ \hline C^* & \vdots & D^* \end{bmatrix} \begin{bmatrix} N \\ \hline k \end{bmatrix} \qquad 3.40$$

or completely inverted to give

$$\begin{bmatrix} \varepsilon^0 \\ \hline k \end{bmatrix} = \begin{bmatrix} A' & \vdots & B' \\ \hline C' & \vdots & D' \end{bmatrix} \begin{bmatrix} N \\ \hline M \end{bmatrix} \qquad 3.41$$

where
$$[A'] = [A^*] - [B^*][D^{*-1}][C^*]$$
$$[B'] = [B^*][D^{*-1}]$$
$$[C'] = -[D^{*-1}][C^*] \qquad 3.42$$
$$[D'] = [D^{*-1}]$$

and
$$[A^*] = [A^{-1}]$$
$$[B^*] = -[A^{-1}][B]$$
$$[C^*] = [B][A^{-1}] \qquad 3.43$$
$$[D^*] = [D] - [B][A^{-1}][B]$$

3.9 Bending-extensional coupling

The inter-dependence of the stress resultant with the mid-plane strains and curvatures has been shown by equation 3.34. If we consider the normal stress resultant N_x we have:-

$$N_x = A_{11}\varepsilon_x^0 + A_{12}\varepsilon_y^0 + A_{16}\gamma_{xy}^0 + B_{11}k_x + B_{12}k_y + B_{16}k_{xy}$$

Here the normal stress resultant in the X direction is developed by the mid-plane normal strains in the X and Y directions, ε_x^0 and ε_y^0, the mid-plane shear strain γ_{xy}^0 and the three curvatures k_x, k_y and k_{xy}. In order to eliminate the dependence of the normal stress on the curvatures it is necessary for $B_{11}=B_{12}=B_{16}=0$. B_{ij} are functions of Q_{ij} and the distance z (see equation 3.36) and hence cannot be zero unless z=0. However as B_{ij} are an even function of z it is possible to construct a laminate with identical layers equally spaced either side of the mid-plane so that the laminate B_{ij} terms cancel each other out. If B_{ij} is zero the stress couples will only be dependent on the plate curvatures (equation 3.37). This type of laminate is termed a balanced or symmetric laminate and is one of the most common classes of laminate used. The reason for its common

-68-

usage in fibre reinforced composites is that the resin shrinkage during
cure can give rise to stresses in a laminate which if not balanced out
can cause warping.

To produce a laminate in which the normal stresses are not functions
of the in-plane shear strains it is necessary to reduce A_{16} and A_{26} to
zero. A_{16} and A_{26} are functions of Q_{16} and Q_{26} which are in turn functions
of C_{11}, C_{12}, C_{22} and C_{66} (equation 3.13). Hence for angles of $\Theta = 0^{\circ}$ or 90°
A_{16} and A_{26} are zero. As A_{16} and A_{26} are odd functions of $\text{Sin}\,\Theta$ and $\text{Cos}\,\Theta$
they have equal and opposite values for equal and opposite angles of Θ.
Thus in a laminate composed of equal numbers of laminae with equal and
opposite angles, (and of the same thickness) the A_{16} and A_{26} will cancel
out and the laminate will behave as an orthotropic material.

Although D_{16} and D_{26} are also odd functions of $\text{Sin}\,\Theta$ and $\text{Cos}\,\Theta$ they
do not cancel out in a symmetric laminate because they are also functions
of the thickness to the power three.

3.10 Invariant properties of composite materials

In the early days of fibre reinforced composites, manufacturers of
fibres and composites tended to only quote the longitudinal properties
when comparing their products with others, thus giving a misleading
impression. Tsai and Pagano (87) introduced the concept of the invariant
properties of composite materials to provide a more realistic assessment
of the overall material properties for comparison with others and design
purposes.

The transformation of the stiffness matrix $\left[Q_{ij} \right]$ for an orthogonal
composite is given in terms of U_n by:

$$Q_{11} = U_1 + U_2 \text{Cos}\,2\Theta + U_3 \text{Cos}\,4\Theta$$
$$Q_{12} = U_4 - U_3 \text{Cos}\,4\Theta$$
$$Q_{22} = U_1 - U_2 \text{Cos}\,2\Theta + U_3 \text{Cos}\,4\Theta \qquad\qquad 3.44$$
$$Q_{66} = U_5 - U_3 \text{Cos}\,4\Theta$$
$$Q_{16} = -\tfrac{1}{2} U_2 \text{Sin}\,2\Theta - U_3 \text{Sin}\,4\Theta$$
$$Q_{26} = -\tfrac{1}{2} U_2 \text{Sin}\,2\Theta + U_3 \text{Sin}\,4\Theta$$

where
$$U_1 = \tfrac{1}{8}\left(3C_{11} + 3C_{22} + 2C_{12} + 4C_{66}\right)$$
$$U_2 = \tfrac{1}{2}\left(C_{11} - C_{22}\right)$$
$$U_3 = \tfrac{1}{8}\left(C_{11} + C_{22} - 2C_{12} - 4C_{66}\right)$$
$$U_4 = \tfrac{1}{8}\left(C_{11} + C_{22} + 6C_{12} - 4C_{66}\right)$$
$$U_5 = \tfrac{1}{8}\left(C_{11} + C_{22} - 2C_{12} + 4C_{66}\right)$$

3.45

From the above equations the invariant properties L_1 and L_2 are defined by $L_1 = C_{11} + C_{22} + 2C_{12}$ and $L_2 = C_{66} - C_{12}$. Other invariants can be given in terms of L_1 and L_2 as:-

$$U_1 = \tfrac{1}{8}\left(3L_1 + 4L_2\right)$$
$$U_2 = \tfrac{1}{8}\left(L_1 - 4L_2\right)$$
$$U_5 = \tfrac{1}{8}\left(L_1 + 4L_2\right)$$

3.46

3.11 Equations of equilibrium of a thin plate

The conditions for equilibrium of a thin laminated plate are the same as those for a thin homogeneous plate and can be stated mathematically as follows :-

$$\frac{\partial N_x}{\partial x} + \frac{\partial N_{xy}}{\partial y} = 0 \qquad\qquad 3.47$$

$$\frac{\partial N_y}{\partial y} + \frac{\partial N_{xy}}{\partial x} = 0 \qquad\qquad 3.48$$

$$\frac{\partial^2 M_x}{\partial x^2} + 2\frac{\partial^2 M_{xy}}{\partial x\,\partial y} + \frac{\partial^2 M_y}{\partial y^2} = -q(x,y) \qquad 3.49$$

where N_x, N_y, N_{xy} are the stress resultants, M_x, M_y, M_{xy} are the moment resultants and $q(x,y)$ is the transverse loading.

The first two equations are satisfied by a function U, an Airy stress function, defined by

$$N_x = \frac{\partial^2 U}{\partial y^2} \quad 3.50 \qquad N_y = \frac{\partial^2 U}{\partial x^2} \quad 3.51 \qquad N_{xy} = -\frac{\partial^2 U}{\partial x \partial y} \quad 3.52$$

Substituting equations 3.50-3.52 into equation 3.40 we have :-

$$
\begin{bmatrix} M_x \\ M_y \\ M_{xy} \end{bmatrix}
=
\begin{bmatrix} C_{11}^* & C_{12}^* & C_{16}^* \\ C_{21}^* & C_{22}^* & C_{26}^* \\ C_{61}^* & C_{62}^* & C_{66}^* \end{bmatrix}
\begin{bmatrix} \frac{\partial^2 U}{\partial y^2} \\ \frac{\partial^2 U}{\partial x^2} \\ -\frac{\partial^2 U}{\partial x \partial y} \end{bmatrix}
+
\begin{bmatrix} D_{11}^* & D_{12}^* & D_{16}^* \\ D_{16}^* & D_{22}^* & D_{26}^* \\ D_{16}^* & D_{26}^* & D_{66}^* \end{bmatrix}
\begin{bmatrix} -\frac{\partial^2 w}{\partial x^2} \\ -\frac{\partial^2 w}{\partial y^2} \\ -2\frac{\partial^2 w}{\partial x \partial y} \end{bmatrix}
\qquad 3.53
$$

If these expressions for the moment resultants are now substituted into equation 3.49 we obtain the first of the differential equations governing laminated plates.

$$C_{12}^{*}\frac{\partial^4 U}{\partial x^4} + (2C_{12}^{*}-C_{16}^{*})\frac{\partial^4 U}{\partial x^3 \partial y} + (C_{11}^{*}+C_{22}^{*}-2C_{66}^{*})\frac{\partial^4 u}{\partial x^2 \partial y^2} + (2C_{61}^{*}-C_{26}^{*})\frac{\partial^4 U}{\partial x \partial y^3} + C_{21}^{*}\frac{\partial^4 U}{\partial y^4}$$

$$-D_{11}^{*}\frac{\partial^4 \omega}{\partial x^4} - 4D_{16}\frac{\partial^4 \omega}{\partial x^3 \partial y} - 2(D_{12}^{*}+2D_{66}^{*})\frac{\partial^4 \omega}{\partial x^2 \partial y^2} - 4D_{26}^{*}\frac{\partial^4 \omega}{\partial x \partial y^3} - D_{22}^{*}\frac{\partial^4 \omega}{\partial y^4} = -q(x,y) \tag{3.54}$$

Equation 3.54 is a fourth order partial differential equation in terms of
two unknowns, and thus cannot be solved without a further equation. The
other equation is the compatibility equation for thin plates which is
derived from the consideration of the normal and shear strains. The mid-
plane strains are defined by:

$$\varepsilon_x^{o} = \frac{\partial u^o}{\partial x} \qquad \varepsilon_y^{o} = \frac{\partial v_o}{\partial y} \qquad \gamma_{xy}^{o} = \frac{\partial u_o}{\partial y} + \frac{\partial v_o}{\partial x}$$

and the compatability equation is as follows.

$$\frac{\partial^2 \varepsilon_x^{o}}{\partial y^2} + \frac{\partial^2 \varepsilon_y^{o}}{\partial x^2} + \frac{\partial^2 \delta_{xy}}{\partial x \partial y} = \frac{\partial^3 u_o}{\partial x \partial y^2} + \frac{\partial^3 v_o}{\partial x^2 \partial y} \tag{3.55}$$

Expressing the strains in terms of the Airy stress function U and substitut-
ing into equation 3.40 we have:

$$\begin{bmatrix} \varepsilon_x^{o} \\ \varepsilon_y^{o} \\ \gamma_{xy}^{o} \end{bmatrix} = \begin{bmatrix} A_{11}^{*} & A_{12}^{*} & A_{16}^{*} \\ A_{12}^{*} & A_{22}^{*} & A_{26}^{*} \\ A_{16}^{*} & A_{26}^{*} & A_{66}^{*} \end{bmatrix} \begin{bmatrix} \frac{\partial^2 U}{\partial y^2} \\ \frac{\partial^2 U}{\partial x^2} \\ -\frac{\partial^2 U}{\partial x \partial y} \end{bmatrix} + \begin{bmatrix} B_{11}^{*} & B_{12}^{*} & B_{16}^{*} \\ B_{21}^{*} & B_{22}^{*} & B_{26}^{*} \\ B_{61}^{*} & B_{62}^{*} & B_{66}^{*} \end{bmatrix} \begin{bmatrix} -\frac{\partial^2 \omega}{\partial x^2} \\ -\frac{\partial^2 \omega}{\partial y^2} \\ -2\frac{\partial^2 \omega}{\partial x \partial y} \end{bmatrix} \tag{3.56}$$

Substituting this equation into the compatibility equation we obtain
the second governing differential equation for laminated plates.

$$A_{22}^{*}\frac{\partial^4 U}{\partial x^4} - 2A_{26}^{*}\frac{\partial^4 U}{\partial x^3 \partial y} + (2A_{12}^{*}+A_{66}^{*})\frac{\partial^4 U}{\partial x^2 \partial y^2} - 2A_{16}^{*}\frac{\partial^4 U}{\partial x \partial y^3} + A_{11}^{*}\frac{\partial^4 U}{\partial y^4} - B_{21}^{*}\frac{\partial^4 \omega}{\partial x^4}$$

$$-(2B_{26}^{*}-B_{61}^{*})\frac{\partial^4 \omega}{\partial x^3 \partial y} - (B_{11}^{*}+B_{22}^{*}-2B_{66}^{*})\frac{\partial^4 \omega}{\partial x^2 \partial y^2} - (2B_{16}^{*}-B_{62}^{*})\frac{\partial^4 \omega}{\partial x \partial y^3} - B_{12}^{*}\frac{\partial^4 \omega}{\partial y^4} = 0 \tag{3.57}$$

Theoretically it is now possible to solve the equations for the stress
function U and the deflection w, but in practice only certain special
cases have been solved.

Symmetric laminates which do not exhibit extensional-bending coupling
because $B_{ij}=0$ can be solved for. If $B_{ij}=0$, then $[B]=[C]=0$ and $[D^{*}] = [D]$.
Substitution of this information into equation 3.57 yields :-

$$A_{11}^{*}\frac{\partial^4 U}{\partial y^4} - 2A_{16}^{*}\frac{\partial^4 U}{\partial x \partial y^3} + (2A_{12}^{*}+A_{66}^{*})\frac{\partial^4 U}{\partial x^2 \partial y^2} - 2A_{26}^{*}\frac{\partial^4 U}{\partial x^3 \partial y} + A_{22}^{*}\frac{\partial^4 U}{\partial x^4} = 0 \tag{3.58}$$

which is the same as the equation which governs a homogeneous plate, which

obeys the following constitutive law:

$$\begin{bmatrix} \sigma_x \\ \sigma_y \\ \tau_{xy} \end{bmatrix} = \frac{1}{h} \begin{bmatrix} A_{11} & A_{12} & A_{16} \\ A_{12} & A_{22} & A_{26} \\ A_{16} & A_{26} & A_{66} \end{bmatrix} \begin{bmatrix} \varepsilon_x \\ \varepsilon_y \\ \gamma_{xy} \end{bmatrix} \tag{3.59}$$

Applying the same simplifications regarding symmetrical laminates to equation 3.54 we obtain the differential equation governing the bending behaviour:

$$D_{11}\frac{\partial^4 w}{\partial x^4} + 4D_{16}\frac{\partial^4 w}{\partial x^3 \partial y} + 2(D_{12}+2D_{66})\frac{\partial^4 w}{\partial x^2 \partial y^2} + 4D_{26}\frac{\partial^4 w}{\partial x \partial y^3} + D_{22}\frac{\partial^4 w}{\partial y^4} = q(x,y) \qquad 3.60$$

This equation is also identical to the one governing homogeneous plates, which also obeys the constitutive law following.

$$\begin{bmatrix} \sigma_x \\ \sigma_y \\ \tau_{xy} \end{bmatrix} = \frac{12}{h^3}\begin{bmatrix} D_{11} & D_{12} & D_{16} \\ D_{12} & D_{22} & D_{26} \\ D_{16} & D_{26} & D_{66} \end{bmatrix}\begin{bmatrix} \varepsilon_x \\ \varepsilon_y \\ \gamma_{xy} \end{bmatrix} \qquad 3.61$$

If the laminate is also orthotropic, then $A_{16}= A_{26}= 0$ and the plane stress equation becomes:

$$A_{11}^*\frac{\partial^4 U}{\partial y^4} + (2A_{12}^* + A_{66}^*)\frac{\partial^4 U}{\partial x^2 \partial y^2} + A_{22}^*\frac{\partial^4 U}{\partial x^4} = 0 \qquad 3.62$$

and the bending equation becomes:

$$D_{11}\frac{\partial^4 w}{\partial x^4} + (2D_{12}+D_{66})\frac{\partial^4 w}{\partial x^2 \partial y^2} + D_{22}\frac{\partial^4 w}{\partial y^4} = q(x,y) \qquad 3.63$$

As these equations are essentially similar to those for isotropic material they can be solved by similar techniques.

4 EXPERIMENTAL WORK

4.1 Materials

Four resin systems and two types of fibre were used in the making
of the composites. A brief description will be given of each.

Polyester resin

Crystic D351 polyester resin manufactured by Scott Bader Company Limited
was used for the majority of the work concerned with polyester. The resin
consists of 86% (by weight) of a high molecular weight isophthalic
unsaturated polyester and 14% of di-allyl phthalate monomer. The resin
is the product of a condensation reaction between orthophthalic anhydride
and propylene glycol.

Normally polyester resins use styrene as the cross-linking monomer in
a 2:1 ratio producing a highly volatile resin system with a consistency of
thin syrup. Crystic D351 is solid at room temperature and is therefore
normally sold as a 75% solids solution in acetone. This particular polyester
system was selected because it can be used in a high temperature curing
preimpregnating system, unlike the majority of polyester resins.

The gel time of the resin with 1% benzoyl peroxide as a catalyst was
about 1-2 minutes at $400\,^{\circ}$K, complete curing taking about 1 hour. No propert-
ies of the cured resin were supplied by the manufacturer.

A few test pieces were made using Crystic 272 which is another
isophthalic polyester resin manufactured by Scott Bader. This resin uses
styrene as the monomer and hence has a low viscosity at room temperature
(3.5 poise). Methyl ethyl ketone peroxide was used as the catalyst (2%)
with cobalt napthanate as the accelerator (2%) to provide a room temperature
cure.

The properties claimed by the manufacturer are:- tensile strength
62 MPa, tensile modulus 3.9 GPa, tensile elongation 2.3%, specific gravity 1.21.

Epoxy resins

For initial investigations on this work some composites were made
from Scotchply 1002 prepreg material. Scotchply 1002 is produced by the

Minnesota, Mining and Manufacturing Company Limited and consists of a
sheet of unidirectional E glass fibres impregnated with a hot curing B
staged epoxy resin of high viscosity. The prepreg material contains 36%
resin by weight and is 0.27mm thick. The type of epoxy and curing agent are
unfortunately unknown but the quoted shelf life at room temperature is
6 months. Gel time was about 4 minutes at 430°K, and 2 hours at 440°K were
allowed for curing.

The properties quoted by the manufacturer for a cured composite are
as follows:- tensile strength 1·10 GPa, tensile modulus 39.3 GPa, flexural
strength 1.14 GPa, flexural modulus 36.5 GPa, specific gravity 1.80.
No fibre volume fraction was given.

For most of the work carried out with epoxy resin Shell Epikote DX210
was used. It has an epoxy equivalent of 388 and was used with Shell Epikure
BF_3-400, a boron trifluoride monoethylamine complex. At room temperature
the resin is almost solid (viscosity 19 poise) and is normally sold as
DX 210 B-90 which is an 80% solids solution in methyl ethyl ketone. It was
used to produce a prepreg material in a similar way to Crystic D351 and
was cured at 440°K for 4 hours.

The manufacturers quote the following properties for the cured resin:-
tensile strength 53.2 MPa, elongation 3%, flexural strength 93.8 MPa,
flexural modulus 2.78 GPa, specific gravity 1.21.

Glass fibre

The glass fibre used in this work was E type glass roving manufactured
by Fibreglass Limited and sold under the name Equerove. Fibres coated with
two types of coupling agent were used, one with an epoxy compatible comp-
ound and one with a polyester compatible compound. The actual coupling
agents are not disclosed by the manufacturer, but are thought to be silane
based. Equerove roving is made commercially for fibre winding processes
and is untwisted and equi-tensioned so that there is no catenary between
the strands which make up the roving. The fibre is supplied in the form
of a cheese on a tubular former. The properties claimed by the manufacturer

are as follows:-tensile strength 3.7GPa(newly drawn),tensile modulus 76 GPa,
specific gravity 2.56, fibre diameter 12 m.

The carbon fibre used was manufactured by Courtaulds Limited and sold
under the name Grafil. Most of the carbon fibre work was carried out with
Grafil A, but a few test pieces were also made with Grafil HM. Both types
of fibre are manufactured from Courtaulds polyacrylonitrile fibre (Courtelle)
and were supplied in a non surface treated form. Some of the Grafil A type
fibres were made into a unidirectional prepreg sheet by the manufacturers
using Shell Epikote DX210/Shell Epikure BF_3400 resin system.

The properties claimed for the fibres are as follows:-

	Grafil A	Grafil HM
Minimum U.T.S.	2.3 GPa	2.10 GPa
Mean U.T.S.	2.64 GPa	2.35 GPa
Tensile modulus	175-200 GPa	310-345 GPa
Specific gravity	1.80	1.87

4.2 Preparation of test pieces

Resin samples

The high viscosity of resin systems used in the production of prepreg sheet makes it difficult to cast a satisfactory sheet of resin without trapping any bubbles of air or solvent. Epikote DX210 is sufficiently viscous at room temperature to prevent pouring from a container. At 393°K the resin is much less viscous and can be poured reasonably easily . To cast a sheet of resin, the mould (consisting of 2 glass plates separated by metal spacers) and a beaker of resin were pre-heated to 393°K in an air circulating oven. The powdered curing agent was added and stirred rapidly to dissolve and disperse it uniformly. The resin was then poured slowly into the mould allowing most of the entrapped air to escape, before curing the resin for 4 hours.

The main problem associated with the hot casting of resin is the short gel time. At 400°K the mixed DX210 resin has a gel time of about 5 minutes, which is just sufficient to mix the resin, pour it into the mould and allow any entrapped air bubbles to rise to the surface. As the sheets were cast vertically the top surface was easily removed when cured.

Crystic D351 is completely unpourable at room temperature and it is necessary to heat it to about 393°K before it is possible to pour it. Unfortunately after adding the catalyst (benzoyl peroxide and di-allyl phthalate 1:1) the gel time is only about 2 minutes at 393°K, and insufficient time is available to remove the entrapped air. To overcome this problem a different approach was used.

The resin and di-allyl phthalate were mixed together with an equal weight of acetone at 323°K and allowed to cool before adding the catalyst. The acetone was removed after mixing was complete by allowing most of the acetone to evaporate and removing the remainder by use of a vacuum oven at 323°K and 60mm of mercury. When this was completed the resin was cooled to 258°K in a deep freeze and ground into a powder and stored in a desiccator to prevent condensation. When at room temperature the powdered resin was slowly shaken into the preheated mould to allow the powder to melt without

enclosing any air.None of the D351 resin samples made were entirely void-free but with the benefit of experience the latter ones had a reduced porosity.

The Scotchply prepreg material used at the begining of the experimental work to develop manufacturing techniques was made with an unidentified epoxy resin. All attempts to (a) identify the resin system,(b)obtain a sample of resin from the manufacturers, or (c) obtain data on the resin properties, were not successful. However by moulding a large composite plate it was possible to collect sufficent resin squeezed out of the mould to produce a sample about 130x20x5mm. Although this method of casting a resin sample is far from perfect it was the only course open.

Crystic 272 presented no problems in casting a sheet sample as it is a low viscosity low temperature curing system.

Manufacture of preimpregnated fibre sheet.(prepreg)

The number of techniques available to make multiangled,many layered composites are few in number. Of the most common two, fibre winding and prepregging the latter is by far the simpler as regards experimental apparatus. It was decided at an early stage to use prepreg materials because of the limited equipment available,the freedom of design and the high quality of composites possible.Some early investigations with Scotchply prepreg were carried out to study mould design and general experimental technique. It became apparent that the fibre volume fraction of composites made from Scotchply were very limited by the fixed resin content and the high viscosity of the resin. It was possible to make a low fibre volume fraction sample by adding extra resin from other prepreg ,but the results were not really satisfactory. To overcome this problem and to have complete freedom in choice of materials a machine was constructed to make prepreg sheet in small quantities. See figures 50 & 51.

The fibre was pulled through a bath of resin diluted with acetone or methyl ethyl ketone and wound on to a drum covered with Tygadure (PTFE coated glass cloth from Fothergill and Harvey).Excess resin was removed by the spring loaded rollers immediately after the resin bath. An adjustable automatic tensioning device was incorporated to keep the fibre tension

-77-

constant so that the resin pick-up did not vary and also to prevent the uncontrolled unwinding of the glass fibre spool should the roving break or get jammed. The resin bath was easily accessible for changing the resin and cleaning the machine. Immediately before being wound on to the drum the impregnated fibres were spread horizontally to a width of 2-3mm by a PTFE roller to reduce the thickness of the prepreg sheet. The drum was electrically driven and was geared to the traverse mechanism so that there was a constant ratio between the two drives to keep the thickness of the prepreg constant. A complete traverse of the drum took about 10-15 minutes and produced a sheet of prepreg about 1 metre square. After 3 hours most of the solvent in the resin had evaporated and the prepreg was cut normal to the fibre direction and removed from the drum. The prepreg initially had some curvature, but if left for a day tended to flatten under its own weight without buckling the fibres.

By varying the dilution of the resin with solvent and the pressure of the resin wipers, it was possible to produce prepreg sheet with resin volume fractions from 85 to 10%, although the system had an optimum performance with a resin volume fraction of 30 to 50%.

The prepreg made with Crystic D 351 and acetone was less tacky at room temperature than those with Epikote DX210 and methyl ethyl ketone. Before cutting up the prepreg sheets they were heated in an air circulating oven at 353°K for ten minutes to remove any residual solvent and B stage the resin.

Early attempts at making prepreg sheet from Grafil A fibre failed due to the difficulty in unwinding the fibre from the cardboard tubes on which it was supplied without snagging or breaking. However with the newer type of packing consisting of loose coils of fibre inside a plastic drum, the machine produced satisfactory prepreg. A typical glass fibre prepreg and composite are shown in figures 52 and 53 respectively.

Moulding the composites

Two moulds of similar design but different size were used for making

samples.(figure 54). Both moulds used metal spacers to control the thickness of the samples, and both could be used as wet lay up moulds if the end pieces were removed.

For making samples from prepreg, the required number of sheets of prepreg (of known fibre volume fraction) were stacked in the mould and consolidated by hand pressure before being removed as a prepreg block. Both halves of the mould were sprayed with release agent and preheated to the required temperature on the platte ns of the hot press (40tonnes Daniels) before the prepreg block was placed in the mould. The resin was left to gel for the requisite time during which the pressure was applied gently and released a few times before finally closing the mould. The final pressure was not critical as the mould had fixed stops but was about 8000 Pa. The composite was cured for 1 hour in the press before it was removed (still in the mould) and post-cured in a preheated oven. The composite was removed from the mould when cool.

A few samples were made by the wet lay-up of fibres wrapped round an open frame. The frame was made in two halves held together by bolts. After the fibre had been wound round the frame it was possible to increase the tension in the fibres by forcing the two halves apart by use of the bolts. The frame was laid round the mould so that the fibres ran through the mould. Crystic 272 + catalyst and accelerator was poured on to the fibres and spread manually before closing the lid and applying pressure in the cold press to close the lid to the stops. The samples made by the wet lay-up were generally inferior to the prepreg made samples due to inhomogeneity of the fibre distribution.

To produce samples with varying degrees of fibre/matrix bond strength, some glass fibre samples were made using the fibre with a polyester compatible size with Epikote DX210 and fibres with the epoxy compatible size were used with Crystic D351. Some samples were also made with glass fibre which had been partially coated with silicone grease which reduced the transverse strength considerably.

Cutting and machining of the composite samples

Unidirectional composite materials can be fairly easily damaged by unsuitable machining techniqes so considerable care was taken in the cutting of the samples. A circular saw fitted with a diamond impregnated blade was used for cutting up the moulded plates.As no water cooling/lubricant was used the samples were cut slowly to avoid overheating, especially at 90° to the fibre direction. The specimens used for tensile and bending tests were ground on a surface grinder to ensure that the edges were accurately parallel.After grinding,the samples were washed and stored in a desiccator As a check on the effect of the water/oil emulsion used in grinding on the composites,one composite plate was cut into 8 strips, 4 of which were wet ground and the other 4 sand papered dry. On testing the samples no significant difference in the moduli (transverse) or strength was detected so all other samples were wet ground.

Mechanical testing of fibres, matrices and composites.

It has been proposed in section 2 that the elastic properties of a unidirectional fibre reinforced composite are functions of the fibre and matrix moduli and Poisson's ratio and of relative proportions and geometry The methods available to measure the required elastic properties are numerous but tend to give slightly different values under diferent conditions for properties which are normally assumed to be constant.For example, the Young's modulus of a matrix or fibre may not be the same under tensile and compressive loading.This is due to inherent properties of the material, inaccuracies and assumptions in the test procedures,and corrections which may be applied to alleviate some of them.An additional large source of error concerned with the testing of composite materials is that of structural variations. In the simplest case of a'unidirectionally'fibre reinforced composite, it is possible to have a fixed ratio of fibre and matrix but to change the composite properties by the internal arrangement of the fibres. The more complicated composites are open to numerous variations and unless the description of the composite (and test)

is complete confusion can arise. One of the most common cases is that of an "angle ply composite" where it is not made clear whether the stacking sequence is symmetric or anti-symmetric about the centre plane.

Thus the need for test procedures which measure the property under specific conditions can be fully appreciated. As this thesis is concerned with the prediction of composite properties from the properties of the components, the tests used have been chosen because (a), they measure the required property, and (b) because the component properties are measured under the same or similar conditions that they experience in a composite. The compressive properties of composites are not easy to carry out accurately without special apparatus so they have not been measured. However in addition to the tests necessary to obtain the required data some other tests were carried out for the purpose of comparing experimental techniques.

Selection of tests

Ideally for the fibres we would like to know the transverse and longitudinal moduli, two shear moduli and three Poisson's ratios. In practice we can only measure the longitudinal properties. There is little choice in the broad manner in which this is done, although there are differences in the way the same objective may be achieved. Single and multiple fibre tensile tests, and single fibre torsional pendulum and three point bend tests were used.

For the resins and composites it was decided to use simple tensile tests to establish the Young's moduli and Poisson's ratio and to also carry out three and four point flexural tests. The measurement of the shear modulus was the most difficult and several methods were considered. The methods considered are listed below.

1) Filament wound tube loaded in torsion. ---Samples difficult and costly to make. Would require separate specimen for test.

2) Douglas ring test. (83)--- Too costly to make specimens. Separate specimen for test. Only applicable to 0 degree specimens.

3) Cross-sandwich beam sample with aluminium honeycomb core loaded in tension. ---Very expensive test piece. Separate test piece required.

4) Sample approximately 200mm square loaded in shear by complicated
clamp and pulley system. ---Large expensive test pieces, expensive
complicated apparatus.

5) $\pm 45^{0}$ strip test piece loaded in tension with strain gauges.---limited
to $\pm 45^{0}$ samples.

6) Torsional pendulum using rectangular cross-section strip sample.---
Require long sample to give reasonable results. Care required when using
$\pm\theta$ samples.

7) Plate twisting test.---requires fairly large test piece.

After some consideration it was decided that the plate twist test was most
suitable as it was reasonably easy to carry out ,used the same type of sample
for the tensile and bending tests, could give other information on the
test piece and used moderately priced test pieces.

Further details of the test are given in appendix D.

Fibre properties

Although glass fibres are isotropic and carbon fibres are anisotropic
the tests carried out were the same in both cases because it was only
possible to measure the longitudinal properties due to the small fibre
diameters.

A single fibre 400mm long was stretched across a rectangular annulus
made of stiff paper 350mm long and bonded to each end with Durofix. One
end of the rectangle was attatched to the lower side of the crosshead of
an Instron universal testing machine, the other end to a 500 g weight
standing on the pan of a top pan balance and the annulus cut either side.
The load on the fibre was calculated from the reading on the balance, the
fibre elongation was calculated from the cross head movement after correct-
ions had been made for the movement of the balance pan. This unorthodox
load measuring system was used because no suitable load cells were available.
Although the test worked satisfactorily the results indicated a large
variation in fibre strength and a smaller variation in fibre modulus (worse
for carbon). This is partly due to the nature of brittle materials and

-82-

partly due to the estimate of the fibre diameter by means of optical exam-
ination of a polished cross-section of the fibre set in resin. Single fibre
tests are also open to the criticism that in selecting a fibre from a tow
one tends to pick the 'best looking'fibres.In an effort to gain a truer
average value of the fibre tensile properties a fibre tow test was tried.

One end of a 400mm long tow was bonded to tapered,etched aluminium tab
with epoxy resin and the tow pulled through a folded tissue to remove any
broken or loose fibres. The other end of the tow was then bonded to another
aluminium tab and the tow loaded in tension at 1mm/min on the Instron.
The cross-section of the tow was calculated from the weight and density,
but the strengths recorded were lower than expected due to non-uniform stress
in the individual fibres in the tow causing some fibres to break before
others.This situation was improved by impregnating the fibres with a solution
of DX210 resin in methyl ethyl ketone.The excess resin was removed by pull-
ing the tow through lightly pinched rollers. This also had the effect of
removing most of the broken fibres and straightening the rest, thus helping
to create a uniform stress situation.The two ends of the impregnated tow
were laid on two hot prepared tabs. The hot tabs caused the resin to cure
locally and bond on to the tabs and create a transition region from fully
cured resin on the tabs to fully uncured resin on the tow.In this way the
stress concentration at the tab/tow joint is reduced and tow failure at
this point is less likely,although the gauge length is less accurate.
However the uncertainty in the gauge length is only about $\pm$ 0.5% on a length
of 400mm.

The fibre tow test was also tried with the resin on the tow
fully cured along the whole length, to compare the results with the uncured
tow.

A load versus extension graph was plotted for each test and the
modulus calculated from the straight portion after corrections had been
made for the compliance of the tabs and grips.

It was not possible to carry out meaningful torsional tests on a

fibre tow so only single fibre tests were carried out.

A single fibre about 200mm long was extracted from a tow and a piece of aluminium wire with a Vee cut in the centre was bonded to the fibre about 20mm from one end so that the fibre passed through the Vee. The wire was 1mm in diameter and 10mm long and was trimmed with a razor blade so that it was balanced about the fibre. The other end of the fibre was glued to the apex of large Vee cut in a cardboard disc 80mm in diameter, and the fibre lowered into a measuring cylinder so that the cardboard disc rested on top of the cylinder. The measuring cylinder was used to support the fibre and to protect it from draughts. Any electrostatic force between the cylinder and fibre was cylindrically symmetrical to the fibre and had no effect on the torsional oscillation. By twisting the disc it was possible to set up a twisting motion in the fibre without any swinging motion. A period of approximately 5 seconds was obtained by adjusting the length of the aluminium wire. The periods of oscillation for several different lengths of fibre were measured for each fibre.

To examine the effect of tension on the fibre due to the weight of the aluminium wire, several tests were carried out using different lengths of wire. The length of the fibre was adjusted to keep the period approximately equal.

A three point loading test was used for bending single fibres. Two vertical razor blades were used as the outer loading points and pieces of bent fuse wire as the combined third loading point and load. The whole 'apparatus' was placed in a glass tank to protect it from draughts and the deflection of the fibre measured with a travelling microscope. Several different lengths of wire were used with each fibre. The weights of the wires were measured to four decimal places on an electronic balance.

In the single fibre tests the same fibre was measured on all three tests, the order of tests being, torsion, tension and bend. A section of each fibre tested was mounted in resin, polished and examined optically to estimate the diameter. The magnification used was X1000 and this was

-84-

checked against a known calibration, but the main error lay in deciding where the edge of the fibre was, as it was not very sharp.

The specific gravity of the fibres was measured in the standard manner using a specific gravity bottle. Reduced pressure was used to help remove any trapped air bubbles.

Resin properties

The available 3 and 4 point flexural rigs had guide pins which suffered from varying degrees of friction, and thus made the resin flexural tests unreliable because of the small loads involved. To overcome this defect a new rig was made which had a larger span ,no friction and a built-in transducer to measure deflection.(figure 61)Four point bending was chosen rather than three point because the stress pattern is better defined, the shear stress being zero between the inner loading points. Some three point bending test were also carried out for comparison with other published data.

The test pieces were cut from a 5mm thick cast sheet of resin and measured 20x150mm. For four point loading an inner span of 70mm and an outer span of 140mm was used with a loading speed of 1mm per minute.The load was measured from the load cell and the deflection from the transducer; both were recorded continuously on a Bryans X-Y plotter. Several tests were carried out on each sample, increasing the load range each time until half the estimated maximum stress had been reached.The compliance of the rig was measured by using a 15x15mm cross-section steel bar in place of a test piece. A similar test procedure was used with the three point tests except that the deflection was measured from the cross-head movement rather than use the transducer.

A test piece measuring 105x105mm was cut from the cast sheet and was loaded in torsion by using the plate twisting rig shown in figures 62&63. The plate twisting apparatus has 3 fixed loading points and 1 moving point. These are so arranged that when the moving point is pulled upwards with a force P,a force of $P/2$ is applied upwards to the two opposite corners of the plate and downwards in the other two corners. This results in an

overall twisting moment being applied to the plate, similar to the cross-sandwich beam tests used for composite materials. The loading points (12mm diameter steel balls) are arranged to form a 100mm square allowing a 2.5mm overhang of the test-piece.To position the test-piece accurately in the rig each was marked out with the position of the loading points(figure 53) and adjusted using the retractable indicators.The deflection of the plate with respect to the base plate was measured by means of a LVDT transducer mounted in a block clamped to the base plate . The transducer block could be fixed anywhere on the plate within a 35mm radius of the centre, but was normally fixed at the centre.Before the actual test was started the test piece was loaded to the maximum required load and unloaded to take up any 'slack' in the system. Loading was carried out at 1mm per minute by lowering the cross-head. Load and deflection were recorded continuously on the X-Y plotter for both increasing and decreasing loads. The maximum load was governed by the deflection of the sample which did not exceed one quarter of the plate thickness. No attempts to break the test piece by torsional loading were made.

As a check on this test, many tests were carried out on a glass plate using different positions of the transducer. Two strain gauges were also bonded to the plate to measure surface strains.

The compliance of the rig was measured using a 6mm thick steel plate.

To compare the values obtained from the plate twisting test with results from a more conventional test,some tests were carried out on a torsional pendulum using the samples used in the bend tests. The torsional pendulum apparatus is shown in figure 58. The torsional modulus of the sample is given by $G = 64 \pi^2 (I_x + I_s) L f^2 / b t^3 \mu$ where I_x is as shown in the diagram, I_s is the total moment of inertia without the weight, L is the sample length betweeen clamps, f is the frequency, b is the sample width, t is the sample thickness and μ is a shape factor. In order to eliminate the unknown factors in the calculation of the torsional modulus of the sample several different values of were used for each test piece and a graph of I_x / f^2 was plotted.

For tensile testing the test pieces used in the flexural tests were waisted down in the centre to a width of 10mm over a length of 50mm and aluminium tabs were bonded to the ends. Strain gauges were bonded on to measure the transverse strain and a clamp-on transducer was used to measure the longitudinal strain, because of the high strain to failure anticipated . The samples were held in self tightening jaws on the Instron (figure 60) and loaded to half the estimated maximum stress to take up any play in the system.The tests were carried out at a loading rate of 1mm per minute and both the longitudinal and transverse strain were recorded continuously against load on two X-Y plotters. Figure 61 shows an overall view of the apparatus.The samples were loaded and unloaded several times increasing the maximum load each time until fracture occured.

Specific gravity

The specific gravity of the resin samples was determined using pieces of crushed resin in a specific gravity bottle in the standard manner.

Composite properties

Two moulds were used for producing composites, both of the plunger type with sides 20mm deep, using spacers to control the sample thickness. The larger mould made samples 300x150x2mm and was used mainly for making off-angle test pieces. The smaller mould made samples 130x130x2mm and was used for the majority of the time in view of economy of material.The 130 x130mm mouldings were cut up as shown in figure 59. The 105x105mm sample was used on the plate twisting rig, the two strip samples were used for bending, tensile and torsional pendulum tests and the 15x15mm sample was used for specific gravity and volume fraction measurements.

Volume fraction and specific gravity

The specific gravity and fibre volume fraction of every sample made was measured to make sure that there were no voids in the test pieces. On some early composites the entire plate was cut up to measure the variation of specific gravity and volume fraction.

A 15x15mm specimen was cut from the composite so that the edges were

at least 4mm from the edges of the 'as moulded' composite. The specimens were weighed in air and suspended in iso-propyl alcohol to determine the specific gravity. The alcohol was used because it had better wetting properties than water. The weight of the wire used to suspend the specimen and the effects of suface tension were taken into account in calculating the specific gravity.

To remove the resin from the glass fibre composites the specimen was heated in a furnace at $900\,^{o}K$ until a constant weight was achieved (about 2 hours). The carbon fibre specimens were treated by the 'acid digestion' method using concentrated sulphuric acid and hydrogen peroxide. After removal of the resin the fibres were washed and dried to constant weight. The amount of fibre weight lost during both types of resin oxidation was measured by using virgin fibre in place of the composite specimens. The volume fractions of the specimens were calculated from the composite, fibre and resin densities with the following assumptions.

a) composite mass = fibre mass + resin mass.

b) composite volume = fibre volume + resin volume + void volume.

c) resin density measured from cast resin is the same as resin density in
   a composite.

Mechanical tests

The types of mechanical tests used for the composites were the same as those used for the resin samples, but before measuring the composite properties various parameters of the test techniques were investigated. The parameters of interest were the loading speed, span-to-depth ratio and span-to-width ratio.

Both three and four point flexural tests were used to measure the composite properties, the maximum deflection for most samples being limited to the thickness of the sample, but for transverse unidirectional samples the maximum was only 50% of the sample thickness.

Some of the flexural samples were also tested on the torsional pendulum apparatus in the same manner as the resin samples, but most were too short to give reliable results.

-88-

The plate twisting tests were carried out in the same manner as for the resin samples but more measurements were made on each sample. On all the samples the central deflection versus load was recorded normally and then the plate was turned horizontally through 90° and re-tested. On some of the plates,measurements were also made after turning the plate over. In addition to these tests the deflection was also recorded at points other than the centre on certain plates, as the results show.

The tensile tests were carried out under the same conditions as the resin samples, again using the transducer to measure the longitudinal strain to failure. On the unidirectional samples with the fibres running parallel to the length, failure of the sample was usually initiated in the tab region due to stress concentration effects and the compressive stress imposed by the grips. It was found that by reducing the central 80mm to a width of 8mm and having a gentle taper to the tabs on a specimen 300mm long that failure in the central section could be achieved with a reasonable degree of success.This was generally easier to achieve on composites with an epoxy matrix. However the majority of the test pieces were too short to reduce the central portion and leave sufficient length for tapering and for the tabs, so with the exception of a few samples the tensile test pieces had parallel sides. On the $\pm\Theta$ test pieces most of them failed by inter-laminar pull out so the problem of a reduced section did not arise. Most unidirectional transverse composites failed at the tabs , but it is difficult to reduce the section without creating transverse cracks ,so again most samples were left with parallel sides.Figures 62 and 63 show a series of $\pm\Theta$ glass and carbon fibre tensile test pieces.

As an indication of the fibre/matrix bond strength and general 'quality' of the composite some short beam three point bend interlaminar shear tests were carried out in a specially made jig.

Some early tests were made on unidrectional composite plates in a manner devised by Hearmon (84) for testing plywood.As the test required large samples, was not particularly easy to carry out and produced unreliable reslts ,the test was dropped. Fuller details are in appendix D.

5.1 Fibre properties

Single fibre tests

Fibre type	Torsional modulus (GPa)	Tensile modulus (GPa)	Tensile strength (GPa)	Flexural modulus (GPa)	Poisson's ratio	Measured diameter (μm)	Number of tests
Glass	16-53	62-88	0.83-.41	42-126	0.15-.27	10-16	10
Grafil A	9-47	123-290	0.77-.35	33-250	0.11-8.6	6-12	10
Grafil HM	3-61	237-387	0.61-.17	83-420	0.17-21	6-11	10

The diameter of the fibre was based on measurement of a x 1000 photograph of a fibre cross-section. The torsional modulus was measured by a torsional pendulum and is given by $\dfrac{128 \pi \, l_1 \, I}{d^4 \, T^2}$

where

l_1 = fibre length

I = moment of inertia

d = fibre diameter

T = period of oscillation

The flexural modulus was measured from a three point loading test and is given by $\dfrac{4 \, P \, l_2^3}{3 \pi \, d^4 \, x}$ where l_2 = span

d = fibre diameter

x = central deflection

Poisson's ratio ν_f is calculated on the assumption that the fibre are isotropic and is given by $\dfrac{E}{2 G} - 1$

Hence $= \dfrac{P \, l_2^3 \, T^2}{192 \pi^2 I \, l_1 \, x} - 1$

Fibre tow tests

Dry fibre test

Fibre type	Maximum stress	Maximum strain	Modulus	Number of tests
Glass	0.76± 0.35 GPa	1.10± 0.40 %	69± 3 GPa	10
Grafil A	0.41± 0.20	0.23± 0.11 %	175±21	10
Grafil H M	0.39± 0.19	0.13± 0.07 %	295±34	10

Impregnated tow test (uncured)

Fibre type	Maximum stress	Maximum strain	Modulus	Number of tests
Glass	1.84±0.19 GPa	2.43±0.25 %	75.8±1.1 GPa	10
Grafil A	1.06±0.42	0.57±0.23 %	187±5.4	10
Grafil HM	1.07±0.41	0.33±0.12 %	327±8.3	10

Impregnated tow test (cured)

Fibre type	Maximum stress	Maximum strain	Modulus	Number of tests
Glass	1.99±0.16 GPa	2.63±0.19 %	75.6±0.9 GPa	10
Grafil A	1.73±0.33	0.92±0.18 %	197±6.3	10
Grafil HM	1.57±0.19	0.47±0.18 %	335±8.1	10

Specific gravity

Fibre type	Specific gravity
Glass	2.54±0.01
Grafil A	1.79±0.01
Grafil HM	1.87±0.01

Using the average fibre modulus values from the cured tow test, the
cross-sectional area of the fibres in the single fibre tests were
calculated and used to re-calculate the values of the torsional moduli
of the single fibres. The results are shown in the following table.

Re-calculated single fibre torsional moduli

Fibre type	Torsional modulus
Glass	33.1±3.3 GPa
Grafil A	14.3±5.8
Grafil HM	11.1±5.2

Effect of tension on the torsional modulus

	Glass fibre			Grafil A		
Mass of wire	0.0434g	0.0740g	0.0988g	0.0434g	0.0740g	0.0988g
Length of fibre	320mm	178mm	156mm	198mm	126mm	83mm
Torsional mod.	30.3GPa	28.7GPa	32.6GPa	17.7GPa	19.2GPa	16.9GPa

Fibre weight loss during volume fraction assessment

Glass	0.9 %
Carbon	1.2 %

5.2 Resin properties

Three point flexure tests (Average values of 10 tests)   Span=140mm

Resin system	Maximum deflection	Maximum stress	Modulus	Repeatability
Scotchply 1002	5mm	27.2 MPa	2.38 GPa	± 3%
Epikote DX210 Epikure $BF_3$400	5mm	20.8 MPa	2.77 GPa	± 2%
Crystic D351	5mm	26.1 MPa	3.43 GPa	± 4%
Crystic 272	5mm	23.7 MPa	3.54 GPa	± 3%
Special resin	Too soft to test			
Aluminium	4mm	18.5 MPa	64.7 GPa	± 1%

Four point flexure tests (Average values of 10 tests) Inner span=70mm

Resin system	Maximum deflection	Maximum stress	Modulus	Repeatability
Scotchply 1002	3mm	44.3 MPa	2.52 GPa	± 2%
Epikote DX210 Epikure $BF_3$400	3mm	33.8 MPa	2.83 GPa	± 2%
Crystic D351	3mm	40.7 MPa	3.51 GPa	± 3%
Crystic 272	3mm	43.3 MPa	3.68 GPa	± 2%
Special resin	Too soft to test			
Aluminium	2mm	27.6 MPa	67.1 GPa	± 1%

Tensile tests (Average values of 10 tests)

Resin system	Maximum stress	Maximum strain	Modulus	Poisson's ratio	Repeatability
Scotchply 1002	39.7 MPa	1.24 %	2.65 GPa	0.354	± 4%
Epikote DX210 Epikure $BF_3$400	43.3 MPa	2.13 %	2.77 GPa	0.349	± 4%
Crystic D351	42.5 MPa	1.27 %	3.65 GPa	0.352	± 3%
Crystic 272	51.0 MPa	1.82 %	3.72 GPa	0.346	± 4%
Special resin	26.7 MPa	6.41 %	1.02 GPa	0.331	± 7%
Aluminium	200 MPa	0.3 %	67.5 GPa	____	±0.5%

Torsional tests

Plate twisting test

Resin system	Modulus	Repeatability
Epikote DX210/Epikure BF$_3$400	1.01 GPa	± 5%
Crystic D351	1.47 GPa	± 5%
Crystic 272	1.39 GPa	± 3%
Special resin	Too soft to test	
Aluminium test piece	28.6 GPa	±1.5

Torsional pendulum (average of ten tests)

Resin system	Modulus	Repeatability
Scotchply 1002	1.05 GPa	± 4%
Epikote DX210/Epikure BF$_3$400	1.13 GPa	± 6%
Crystic D351	1.32 GPa	± 7%
Crystic 272	1.27 GPa	± 7%
Special resin	Too soft to test	
Aluminium test piece	27.2	± 3%

Specific gravity

Resin system	Specific gravity
Scotchply 1002	1.20
Epikote DX210/Epikure BF$_3$400	1.21
Crystic D351	1.31
Crystic 272	1.21
Special resin	1.26

Ash content

Scotchply 1002	0.8 %
Epikote DX210/Epikure BF$_3$400	0.9 %
Crystic D351	0.6 %
Crystic 272	0.5 %
Special resin	0.5 %

Repeatability

The repeatability was determined by re-measurement of the modulus at approximately 3 monthly intevals over a period of a year.

5.3 Test variables (Unidirectional samples)

Three point flexure — Glass/Epikote DX210 composite

Span to depth ratio	Flexural modulus	Loading speed	Flexural modulus
69.2	37.5 GPa	30 mm/min	46.9 GPa
65.7	44.3	60	45.0
56.3	42.8	120	43.6
46.9	43.6	300	43.6
37.6	43.1	600	42.9
28.2	40.1		
18.8	41.6		

Three point flexure — Grafil A/Epikote DX210 composite

Span to depth ratio	Flexural modulus	Loading speed	Flexural modulus
67.3	131.5 GPa	30mm/min	140.0 GPa
57.7	135.1	60	131.5
48.1	131.7	120	128.8
38.5	128.9	300	128.9
28.2	123.4	600	128.9
19.2	101.4		

Three point flexure

Span = 140mm

Span to width ratio	Flexural modulus	
	Grafil composite	Glass composite
35	140.8 GPa	44.1 GPa
17.5	135.5	43.8
11.61	129.7	43.5
8.75	127.8	43.7
7.00	128.4	43.4
5.83	128.1	43.4

Four point flexure (inner to outer span constant at 1:2)

Inner span to depth ratio	Glass composite flex. modulus	Inner span to depth ratio	Carbon composite flex. modulus
25.9	46.3 GPa	23.8	138.6 GPa
36.3	45.7	33.3	139.2
51.8	45.1	47.6	136.4

Torsional pendulum [*]

Effect of sample length

Sample length	Unidirectional glass composite. Shear modulus	$\pm\ 45°$ symmetric glass composite. Shear modulus
80mm	4.53 GPa	15.3 GPa
100	4.49	16.1
120	4.51	16.3
140	4.50	16.5

* For discussion regarding torsion and shear see appendix E

Plate twisting test.
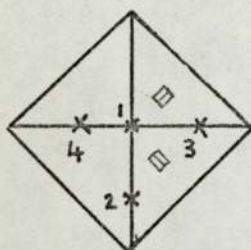
▥ Strain gauges--registered no strain.

Deflection measuring position.	Glass plate torsional modulus.	Grafil composite plate $=\pm30°$. Torsional modulus
1	33.7 GPa	22.2 GPa
2	33.5	22.1
3	33.0	22.7
4	33.3	22.2

5.4 Composite results

Volume fraction variation

The sketch below shows the variation in fibre volume fraction in a 130x 130x2mm unidirectional glass fibre composite plate which was considered to be of average quality.

0·58	0·59	0·59	0·60	0·62
0·59	0·60	0·60	0·61	0·63
0·59	0·59	0·61	0·62	0·63
0·60	0·60	0·63	0·63	0·62
0·57	0·58	0·57	0·63	0·62

Effect of fibre pre-tension on composite properties

The tension in the fibres wound round the frame was judged by the amount the two halves of the frame were forced apart.

Distance between 2 halves of frame	Fibre volume fraction	Longitudinal modulus	Transverse modulus	Shear modulus
0mm	0.42	31.1 GPa	10.2 GPa	4.7 GPa
1.7	0.44	32.3	9.9	4.7
2.6	0.43	31.8	9.8	4.5
3.8	0.46	33.6	10.5	4.9

Effect of reduced bonding between fibre and matrix

The reduction in the bond was caused by silicon grease applied to the fibres and was estimated from the composite interlaminar shear strength.

Interlaminar shear strength	Fibre volume fraction	Longitudinal modulus	Transverse modulus	Shear modulus
76 MPa	0.58	42.9 GPa	15.7 GPa	6.3 GPa
52	0.60	43.4	14.5	5.7
47	0.61	42.1	14.6	4.1
23	0.57	39.7	11.4	1.9

The following two samples used epoxy resin with glass fibre coated in a polyester compatible size, and polyester resin with glass fibres coated in an epoxy compatible size.

59 MPa (Epoxy resin)	0.59	43.2 GPa	13.7 GPa	5.9 GPa
33 (Polyester resin)	0.57	41.7	10.4	2.6

Comparison of three and four point flexural tests and tensile tests

Test piece	Flex. modulus three point	Flex. modulus four point	Tensile modulus
Crystic D351/glass 0 V_f=0.61	42.7 GPa	45.3 GPa	44.1 GPa
Crystic D351/glass 90 V_f=0.61	17.1 GP	17.8	16.5
Crystic D351/glass±45 V_f=0.59	18.5	20.6	11.2
Epikote DX210/Grafil 0 V_f=0.62	119.8	125.7	121.3
Epikote DX210/Grafil 90 V_f=0.62	7.6	7.9	7.8

Effect of low modulus matrix on composite properties

Material: Special resin/glass fibre unidirectional composite

Special resin: Crystic 272/Crystic 182 2:1

Fibre volume fraction	Longitudinal modulus	Transverse modulus	Shear modulus
0.27	18.8 GPa	4.2 GPa	Too soft to measure
0.48	32.4	6.7	Too soft to measure
0.62	41.3	9.1	1.8 GPa

Longitudinal and transverse moduli measured in tension.

Effect of voids on composite properties

Material: Crystic D351/glass fibre unidirectional composite

Void volume fraction	Fibre volume fraction	Longitudinal modulus	Transverse modulus	Shear modulus
0.0008	0.43	31.3 GPa	10.2 GPa	4.8 GPa
0.021	0.41	30.7	9.9	4.6
0.037	0.44	31.0	10.2	4.4
0.066	0.45	32.0	9.8	4.1
0.12	0.43	31.3	7.8	3.2
0.18	0.41	30.9	5.3	1.8

Longitudinal and transverse moduli measured in tension.

5.5 Graphical results

The majority of the experimental results are shown in graphical form in figures 72-103 and the results are not given in tabular form. There were many more glass fibre composites made and tested than carbon fibre composites because of the cost of the carbon fibre. The 'bunching' effect of some of the results is due to the method of making the composites from prepreg material; to vary the volume fraction a number of sheets of prepreg were added or subtracted, thus tending to vary in steps.

The longitudinal and transverse moduli and the Poisson's ratios were all measured in tension unless otherwise stated. The shear moduli were measured on the plate twisting rig unless otherwise stated. The fibre volume fractions were measured by the methods previously mentioned, and

in no case did the calculated void volume fraction exceed 1%.

Grafil HM samples

Only two composites were made using Grafil HM fibre. The results are shown below.

Composite type:Unidirectional Epikote DX210/Epikure BF$_3$400 GrafilHM				
Fibre volume fraction	Longitudinal modulus	Transverse modulus	Shear modulus	Poisson's ratio
0.66	208 GPa	6.3 GPa	3.9 GPa	0.31
0.38	121 GPa	4.1 GPa	3.1 GPa	0.33

6 DISCUSSION OF RESULTS AND CONCLUSIONS

6.1 Fibre results

The variation in the initial results of the single fibre tests make the figures useful only as a guide to the correct values. The principle cause of the variation is thought to be errors involved in measuring the fibre cross-section on the microscope, but with any brittle material there is always some spread in the results.

The dry tow test allowed the fibre tow cross-sectional area to be computed more accurately by measuring the weight, length and density. However there is always a number of broken fibres in a tow despite efforts made to remove them, and these will contribute to the weight but not the strength or stiffness. Apart from the broken fibres not all the continuous fibres are under the same initial tension so that at any one time different fibres are under different stresses. The effect on the measured modulus will be greatest at low strains where some fibres are not stressed at all, and high strains where some fibres may have already broken. Fortunately the modulus is normally measured between these two extremes.

Both the single fibre and dry tow test suffer from premature fibre failure initiated by the stress concentration where the fibres are bonded to the tab. The wet tow test overcomes this problem to a large extent.

Impregnating the tow with resin enabled broken fibres to be removed more easily without damaging other fibres and to align the continuous fibres so that constant strain conditions were more likely under loading. This is reflected in the results where the maximum stress and strains reached were far in excess of those for the dry test, but the increase in modulus is less. This is to be expected because the modulus is calculated from the slope of the stress/strain curve over the central portion where most of the fibres will be contributing in either a wet or dry test.

The cured impregnated tow test has some of the advantages and some of the disadvantages of the previous tests, in that the fibres are more equally

strained but are more likely to fail at the tab bond than the wet tow test. The main difference between this and other tests is the ability of the fibres to transmit stress from broken fibre to other fibres via the matrix, thus behaving like a composite. The strength values calculated from this test (after taking the resin strength into account) are noticeably higher for the carbon fibre,and less so for the glass fibre. This indicates that generally in a glass tow there are far fewer broken fibres than in a carbon tow.The moduli were also slightly higher, particularly for the high modulus carbon.

The measured values of the moduli are in reasonable agreement with the manufacturer's figures but the strengths are slightly lower.

The specific gravity results were very consistent and in good agreement with the manufacturer's figures.

The justification for re-calculating the torsional moduli of the single fibres on the assumption that the tensile modulus of any one type of fibre is constant could be called into doubt. However in defence of the move it must be said that the re-calculated value probably represents a good average, and the properties of the composites in which we are interested depend on the average fibre properties.For glass fibre with a Poisson's ratio of 0.2 (from literature) and a Young's modulus of 76 GPa the theoretical shear modulus is 31.6 GPa which is in good agreement with the experimental value. The experimental values for the carbon fibres cannot be compared in this manner because of the fibre anisotropy.

The effect of tension in the fibre during the torsional pendulum measurements is assumed to be zero from the results obtained.

The fibre weight loss during fibre volume fraction measurements is small compared with the variation of fibre volume fraction found in the average composite.However if not taken into account it can lead to the phenomena of negative voids.

6.2 Resin results

The maximum stress values quoted in the flexural results are the maximum stress levels reached during testing and not the failure stress

values; the maximum stresses in the tensile tests are failure stresses
and the maximum strains are the strains up to the maximum stress levels.
The repeatability of the tests is worst for the tensile tests and the
only reason that can be thought of is that the complexity of the strain
measuring equipment may lead to slight errors, although the equipment
was calibrated each time it was used.

Generally the modulus values from the three point flexural test were
the lowest because the deflections due to shear stresses are not taken
into account in simple bending theory. The flexural modulus of DX210 resin
is in good agreement with the manufacturer's figure for flexural
modulus , but the tensile properties were less than those quoted. The
tensile properties of Crystic 272 were also slightly less than the
manufacturer's figures.

All the shear modulus results form the plate twisting test are higher
than those calculated from the tensile results. The shear modulus of the
aluminium sample measured on the rig is 28.6 GPa compared with a
quoted value of 27.2 GPa. Greszezuk (88)states that the plate twisting
test generally gives slightly higher values of shear modulus than other
tests.For the calculations based on the matrix shear modulus the plate
values are used.

6.3 Calulated fibre values

Following the method of Goggin and Reynolds the Reuss and Voigt
limits of the fibre properties were calculated for Grafil A and HM
using assumed orientation values of 12 and 8 respectively.(average
values figure 20)

	E_{f1}		E_{f2}		G_f	
	Reuss	Voigt	Reuss	Voigt	Reuss	Voigt
Grafil A	121 GPa	947 GPa	5.5 GPa	63 GPa	11.7 GPa	92 GPa
Grafil HM	177 GPa	963 GPa	5.1 GPa	57 GPa	9.5 GPa	85 GPa

If the Reuss values are considered to be closest to the real fibre
properties, the above may be taken as a guide only.

This is a brief summary of the information contained in tables 6-32 and figures 29-48.

From table 7 it can be seen that only Tsai's expression (no 3) with its K factor differs to any degree from the law of mixtures and tables 11-14 show the reason why. The longitudinal modulus E_{11} is a function of the fibre volume fraction and the two constituent moduli only .This simple relationship should also apply to composites made with anisotropic fibres according to Rabinovich's and Whitney's work. (Tables 25-32)

Figure 30 and table 8 give the predicted values of Poisson's ratio. Hill's expression for the upper and lower bounds gives almost exactly the same values as those of Tsai for C=0 and C=1.Expression 11 is the odd one out in the sense that it predicts an increasing value for the composite Poisson's ratio with increasing fibre volume fraction, but for certain values of ν_f and ν_m, ν_n can be negative. It is believed that there is an error in the equation.Figures 40-42 and tables 15-18 show that once the fibre modulus is over an intitial value of approximately 40 GPa and the matrix modulus is greater than 2 GPa then ν_n is almost a linear function of ν_f and ν_m in a law of mixtures relationship.

Whitney suggests that for composites made with anistropic fibres the composite Poisson's ratio is also given by the law of mixtures ; Rabinovich has a modified version in which the composite Poisson's ratio is reduced for highly anisotropic fibres.(See tables 25-32)

The predicted values of the transverse composite modulus are shown in figure 31 and table 9. From figures 44-47 and tables 19-22 it is clear that most theories treat the transverse modulus as a function of only E_f,E_m and V_f, but derive considerably differing values for E_{22}. Only by comparing the results with experimental values is it possible to tell which of the predictions is most correct.

The variation of the transverse modulus of a composite made with anisotropic fibres is shown in figures 35 and 36 and tables 25-32. The values generated are similar and are highly dependent on the transverse

fibre modulus.

The variation of the composite shear modulus with fibre volume fraction
is shown in figure 32 and table 10. There is some disagreement in the
value of the shear modulus but all the theories assume that it is only
a function of G_f, G_m and V_f, where the relationship with V_f is almost
linear if G_f is greater than 20 GPa (expressions 27 & 28 excepted).

The shear modulus of a composite made with anisotropic fibres as
predicted by Whitney and Rabinovich in shown in figure 37 and 38 and
tables 25-32. In both cases the fibre shear modulus is the predominating
factor.

6.5 Investigation of test variables

On both the glass and carbon samples the apparent modulus increases
with span to depth ratio but levels off with a ratio of 40:1 or more.
All the three point flexural tests that were carried out had a minimum
span to depth ratio of 48:1. The moduli of both types of sample also
decrease with loading speed. Normally the tests were carried out with a
loading speed of 1mm/minute.

Except at very narrow widths, the width to depth ratio has little
apparent effect on the measured modulus over the range considered here.

When using a torsional pendulum to determine the shear modulus the
length of the sample has little or no effect if the the sample is a
unidirectional one, but does affect the measured modulus when using
off-angle composites. This is due to the change in the relative
directions of the the strain and fibre as the length is changed, so
if a very long sample was used there would be little change in modulus
for a small change in length. The maximum sample length on the available
apparatus was limited to 140 mm so the technique was only used to compare
results with those from the plate test.

The results of the glass plate (isotropic) and the $\pm 30°$ Grafil
plate from calculating the torsional modulus by measuring the deflections
at various points agree well with the theory (appendix E). The strain
gauges also registered no strain as expected.

-103-

The variation of fibre volume fraction in a typical composite plate shows that the volume fraction quoted for any one sample may only be considered to have an accuracy of about ±5 %.

6.6 Composite results

The attempts to pre-stress the fibres during the production of a composite test piece were rather crude but did actually stress the fibre (by an unknown amount).The results obtained were inconclusive and it is assumed that a low value of pre-stress may help to straighten the fibres but has no effect on the elastic properties. At higher stress levels it is thought that using pre-stressed fibres would help to stop the matrix failing under tensile loads in a method analogous to that used in pre-stressed concrete beams.

The table comparing three point and four point flexural tests with tensile tests clearly shows the tremendous difference in modulus for a $\pm \Theta$ composite measured in tension and flexure. The difference in the measured moduli of the unidirectional samples is considerably less and is due to the effect of shear stress in the composite. The longitudinal to shear modulus ratio for a 0^0 sample is high and thus the effect of ignoring the deflection due to shear stress is greater than for a 90^0 sample where the difference is much less.The difference in apparent moduli for angle ply composites measured in tension and flexure is due to the B_{ij} and D_{ij} matrices explained in section 3.

The composites made with the 'special' low modulus, high elongation resin demonstrate that the resin properties control the transverse and shear properties of the composite but have little effect on the long-itudinal properties.

Normally every effort is made to produce composites without any voids,but the results suggest that a relatively low void content has little effect on the composite properties. At larger void contents the reduction in the shear and transverse moduli increases rapidly.

The bonding between the fibre and matrix (as indicated by the inter-

-104-

laminar shear strength) has an effect on the transverse and shear moduli in the sense that they are reduced by weak bonding.It is difficult to control the bonding in a controlled manner so that it is not known how sensitive the elastic properties are to the bond strength.

Unidirectional composite results

The experimental variation of longitudinal modulus, transverse modulus, shear modulus and major Poisson's ratio are shown in figures 72-87.The longitudinal modulus of all four systems considered is a linear function of the fibre volume fraction. On extrapolating the graphs the tensile modulus of glass varies from 72 to 74 GPa, the tensile modulus of Grafil A is 188 GPa, and the tensile moduli of the resins vary from 1.5-3.0 GPa. The scale of the Y axis makes it difficult to determine the resin moduli from the graph. Comparing these results with the fibre experimental results,the glass and Grafil moduli are about 5% lower than the tow test results.The theoretical values of the composite moduli based on the law of mixtures and using the experimental data is shown on each graph. All the experimental traces are below the theoretical ones but are within the 'lower limit' set by Tsai's K factor = 0.9.The reasons why the traces do not agree exactly are thought to lie partly in the testing and measuring techniques (some points are above the theoretical maximum), and partly in non-perfect composites.

To measure the alignment of fibres in composites some stretches of glass fibre were sprayed with paint as the prepreg was being made. The angular spread of the fibres were measured in the prepreg and found to almost zero, and in a composite where the spread was estimated at $\pm 2^{o}$, although accurate measurement was difficult.The longitudinal modulus is related to the fibre modulus by Cos Θ , so $\pm 2^{o}$ would reduce the modulus by about 2%.The other main error in the composites is the possible variation of the fibre volume fraction, which can be as much as 5%.

The scatter in the results of the Poisson's ratio is greater than in the longitudinal modulus results, possibly because the Poisson's ratio

depends on measuring two strains without error, but again the relationship is a linear one for the glass fibre composites.The relationship for the Grafil composites is possibly also linear but the scatter makes it uncertain.The extrapolated values for the Poisson's ratio of glass vary from 0.208 to 0.22,and for the resins as follows:- Crystic D351, 0.31, Scotchply,0.32 and Epikote,DX210 0.348.If this value of Poisson's ratio for Epikote is used as one end of a straight'best fit' line drawn through the Grafil composite results, the extrapolated value for the Poisson's ratio of Grafil A is 0.36. The experimental value of the Poisson's ratio of glass fibre is between 0.15-0.27 and the values found by Brannan and Kroenke (section 1) are between 0.18 and 0.34. Using an average experimental value of 0.21 and the experimental value for the tensile modulus of 75.8,the calculated value of the fibre shear modulus is 31.32GPa and this value is in good agreement with the re-calculated fibre shear modulus.Using 0.21 as the glass Poisson's ratio and experimental values for the resin Poisson's ratios,the 'theoretical ' values are shown on the graphs.The theoretical and experimental values for Epikote/glass agree well, but the theoretical values for Crystic D351 and Scotchply are both higher than the experimental values at low fibre volume fraction.

The extrapolated Poisson's ratio value for Grafil A of 0.36 agrees with the generally accepted level for carbon fibre, but there is no other experimental confirmation.

Figures 74,78 and 82 show the experimental relationships between composite transverse modulus and fibre volume fraction for three different resin systems with glass fibre.All the graphs have a similar shape but the modulus values of the Scotchply system are lower than the other two at low fibre volume fractions.In section 6.4 it was concluded that most theoretical approaches to predicting the transverse modulus have assumed that the transverse modulus is a function of the fibre and matrix Young's moduli and the fibre volume fraction. If this is the case,then the differences in the values of the transverse moduli of the three composite

resin systems should be a function only of the resin properties as the other two variables are common. However by comparing the modulus values of the graphs at common fibre volume fractions it is apparent that either the hypothesis is wrong or that a complicated relationship is involved.

From a study of tables 19-22 and figures 9,19 and 20 several expressions were selected as being the most likely to fit the experimental results. Substituting the experimental values in for the constituent properties it was concluded that expression 17 gave the best fit, but in all cases the theoretical values were lower than experimental ones at high volume fractions. The theoretical values based on expression 17 are shown for each system.

Figure 86 shows the relationship between transverse modulus and fibre volume fraction for Epikote/Grafil composites, but due to the scatter in the results the relationship has been interpreted simply as a linear one because there is no real justification for doing anything else. If the linear relationship is extrapolated the fibre shear modulus is 12 GPa and the matrix shear modulus is -0.5 GPa. Working on the assumption that expression 17 provides the best overall agreement between theory and experiment it is found that the best fit is obtained when the fibre modulus = 23 GPa. However because the values of fibre modulus and matrix modulus are much closer the differences between the various expressions are reduced. A plot of the values from expression 17 with $E_f = 23$ GPa is shown in figure 86.

Rabinovich and Whitney's expressions for the transverse modulus generate much higher values than the experimental values when $E_{f1}/E_{f2} = 9$.

The experimental results of the shear moduli of the three glass composite systems are shown in figure 75,79 and 83. By reasoning in a similar manner to that employed for the transverse modulus it is concluded that expression 30 gives the best overall fit between theory and experiment. Using the experimental values for the constituent

properties the theoretical values according to expression 30 with zeta=2.5 are shown for the three systems. The agreement at higher fibre volume fractions is again not very good.

In figure 87 the experimental results of shear modulus of the Grafil composites are shown with a theoretical plot based on expression 30 with zeta = 2.5 and E_f=23 GPa. The values predicted by both Whitney and Rabinovich are much lower than the experimental values.

We have seen that the longitudinal modulus and Poisson's ratio cf composites made from either isotropic or anisotropic fibres can be predicted reasonably well from the law of mixtures equations. The relationship between transverse and shear moduli of the composite and the composite constituent properties is not so well understood. An expression which allows the composite transverse modulus to be predicted approximately from the constituent properties has been used in conjunction with the carbon fibre composite, and it was found that an assumed fibre modulus of approximately 23 GPa gave reasonable agreement between theory and experiment.

The situation is even more open for the composite shear modulus ; The values of the composite shear modulus are approximately given by expression 30 where zeta = 2.5. Using the same expression for a composite made from anisotropic fibres (fibre shear modulus calculated from fibre transverse modulus) the theoretical values are greater than the experimental ones.

One of the reasons why there is a difference between experimental and theoretical values is that the composites do not conform exactly to the assumptions of section 2. For example, the spread of fibres at low fibre volume fractions tends to be inhommogeneous. Figure 64 shows a typical area in a low fibre volume fraction sample and figure 65 shows how it is possible to get resin rich layers between the layers of the original prepreg due to incorrect manufacture. Figures 66 and 67 show areas of high volume fraction glass and carbon composites respectively.

The packing in both is tending towards hexagonal and the dispersal of fibre is more hommohgeneous. A close up of a carbon fibre composite is shown in figure 68 where it can be seen that the fibres aren't perfectly round and vary in size quite considerably compared with glass.

We have seen how the anisotropy of carbon fibre has a major influence on the transverse and shear properties of a unidirectional composite especially at high fibre volume fractions. The next area of study is the effect of the unidirectional composite properties on angular properties.

There are two basic types of angular composites; a unidirectional composite stressed at an angle to the fibre direction, and a multilayered laminate. The experimental and theoretical values of the off-angle properties of a unidirectional composite are shown in figure 89. These results show the effect of the B_{ij} and D_{ij} (mentioned in section 3) where it can be seen that the constraints of the testing procedure have had a major influnce on the properties measured between $0°$ and $90°$. It was also shown in section 3 that the elastic response of a symmetrical laminate is easier to deal with both in theory and practice.

Figure 69 shows a section of a typical balanced or symmetric laminate. The thick section is the centre section. It is often assumed that there must be a resin rich layer between each ply of a laminate, although figure 69 shows that this is not necessarily the case.

Figure 90 shows the typical stress-strain curves for the tensile tests on a series of $\pm\theta$ laminates. Note that only a small portion of the total is linear and elastic. The results from the torsional pendulum and plate twisting test are compared in figures 91 and 92. The difference between the results for the unidirectional samples is relatively small, but gets considerably larger for angles between $0°$ and $90°$ due to the interaction between the B_{ij} and D_{ij} and the constraints of the test technique. A similar effect is illustrated in figure 93 for the tensile and four point flexure of a series of $\pm\theta$ samples. The theoretical values shown are calculated using the experimental data from the uni-

directional composites, and the theory shown in section 3.

Figures 93-101 are the experimental and theoretical results for three series of $\pm\Theta$ laminates made from two different resin systems and two types of fibre, one of them being anisotropic. Although the theoretical results do not agree exactly with the experimental ones, the error is approximately equal for all three types of laminate. It can then be said that the anisotropy of the carbon fibre does not invalidate the use of conventional laminate theory, at least for use with the type of laminate used here. However the use of highly anisotropic fibre can produce some unusual effects such as a Poisson's ratio greater than 1 for a $\pm 30^{\circ}$ laminate. (This particular property could be very helpful in removing a filament wound article from the mandrel.) The experimental and theoretical results for modulus E_y at 90° to modulus E_x are a mirror image of the E_x results. The minor Poisson's ratio ν_{yx} is given by $\nu_{yx} = (\nu_{xy}E_y)/E_x$.

The maximum stress and strain at failure variations with angle Θ are shown in figures 102 and 103 respectively. The maximum stress curve has a very similar shape to that of E_x for the system shown but this need not be the case. The sample used was a glass/epoxy one which had a reasonable interlaminar shear strength, but the failure of the samples between angles of 10° and 70° were all due to interlaminar tensile failure. The 0° sample failed by tensile fibre fracture and the samples between 70° and 90° by a combination of interlaminar tensile failure and transverse fracture. Figure 71 shows the fractured end of a $\pm 70^{\circ}$ sample. If a $\pm\Theta$ sample with a greater interlaminar tensile strength was tested in a similar manner, the maximum stress curve would probably not be the same as the one shown.

The failure strain is defined here as the strain up to initial failure of the composite. The large strains recorded are the result of the type of 'sliding' failure of the laminate. Even after failure the composite is still capable of carrying a stress and 'strains' of greater than 10% can be recorded for total separation of the two parts of a sample.

6.7 Final conclusions

Although the measurement, and even calculation of the basic properties of the composite constituents was not entirely satisfactory, sufficient information was obtained to show that some properties of a unidirectional composite may be calculated reasonably accurately. In particular the longitudinal modulus can be calculated for composites made from isotropic or anisotropic fibres from a knowledge of the fibre longitudinal modulus, matrix modulus and fibre volume fraction. The major Poisson's ratio of a composite may also be calculated with reasonable accuracy for fibre volume fractions greater than 20% and possibly over the whole range for composites made from isotropic fibre. It may also be possible to calculate the major composite Poisson's ratio for composites made from anisotropic fibres, but until an accurate measurement of the fibre Poisson's ratio is made we will not have certain proof.

The composite transverse modulus can be calculated reasonably accurately for low to medium fibre volume fraction composites made from isotropic fibres but becomes less reliable at higher volume fractions. As the transverse modulus of carbon fibre is not known accurately no attempts can be made to calculate the composite properties, but working in reverse using the expressions used for isotropic fibres a value of the fibre modulus may be obtained.

The shear modulus of composites made from isotropic fibres is in a similar position to that of the transverse modulus, in that it can be calculated reasonably well for low to medium fibre volume fractions but the disagreement with experimental values increases at higher volume fractions. By using the value of the carbon fibre transverse modulus determined from measurement of the composite transverse modulus it is possible to calculate the shear modulus of a composite made from carbon fibre. However the results generated in this manner do not agree very well with the calculated values based on the shear modulus of the fibre determined from torsional pendulum measurements.

The situation regarding the calculation of unidirectional composite properties is thus only partly satisfactory, but until the transverse properties of anisotropic fibres are known more accurately any improvement will be difficult.

The present theory used for calculating the properties of laminates appears to be satisfactory for composites made from both isotropic and anisotropic fibres.

Regarding the experimental techniques employed for the practical work it has been found that the procedure for producing composites gives great freedom of choice of material while producing composites of reasonable quality of a variety of geometries. The types of tests used are fairly standard apart from the plate twisting type. This test is not entirely satisfactory in that it produces slightly higher results than others, but overall represents a good compromise between reasonable results and reasonable cost. In combination with the tensile tests (and flexural if required) sufficient information may be acquired for assessment of new materials or to calculate the properties of a complicated structure.

RECOMMENDATIONS FOR FURTHER WORK

There two main areas where further knowledge would be of help. Firstly in obtaining more accurate values for the transverse and shear properties of anisotropic fibres either by direct/indirect measurement or by calculation. Secondly an improvement in calculating the transverse and shear properties of unidirectional composites is required.

Table 6 Expressions for predicting the elastic properties of composites

Longitudinal Young's modulus

Author	Expression	Number
Abolinish		
Halpin/Tsai		
Hashin/Rosen(approximate)		1
Rabinovich(isotropic)	$E_{11} = E_f V_f + E_m V_m$	
Paul(upper bound)		
Van Fo Fy		
Whitney(approximate)		

Ekvall $\qquad$ $E_{11} = E_f V_f + E_m' V_m$ $\qquad$ 2

$\qquad$ where $\qquad$ $E_m' = E_m / (1 - 2 V_m^2)$

Tsai $\qquad$ $E_{11} = k(E_f V_f + E_m V_m)$ $\qquad$ 3

Hashin/Rosen
Hill(lower bound)
Kilchinski
Whitney(isotropic)

$$E_{11} = E_f V_f + E_m V_m + \dfrac{4(V_f - V_m)^2 V_f V_m}{\dfrac{V_f}{K_m} + \dfrac{V_m}{K_f} + \dfrac{1}{G_m}}$$

4

$\qquad$ where $\qquad$ $k_m = E_m / (2(1 - V_m - 2V_m^2))$
$\qquad\qquad\qquad$ $k_f = E_f / (2(1 - V_f - 2V_f^2))$

Hill(upper bound) $\qquad$ $E_{11} = E_f V_f + E_m V_m + \dfrac{4(V_f - V_m)^2 V_f V_m}{\dfrac{V_f}{K_m} + \dfrac{V_m}{k_f} + \dfrac{1}{G_f}}$ $\qquad$ 5

Major Poisson's ratio

Abolinish
Ekvall
Halpin/Tsai
Rabinovich(isotropic)

$\qquad$ $V_{12} = V_f V_f + V_m V_m$ $\qquad$ 6

Author	Expression	Number

Hashin/Rosen
Hill(lower bound)
Kilchinski
Whitney(isotropic)

$$\nu_{12} = \frac{\nu_j V_j + \nu_m V_m + (\nu_j - \nu_m) V_j V_m \left(\frac{1}{K_m} - \frac{1}{K_j}\right)}{\frac{V_m}{K_j} + \frac{V_j}{K_m} + \frac{1}{G_m}}$$

7

$$\text{where} \quad K_m = E_m / (2(1 - \nu_m - 2\nu_m^2))$$
$$K_j = E_j / (2(1 - \nu_j - 2\nu_j^2))$$

Hill(upper bound)

$$\nu_{12} = \frac{\nu_j V_j + \nu_m V_m + (\nu_j - \nu_m) V_j V_m \left(\frac{1}{K_m} - \frac{1}{K_j}\right)}{\frac{V_m}{K_j} + \frac{V_j}{K_m} + \frac{1}{G_j}}$$

8

Tsai

$$\nu_{12} = (1-C) \frac{K_j \nu_j (2K_m + G_m) V_j + K_m \nu_m (2K_j + G_m) V_m}{K_j (2K_m + G_m) - G_m V_m (K_j - K_m)} \qquad (C = 0) \quad 9$$

$$+ C \frac{K_m \nu_m (2K_j + G_j) V_m + K_j \nu_j (2K_m + G_j) V_j}{K_j (2K_m + G_j) + G_j V_m (K_m - K_j)} \qquad (C = 1) \quad 10$$

$$\text{where} \quad K_j = E_j / (2(1 - \nu_j)) \quad \text{and} \quad K_m = E_m / (2(1 - \nu_m))$$

Van Fo Fy

$$\nu_{12} = \nu_m - \frac{4 V_j (\nu_j - \nu_m)(1 - \nu_m) G_m}{(2 - V_j) G_j - V_m G_m}$$

11

Transverse Young's modulus

Shaffer (first)

$$E_{22} = E_j E_m / (E_m V_j + E_j V_m)$$

12

Shaffer (second)

$$E_{22} = \frac{E_m [1 - (1 - E_m/E_j)(0.8247\sqrt{V_j} - V_j)]}{1 - 0.8247\sqrt{V_j}(1 - E_m/E_j)}$$

13

Rabinovich(isotropic)

$$E_{22} = E_j E_m / (E_m V_j + E_j V_m (1 - \nu_m^2))$$

14

Ekvall

$$E_{22} = E_j E_m' / (E_m' V_j + E_j V_m (1 - \nu_m^2))$$

15

$$E_m' = E_m / (1 - 2\nu_m^2)$$

Hashin/Rosen
Whitney

$$E_{22} = \frac{4 K_{23} G_{23}}{K_{23} + G_{23} \left(1 + \frac{4 K_{23} \nu_{12}^2}{E_{11}}\right)}$$

17

$$\text{where} \quad K_{23} = \frac{K_m K_j + G_m (V_m K_m + V_j K_j)}{V_m K_j + V_j K_m + G_m}$$

Author	Expression	Number

Abolinish

$$E_{22} = \frac{E_m E_f (E_m V_m + E_f V_f)}{(E_m V_m + E_f V_f)(E_m V_f + E_f V_m) - (E_f V_m - E_m V_f)^2 V_f V_m} \qquad 18$$

Van Fo Fy

$$\frac{1}{E_{22}} = \frac{(1-V_m^2)}{E_m}\left[\frac{2G_f - G_m}{(2-V_f)G_f - V_m G_m} - \frac{2V_f(G_f - G_m)}{V_f G_f + V_m G_m}\right] \qquad 19$$

Tsai

$$E_{22} = 2\left(1-V_f + (V_f - V_m)V_m\right)\left[(1-C)\frac{K_f(2K_m + G_m) - G_m(K_f - K_m)V_m}{(2K_m + G_m) + 2(K_f - K_m)V_m}\right.$$

$$\left. + C\,\frac{K_f(2K_m + G_f) + G_f(K_m - K_f)V_m}{(2K_m + G_f) - 2(K_m - K_f)V_m}\right] \qquad \begin{array}{l}(C=0)20\\(C=1)21\end{array}$$

where $K_f = E_f/(2(1-V_f))$ and $K_m = E_m/(2(1-V_m))$

Halpin/Tsai

$$E_{22} = E_m\frac{[E_f(1+\zeta V_f) + E_m V_m \zeta]}{E_f V_m + E_m(\zeta + V_f)} \qquad \begin{array}{l}(\zeta=\tfrac{1}{2})22\\(\zeta=1)23\end{array}$$

where ζ = reinforcement factor

Longitudinal shear modulus

Ekvall

$$G_{12} = \frac{G_f G_m}{G_f(1-R) + G_m R\phi} \qquad 24$$

where $R = 4\left(\frac{1-V_m}{\pi}\right)$ and $\phi = \int_0^{\pi/2}\frac{\sin\theta\, d\theta}{\frac{G_m}{G_f} + \sin\theta\left(1 - \frac{G_m}{G_f}\right)}$

Rabinovich(isotropic)

$$G_{12} = \frac{G_f G_m}{G_f V_m + G_m V_f} \qquad 25$$

Abolinish

Hashin/Rosen(random array)

Kilchinski

Van Fo Fy

Whitney(isotropic)

$$G_{12} = G_m\frac{[G_f(1+V_f) + G_m V_m]}{G_f V_m + G_m(1+V_f)} \qquad 26$$

Rabinovich(mean)

$$G_{12} = G_f\sqrt{\frac{G_m V_f}{G_f V_m}}\sqrt{\frac{1+d}{1+b}} \qquad 27$$

where $d = \frac{V_m G_m}{V_f G_f}$ and $b = \frac{V_f G_m}{V_m G_f}$

Author	Expression	Number

Tsai

$$G_{12} = (1-C)\, G_m \, \frac{2G_f - (G_f - G_m)\, V_m}{2G_m + (G_f - G_m)\, V_m}$$

$$+\, C\, G_f \, \frac{(G_f + G_m) - (G_f - G_m)\, V_m}{(G_f + G_m) + (G_f - G_m)\, V_m}$$

$(C=1)$ 28

Halpin/Tsai

$$G_{12} = G_m \, \frac{\left[\, \zeta\, G_m V_m + G_f (1 + \zeta V_f)\,\right]}{G_f V_m + G_m (\zeta + V_f)}$$

$\left(\zeta = \tfrac{1}{2}\right)$ 29
$\left(\zeta = 2\right)$ 30

Hashin/Rosen (hexagonal array)

upper bound

$$G_{12}^{+} = G_m \left(0.907\, M_G + 0.093\right)$$

31

lower bound

$$G_{12}^{-} = \frac{G_m}{\dfrac{0.907}{M_G} + 0.093}$$

32

where

$$M_G = \frac{G_f (1 + 1.103\, V_f) + (1 - 1.103\, V_f)\, G_m}{G_f (1 - 1.103\, V_f) + (1 + 1.103\, V_f)\, G_m}$$

Other relationships

Hashin/Rosen

$$G_{23} = G_m \, \frac{\left[(\alpha + \beta_m V_f)(1 + \rho V_f^3) - 3 V_f V_m^2 \beta_m^2\right]}{(\alpha - V_f)(1 + \rho V_f^3) - 3 V_f V_m^2 \beta_m^2}$$

33

where $\quad \alpha = \dfrac{\left(\dfrac{G_f}{G_m} + \beta_m\right)}{\left(\dfrac{G_f}{G_m} - 1\right)} \quad \beta = \dfrac{1}{(3-4\nu)} \quad \rho = \dfrac{\left(\beta_m - \dfrac{G_f}{G_m}\beta_f\right)}{\left(1 + \dfrac{G_f}{G_m}\beta_f\right)}$

Van Fo Fy

$$G_{23} = V_f\, G_f + V_m\, G_m$$

34

Foye

$$\nu_{21} = V_f\, \nu_f + V_m\, \nu_m \left[\frac{1 + \nu_m - (\nu_{12}\, E_m)/E_{11}}{1 - \nu_m^2 + (\nu_m\, \nu_{12})/E_{11}}\right]$$

35

Hashin/Rosen

36

$$\nu_{21} = \frac{1}{2}\left(\frac{E_{22}}{G_{23}}\right) - 1$$

Author	Expression	Number

Whitney

$$E_{11} = E_{f_1} V_f + E_m V_m + \frac{2(\nu_{f_1} - \nu_m)^2 V_m V_f}{L_f V_m + L_m V_f + 1 + \nu_m}$$

37

where $L_f = \left[1 - \nu_{f_2} - 2 \left(\frac{E_{f_2}}{E_{f_1}} \right) \nu_{f_1}^2 \right]$ and $L_m = \left[1 - \nu_m - 2\nu_m^2 \right]$

Rabinovich

$$E_{11} = E_{f_1} V_f \frac{(1 - \nu_{12}\nu_{21})}{(1 - \nu_{f_1}\nu_{f_2})} + E_m V_m \frac{(1 - \nu_{12}\nu_{21})}{(1 - \nu_m^2)}$$

38

Whitney

$$\nu_{12} = \nu_m - \frac{2(\nu_m - \nu_{f_1})(1 - \nu_m^2) V_f}{(\nu_m L_f + V_f L_m + 1 + \nu_m) E_m}$$

39

where $L_f = \left[1 - \nu_{f_2} - 2 \left(\frac{E_{f_2}}{E_{f_1}} \right) \nu_{f_1}^2 \right]$ $L_m = \left[1 - \nu_m - 2\nu_m^2 \right]$

Rabinovich

$$\nu_{12} = \frac{E_{f_1} V_f \nu_{f_2} (1 - \nu_m^2) + E_m V_m \nu_m (1 - \nu_{f_1}\nu_{f_2})}{E_{f_2} V_f (1 - \nu_m^2) + E_m V_m (1 - \nu_{f_1}\nu_{f_2})}$$

40

Whitney

$$E_{22} = \frac{2 K_{23} (1 - \nu_{23}) E_{11}}{E_{11} + 4 K_{23} \nu_{12}^2}$$

41

where $K_{23} = \frac{(K_f + G_m) K_m + (K_f - K_m) G_m V_f}{(K_f + G_m) - (K_f - K_m) V_f}$ and $\nu_{23} = \nu_{f_2} V_f + \nu_m V_m$

$K_f = \frac{E_{f_1} E_{f_2}}{2[(1 - \nu_{f_2}) E_{f_1} - 2 E_{f_2} \nu_{f_1}^2]}$

Rabinovich

$$E_{22} = E_{11} \frac{\left[E_{f_2} V_f (1 - \nu_m^2) + E_m V_m (1 - \nu_{f_1}\nu_{f_2}) \right]}{E_{f_1} V_f (1 - \nu_m^2) + E_m V_m (1 - \nu_{f_1}\nu_{f_2})}$$

42

Rabinovich

$$G_{12} = G_f V_f + G_m V_m$$

43

Table 7 Longitudinal Young's modulus/fibre volume fraction

Numbers at the top of the columns refer to expressions in table 6.

V_f	1	2	3	4	5	
0	3.326	4.571	2.993	3.320	3.320	
0.2	17.816	18.825	16.047	17.834	17.997	
0.4	32.312	33.062	29.084	32.339	32.503	
0.6	46.808	47.319	42.138	46.833	46.954	Units GPa
0.8	61.304	61.558	55.177	61.320	61.383	
1.0	75.800	75.800	68.221	75.800	75.800	

Table 8 Major Poisson's ratio/fibre volume fraction

V_f	6	7	8	9	10	11	
0	0.370	0.370	o.370	0.370	0.370	0.370	
0.2	0.338	0.332	0.282	0.333	0.279	0.372	
0.4	0.306	0.298	0.248	0.298	0.246	0.374	
0.6	0.274	0.266	0.229	0.267	0.236	0.377	Units GPa
0.8	0.242	0.237	0.218	0.237	0.217	0.380	
1.0	0.210	0.210	0.210	0.210	0.210	0.385	

Table 9 Transverse Young's modulus/fibre volume fraction

V_f	12	13	14	15	17	
0	3.32	3.32	3.85	5.30	5.87	
0.2	4.11	4.32	4.75	6.51	7.85	
0.4	5.38	5.85	6.20	8.44	10.96	
0.6	7.79	8.28	8.94	11.99	16.47	Units GPa
0.8	14.13	11.93	15.99	20.70	28.79	
1.0	75.80	-	75.80	75.80	79.50	

V_f	18	20	21	22	23
0	3.32	3.32	3.32	3.32	3.32
0.2	4.61	4.47	7.51	4.47	5.44
0.4	6.10	6.34	13.87	6.30	8.72
0.6	8.84	9.81	23.65	9.69	14.44
0.8	15.87	18.47	40.75	18.15	26.93
1.0	75.80	75.80	75.80	75.80	75.80

Units GPa

Table 10 Shear modulus/fibre volume fraction

Units GPa

V_f	25	26	27	28	29	30	31	32
0	1.21	1.21	1.21	1.21	1.21	1.21	1.21	1.21
0.2	1.49	1.76	3.30	1.50	1.63	1.99	1.77	1.75
0.4	1.97	2.63	5.13	1.97	2.31	3.23	2.72	2.52
0.6	2.86	4.24	7.46	2.87	3.58	5.40	4.69	3.89
0.8	5.25	8.13	11.57	5.27	6.80	10.30	71.51	11.31
1.0	31.32	31.32	31.32	31.32	31.32	31.32	-27.21	20.51

Tables 11-14 Variation of longitudinal modulus with constituent properties

Table 11 Variation of E_{11} with fibre modulus, E_f.

E_f	1	2	3	4	5
0	1.66	2.29	1.49	1.66	1.666
20	11.66	12.29	10.49	11.66	11.667
40	21.66	22.29	19.49	21.66	21.667
60	31.66	32.29	28.49	31.66	31.668
80	41.66	42.29	37.49	41.66	51.669

Units GPa

Table 12 Variation of E_{11} with matrix modulus, E_m.

E_m	1	2	3	4	5
0	37.950	37.887	34.113	37.930	37.930
1	38.365	38.582	34.557	38.358	38.364
2	38.907	39.209	35.012	38.907	38.910
3	39.472	39.894	35.458	39.474	39.469
4	39.950	40.664	35.912	39.950	39.950

Units GPa

Table 13 Variation of E_{11} with fibre Poisson's ratio, ν_f.

ν_f	4	5
0	39.720	41.903
0.1	39.654	41.009
0.2	39.593	40.052
0.3	39.556	39.644
0.4	39.561	39.576

Units GPa

Table 14 Variation of E_{11} with matrix Poisson's ratio, ν_m

ν_m	2	4	5
0	39.554	39.608	40.312
0.1	39.586	39.567	39.767
0.2	39.701	39.561	39.704
0.3	39.925.	39.560	39.623
0.4	40.344.	39.558	39.563

Units GPa

Tables 15-18 Variation of Major Poisson's ratio with constituent properties

Table 15 Variation of ν_{12} with fibre modulus, E_f

E_f	7	8	9	10
0	0.290	0.290	0.369	0.0
20	0.265	0.284	0.284	0.264
40	0.246	0.282	0.283	0.249
60	0.237	0.281	0.282	0.240
80	0.232	0.281	0.282	0.235

Units GPa

Table 16 Variation of ν_{12} with matrix modulus, E_m.

E_m	7	8	9	10
0	0.210	0.210	0.0	0.210
1	0.220	0.267	0.283	0.220
2	0.228	0.277	0.284	0.277
3	0.235	0.281	0.284	0.233
4	0.241	0.283	0.284	0.239

Units GPa

Table 17 Variation of ν_{12} with fibre Poisson's ratio, ν_f

ν_f	6	7	8	9	10
0	0.185	0.067	0.166	0.167	0.057
0.1	0.235	0.148	0.221	0.222	0.142
0.2	0.285	0.229	0.276	0.277	0.277
0.3	0.335	0.311	0.331	0.332	0.311
0.4	0.385	0.395	0.387	0.386	0.395

Units GPa

Table 18 Variation of ν_{12} with matrix Poisson's ratio, ν_m

ν_m	6	7	8	9	10
0	0.105	0.193	0.138	0.0	0.186
0.1	0.155	0.200	0.170	0.164	0.197
0.2	0.205	0.213	0.207	0.206	0.209
0.3	0.255	0.220	0.248	0.249	0.223
0.4	0.305	0.250	0.301	0.296	0 242

Units GPa

Tables 19-22 Variation of transverse modulus with constituent properties.

Table 19 Variation of E_{22} with fibre modulus, E_f.   Units GPa

E_f	12	13	14	15	17	18
0	0	3.32	0	0	1.109	0
20	5.694	6.012	6.455	8.371	9.823	6.214
40	6.137	6.602	7.024	9.353	11.558	6.866
60	6.291	6.815	7.232	9.738	12.295	7.113
80	6.365	6.938	7.346	9.932	12.704	7.258

Table 19 continued.

E_f	20	21	22	23	
0	0.592	0	0.830	1.238	
20	6.537	7.469	6.438	7.859	
40	7.314	11.252	7.236	9.775	Units GPa
60	7.623	14.883	7.556	10.689	
80	7.785	18.478	7.728	11.226	

Table 20   Variation of E_{22} with matrix modulus, E_m.   Units GPa

E_m	12	13	14	15	17	18
0	0	0	0	0	0	0
1	1.974	2.201	2.282	3.126	4.362	2.272
2	3.897	4.335	4.489	6.126	8.473	4.459
3	5.772	6.235	6.647	9.007	12.350	6.562
4	7.574	8.228	8.735	11.110	16.010	8.601

Table 20   Variation of E_{22} with matrix modulus, E_m (continued)

E_m	20	21	22	23	
0	0	13.453	0	0	
1	.2.456	14.889	2.442	3.777	
2	4.810	16.299	4.774	7.161	Units GPa
3	7.060	17.681	7.005	10.216	
4	9.230	17.949	9.141	12.994	

Table 21   Variation of E_{22} with fibre Poisson's ratio, ν_f

ν_f	17	18	20	21	
0	8.381	6.374	6.996	20.707	
0.1	8.518	6.378	7.051	19.926	
0.2	9.090	6.502	7.327	19.148	Units GPa
0.3	10.715	6.760	7.493	18.532	
0.4	15.937	7.185	7.921	17.961	

Table 22   Variation of E_{22} with matrix Poisson's ratio, ν_m

ν_m	17	18	20	21
0	10.332	7.276	9.040	20.105
0.1	10.330	7.251	8.277	19.167
0.2	10.327	7.227	7.802	18.208
0.3	10.293	7.204	7.320	17.216
0.4	10.254	7.180	6.829	16.196

Units GPa

Tables 23,24 Variation of shear modulus with constituent properties.

Table 23   Variation of G_{12} with fibre modulus, E_f.   Units GPa

E_f	25	26	27	28	29	30	31	32
0	0	0.403	0	0	0.302	0.484	1.005	1.009
20	2.111	2.645	3.155	3.780	2.408	2.998	3.470	3.103
40	2.210	3.049	4.463	6.560	2.677	3.673	3.674	3.244
60	2.307	3.218	5.478	9.322	2.783	3.985	3.750	3.297
80	2.335	3.311	6.314	12.083	2.839	4.166	3.789	3.333

Table 24   Variation of G_{12} with matrix modulus, E_m.   Units GPa

E_m	25	26	27	28	29	30	31	32
0	0	0	0	10.439	0	0	0	0
1	0.722	1.062	3.285	10.763	0.894	1.388	1.139	1.000
2	1.425	2.060	4.770	11.084	1.749	2.642	2.187	1.949
3	2.116	3.008	5.757	11.402	2.576	3.793	3.202	2.855
4	2.790	3.924	6.577	11.718	3.369	4.847	4.139	3.725

Whitney's predicted composite properties assuming anisotropic fibres

The predicted values are based on expressions 37, 39, 41 and 26 in table 6.

Table 25 Variation of E_{11}, E_{22}, G_{12} and ν_{12} with fibre volume fraction

$E_{f1}/E_{f2} = 1$ (fibre assumed isotropic)

V_f	E_{11}	ν_{12}	E_{22}	G_{12}
0	3.32	0.370	3.401	1.21
0.2	42.656	0.371	7.199	1.909
0.4	81.992	0.372	10.207	2.753
0.6	121.328	0.373	15.953	4.562
0.8	160.664	0.374	30.057	9.511
1.0	200	0.375	198.734	74.069

Units GPa

Table 26 Variation of E_{11}, E_{22}, G_{12} and ν_{12} with fibre volume fraction

$E_{f1}/E_{f2} = 10$

V_f	E_{11}	ν_{12}	E_{22}	G_{12}
0	3.32	0.370	3.401	1.21
0.2	42.656	0.371	6.963	1.617
0.4	81.992	0.372	9.051	2.187
0.6	121.328	0.373	11.608	3.047
0.8	160.664	0.374	15.091	4.489
1.0	200	0.375	20.014	7.409

Units GPa

Table 27 Variation of E_{11}, E_{22}, G_{12} and ν_{12} with fibre volume fraction

$$E_{f1/E_{f2}} = 20$$

V_f	E_{11}	ν_{12}	E_{22}	G_{12}
0	3.32	0.370	3.401	1.21
0.2	42.656	0.370	6.286	1.483
0.4	81.992	0.372	7.255	1.826
0.6	121.328	0.373	8.134	2.268
0.8	160.664	0.374	9.047	2.862
1.0	200	0.375	9.979	3.700

Units GPa

Table 28 Variation of E_{11}, E_{22}, G_{12} and ν_{12} with fibre volume fraction

$$E_{f1/E_{f2}} = 40$$

V_f	E_{11}	ν_{12}	E_{22}	G_{12}
0	3.32	0.370	3.395	1.21
0.2	42.656	0.371	5.910	1.315
0.4	81.992	0.372	5.419	1.431
0.6	121.328	0.373	5.298	1.557
0.8	160.664	0.374	5.154	1.696
1.0	200	0.375	5.000	1.850

Units GPa

Rabinovich's predicted composite properties assuming anisotropic fibres

The predicted values are based on expressions 38,40,42 and 43 in table 6.

Table 29 Variation of E_{11}, E_{22}, G_{12} and ν_{12} with fibre volume fraction.

V_f	E_{11}	ν_{12}	E_{22}	G_{12}
0	3.32	0.370	3.32	1.21
0.2	41.206	0.371	41.206	15.782
0.4	81.305	0.372	81.305	30.354
0.6	121.328	0.373	121.328	44.926
0.8	161.665	0.374	161.665	59.498
1.0	201.702	0.375	201.702	74.071

Units GPa

$$E_{f1/E_{f2}} = 1$$

Table 30 Variation of E_{11}, E_{22}, G_{12} and ν_{12} with fibre volume fraction.

V_f	E_{11}	ν_{12}	E_{22}	G_{12}
0	3.32	0.370	3.32	1.21
0.2	41.206	0.312	6.978	2.456
0.4	81.305	0.305	10.285	3.689
0.6	121.328	0.304	13.498	4.924
0.8	161.665	0.303	16.630	6.168
1.0	201.702	0.302	20.00	7.407

Units GPa

$E_{f1}/E_{f2} = 10$

Table 31 Variation of E_{11}, E_{22}, G_{12} and ν_{12} with fibre volume fraction.

V_f	E_{11}	ν_{12}	E_{22}	G_{12}
0	3.32	0.370	3.32	1.21
0.2	41.206	0.362	5.011	1.708
0.4	81.305	0.357	6.271	2.206
0.6	121.328	0.354	7.517	2.704
0.8	161.665	0.352	8.759	3.202
1.0	201.702	0.363	10.00	3.700

Units GPa

$E_{f1}/E_{f2} = 20$

Table 32 Variation of E_{11}, E_{22}, G_{12} and ν_{12} with fibre volume fraction.

V_f	E_{11}	ν_{12}	E_{22}	G_{12}
0	3.32	0.370	3.32	1.21
0.2	41.206	0.365	4.035	1.338
0.4	81.305	0.361	4.288	1.466
0.6	121.328	0.357	4.522	1.594
0.8	161.665	0.353	4.765	1.722
1.0	201.702	0.350	5.00	1.850

Units GPa

$E_{f1}/E_{f2} = 40$
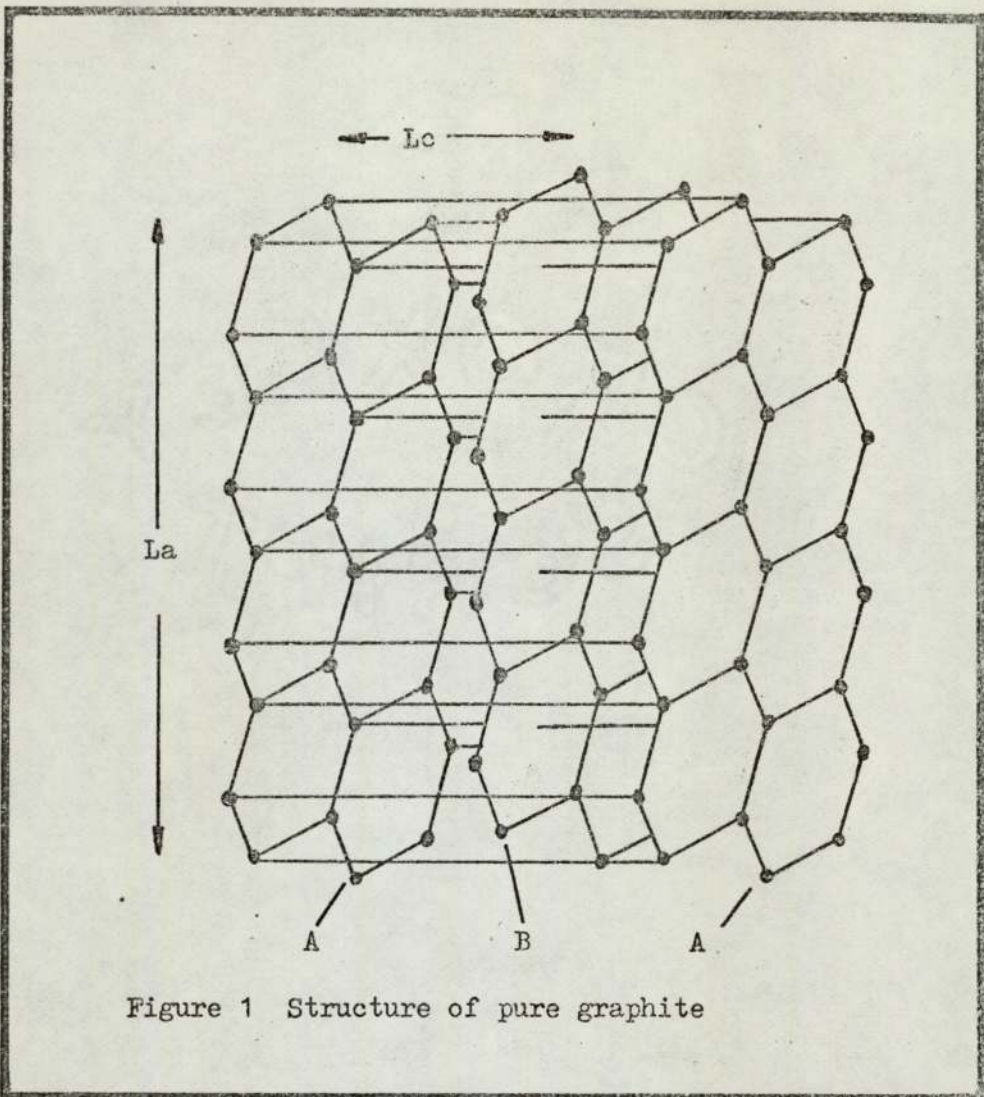
Figure 1   Structure of pure graphite
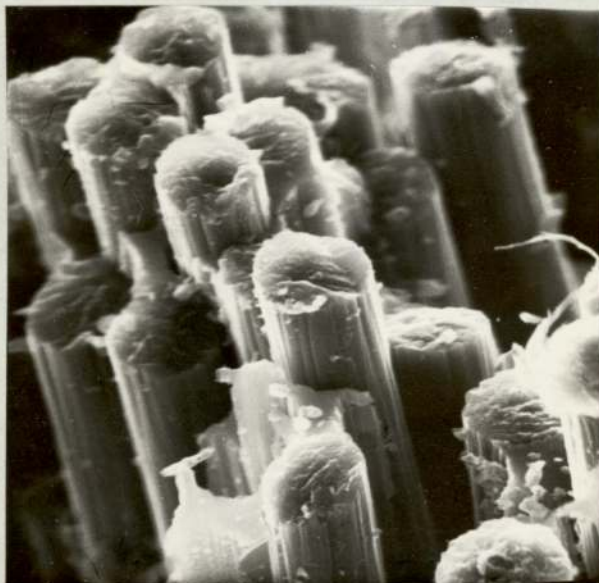
Figure 2   Fractured carbon fibres ✕2400
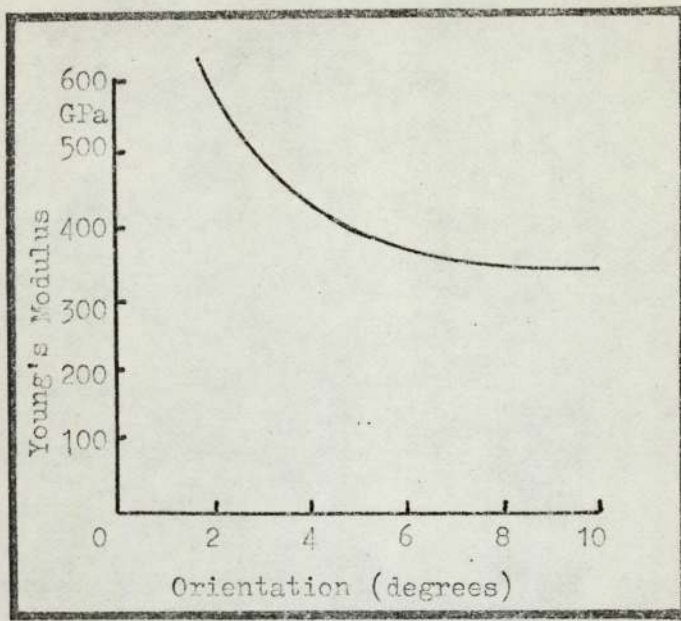
Figure 13 Modulus/orientation.
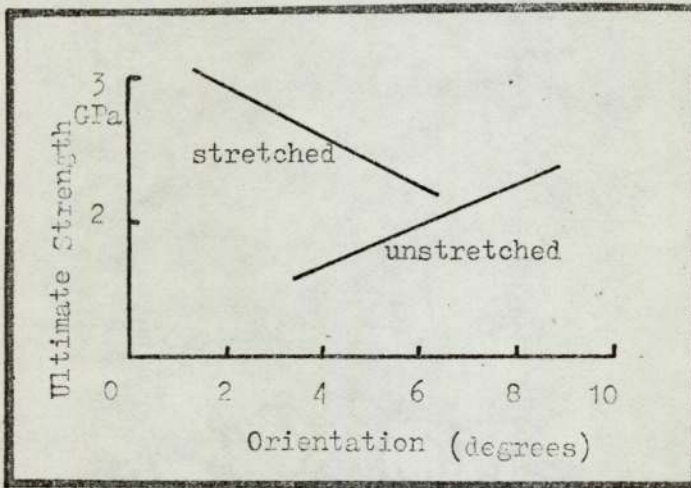
Figure 14 Strength/orientation
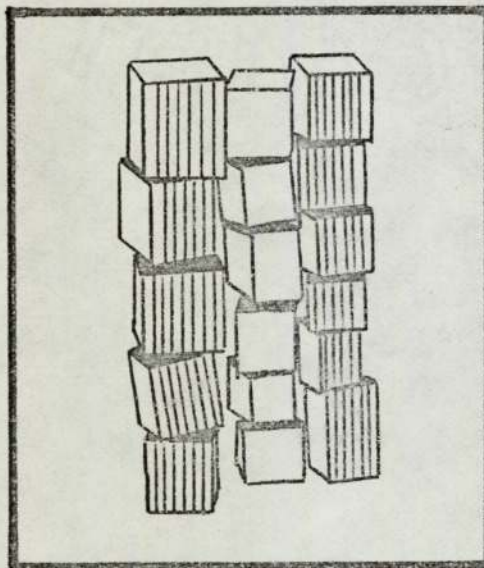
Figure 15 Schematic model of carbon fibre put forward by
Johnson and Tyson.
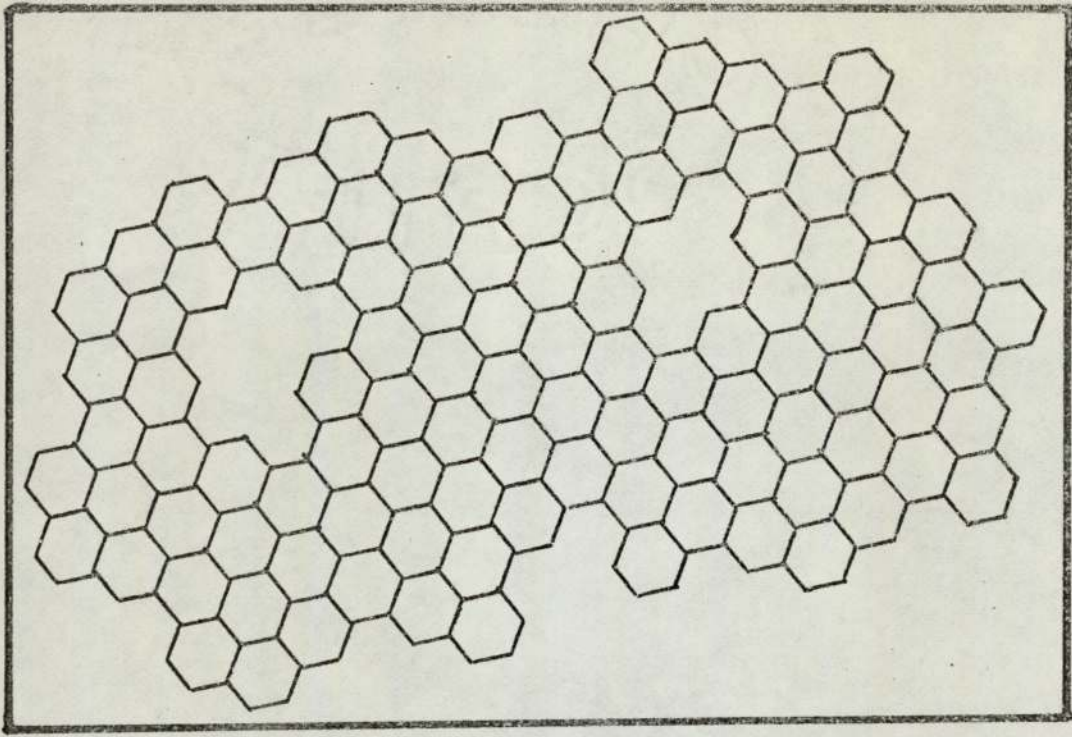
Figure 16 Schematic representation of section of ribbon.
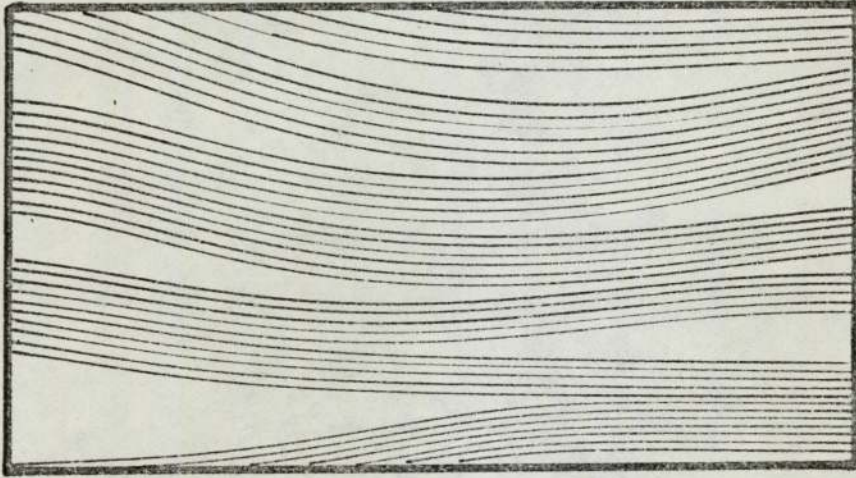
Figure 17 Schematic representation   Figure 18 Schematic representation
of section of fibrils   of branched fibrils

Schematic plan view of fibril.
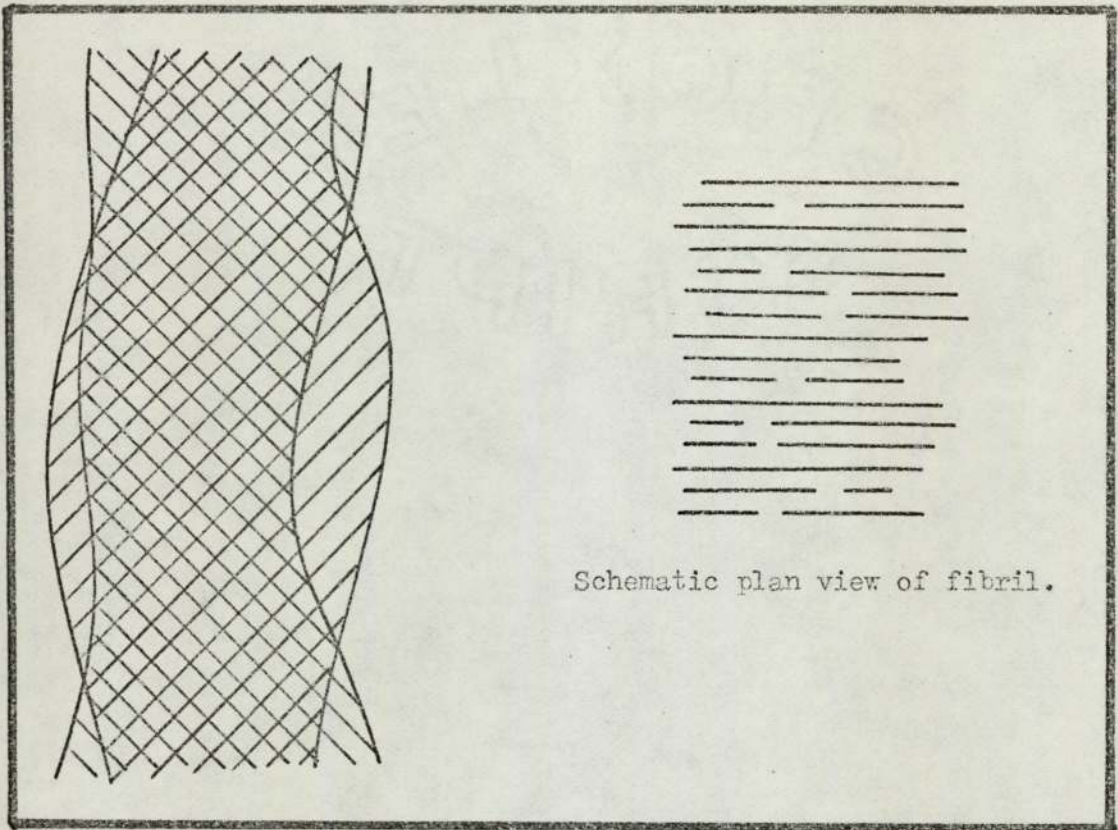
Figure 19. Schematic representation of two parallel ribbons
with irregular edges.

Figure 20   Carbon fibre orientation/modulus
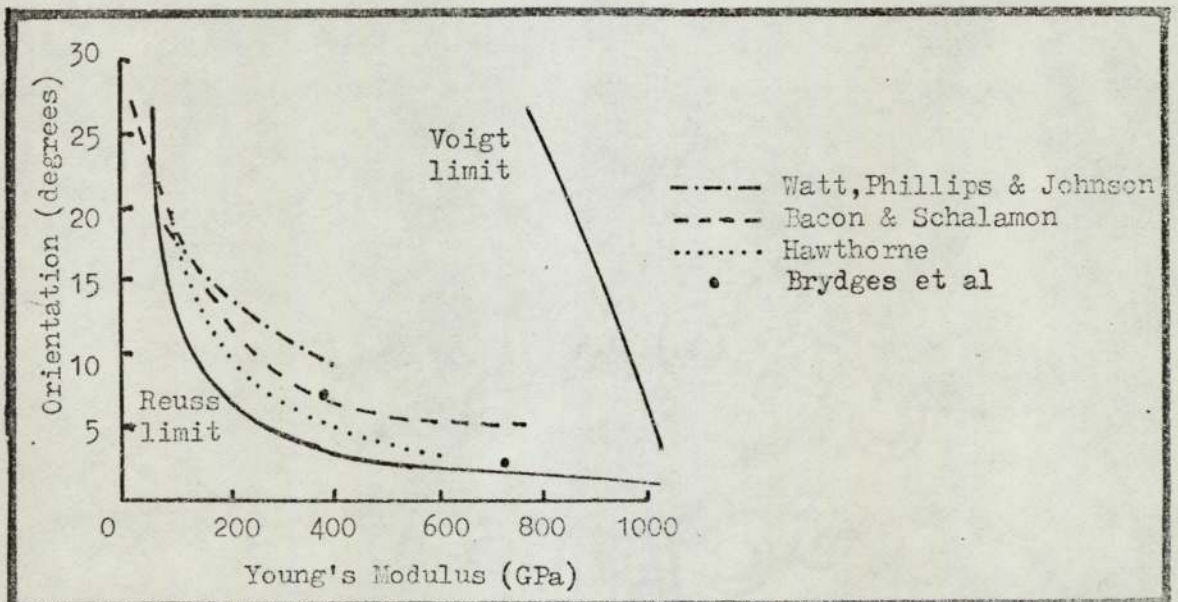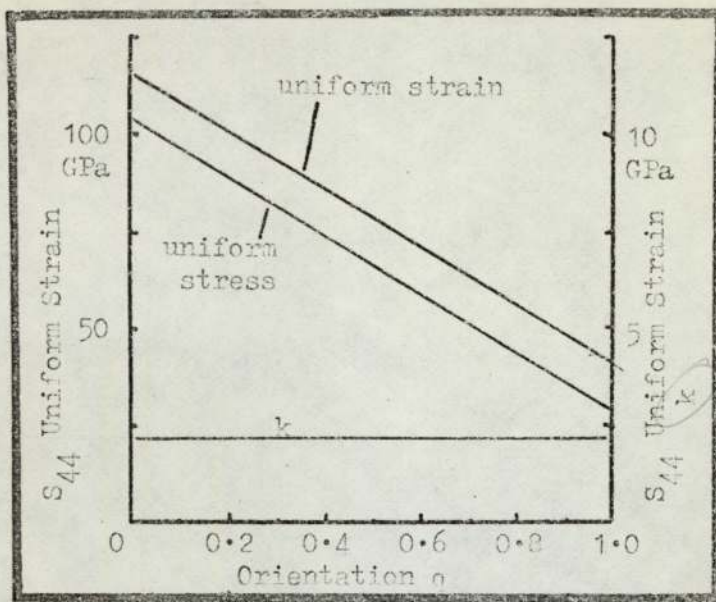
Figure 21 S_{44} and k as a function of orientation q.
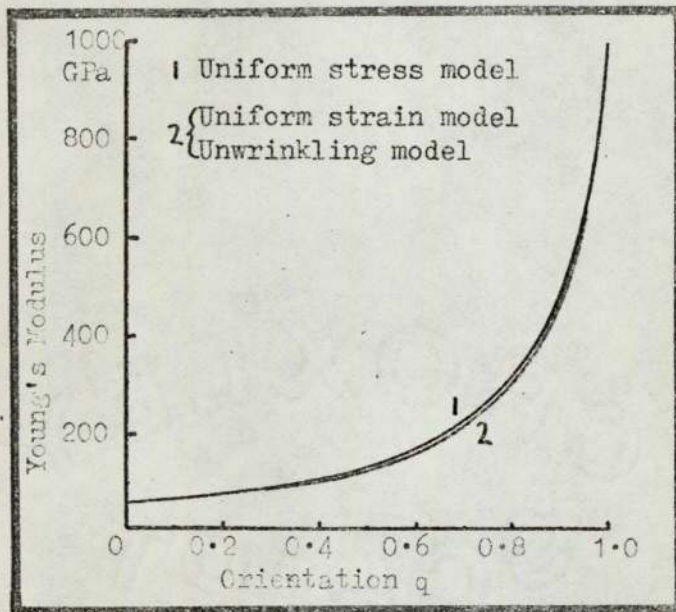
Figure 22 Modulus as a function of orientation q.
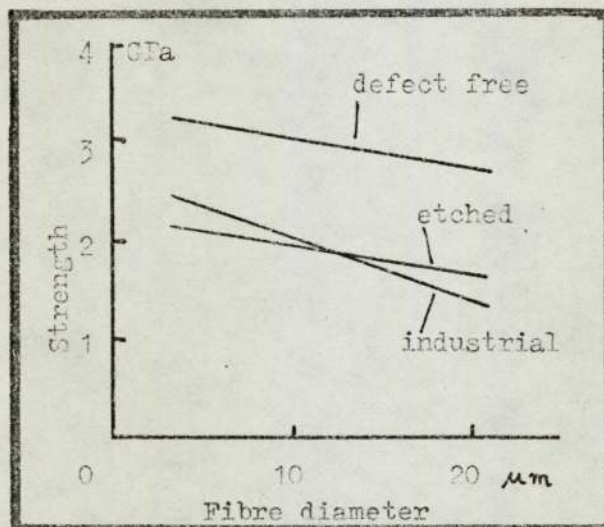
Figure 24 Strength/fibre diameter for glass fibres.
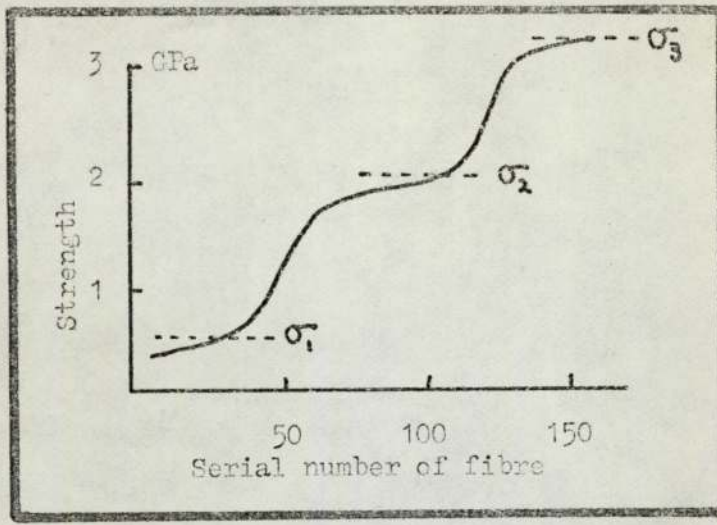
Figure 25 Glass fibre strength distribution.
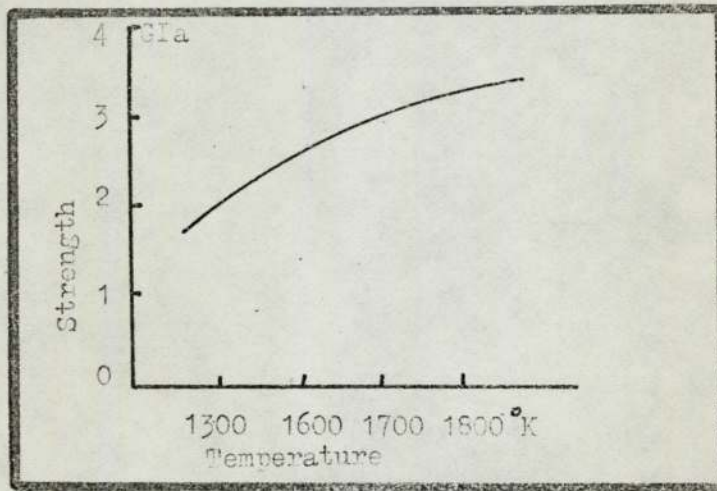
Figure 26 Effect of bushing temperature.
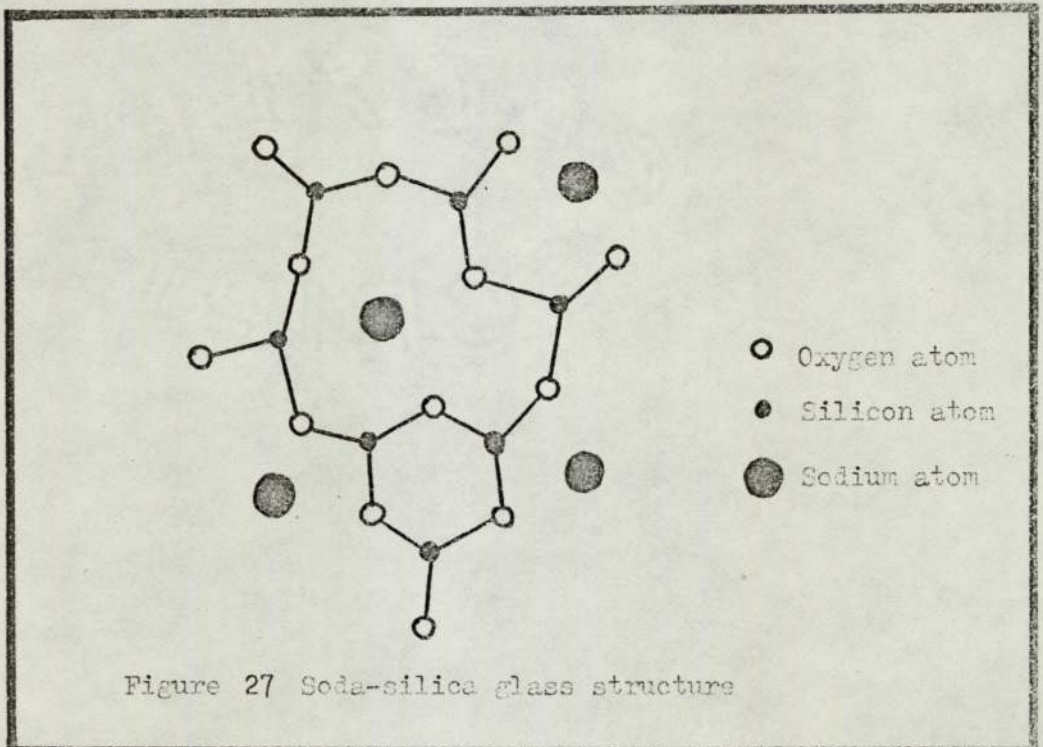
Figure 27 Soda-silica glass structure
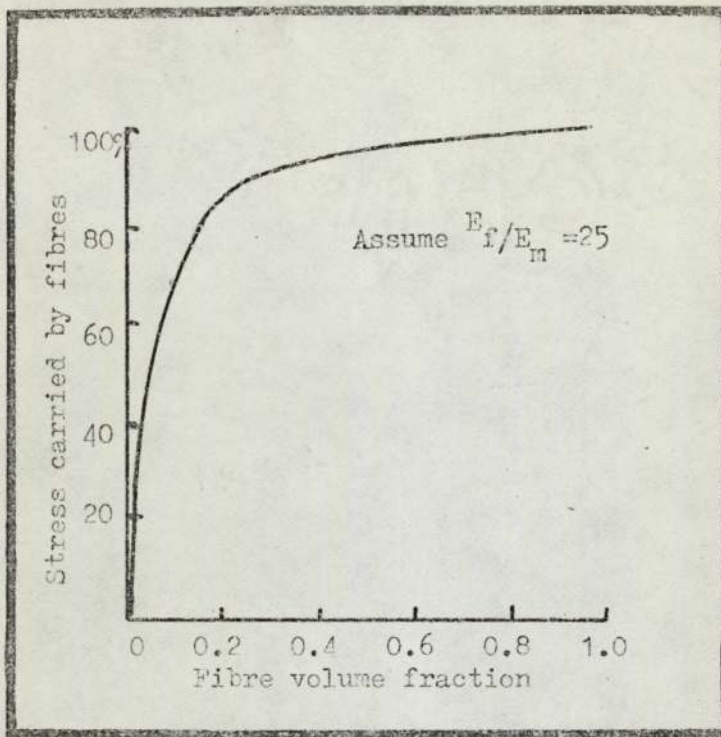
Figure 28   Stress in a glass fibre composite.
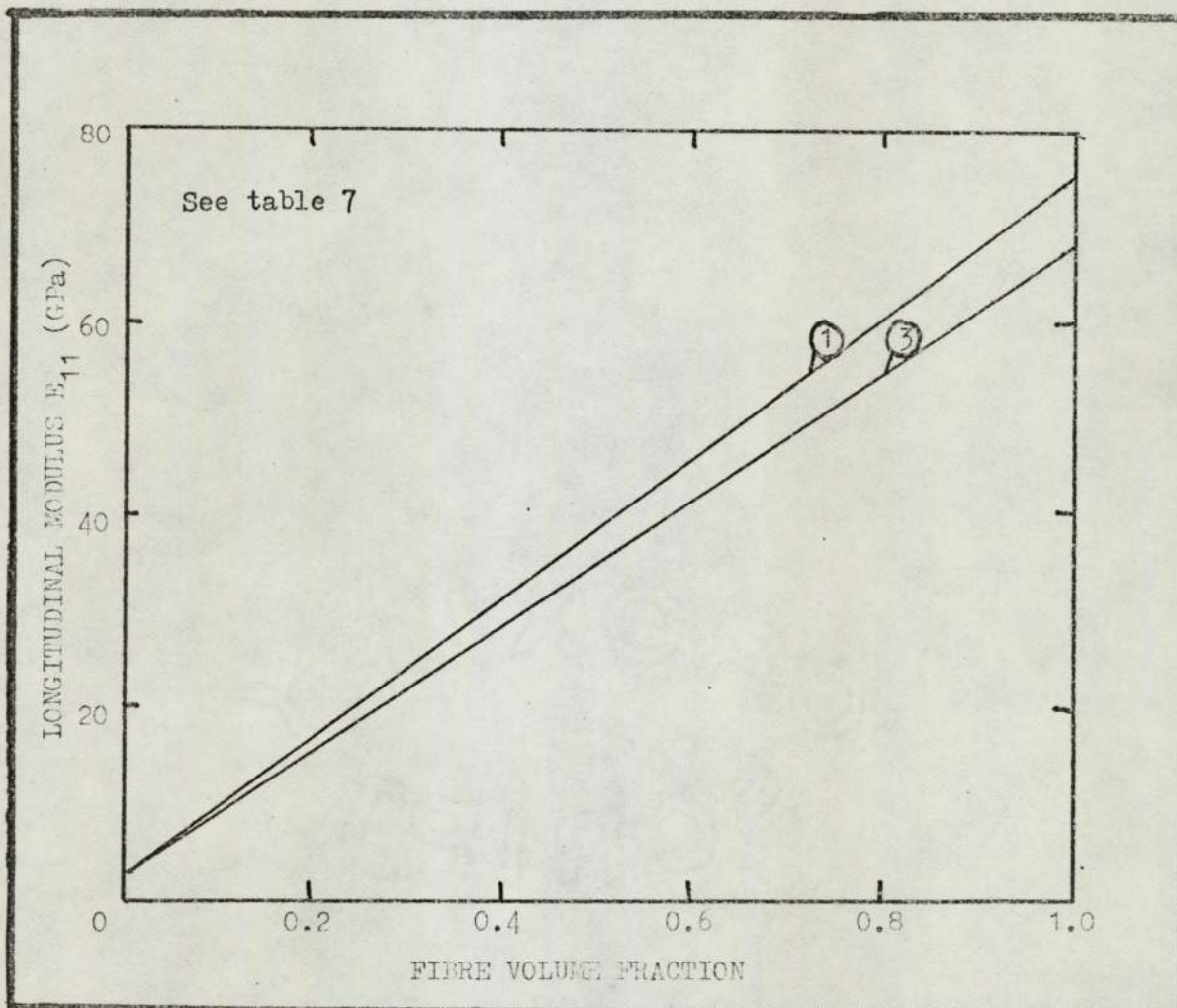
Figure 29   Longitudinal modulus/fibre volume fraction.

-134-
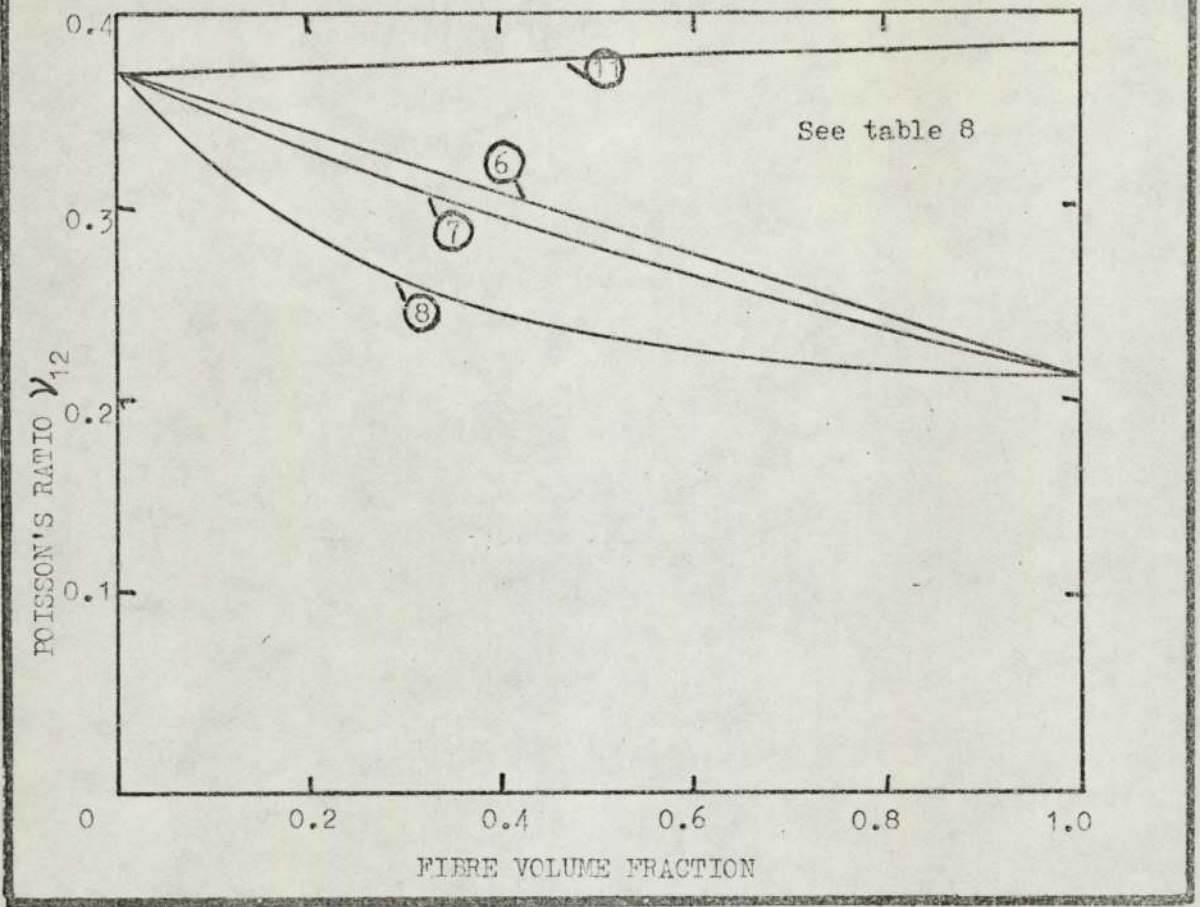
Figure 30 Poisson's ratio/fibre volume fraction.
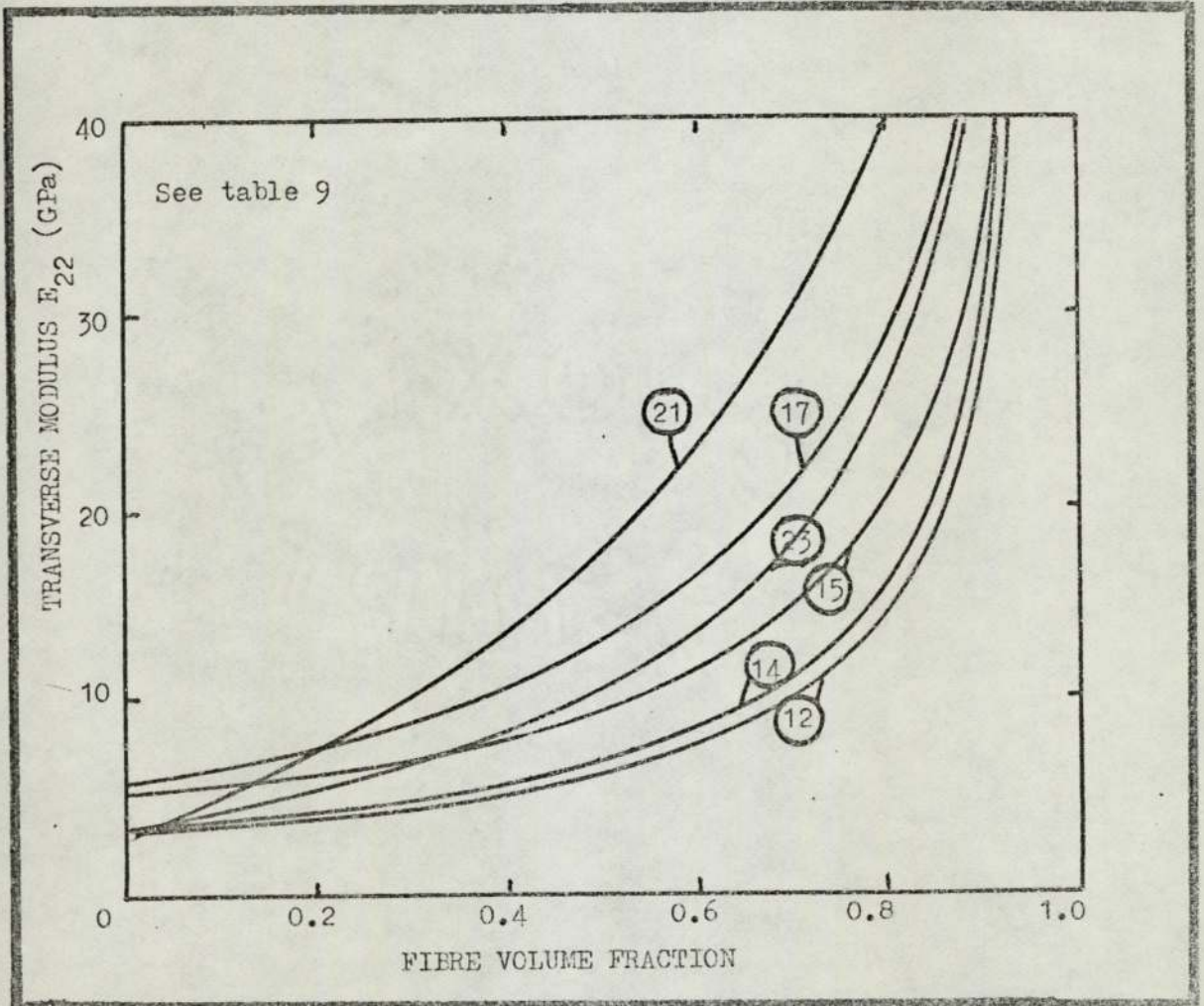
Figure 31 Transverse modulus/fibre volume fraction.
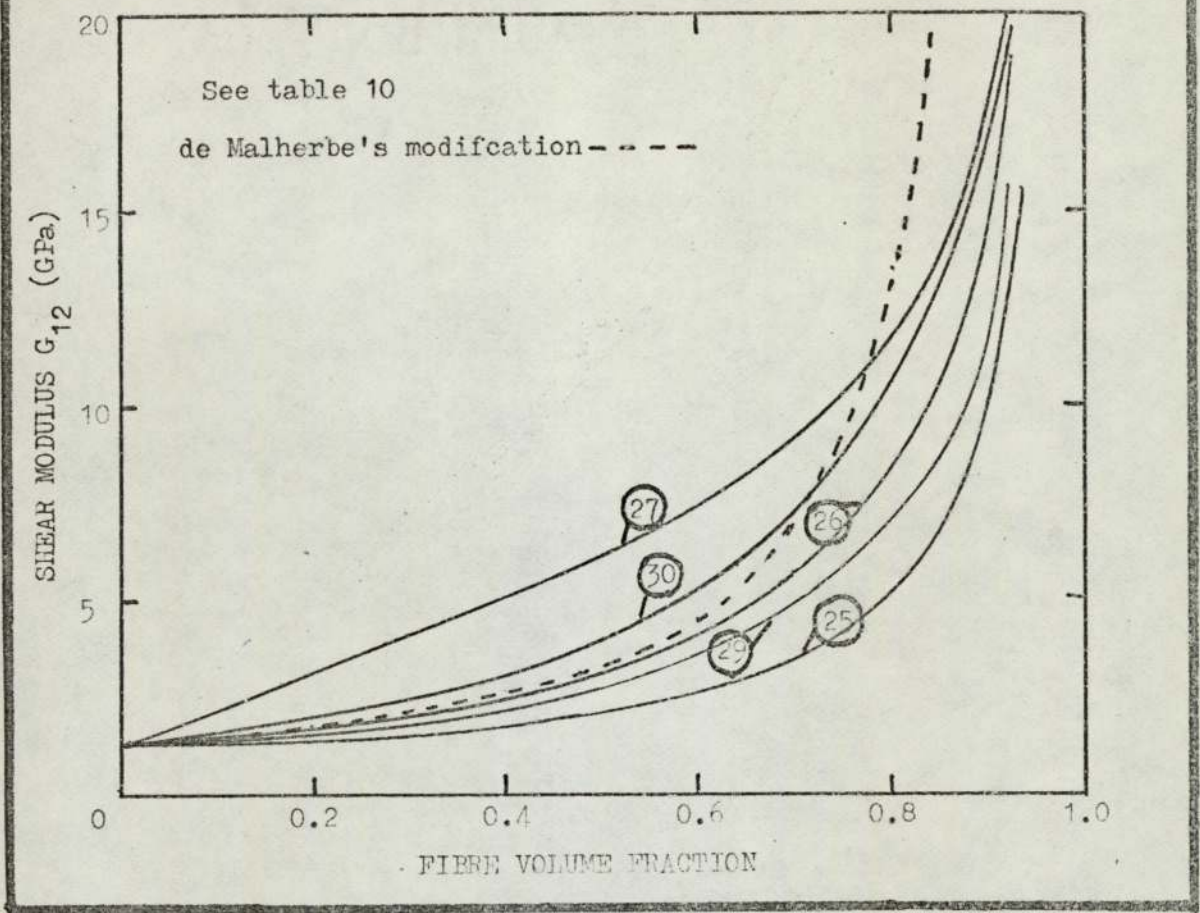
Figure 32 Shear modulus/fibre volume fraction.
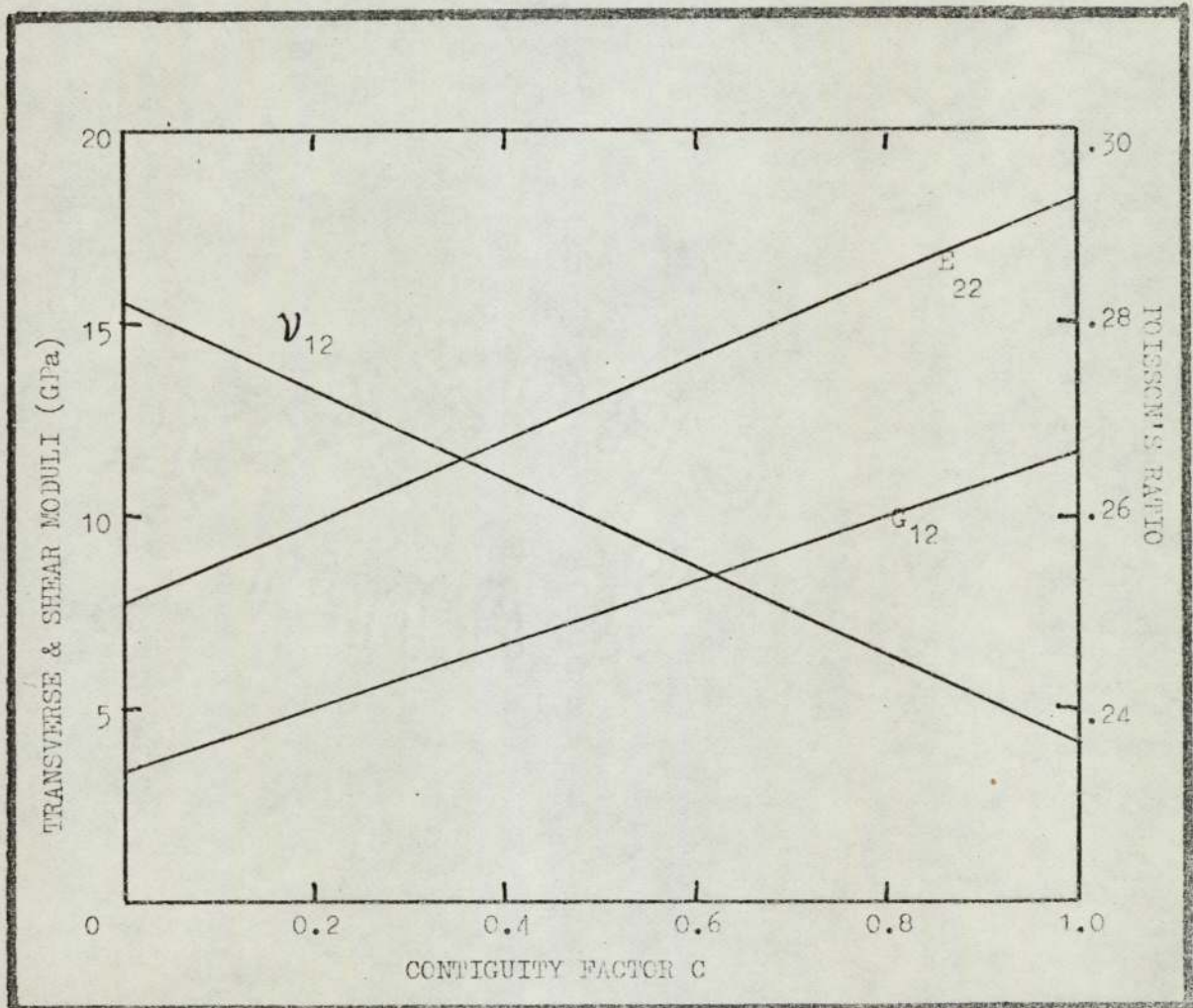
Figure 33 Variation of the contiguity factor.
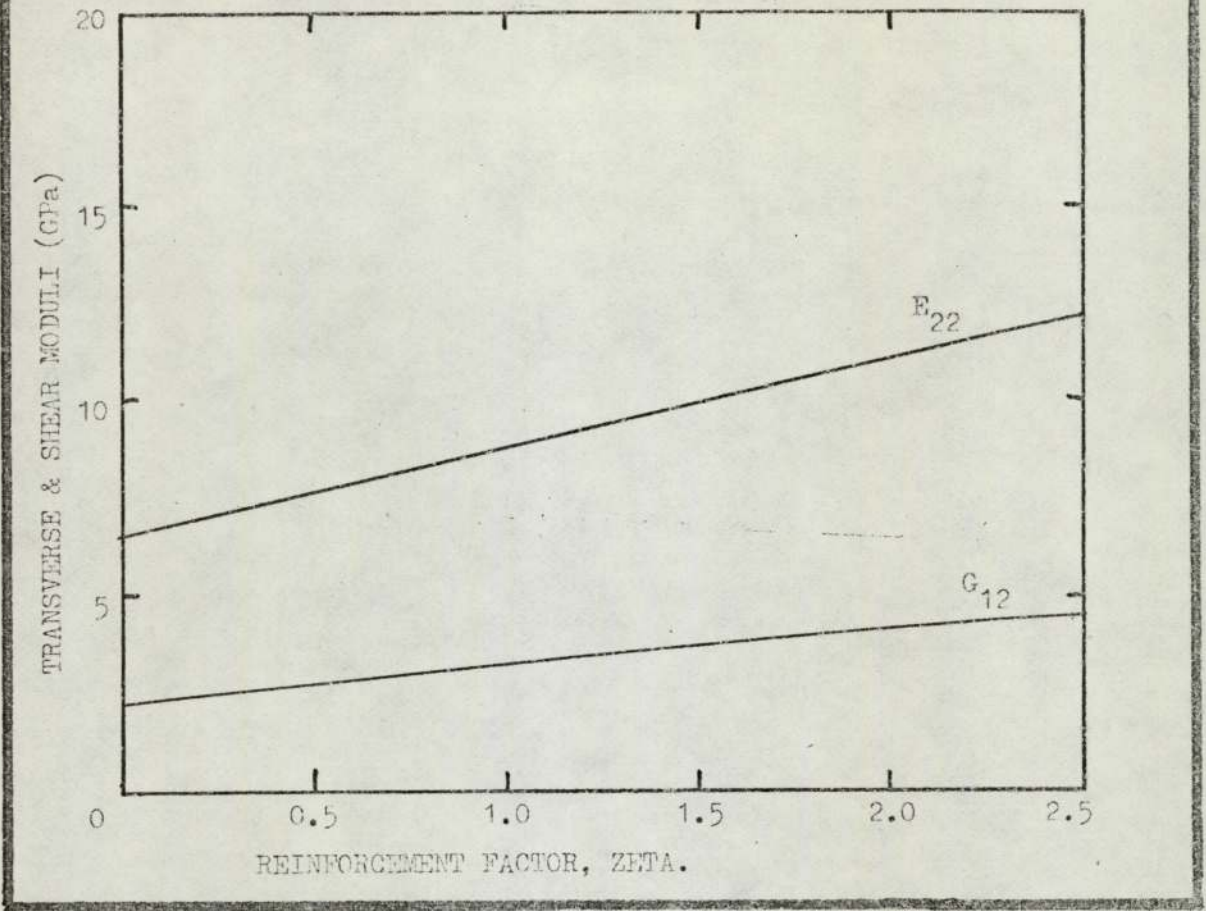
Figure 34 Variation of the reinforcement factor.
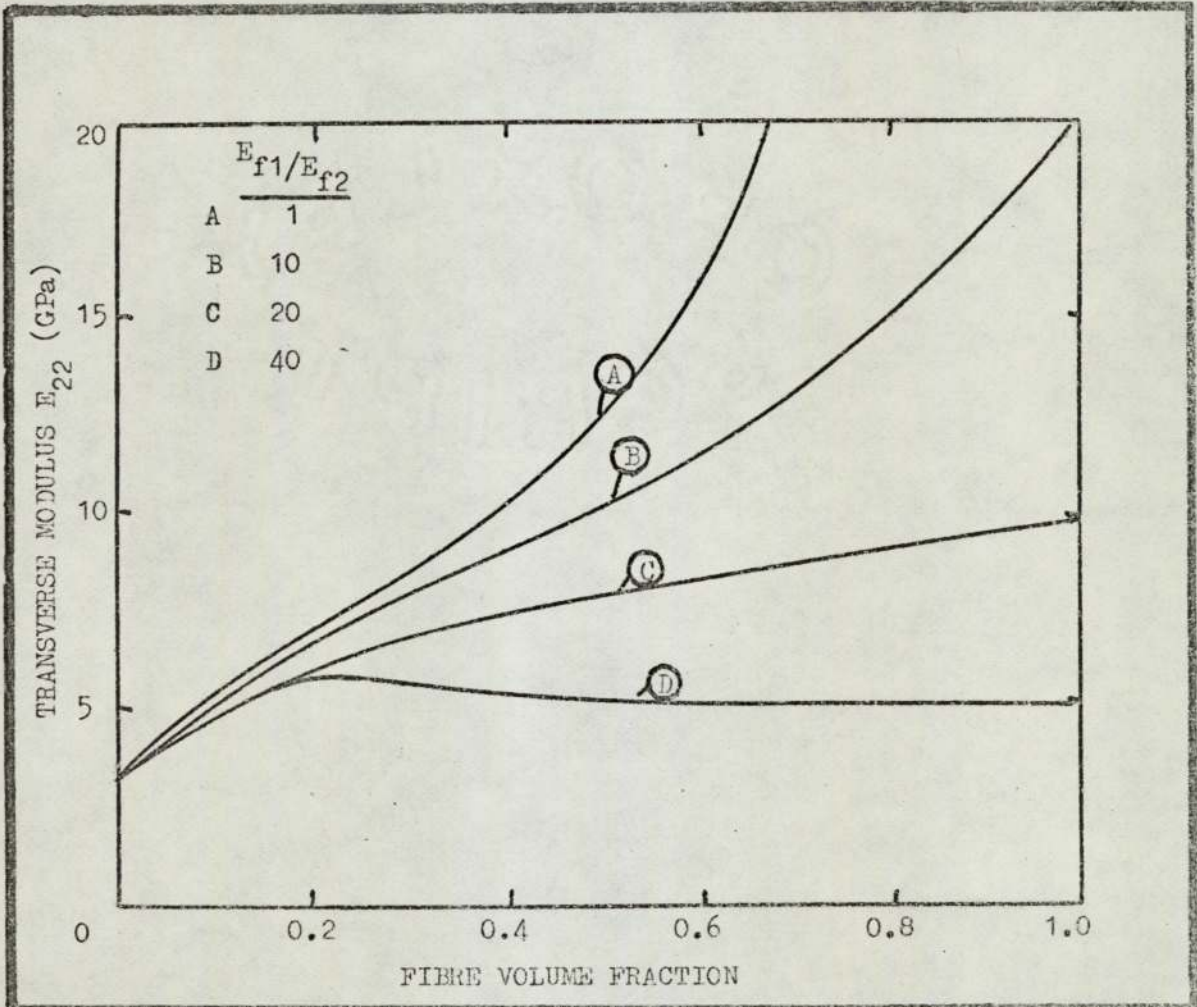
Figure 35 Whitney's transverse modulus for anisotropic fibres.

-137-
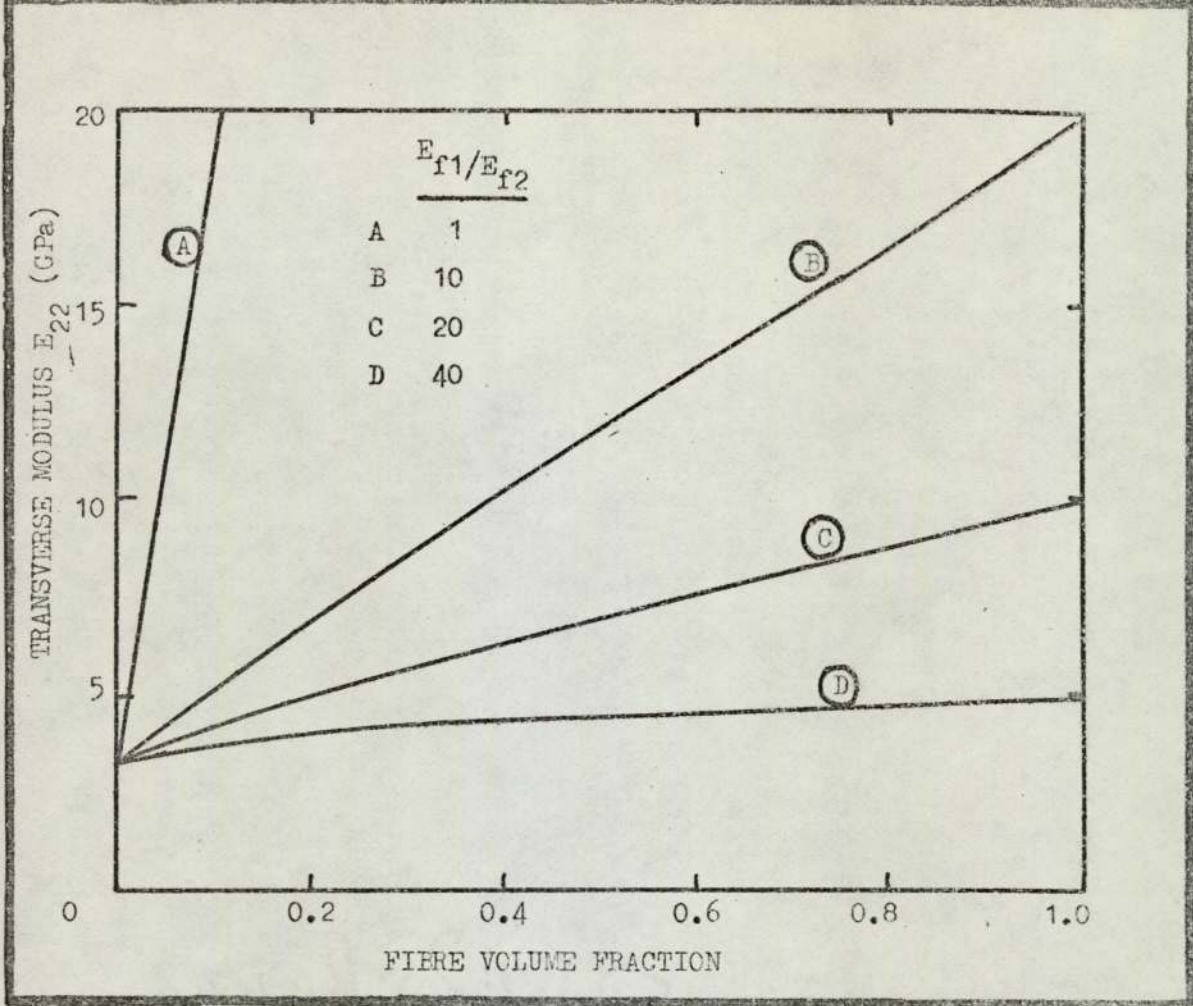
Figure 36 Rabinovich's transverse modulus for anisotropic fibres.
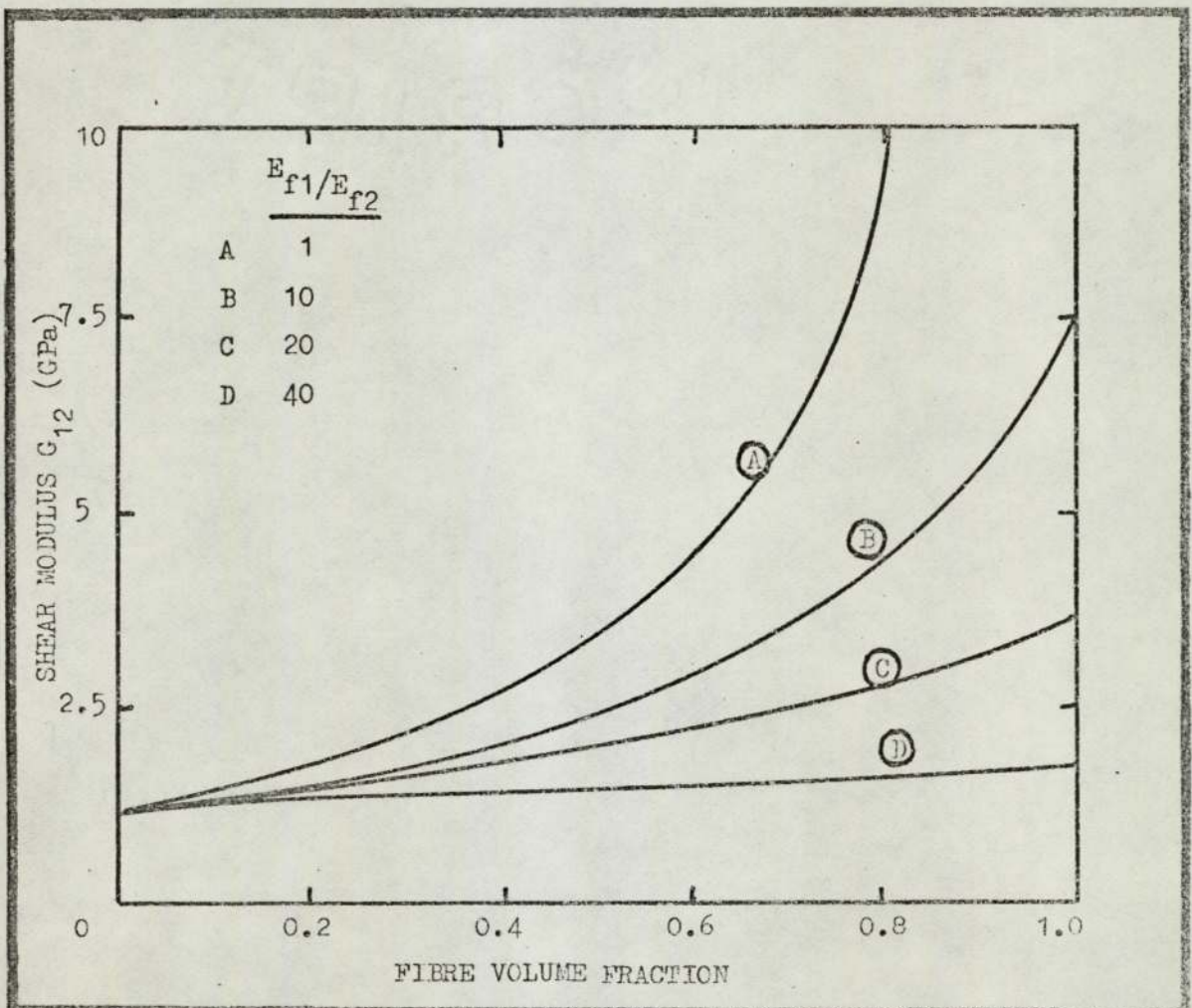
Figure 37 Whitney's shear modulus for anisotropic fibres.
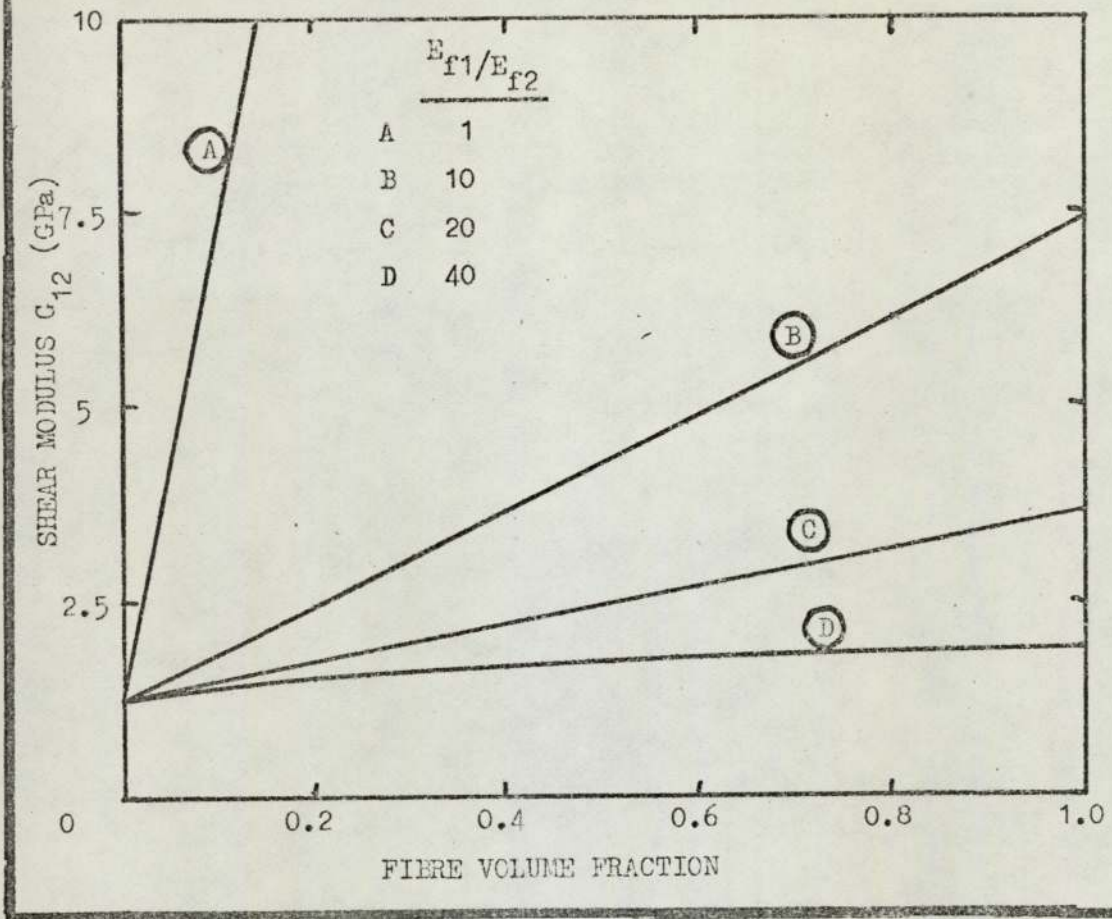
Figure 38 Rabinovich's shear modulus for anisotropic fibres.
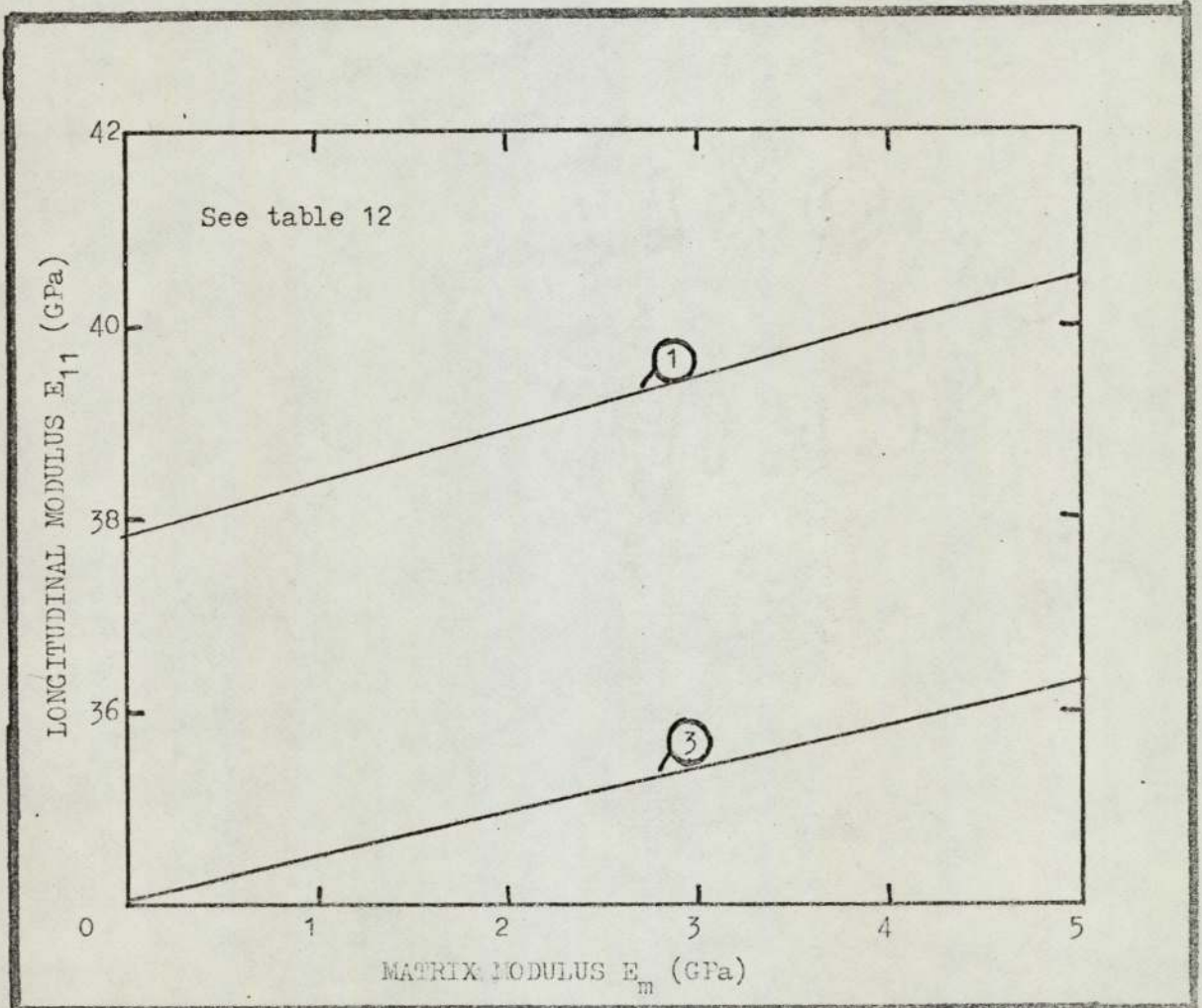
Figure 39 Composite longitudinal modulus/matrix modulus.

Figure 41 Composite Poisson's ratio/matrix modulus

Figure 40 Composite Poisson's ratio/fibre modulus.
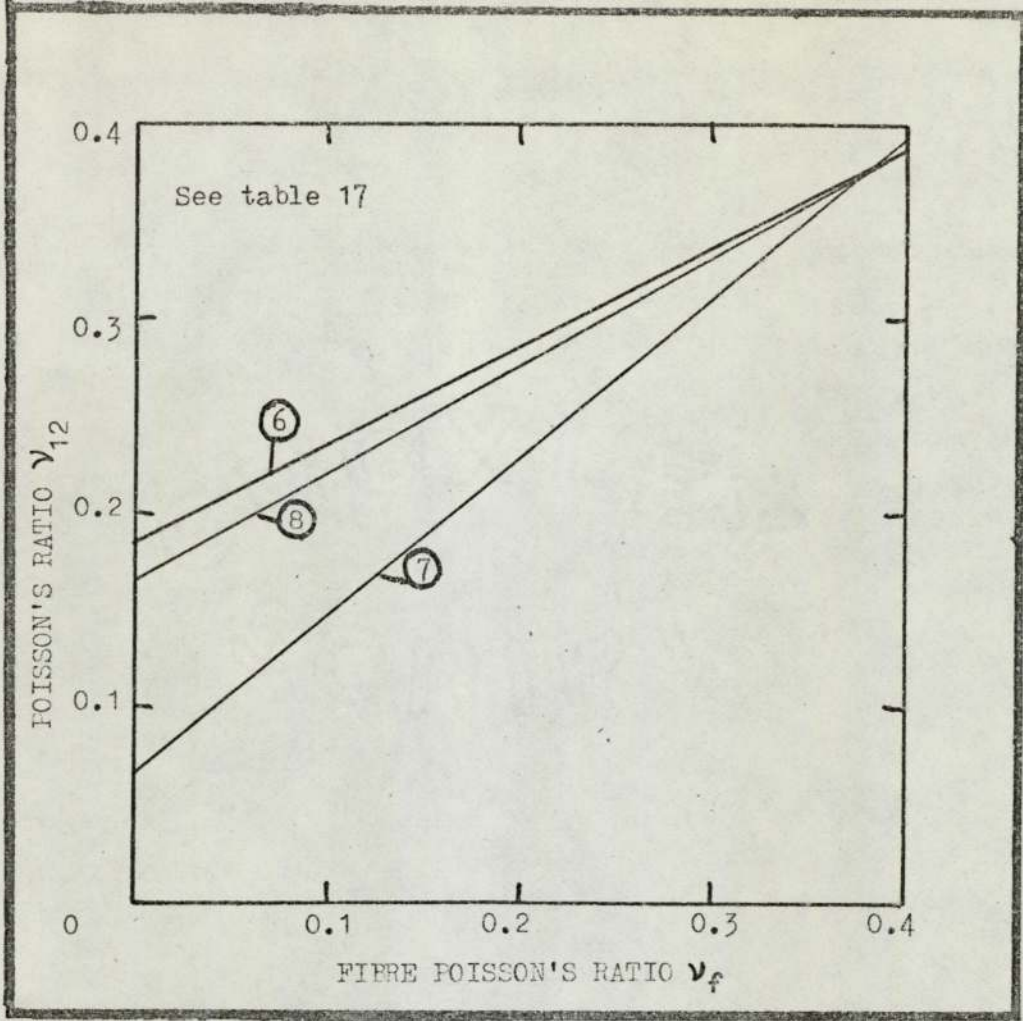
Figure 42   Composite Poisson's ratio/fibre Poisson's ratio.
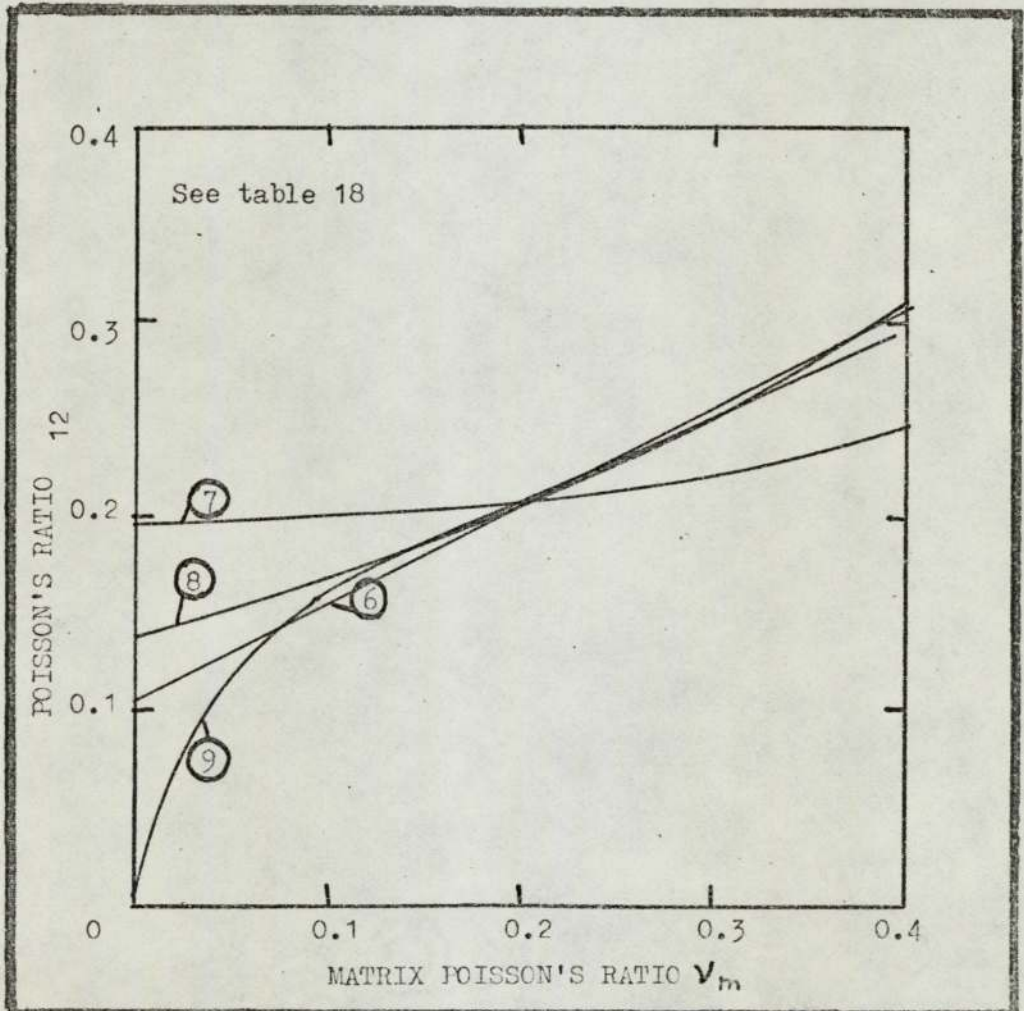
Figure 43   Composite Poisson's ratio/matrix Poisson's ratio.

Figure 45 Composite transverse modulus/matrix modulus.

Figure 44 Composite transverse modulus/fibre modulus.

Figure 47 Composite transverse modulus/fibre Poisson's ratio.

Figure 46 Composite transverse modulus/fibre Poisson's ratio.

Figure 49 Composite shear modulus/matrix modulus.

Figure 48 Composite shear modulus/fibre modulus.

-144-
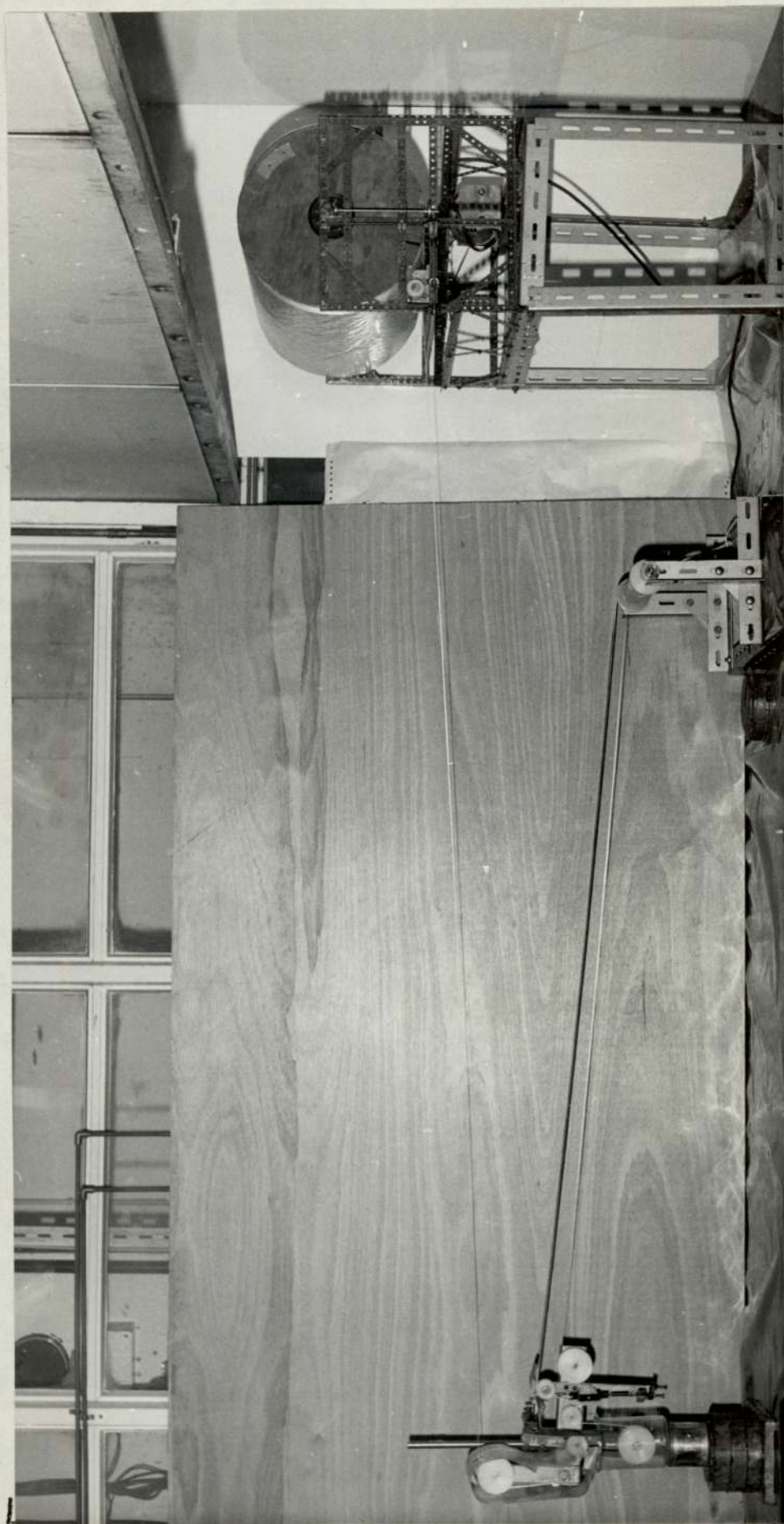
Figure 50 Apparatus for making prepreg sheet.
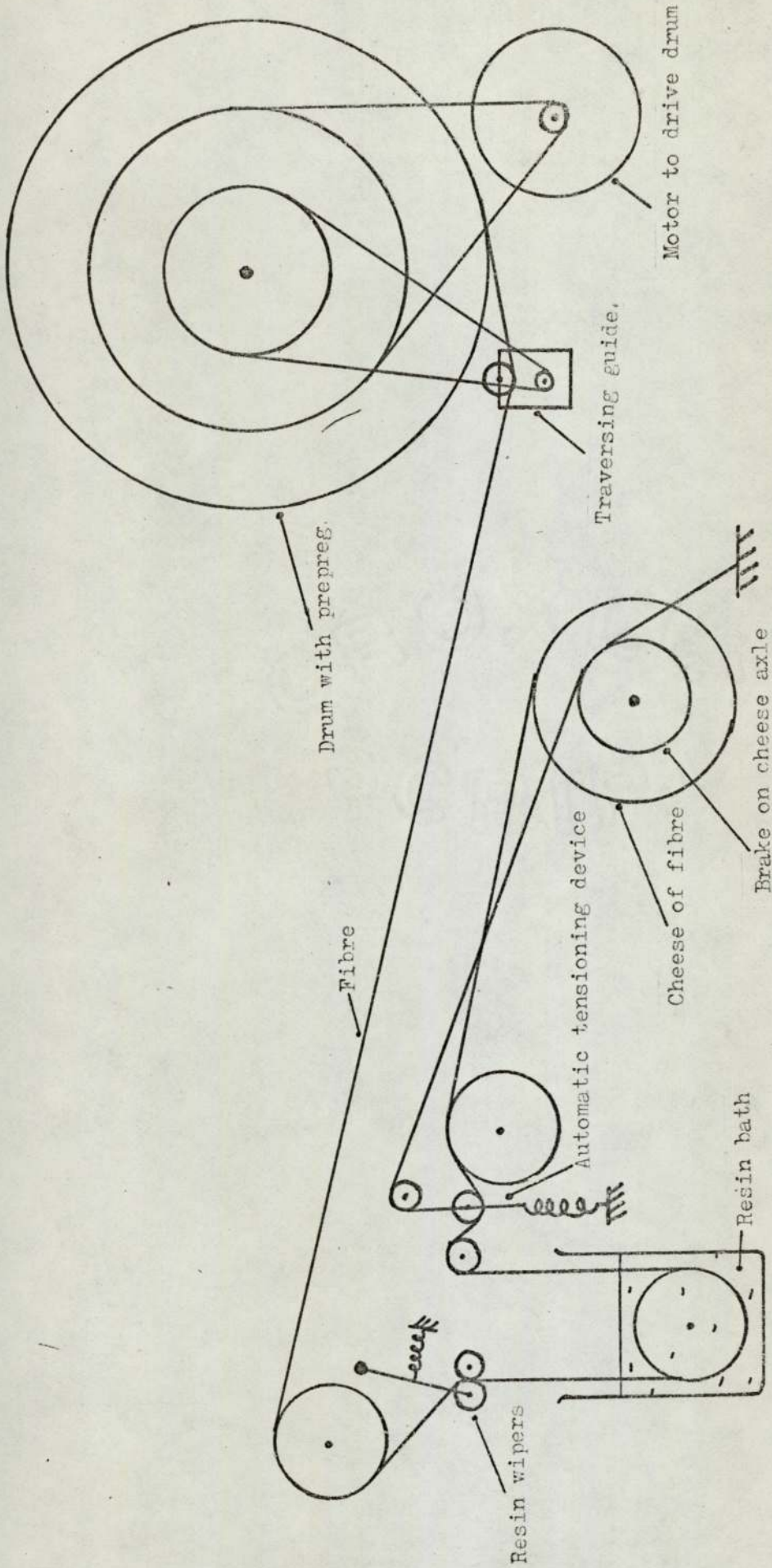
Figure 51 Schematic diagram of prepreg making machine.

Motor to drive drum

Traversing guide.

Drum with prepreg.

Fibre

Automatic tensioning device

Cheese of fibre

Brake on cheese axle

Resin bath

Resin wipers
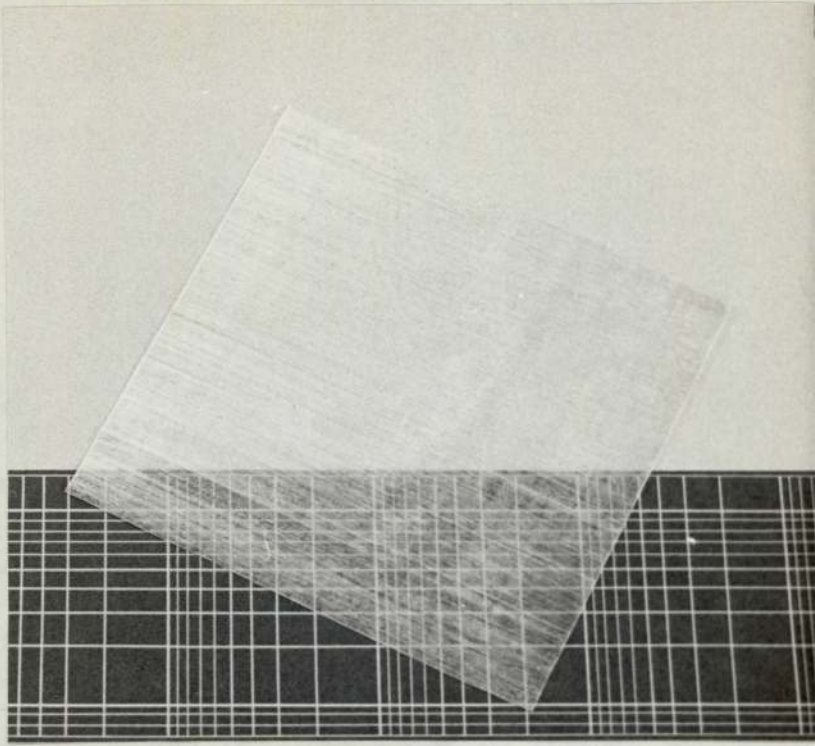
Figure 52   Glass fibre/polyester resin prepreg.
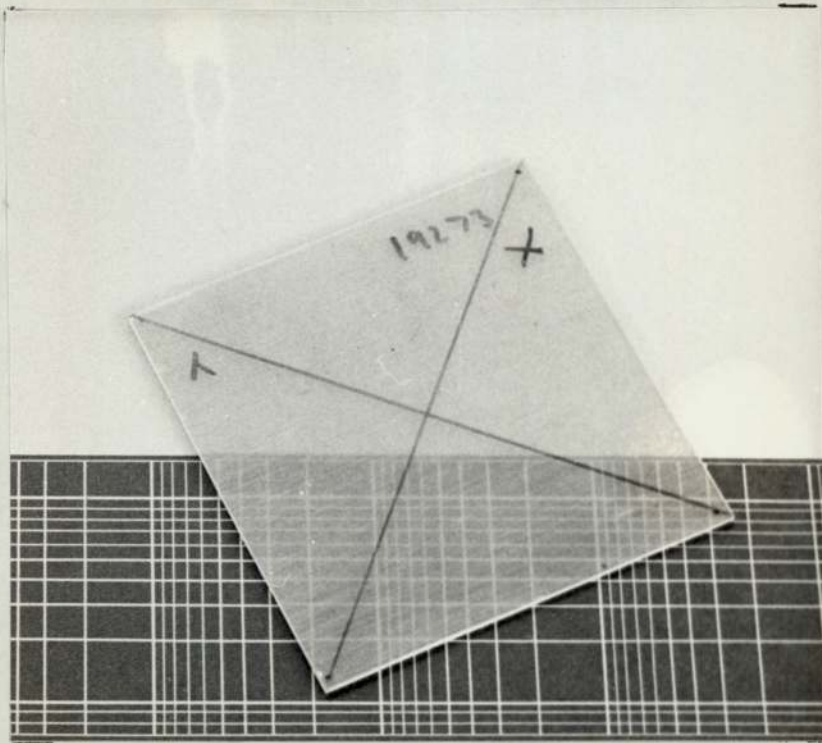
Figure 53   Glass fibre/polyester resin composite.
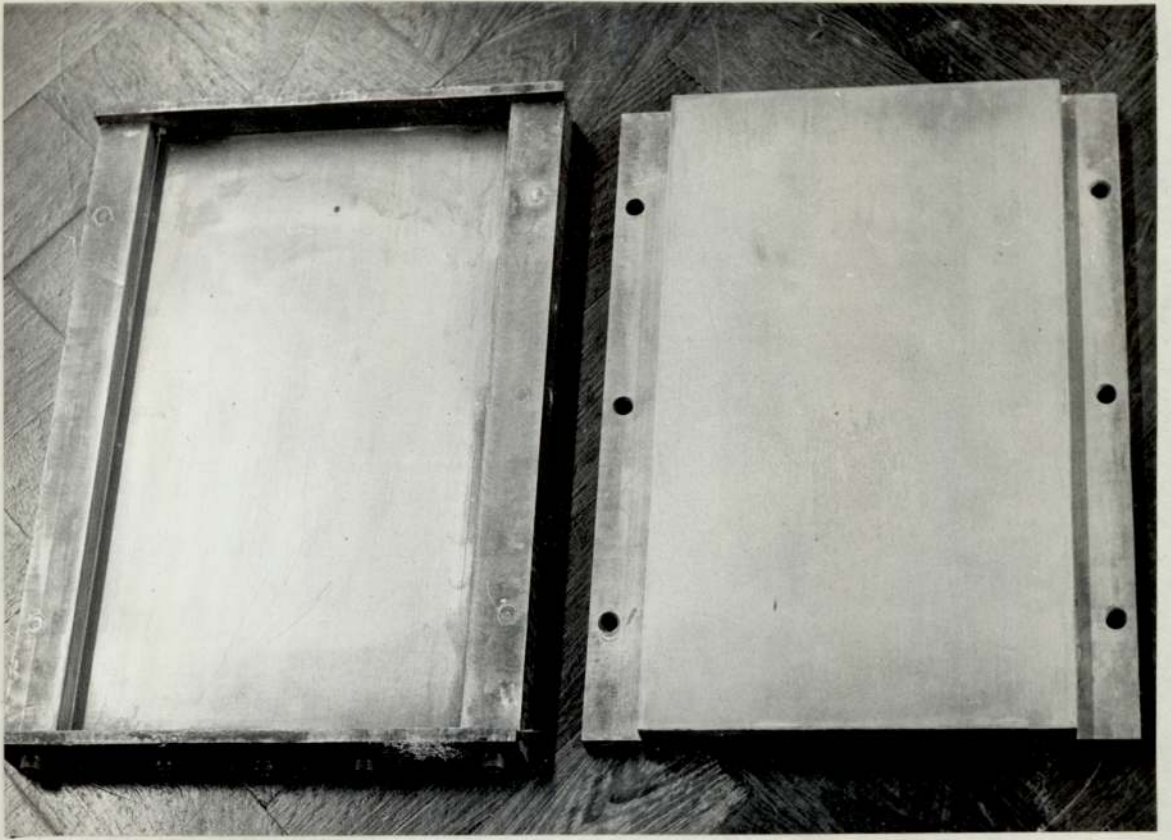
Figure 54 Large composite mould.
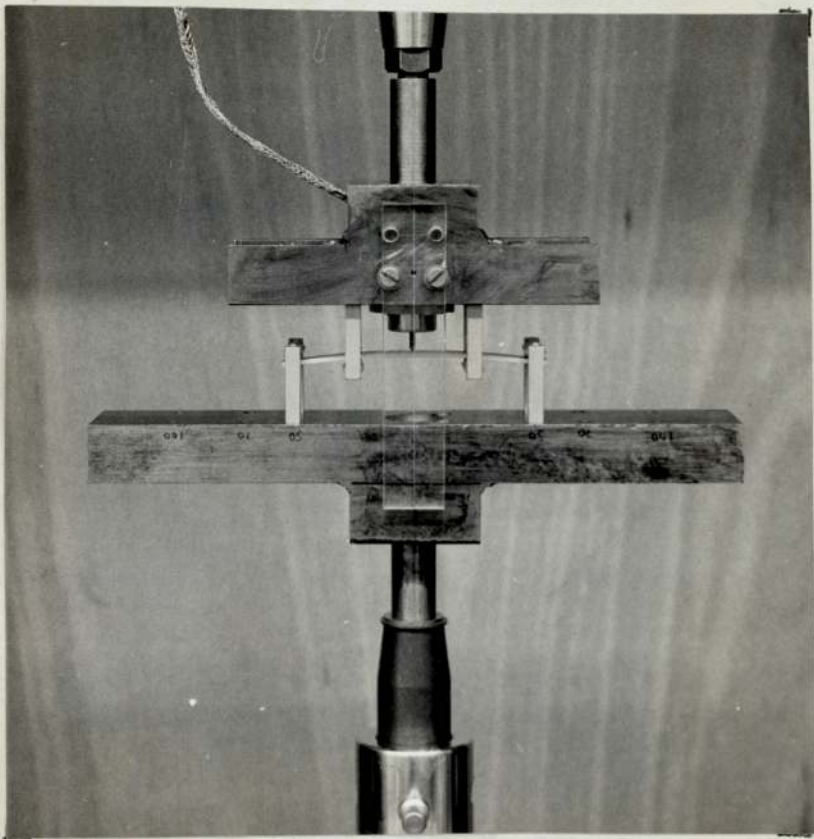
Figure 55 Three and four point flexural rig with built-in transducer.
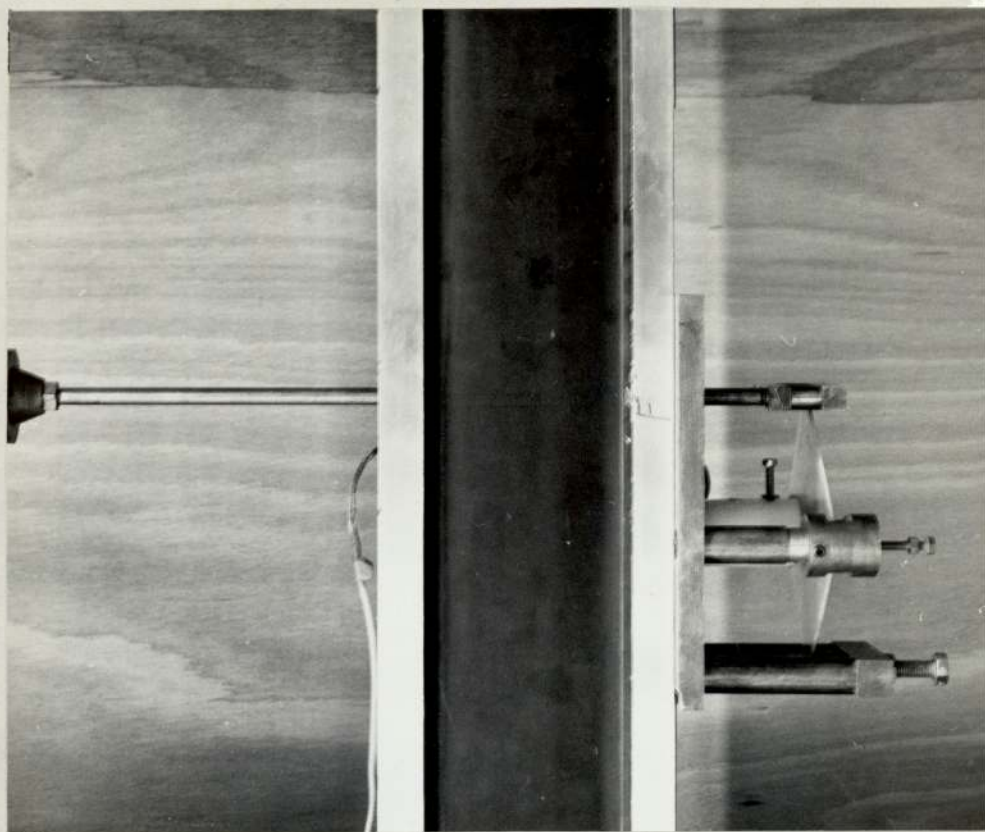
Figure 56 Plate twisting rig on the Instron.
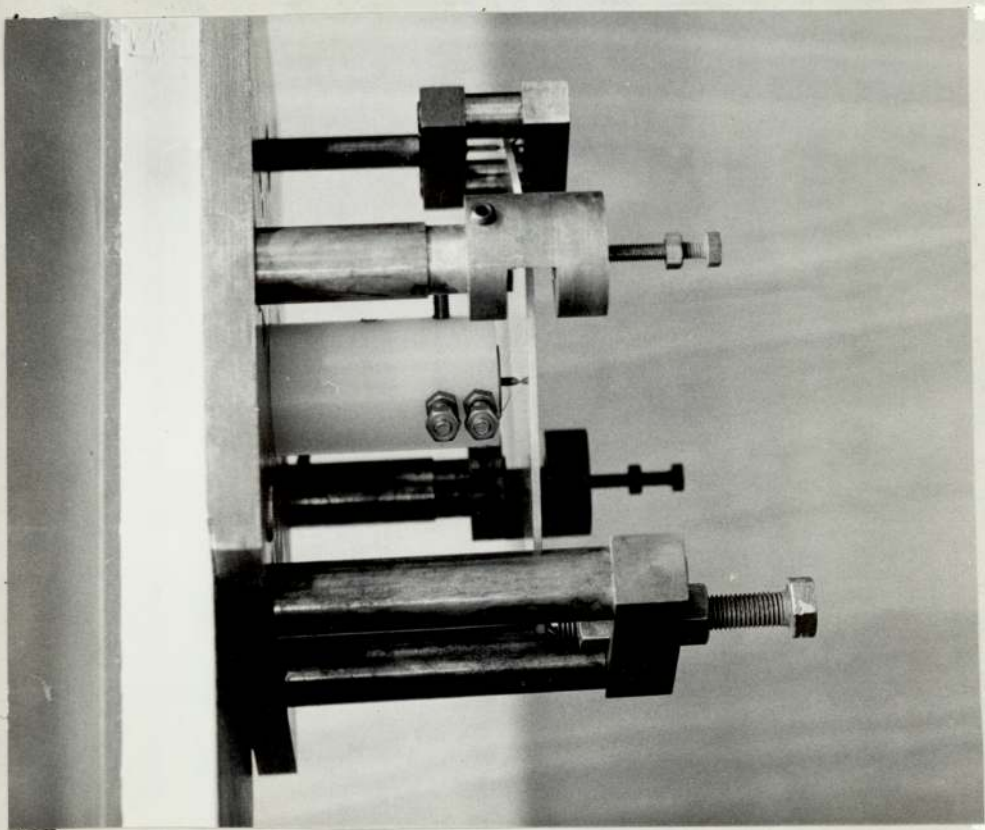
Figure 57 Close-up of plate twisting rig.

Counter balance system

1000 volts

Adjustable weights

Sample

Rotating drum with
teleeltos paper
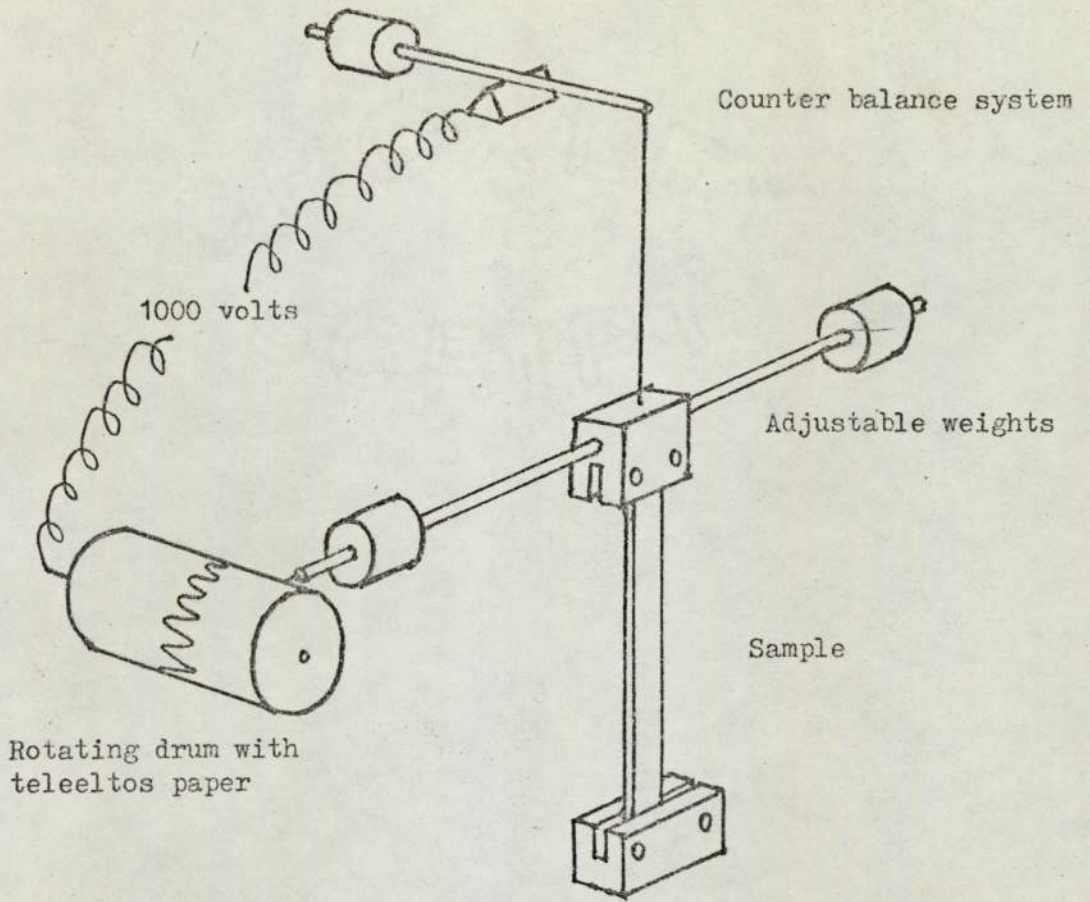
Figure 58 Torsional pendulum

15mm

105mm

15mm

105mm
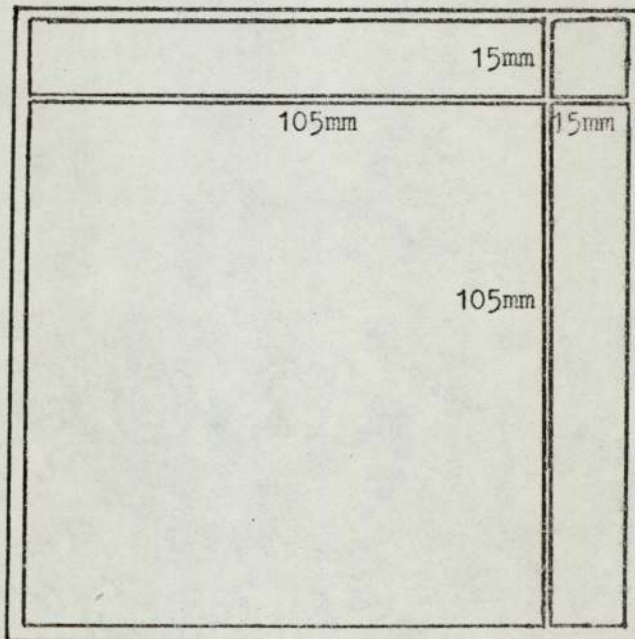
Figure 59 Cutting pattern of 130x130mm composite plate
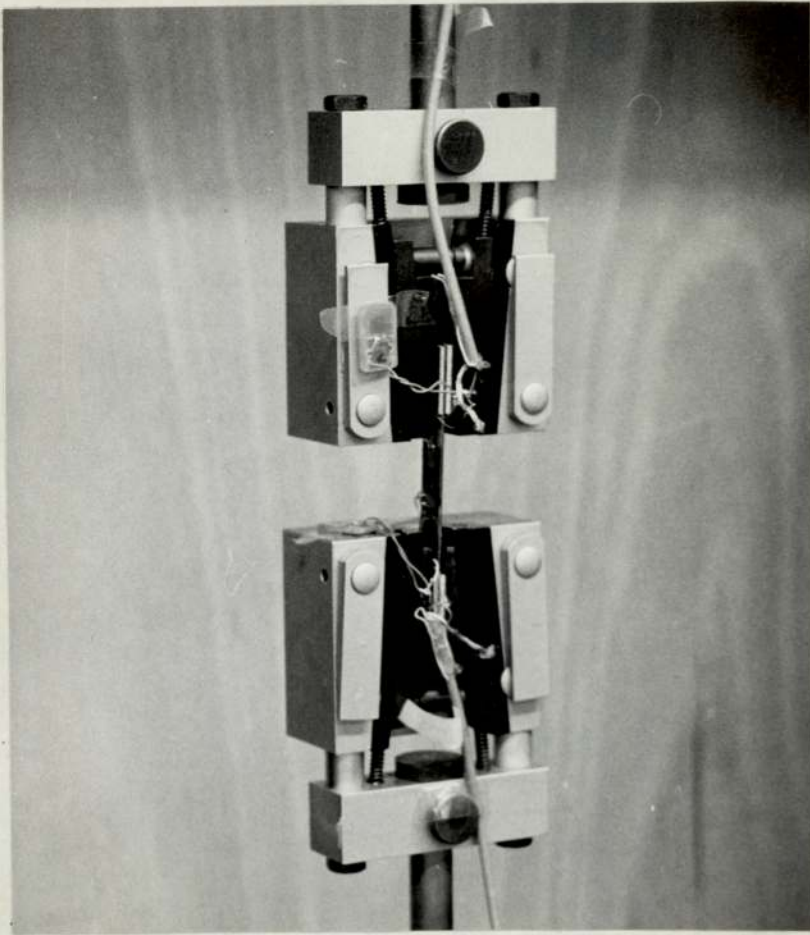
Figure 60   Tensile test sample with strain gauges.

Figure 61   Overall view of test equipment.

Figure 63 Carbon fibre laminated test pieces.

Figure 62 Glass fibre laminated test pieces.

Figure 64 Inhommogeneous glass
fibre distribution. X 30

Figure 65 Inter-ply resin rich
area in carbon composite. X 120
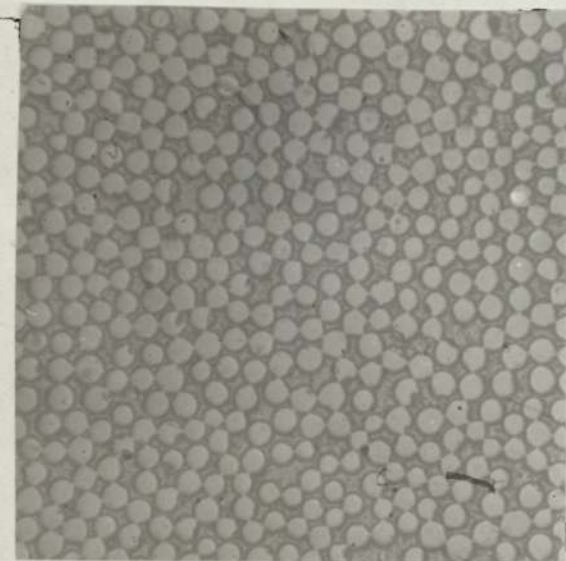
Figure 66 High volume fraction
packing in glass composite. X 250

Figure 67 High volume fraction
packing in carbon composite. X 250
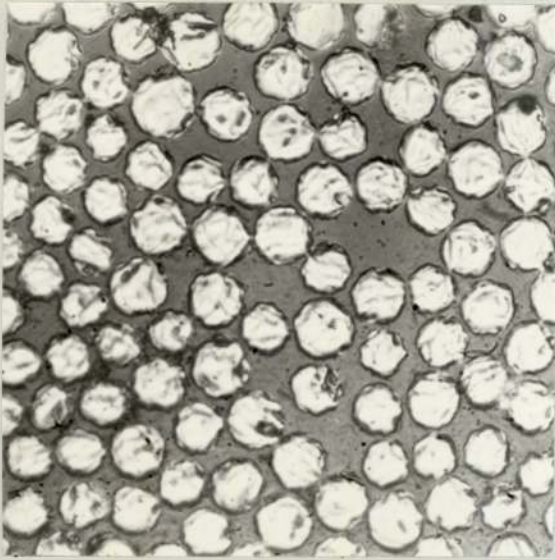
Figure 68 Carbon fibre composite.
X 800
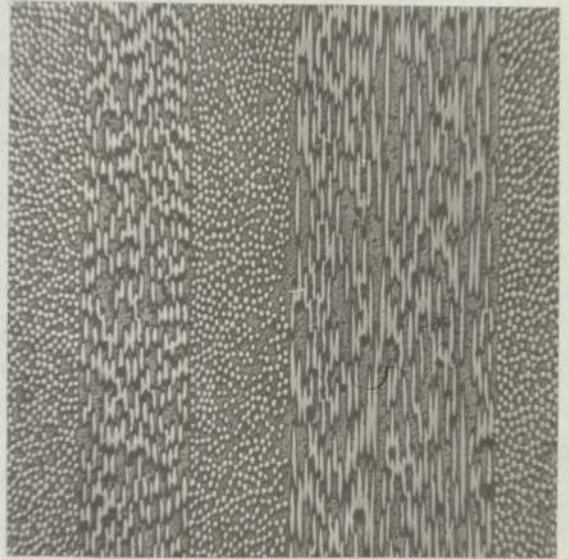
Figure 69 Symmetric ±θ glass
composite. X 25
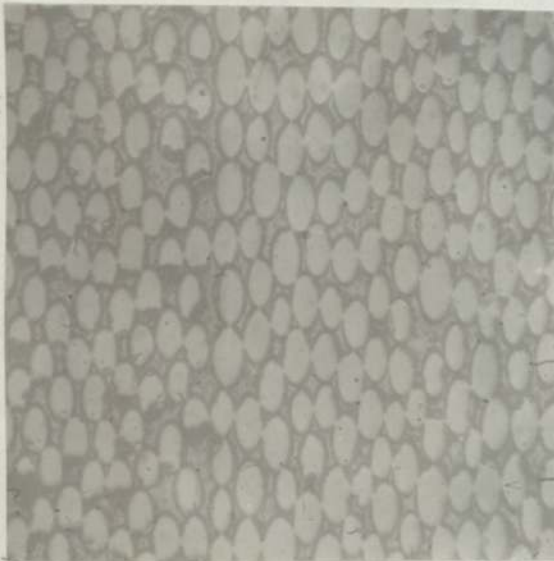
Figure 70 Region between two
lamina on ±θ composite. X 250

Figure 71 Fracture surface of
± 70 carbon composite. X 25
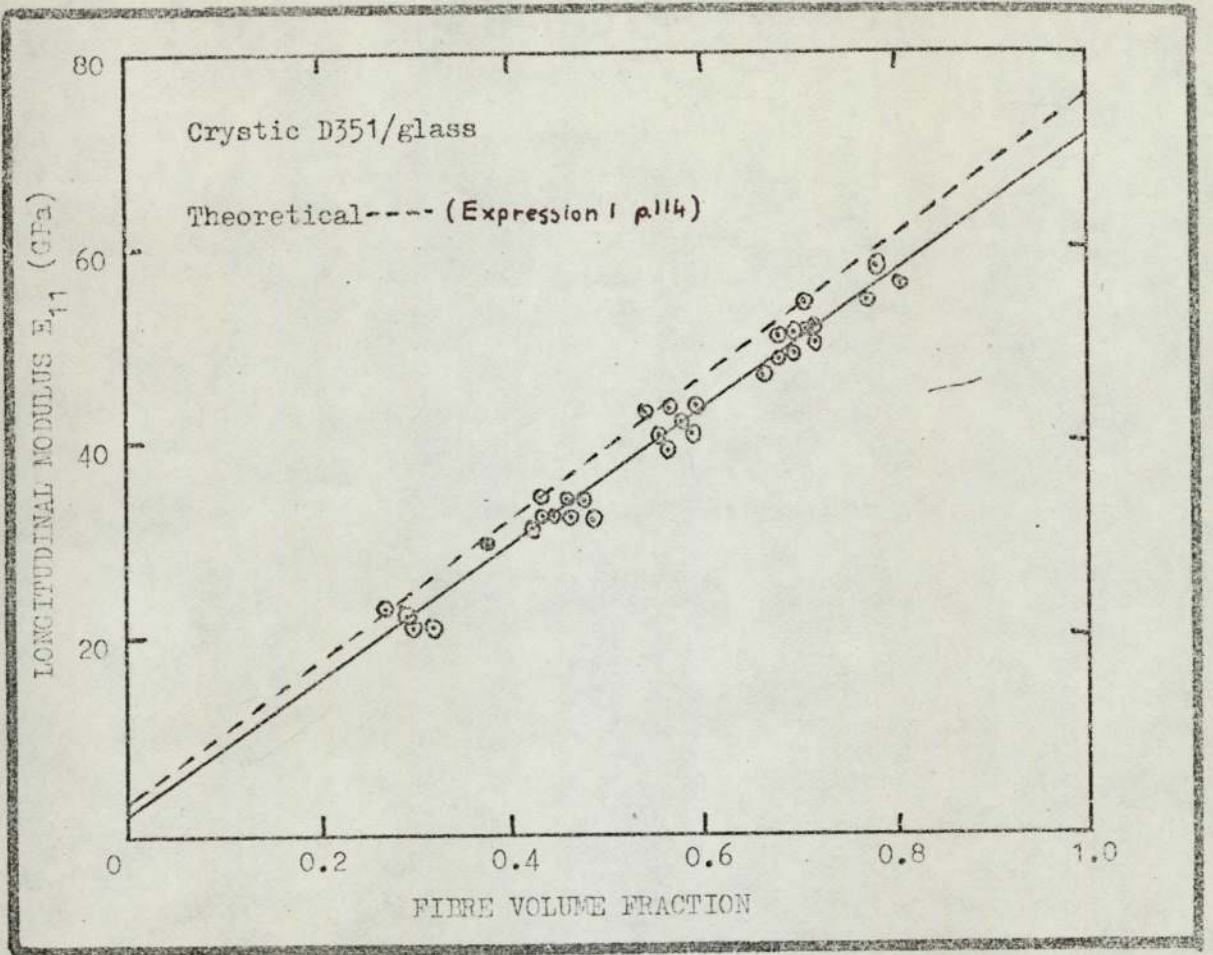
Figure 72 Longitudinal modulus/fibre volume fraction
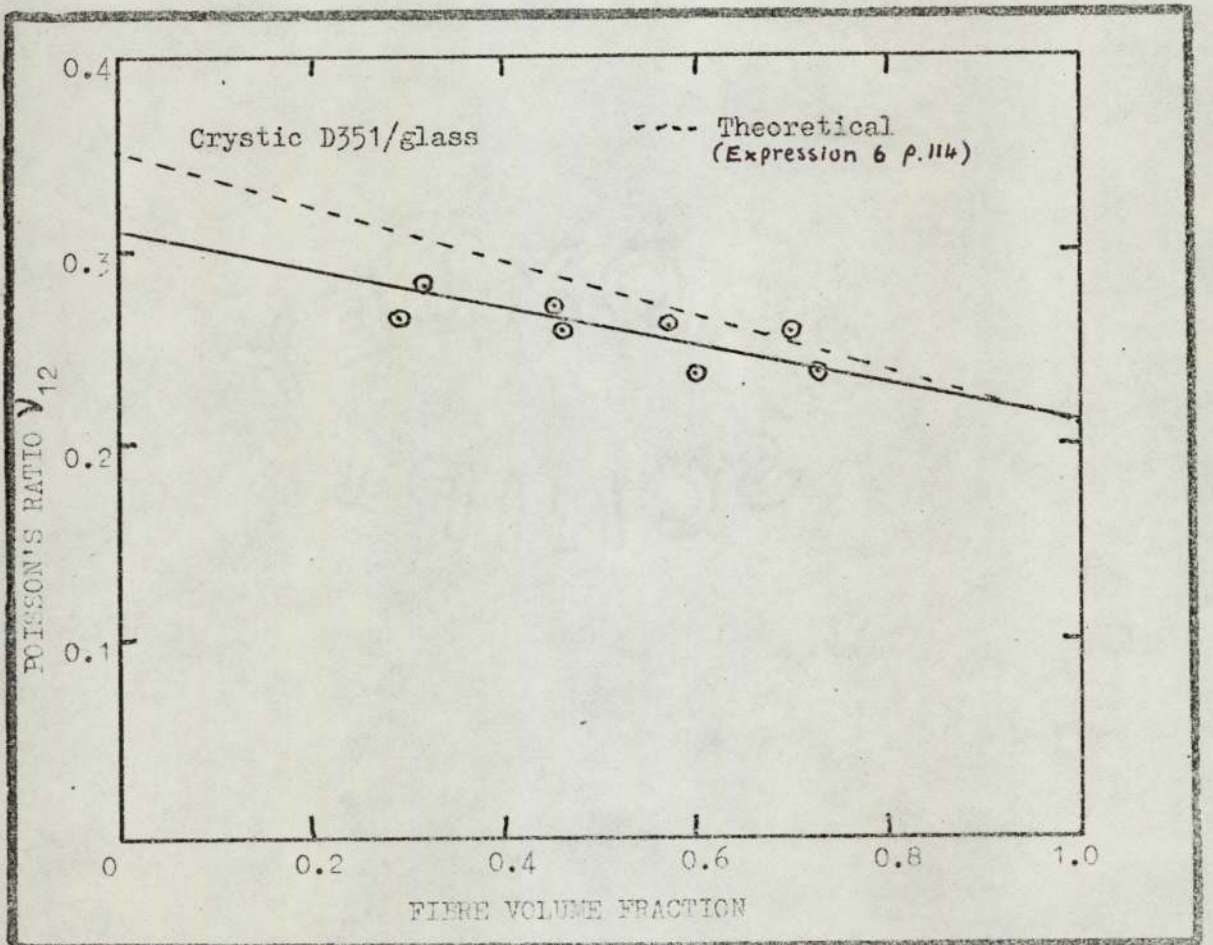
Figure 73 Longitudinal Poisson's ratio/fibre volume fraction
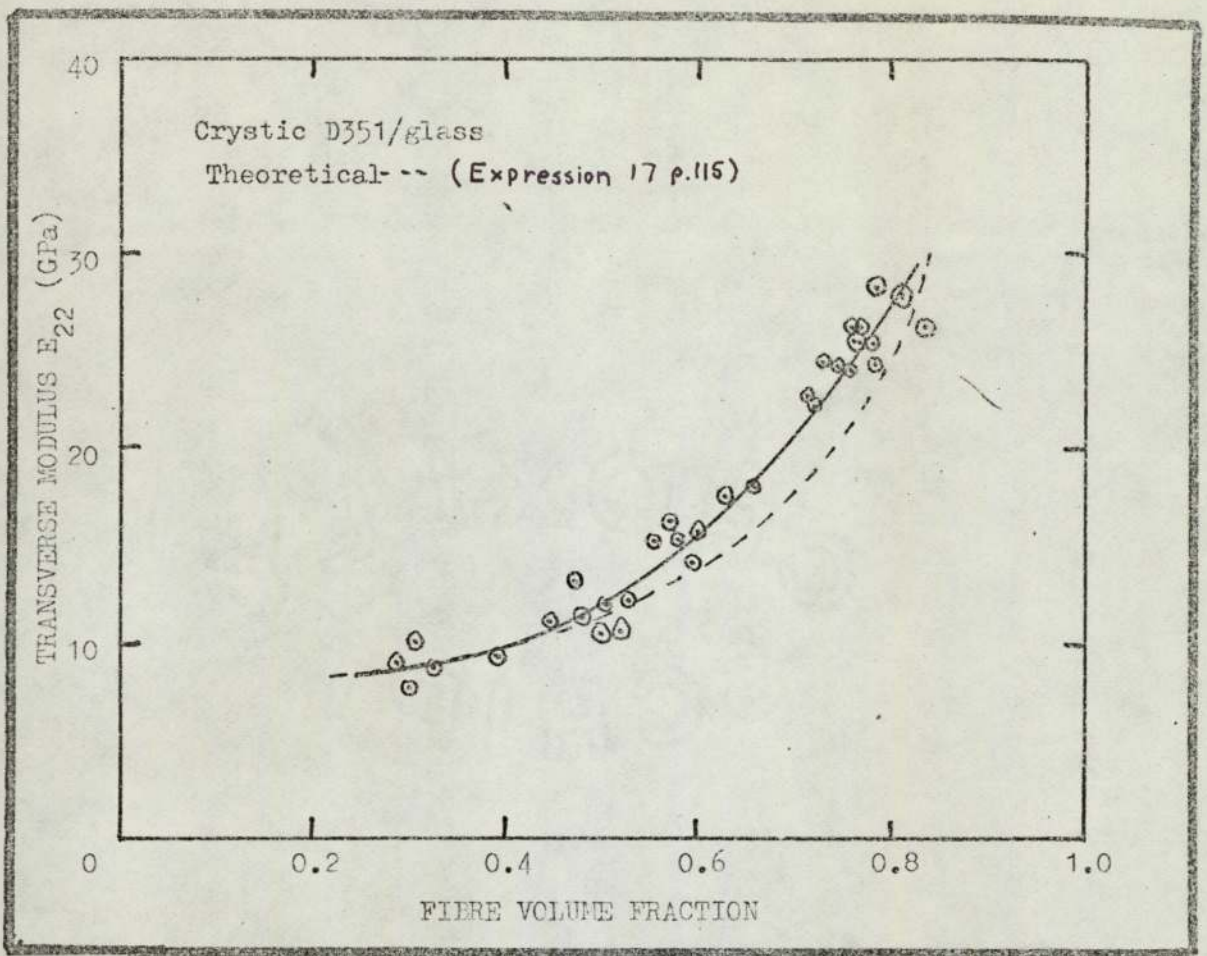
Figure 74 Transverse modulus/fibre volume fraction
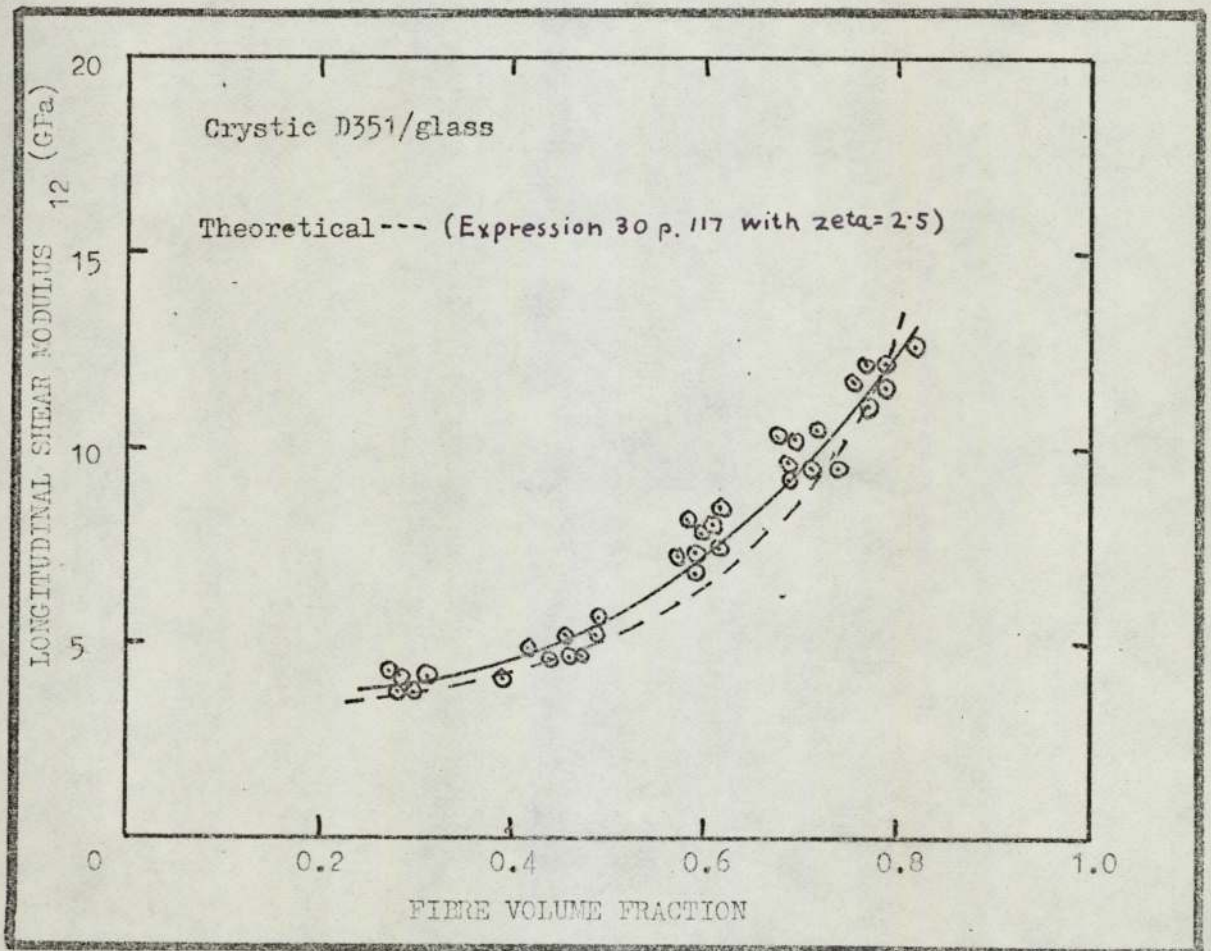
Figure 75 Shear modulus/fibre volume fraction
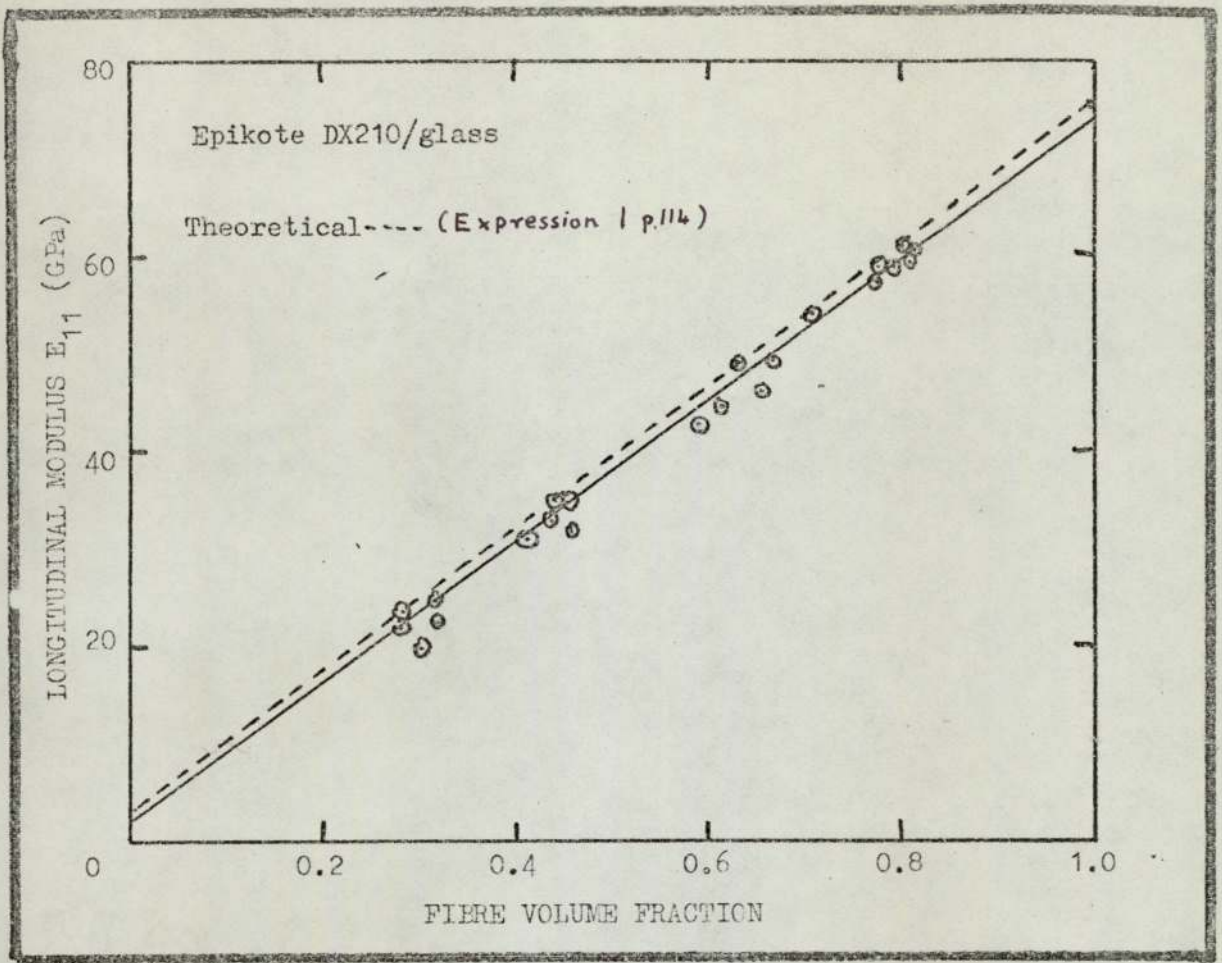
Figure 76 Longitudinal modulus/fibre volume fraction
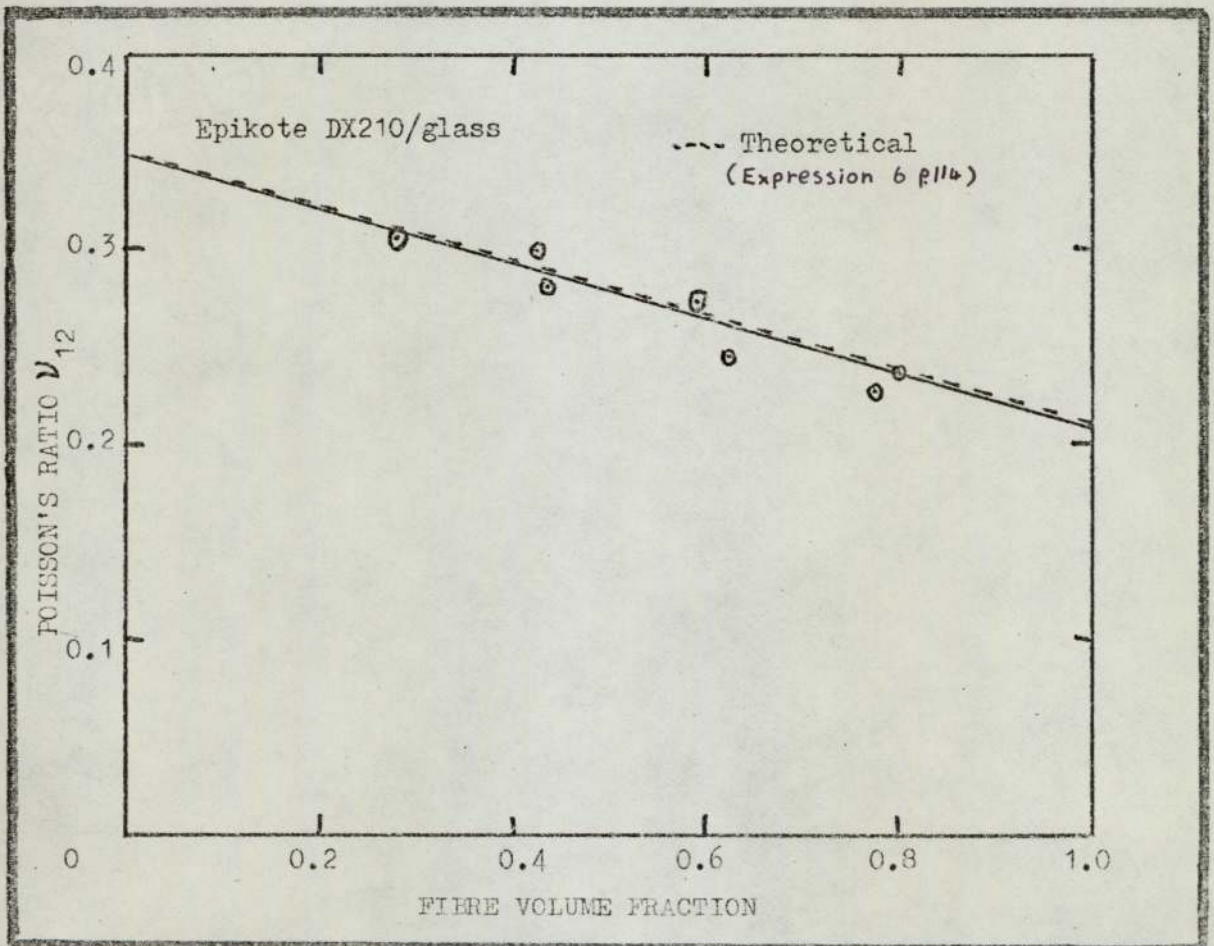
Figure 77 Longitudinal Poisson's ratio/fibre volume fraction

Figure 78 Transverse modulus/fibre volume fraction

Figure 79 Shear modulus/fibre volume fraction
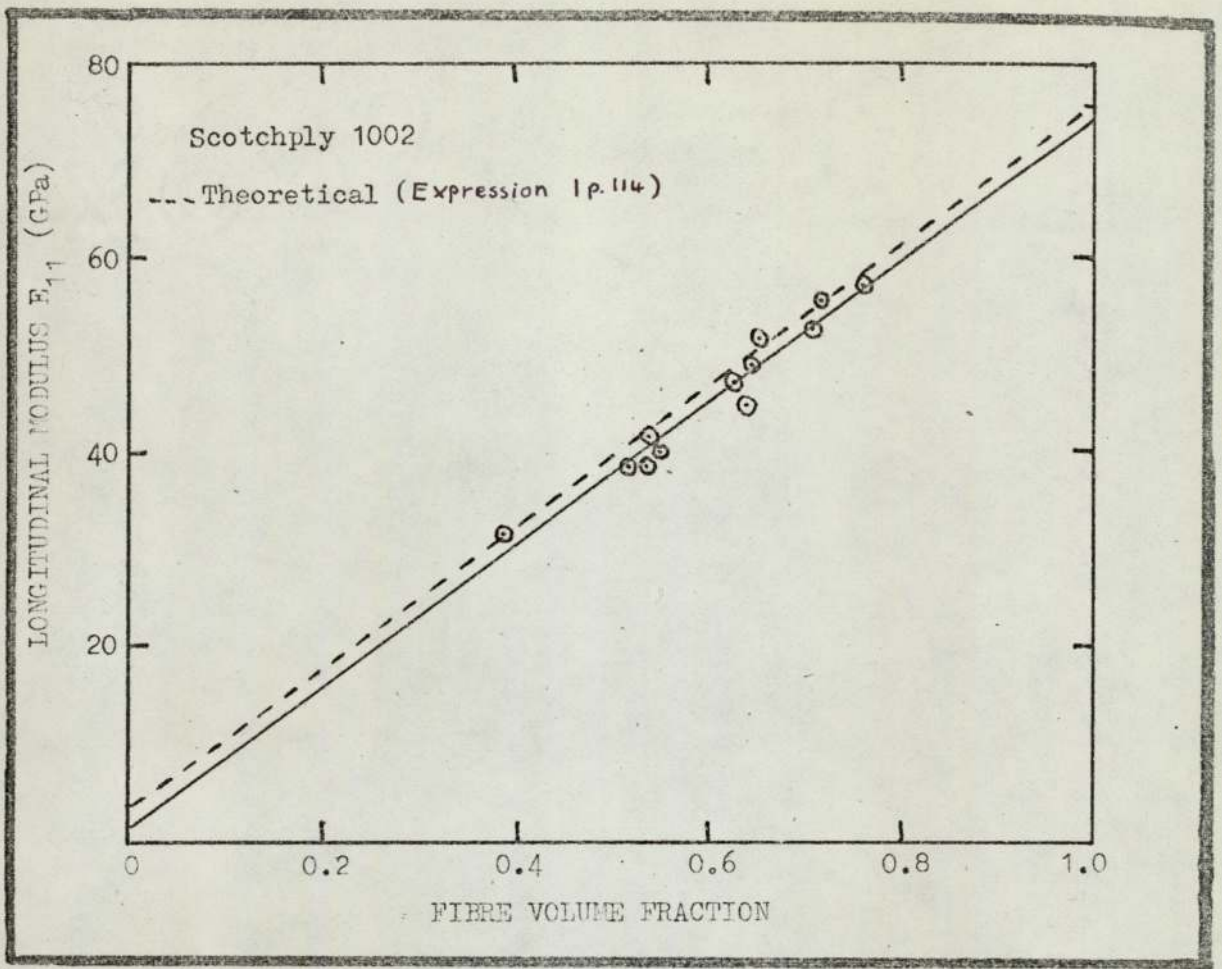
Figure 80 Longitudinal modulus/fibre volume fraction
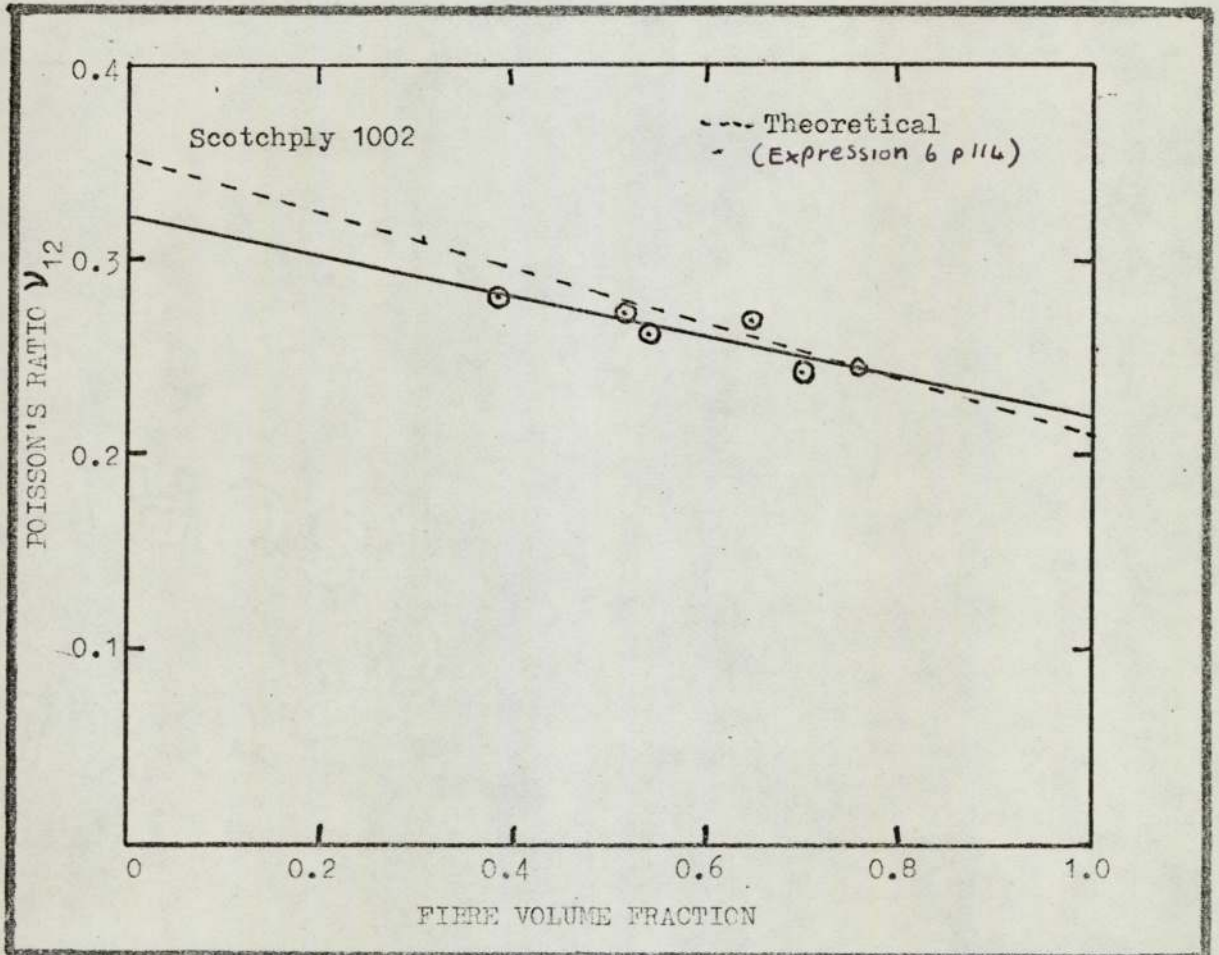
Figure 81 Longitudinal Poisson's ratio/fibre volume fraction
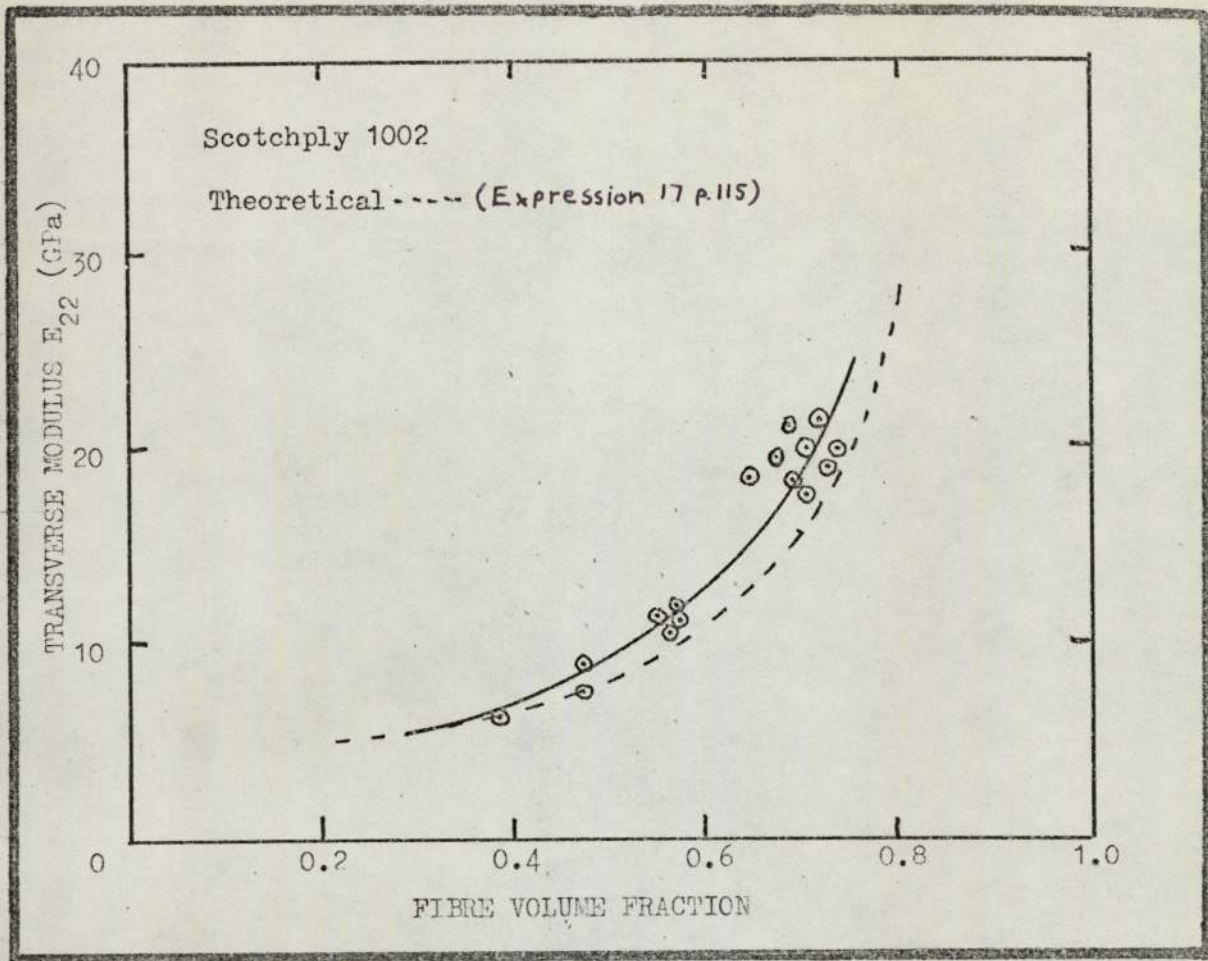
Figure 82   Transverse modulus/fibre volume fraction
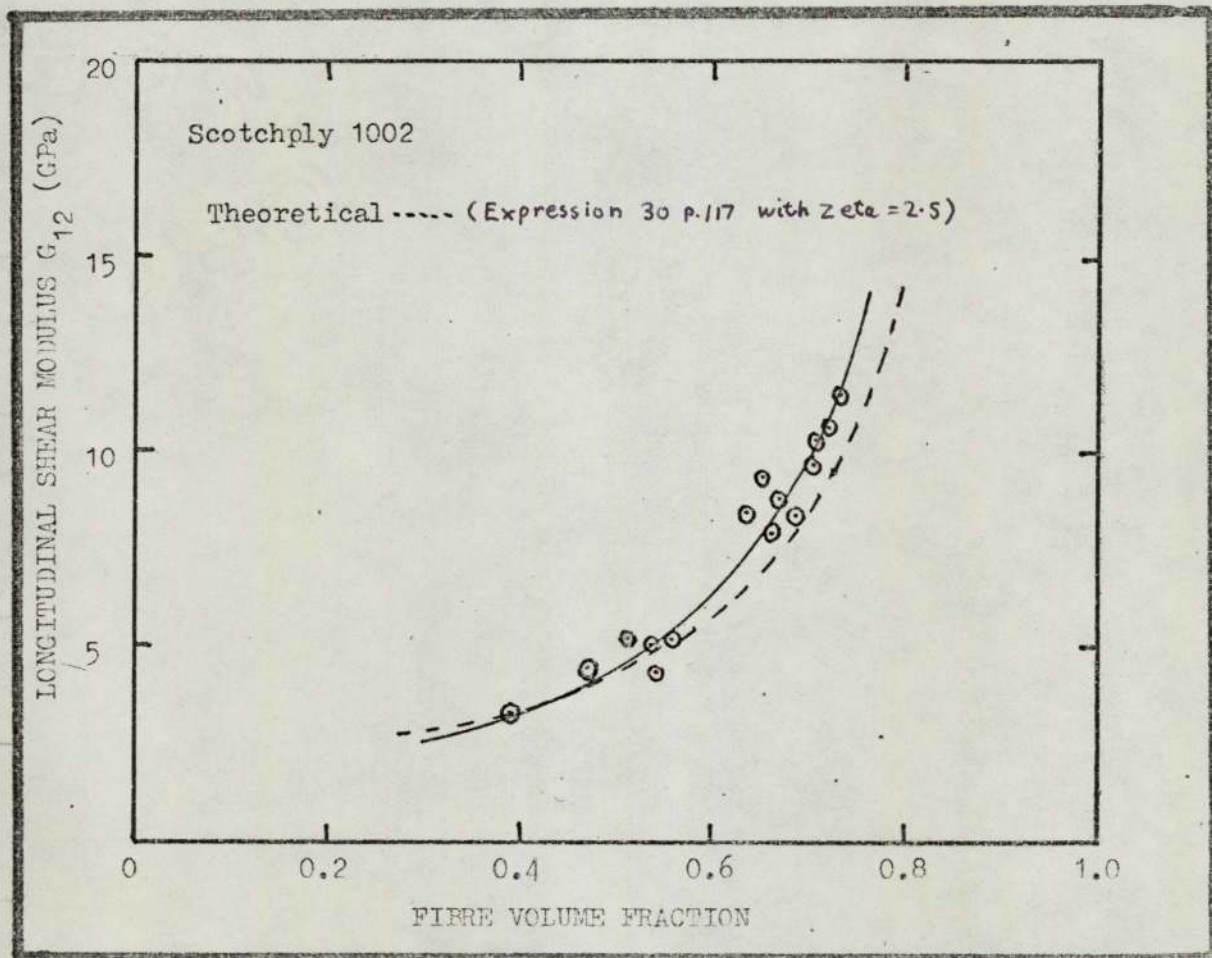
Figure 83   Shear modulus/fibre volume fraction
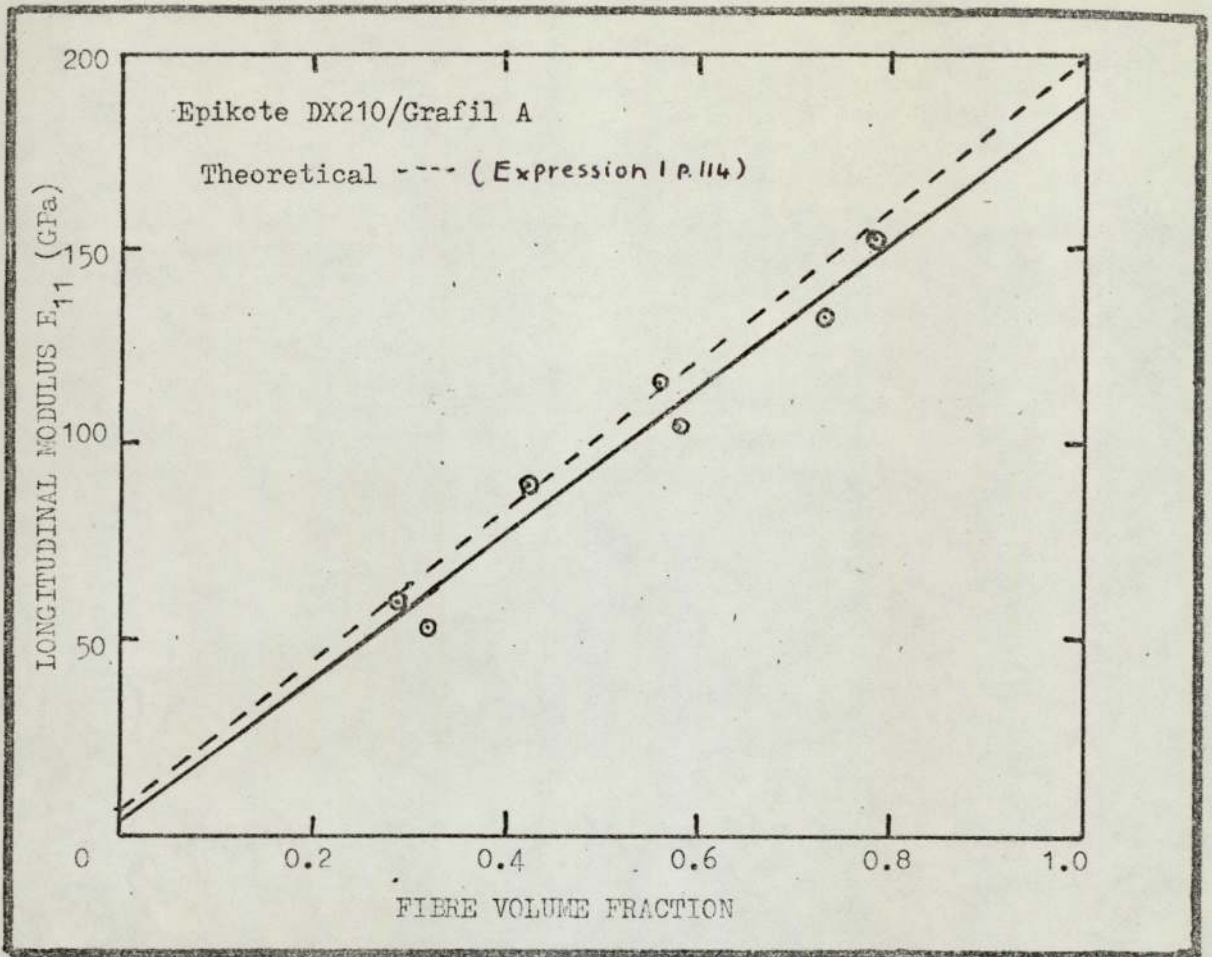
Figure 84 Longitudinal modulus/fibre volume fraction
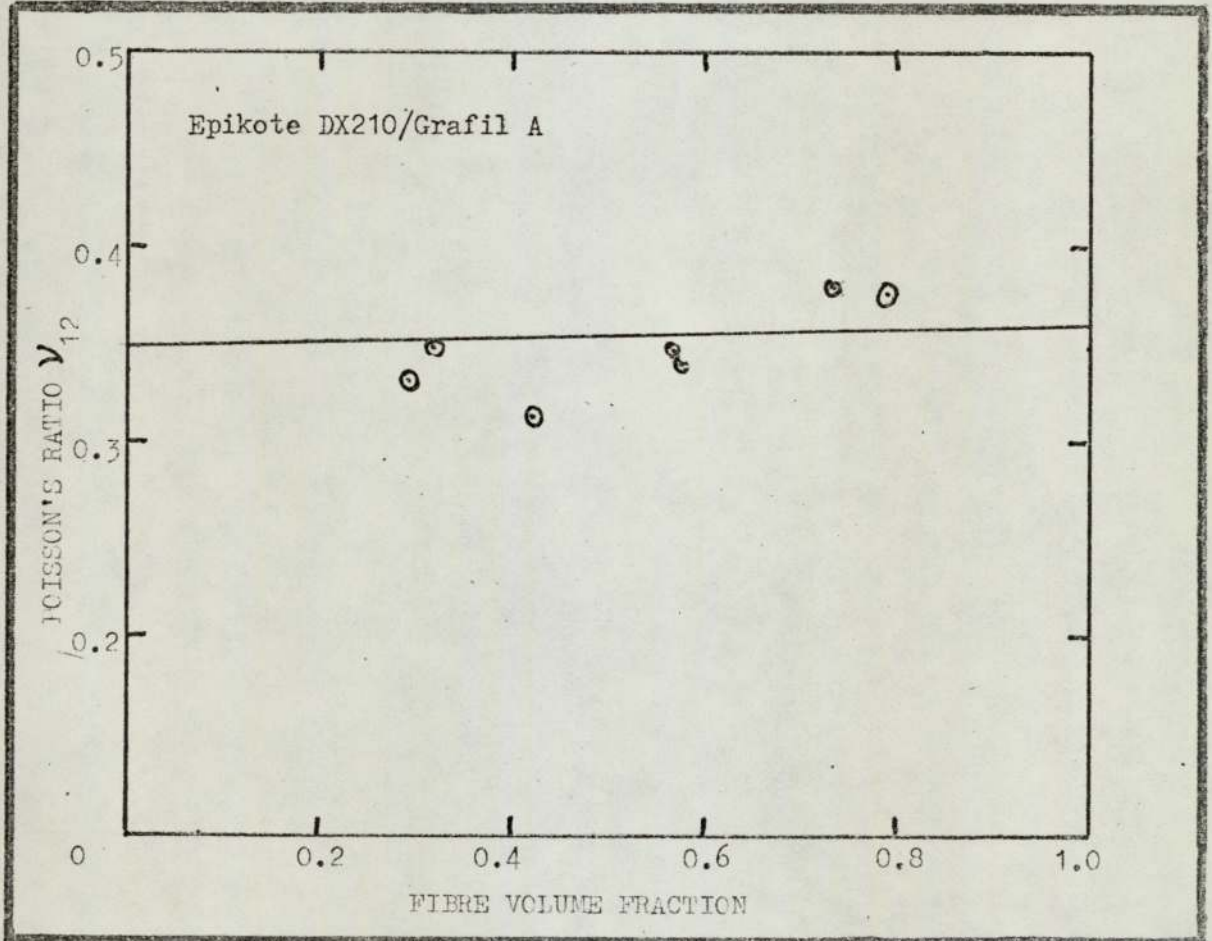
Figure 85 Longitudinal Poisson's ratio/fibre volume fraction
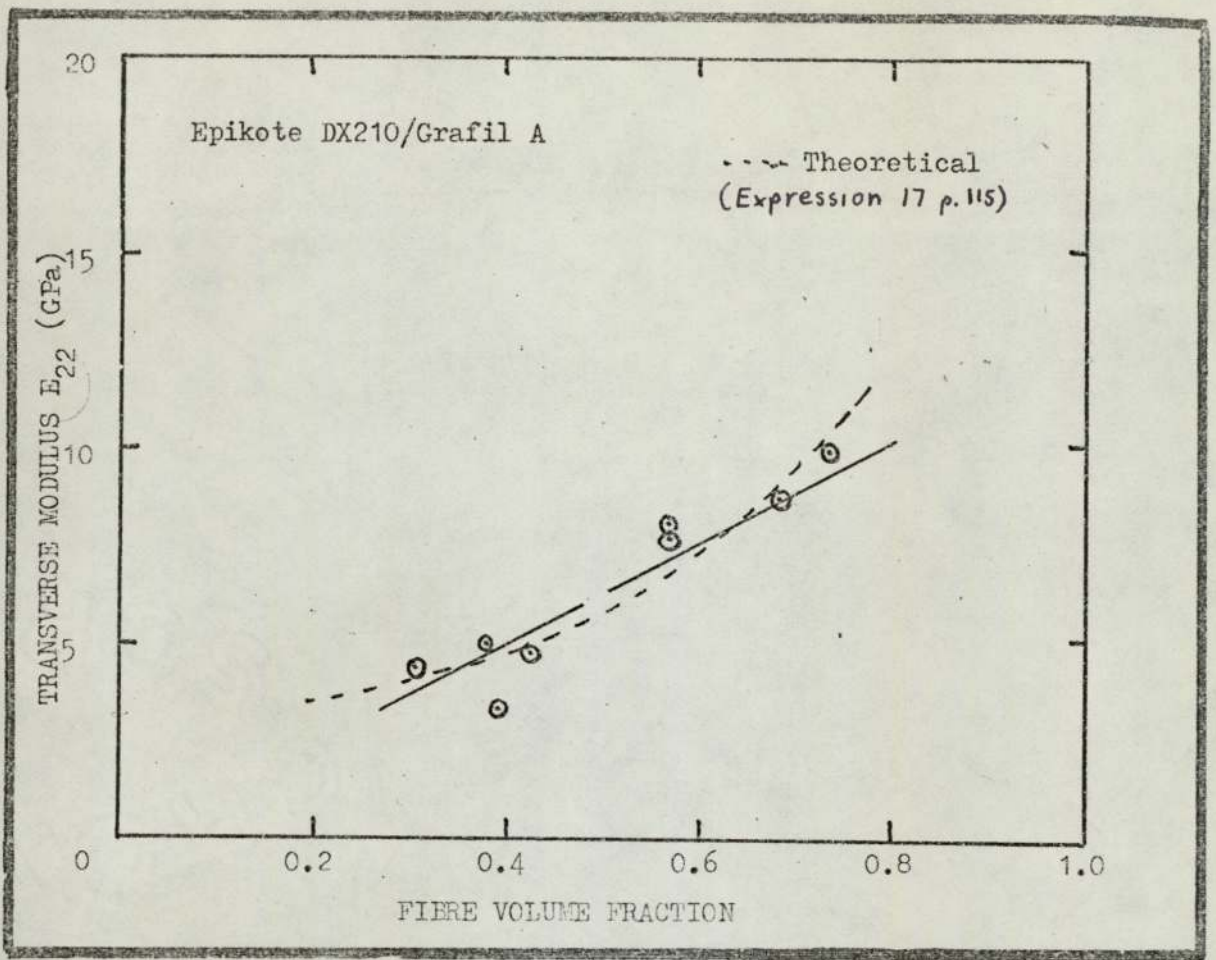
Figure 86 Transverse modulus/fibre volume fraction
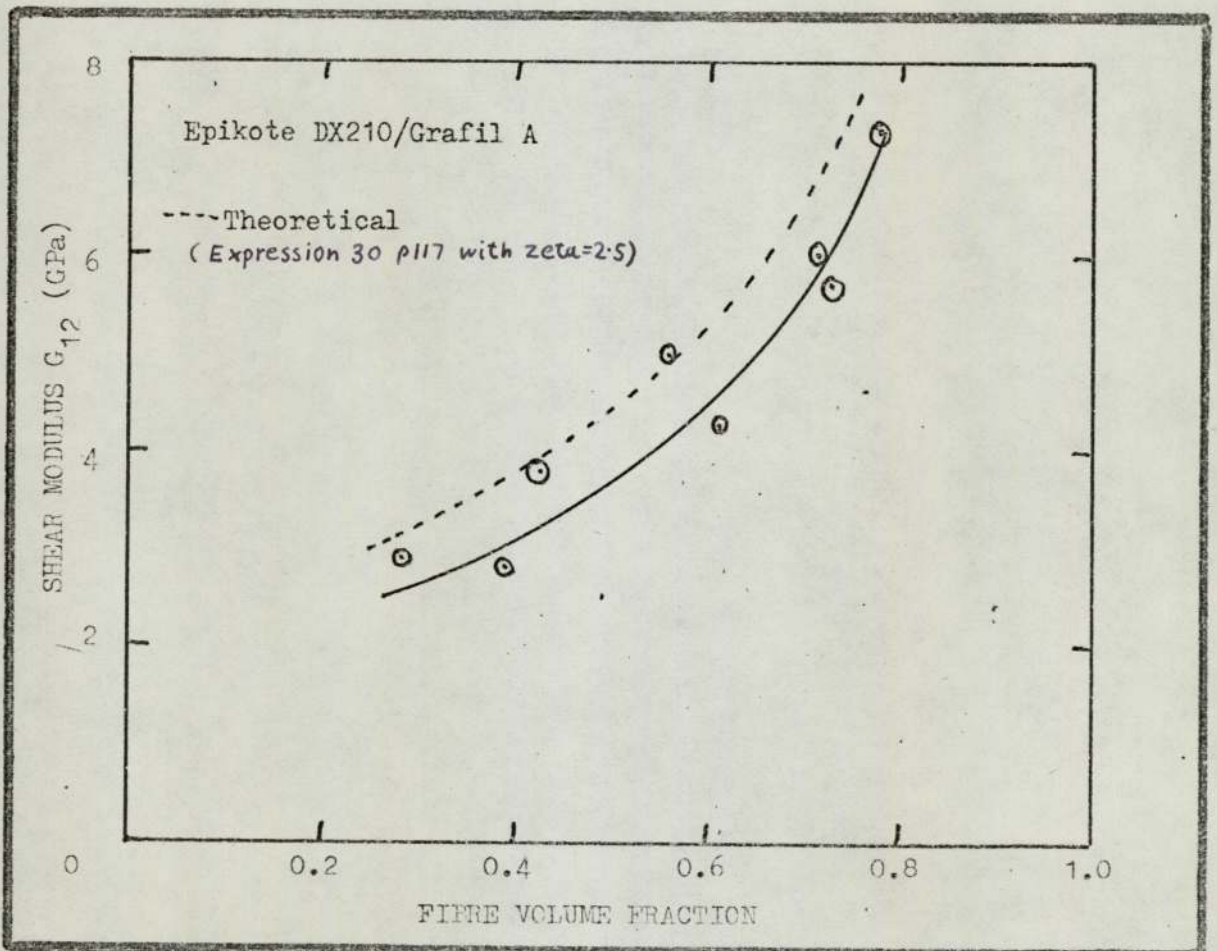
Figure 87 Shear modulus/fibre volume fraction
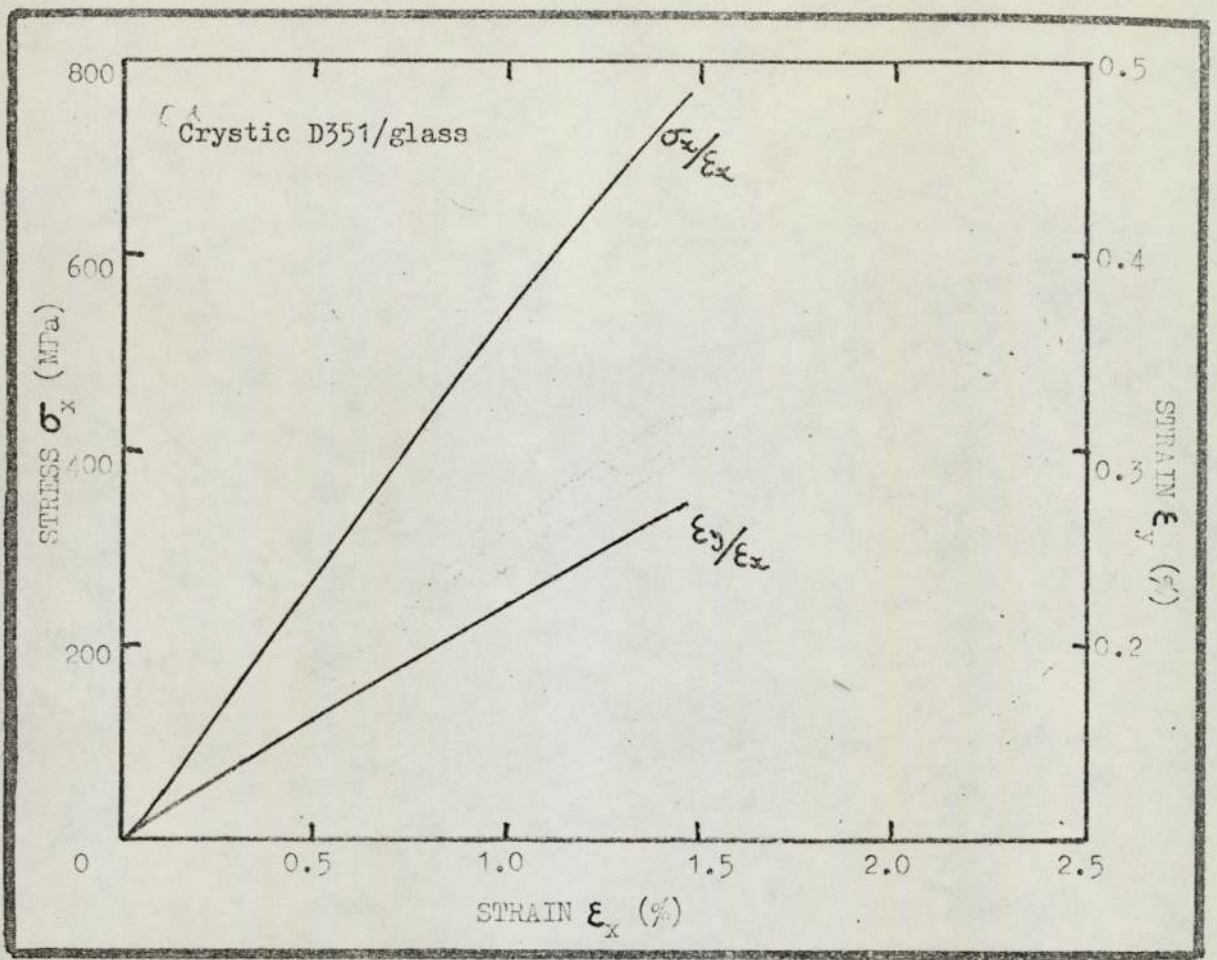
Figure 88 Stress/strain relationship for a unidirectional composite
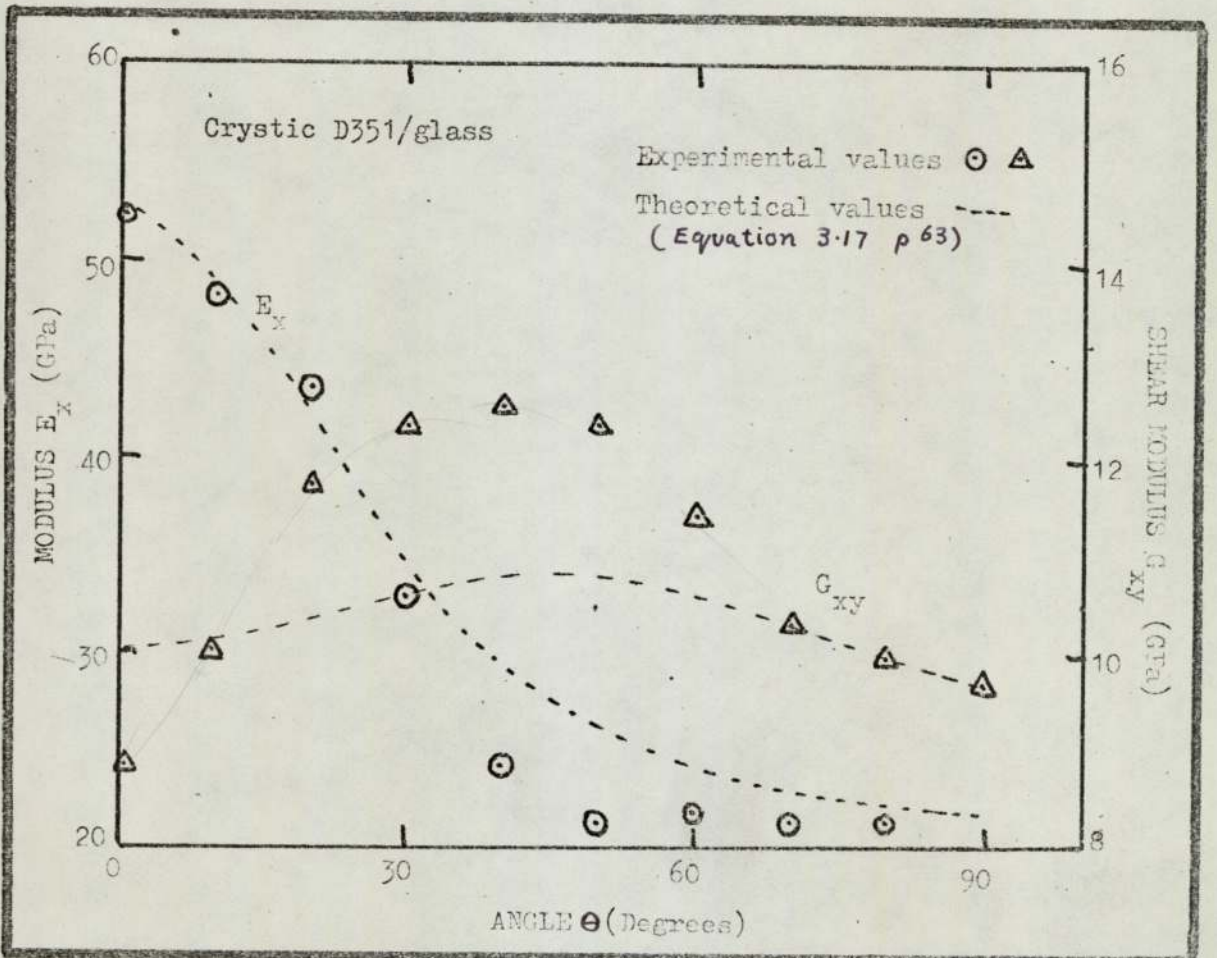
Figure 89 Off-angle properties of a unidirectional composite
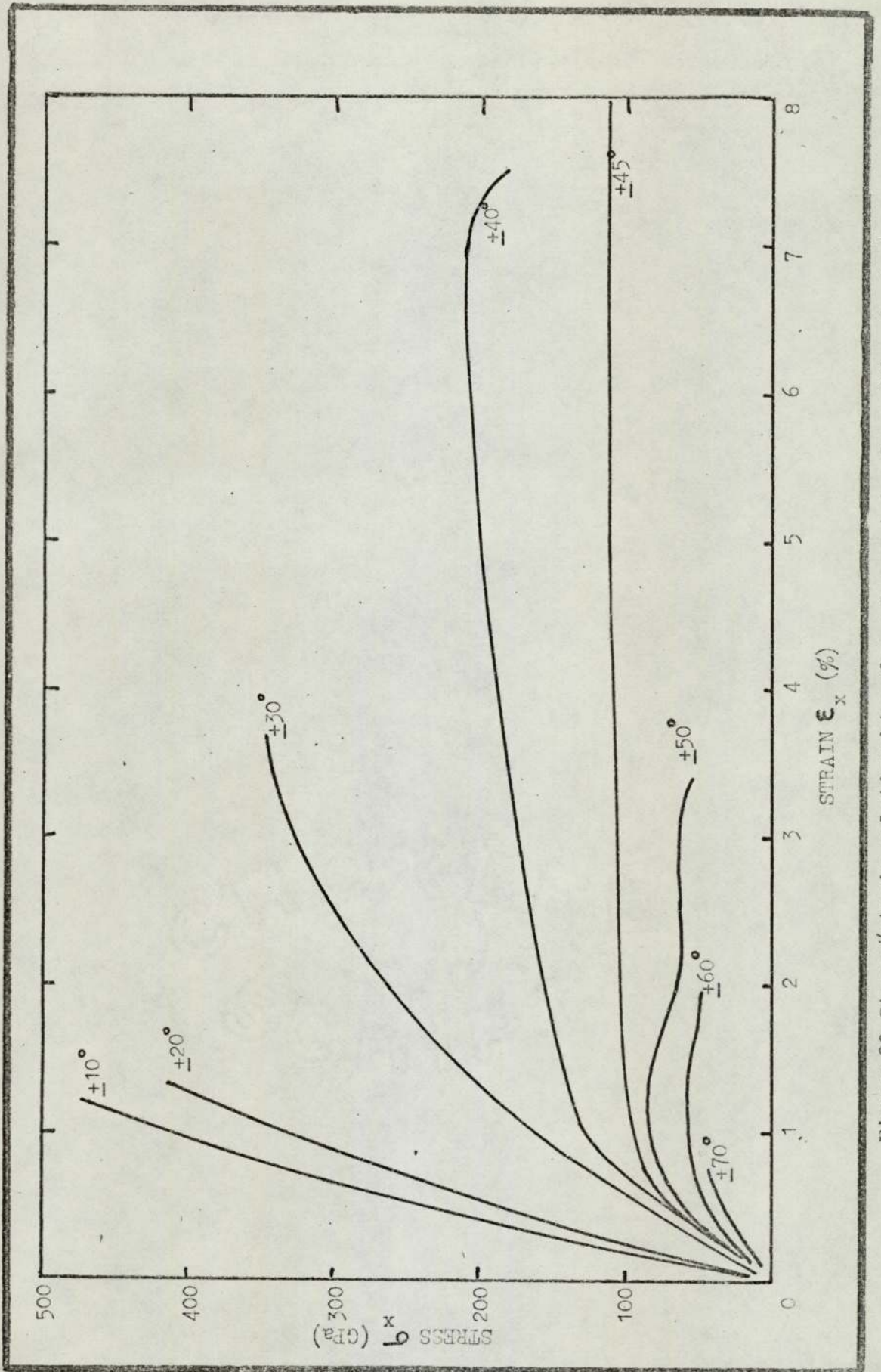
Figure 90 Stress/strain relationships for ±Θ symmetric glass fibre laminates
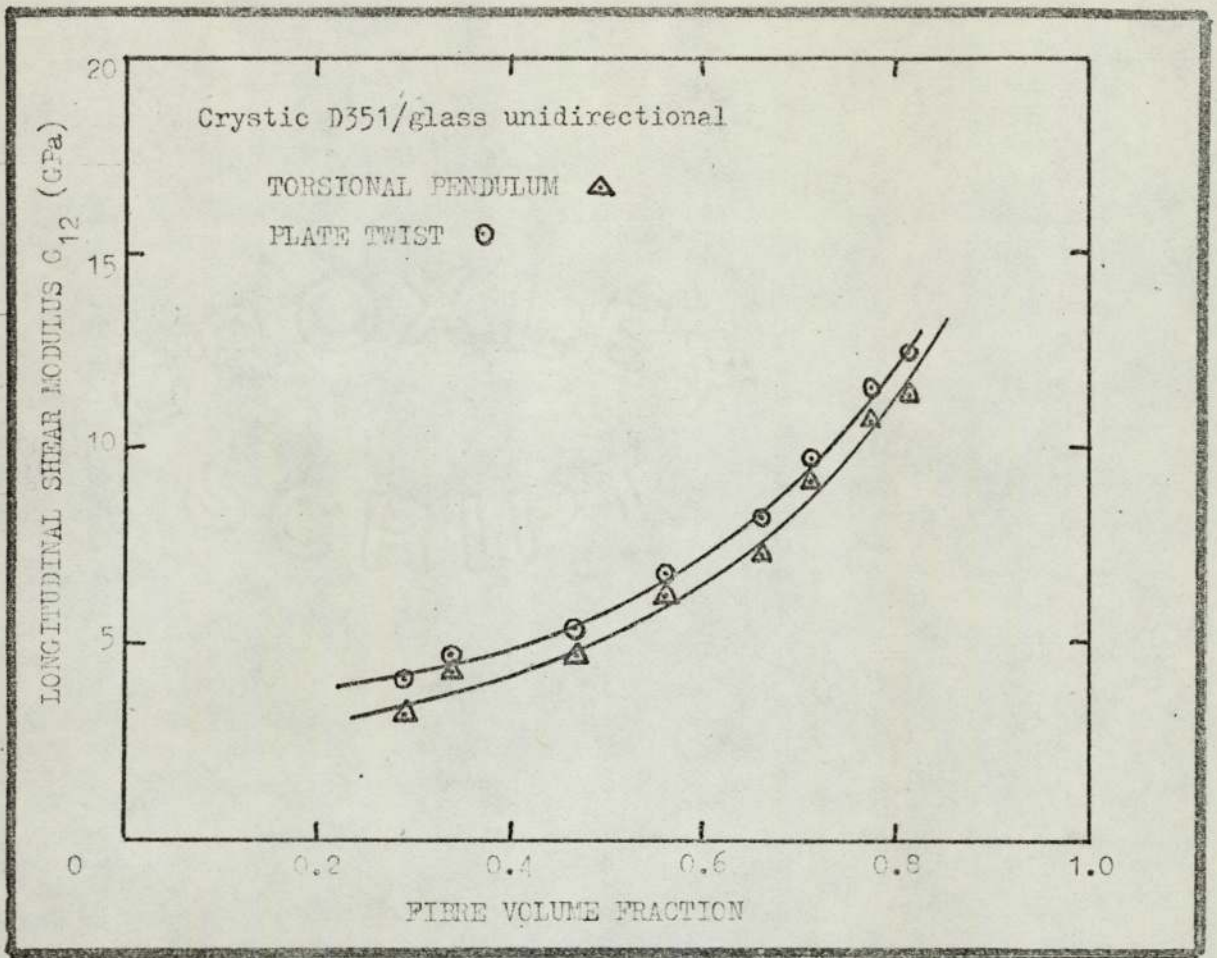
Figure 91 Comparison of torsional pendulum and plate twisting results
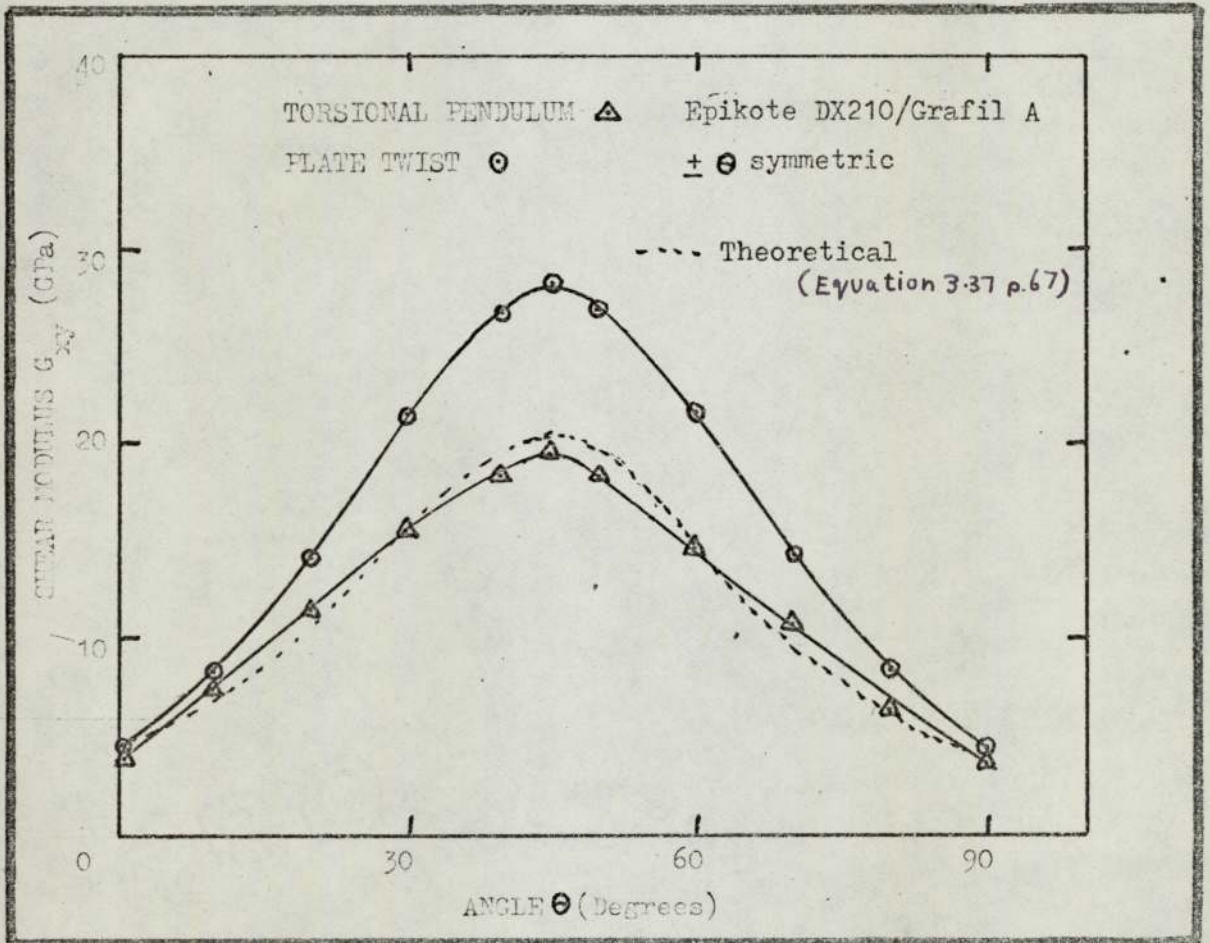
Figure 92 Comparison of torsional pendulum and plate twisting results

-165-
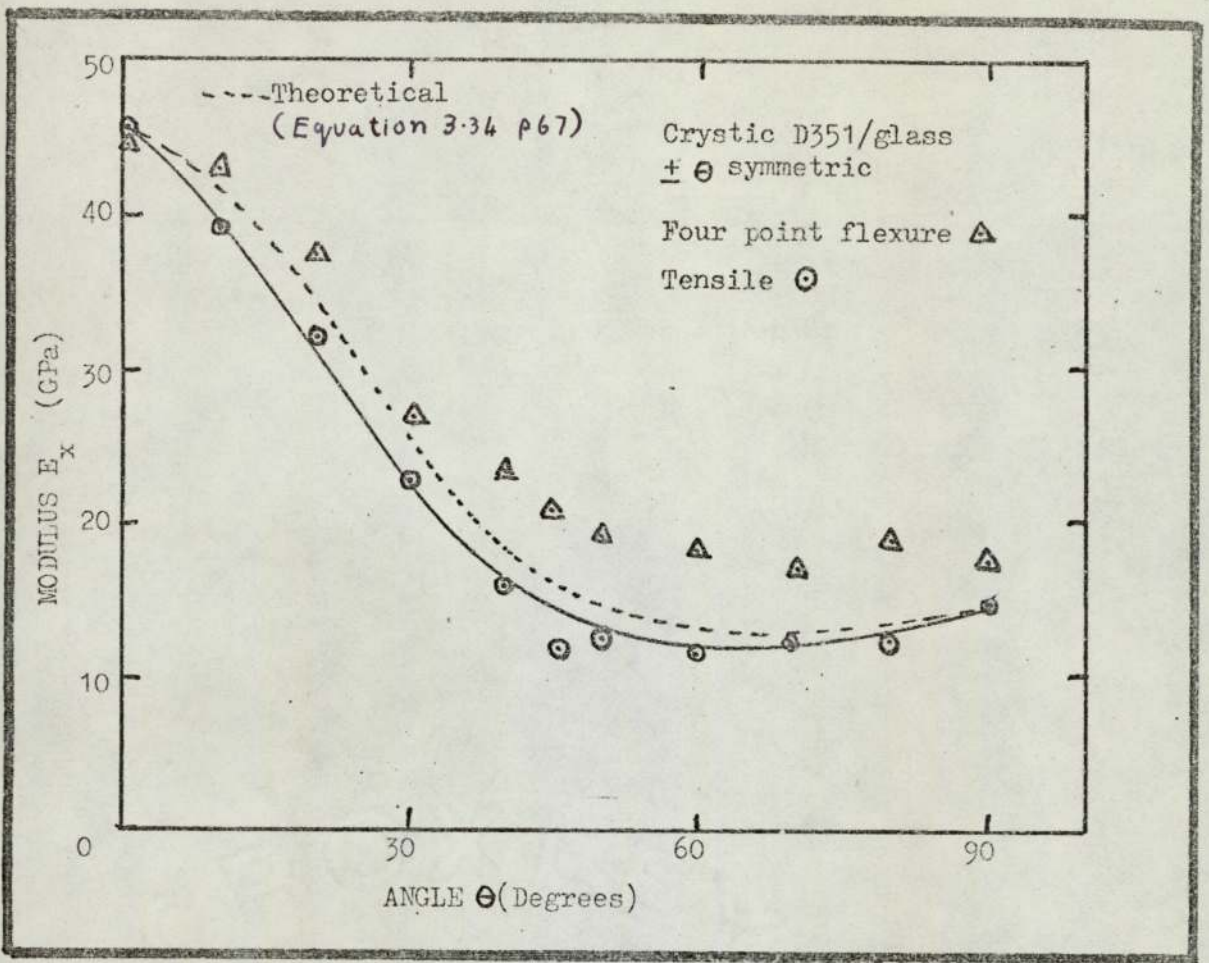
Figure 93 Modulus E_x/angle
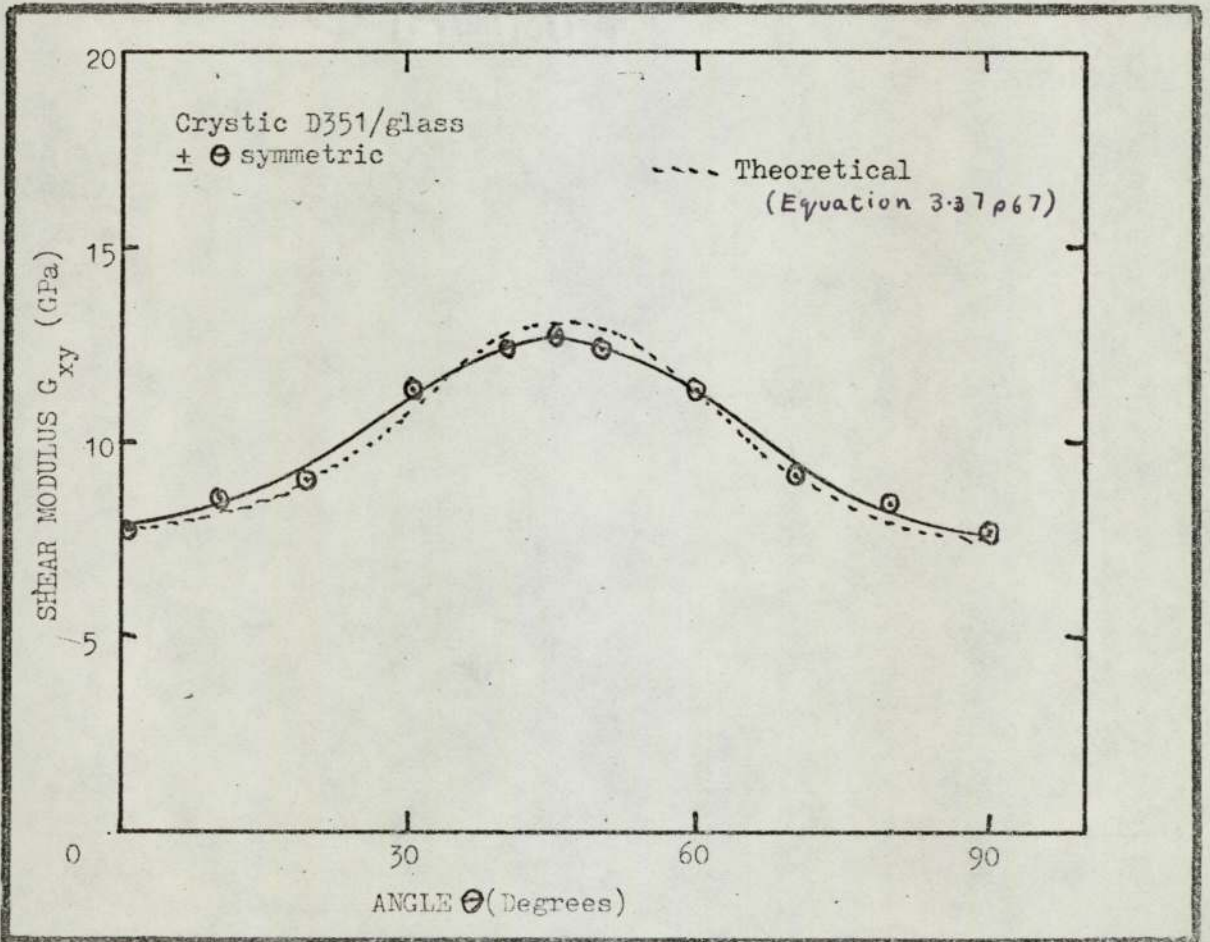
Figure 94 Shear modulus G_{xy}/angle
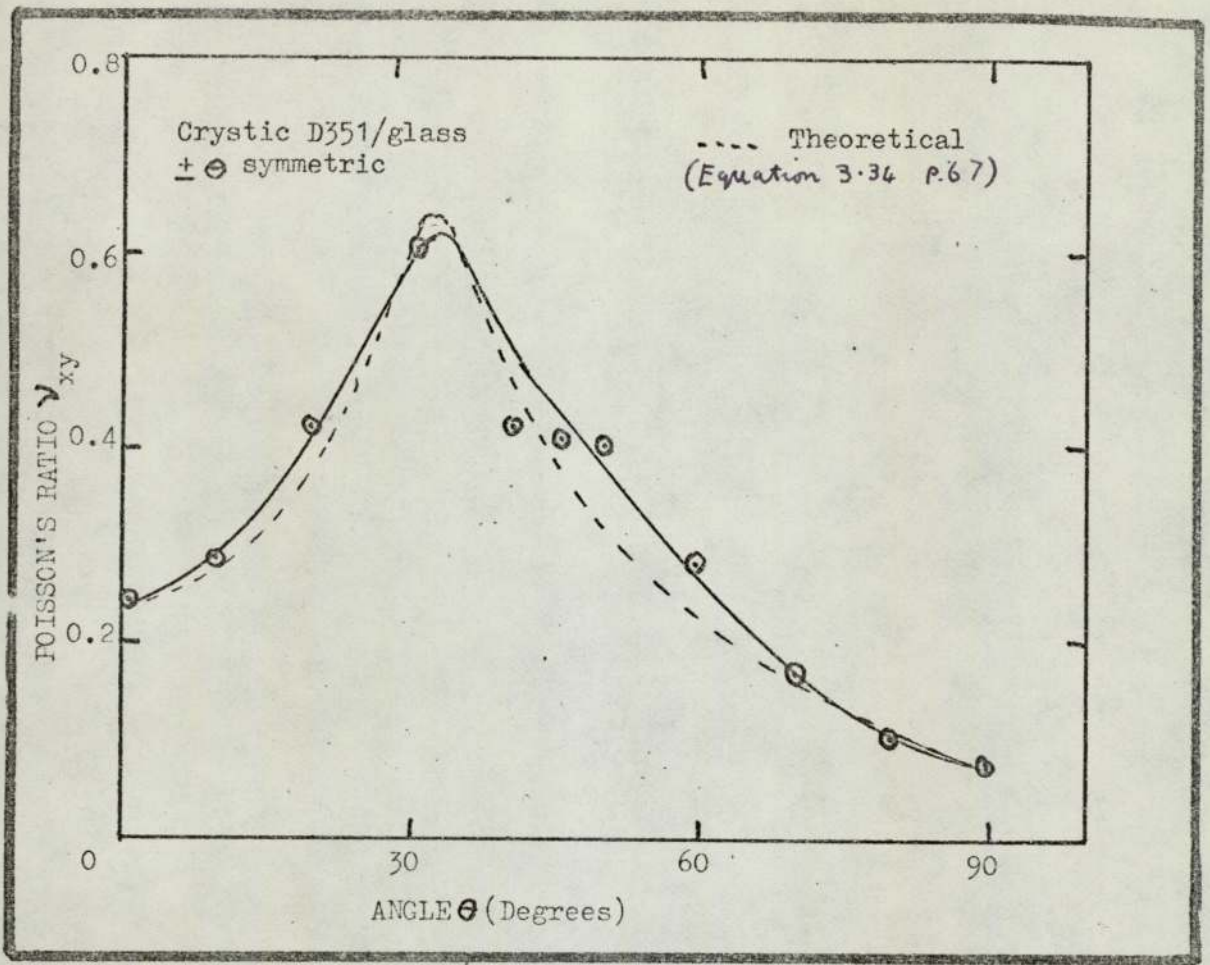
Figure 95 Poisson's ratio ν_{xy}/angle
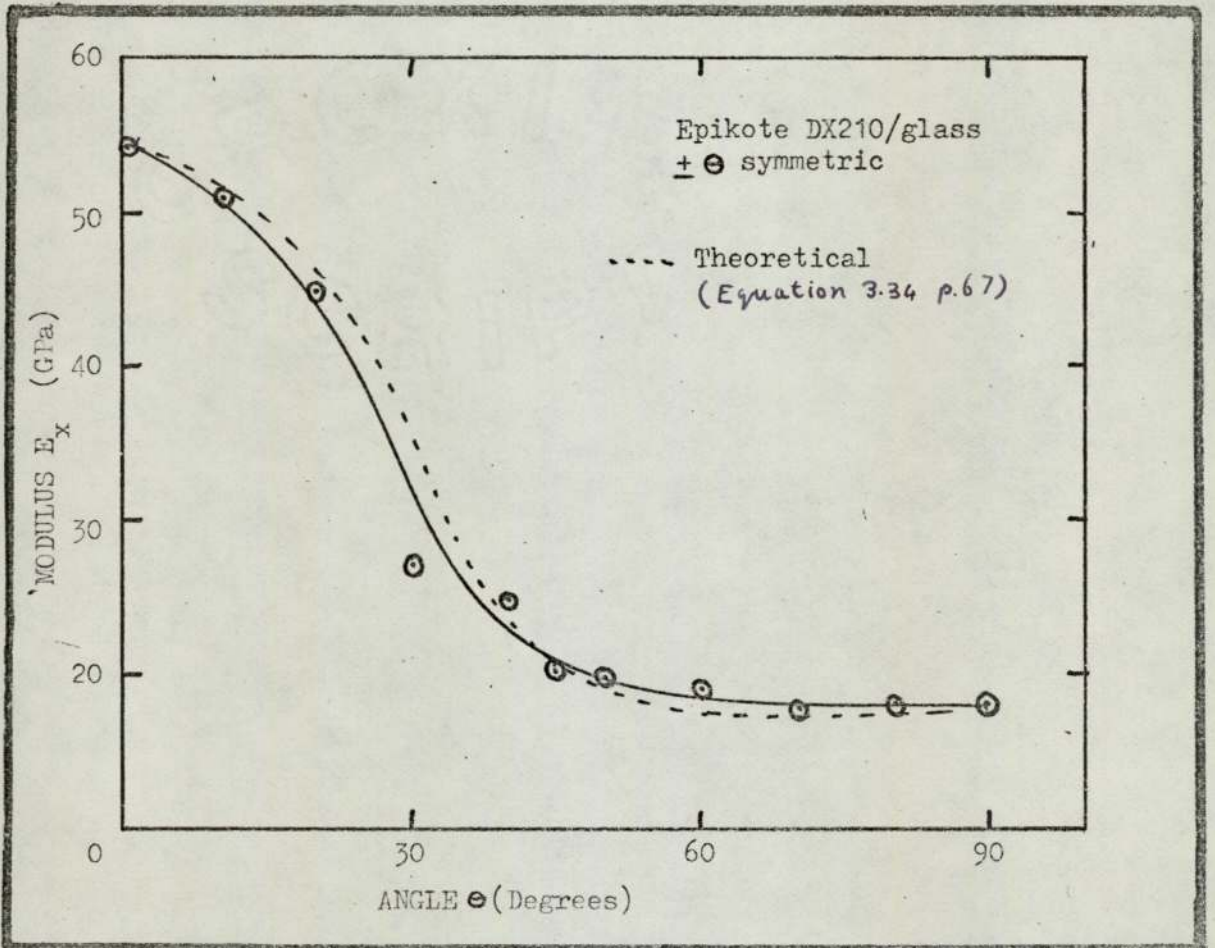
Figure 96 Modulus E_x/angle
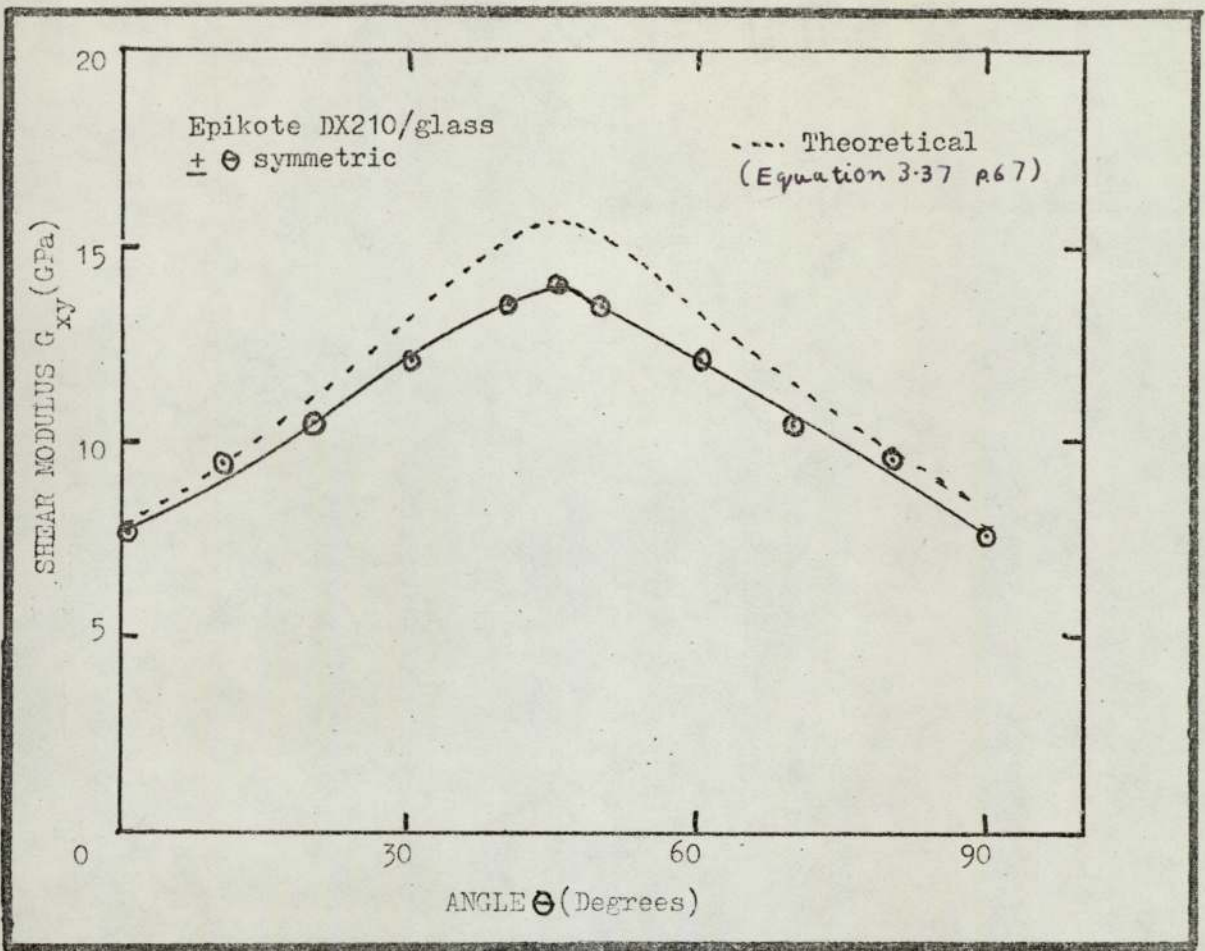
Figure 97 Shear modulus G_{xy}/angle
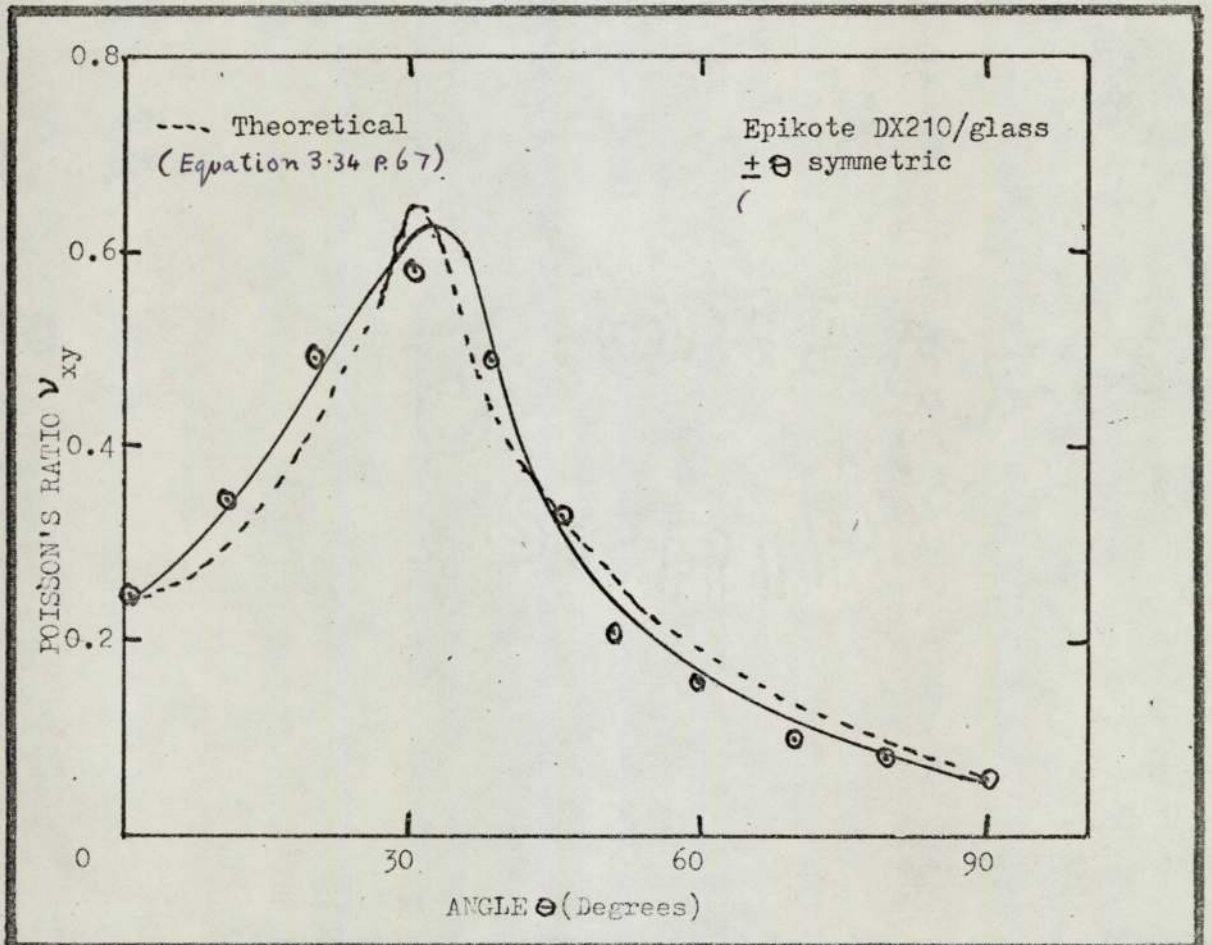
Figure 98 Poisson's ratio ν_{xy}/angle
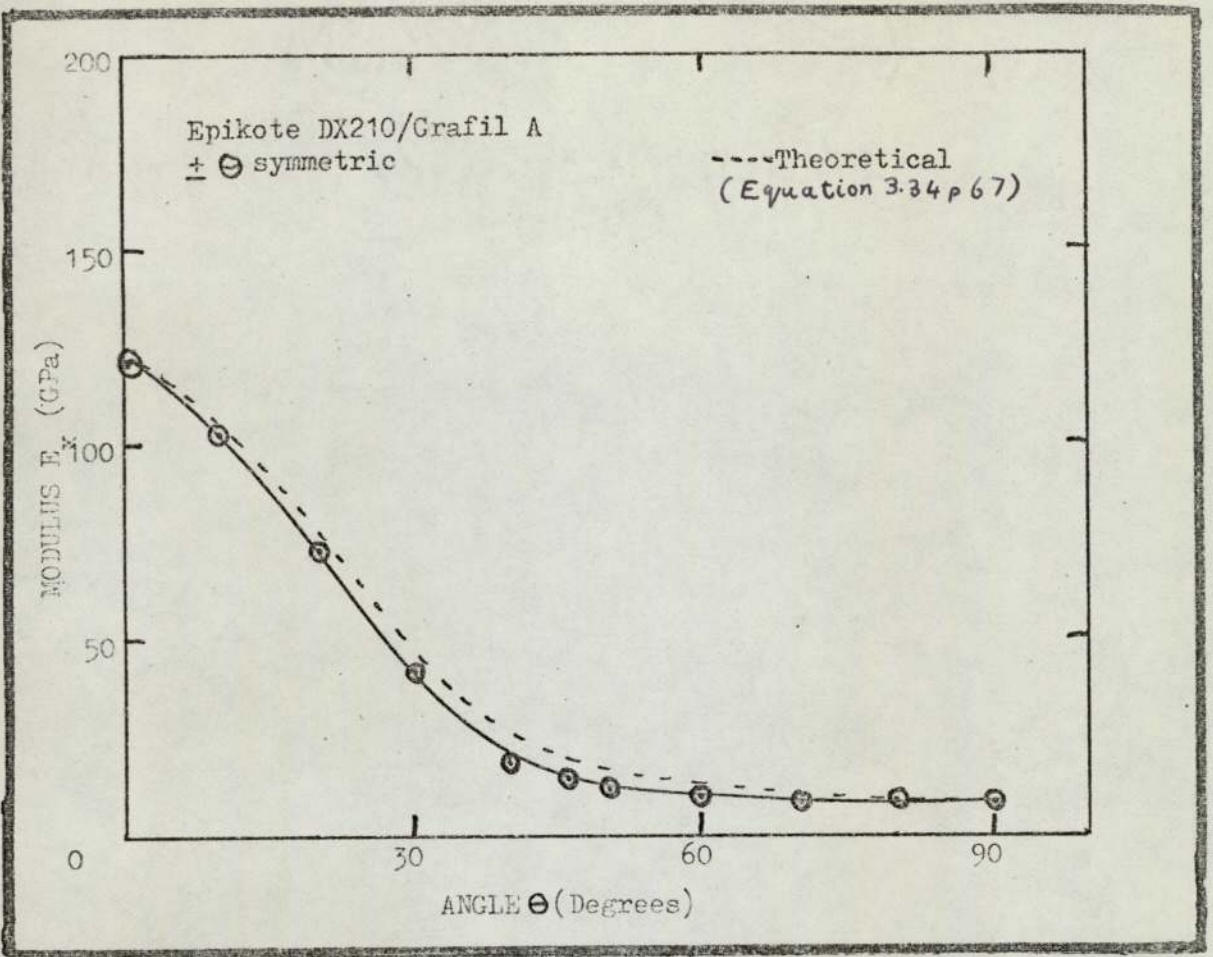
Figure 99 Modulus E_x/angle
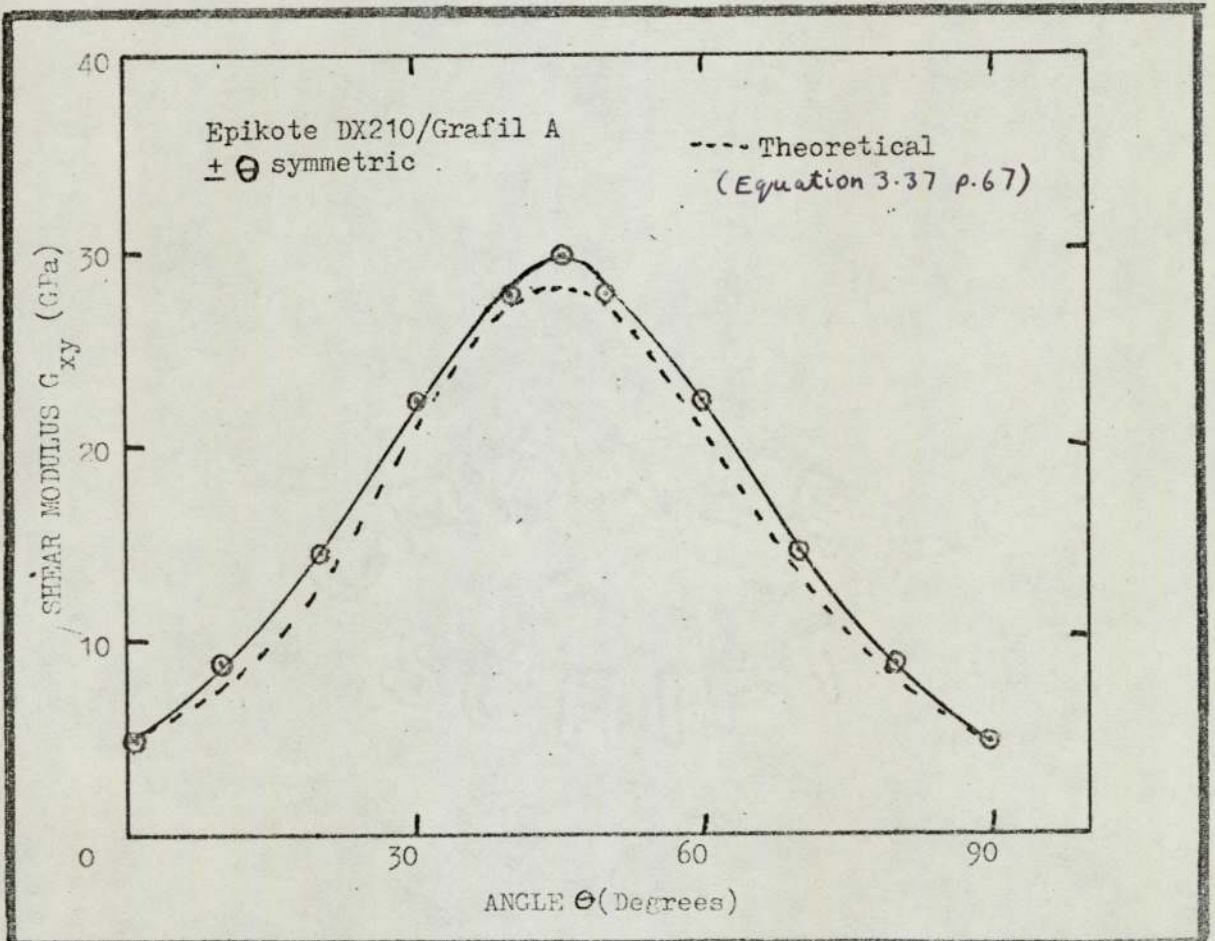
Figure 100 Shear modulus G_{xy}/angle
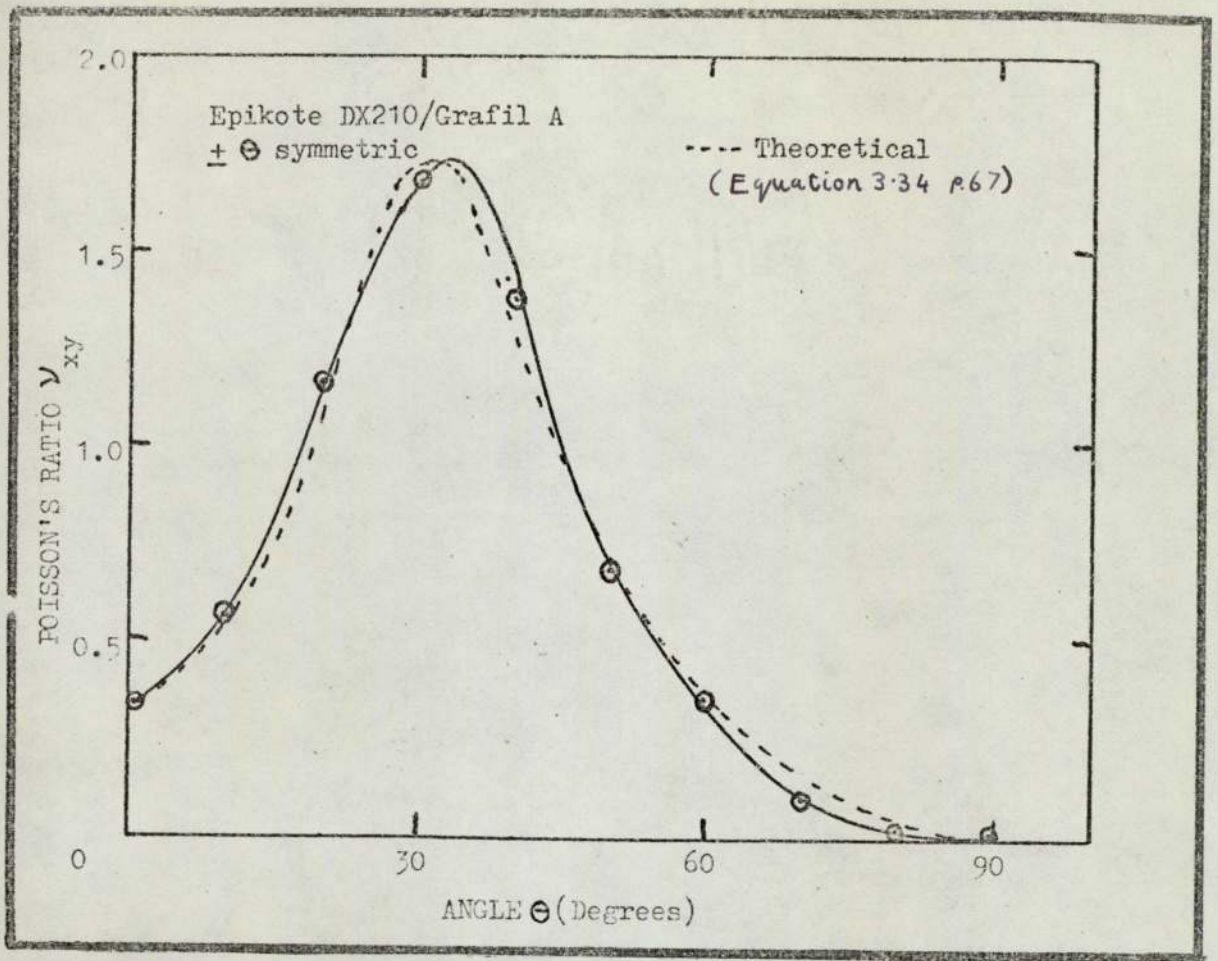
Figure 101 Poisson's ratio ν_{xy}/angle
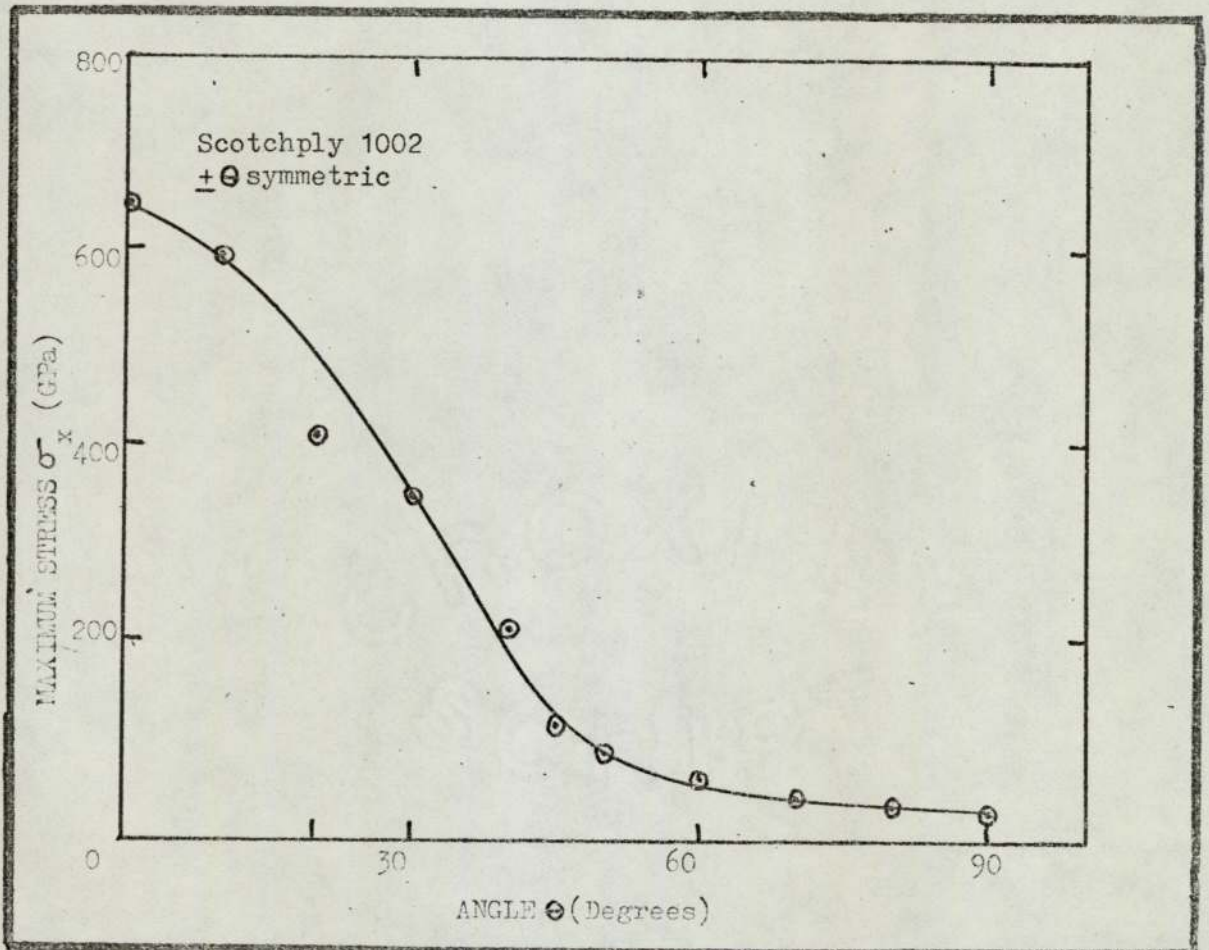
Figure 102 Maximum stress σ_x/angle
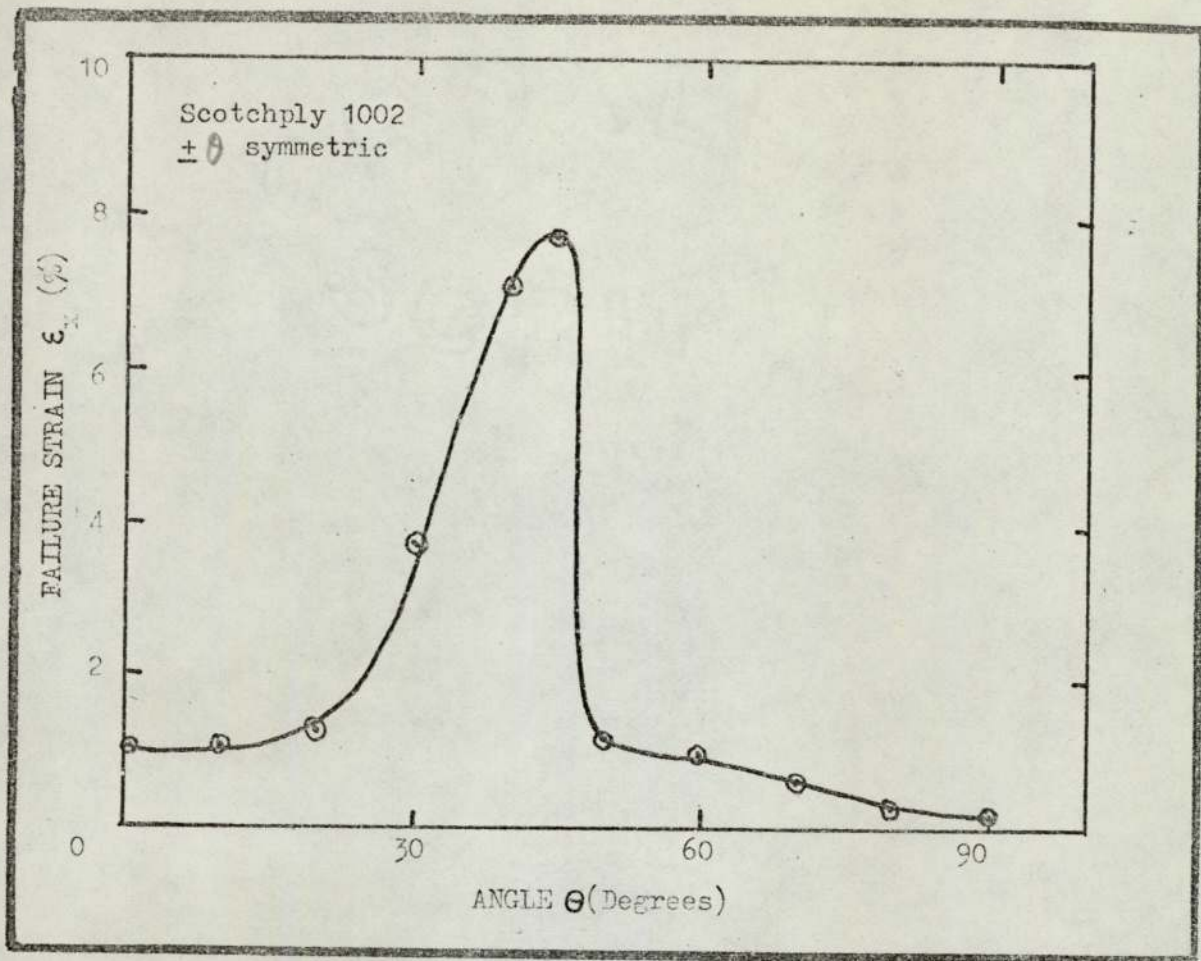
Failure 103 Failure strain ε_x/angle
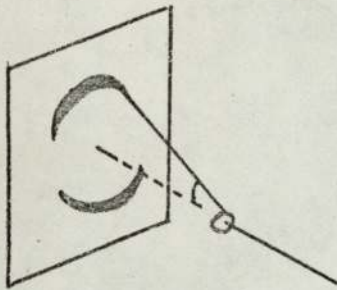
The variation in intensity of the refracted beam with angle $\emptyset$ is recorded using a counter (Ruland) or by a photographic and microdensiometer technique (Bacon). A plot of intensity against angle gives a Gaussian shaped response. The sharpness of the peak is an indication of the preferred orientation. Half the width at half the peak height is often taken as a measure of the average orientation of the crystallites.
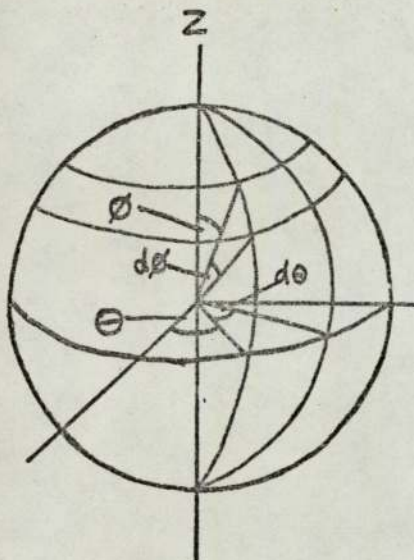
In a multicrystalline graphite with no preferred orientation, the number of crystallites with their c axes within the solid angle defined by $\emptyset$, $\emptyset + d\emptyset$ and θ, $\theta + d\theta$ is proportional to $I(\theta, \emptyset) \sin\emptyset \, d\emptyset \, d\theta$ where $I(\emptyset)$ is the intensity form the X-ray data. In the case of carbon fibres, if they are considered to be cylindrically symmetrical about the fibre axis (Z axis in diagram), the expression can be simp - lified to $I(\emptyset) \sin\emptyset \, d\emptyset$ as it is no longer a function of θ.

Ruland developed this idea and introduced further sophistications to account for line broadening due to crystallite size. His notation differs from that of Bacon so brief details are given.

Ruland represented $g(\emptyset)$ the intensity distribution factor as an infinite series $\sum_{0}^{\infty} P_n \cos 2n\emptyset$ and showed that $g(\emptyset) = \dfrac{1 - q^2}{1 + q^2 - 2q\cos 2\emptyset}$ (Poisson kernel) except for very highly orientated cases. This has a maximum at $\emptyset = n\pi$ for positive q and $\emptyset = \dfrac{(2n+1)\pi}{2}$ for negative q with integral width of the maximum $\dfrac{\frac{\pi}{2}}{(1 - |q|)}$ and maximum to minimum ratio $\dfrac{(1 + |q|)^2}{(1 - |q|)^2}$

The degree of orientation is measured by Ruland in terms of q , where:-

q=0 represents no orientation or random orientation.

q=+1 represents perfect orientation at $\phi = 0$

q=-1 represents perfect orientation at $\phi = \frac{\pi}{2}$

The function $\dfrac{\int g(\phi)\sin^2\phi \, d\phi}{\int g(\phi)\sin\phi \, d\phi}$ is designated as R_z by Ruland and can be

expressed as $\displaystyle\sum_{-\infty}^{\infty} \dfrac{6 P_n}{(1-4n^2)(9-4n^2)} \bigg/ \sum_{-\infty}^{\infty}\dfrac{P_n}{(1-4n^2)}$ or $\left[\dfrac{1+q}{4q^{\frac{1}{2}}\,\text{arth}\,q^{\frac{1}{2}}}\right] - \left[\dfrac{(1-q)^2}{4q}\right]$

if $g(\phi)$ is developed into a Fourier series.

For $q \to 1$ it is shown that $R_z \simeq 1/Log(4/1-q)$

Similarly the function $\dfrac{\int g(\phi)\sin^5\phi \, d\phi}{\int g(\phi)\sin\phi \, d\phi}$ is designated as Q_z and can be

expressed as $\displaystyle\sum_{-\infty}^{\infty}\dfrac{120 P_n}{(1-4n^2)(9-4n^2)(25-4n^2)} \bigg/ \sum_{-\infty}^{\infty}\dfrac{P_n}{1-4n^2}$

or $\left[\dfrac{2}{3} - \dfrac{(1-q)^2}{4q}\right]\dfrac{1+q}{4q^{\frac{1}{2}}\,\text{arth}(q)^{\frac{1}{2}}} + \dfrac{(1-q)^4}{16q^2}$

Appendix B The theoretical basis of the calculated elastic properties of orientated carbon fibres.

The basic unit graphite crystal has hexagonal symmetry and has only 5 independent elastic constants, $S_{11}, S_{12}, S_{13}, S_{33}$ and S_{44} resulting in the compliance matrix shown below. (For comparison with anisotropic composites see appendix C)

$$S_{ij} = \begin{bmatrix} S_{11} & S_{12} & S_{13} & 0 & 0 & 0 \\ S_{12} & S_{11} & S_{13} & 0 & 0 & 0 \\ S_{13} & S_{13} & S_{33} & 0 & 0 & 0 \\ 0 & 0 & 0 & S_{44} & 0 & 0 \\ 0 & 0 & 0 & 0 & S_{44} & 0 \\ 0 & 0 & 0 & 0 & 0 & 2(S_{11}-S_{12}) \end{bmatrix}$$
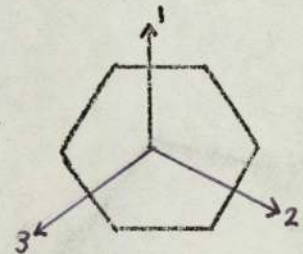
The directions of the axes 1,2,3 are shown in the sketch, the c-axis is the axis of symmetry.

The compliances S'_{ij} of the crystallites in a direction defined by Θ, ϕ (polar coords) with reference to the natural crystallite axes are given by:-

$S'_{33} = S_{11}\sin^4\phi + S_{33}\cos^4\phi + 2\cos^2\phi\sin^2\phi \, S_{13} + S_{44}\cos^2\phi\sin^2\phi$

$S'_{13} = S_{11}\cos^2\phi\sin^2\phi\sin^2\Theta + S_{33}\sin^2\phi\cos^2\phi\sin^2\Theta + S_{12}\sin^2\phi\cos^2\Theta$

$\qquad - S_{44}\cos^2\phi\sin^2\phi\sin^2\Theta + S_{13}(\cos^2\phi + \sin^2\phi\sin^2\Theta - 2\cos^2\phi\sin^2\phi\sin^2\Theta)$

$S'_{44} = 2S_{11}(\cos^2\phi + 2\sin^4\phi\sin^2\Theta\cos^2\Theta) - 8S_{13}\sin^4\phi\cos^2\Theta\sin^2\Theta - 2S_{12}(1-\sin^2\phi)$

$\qquad + 4S_{33}\sin^4\phi\cos^2\Theta\sin^2\Theta + S_{44}(\sin^2\Theta - 4\sin^4\phi\sin^2\Theta\cos^2\Theta)$

However due to the hexagonal symmetry ,the compliances S'_{ij} are independent of angle Θ and are simplified by replacing the functions of Θ by their average values.

$$S'_{11} = \frac{S_{11}}{8}(3\cos^4\phi + 2\cos^2\phi + 3) + \frac{S_{13}}{4}(3\cos^2\phi\sin^2\phi + \sin^2\phi) + \frac{3S_{33}}{8}\sin^4\phi + \frac{S_{44}}{8}(3\sin^2\phi\cos^2\phi + \sin^2\phi)$$

$$S'_{33} = S_{11}\sin^4\phi + S_{33}\cos^4\phi + (2S_{13} + S_{44})\sin^2\phi\cos^2\phi$$

$$S'_{12} = \frac{S_{11}}{8}(\cos^4\phi - 2\cos^2\phi + 1) + S_{12}\cos^2\phi + \frac{S_{13}}{4}(\sin^2\phi\cos^2\phi + 3\cos^2\phi) + \frac{S_{33}}{8}\sin^4\phi + \frac{S_{44}}{8}(\sin^2\phi\cos^2\phi - \sin^2\phi)$$

$$S'_{13} = \frac{S_{11}}{2}(\sin^2\phi\cos^2\phi) + \frac{S_{12}}{2}\sin^2\phi + \frac{S_{13}}{2}(\sin^4\phi + \cos^4\phi + \cos^2\phi) + \frac{S_{33}}{2}(\sin^2\phi\cos^2\phi) - \frac{S_{44}}{2}\sin^2\phi\cos^2\phi$$

$$S'_{44} = S_{11}(2\sin^2\phi\cos^2\phi + \sin^2\phi) - S_{12}\sin^2\phi - 4S_{13}\sin^2\phi\cos^2\phi + 2S_{33}\sin^2\phi\cos^2\phi$$
$$+ \frac{S_{44}}{2}(\cos^4\phi + \sin^4\phi - 2\sin^2\phi\cos^2\phi + \cos^2\phi)$$

The elastic properties of a carbon fibre composed of graphite crystallites are calculated by summing the weighted elastic constants from $0°$ to $90°$. The weighting factor,$I(\phi)$is found by measuring the crystallite orientation.

Reuss model or uniform stress model

For this model the stress in the individual crystallites is assumed to be uniform and equal to the macroscopic stress of the fibre. The modulus of the fibre in the longitudinal direction is given by

$$\frac{1}{E_3} = \frac{\int_0^{\pi/2} \frac{1}{E_3(\phi)} I(\phi)\sin\phi\, d\phi}{\int_0^{\pi/2} I(\phi)\sin\phi\, d\phi}$$

where

$$\frac{1}{E_3(\phi)} = S'_{33} = S_{11}\sin^4\phi + S_{33}\cos^4\phi + (2S_{13} + S_{44})\sin^2\phi\cos^2\phi$$

Hence

$$\frac{1}{E_3} = S_{33} + (2S_{13} - 2S_{33} + S_{44})\frac{\int_0^{\pi/2} I(\phi)\sin^3\phi\, d\phi}{\int_0^{\pi/2} I(\phi)\sin\phi\, d\phi} + (S_{11} - 2S_{13} + S_{33} - S_{44})\frac{\int_0^{\pi/2} I(\phi)\sin^5\phi\, d\phi}{\int_0^{\pi/2} I(\phi)\sin\phi\, d\phi}$$

For the case of an isotropic material (fibre properties independent of ϕ) the integrals $\int_0^{\pi/2} \sin^n\phi\, d\phi$ can easily be evaluated by reduction formulae

to $\quad \dfrac{\int_0^{\pi/2} \sin^3\phi\, d\phi}{\int_0^{\pi/2} \sin\phi\, d\phi} = \dfrac{2}{3} \quad , \quad \dfrac{\int_0^{\pi/2} \sin^5\phi\, d\phi}{\int_0^{\pi/2} \sin\phi\, d\phi} = \dfrac{8}{15}$

In a similar manner the other elastic properties can evaluated, and using the notation of Goggin and Reynolds we have:-

$$\underline{S}_{11} = S_{11} - \frac{1}{2}(2S_{11} - 2S_{13} - S_{44})\frac{I_3}{I_1} + \frac{3}{8}(S_{11} - 2S_{13} + S_{33} - S_{44})\frac{I_5}{I_1}$$

$$\underline{S}_{12} = S_{12} + (S_{13} - S_{12})\frac{I_3}{I_1} + \frac{1}{8}(S_{11} + S_{33} - 2S_{13} - S_{44})\frac{I_5}{I_1}$$

$$\underline{S}_{13} = S_{13} + \frac{1}{2}(S_{11} + S_{33} + S_{12} - 3S_{13} - S_{44})\frac{I_3}{I_1} - \frac{1}{2}(S_{11} + S_{33} - 2S_{13} - S_{44})\frac{I_5}{I_1}$$

$$\underline{S}_{44} = S_{44} + (3S_{11} + 2S_{33} - S_{12} - 4S_{13} - \frac{S_{44}}{2})\frac{I_3}{I_1} - (2S_{11} + 2S_{33} - 4S_{13} - 2S_{44})\frac{I_5}{I_1}$$

where $\quad I_n = \int_0^{\pi/2} I(\phi)\sin^n\phi\, d\phi \quad n = 1, 3, 5.$

-174-

Voigt model or uniform strain model

The stiffness constants C_{ij} of the basic graphite crystallite are related to the general stiffness constants C'_{ij} by expressions similar to those for the compliance constants. Similarly the stiffness constants $\underline{C}_{ij}$ of the carbon fibre can be express in terms of $\underline{C}'_{ij}$ and the correct weighting factor.

e.g.

$$\underline{C}_{11} = C_{11} - (C_{11} - C_{13} - 2C_{44})\frac{I_3}{I_1} + \frac{3}{8}(C_{11} - 2C_{13} + C_{33} - 4C_{44})\frac{I_5}{I_1}$$

The $\underline{C}'_{ij}$ are inverted to obtain the $\underline{S}'_{ij}$ by the normal manner. $\underline{S}'_{ij} = \dfrac{[\underline{C}'_{ij}]\,adj}{\underline{C}'_{ij}}$

The elastic constants for the case of uniform strain can be expressed in terms of $\underline{S}'_{ij}$. As the expressions are quite complicated a computer is normally required for the inversion process.

-175-

Appendix D Plate bending and torsion tests

The two tests described here were originally concieved in this form by Hearmon (89) for the testing of plywood.

The solution to the differential equations of an anisotropic plate under combined uniform bending and twisting moments is given by Lekhnitskii (85) as:-

$$h^3 w = 6 M_x \left(R_{11} x^2 + R_{12} y^2 + R_{16} xy \right)$$
$$+ 6 M_y \left(R_{12} x^2 + R_{22} y^2 + R_{26} xy \right)$$
$$+ 6 M_{xy} \left(R_{16} x^2 + R_{26} y^2 + R_{66} xy \right) \qquad \text{D1}$$
$$+ ax + by + c$$

where h=plate thickness ; w=deflection in the Z direction ; M_x, M_y =bending moments ; M_{xy} =twisting moment ; a,b,c =constants dependent on the frame of reference; R_{ij} is defined by equation 3.15.

Bending
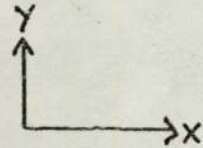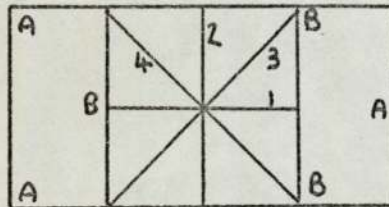
The sample used by Hearmon is shown in the sketch. At points A it was supported by steel balls, and at points B it was loaded by weights. The deflections along lines 1,2,3,4 were measured with a dial gauge held in a clamp which stood on the plate.If x=y=0 at the supporting 'foot' of the clamp (w=0), then a=b=c=0 also.Thus for the bending moment M_x only we have:-

$$h^3 w = 6 M_x \left(R_{11} x^2 + R_{12} y^2 + R_{16} xy \right) \qquad \text{D2}$$

By substituting values for h, x,y and measuring M_x and w on lines 1,2,3,4 the values of R_{11}, R_{12} and R_{16} can be calculated.

If the plate is a unidirectionally fibre reinforced one with the fibres parallel to the long side,then $R_{11} = S_{11}$, $R_{12} = S_{12}$,$R_{16} = S_{16} = 0$. Using a second plate with the fibres transverse, the values of S_{22}, S_{12} may be found.

The deflections measured are fairly small, and in calculating the value of Poisson's ratio (- S_{12} / S_{11}) small errors in any measurement cause a large error in the answer. This problem and the large size of the

test pieces are the principal reasons why the method was not used.

Torsion

Timoshenko (91) showed that loads of P acting on a square plate as shown
will produce a torsional moment M_{xy} per unit length along the sides equal to P/2.
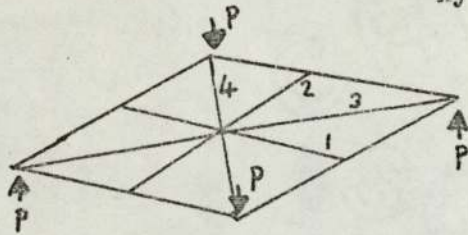
Substituting $M_{xy} = P/2$ into equation D1 we have :-

$$h^3 w = 3P \left(R_{16} x^2 + R_{26} y^2 + R_{66} xy \right) + ax + by + c \qquad \text{D3}$$

If the deflection is measured such that x=y=o when w=o then a=b=c=0.
By measuring the loads and deflections along lines 1,2,3 and 4 it is possible
to calulate R_{16}, R_{26}, R_{66}.

In practice the test was carried out as follows(after Tsai (90)):-
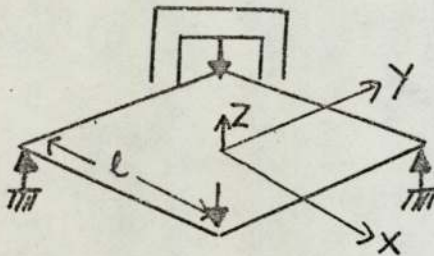
Two fixed loading points , one pre-set point and one moving point were used
as shown above. Thus substituting in equation D3 $\quad w = 0 \quad$ at $\begin{cases} x = +\frac{\ell}{2} , & y = +\frac{\ell}{2} , \\ x = \frac{\ell}{2} , & y = -\frac{\ell}{2} \\ x = -\frac{\ell}{2} , & y = +\frac{\ell}{2} \end{cases}$

we obtain $h^3 w = 3P \left[\left(x^2 - \frac{\ell^2}{4} \right) R_{16} + \left(y^2 - \frac{\ell^2}{4} \right) R_{26} + \left(xy - \frac{x\ell}{2} + \frac{y\ell}{2} - \frac{\ell^2}{6} \right) R_{66} \right]$

By measuring the deflection at different positions on the plate various
relationships involving R_{16}, R_{26}, R_{66} can be derived. Most of measurements
were made at the centre of the plate (x=y=0). Thus we have:-

$$\frac{4 h^3 w}{3 P \ell^2} = R_{16} + R_{26} + R_{66} = \underline{R}$$

Note that if the angle of the fibre $= 0^\circ \quad R_{16} = R_{26} = 0 \quad R_{66} = S_{66}$

$= 45^\circ \quad \underline{R} = 2(S_{22} - S_{12})$

$= 135^\circ \quad \underline{R} = 2(S_{11} - S_{12})$
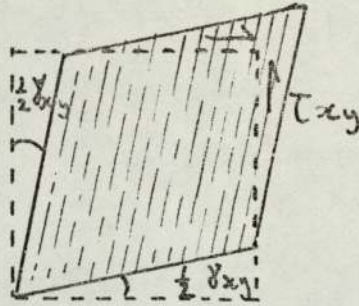
Pure shear as defined in elasticity theory is shown on a two dimensional scale in the sketch, where the engineering strain is given by γ_{xy}. The shear modulus in this case is defined as $G_{xy} = \dfrac{\tau_{xy}}{\gamma_{xy}}$.

If the sketch represents a unidirectional composite plate with the fibres parallel to one edge, then the shear deformation has the effect of creating a shear stress between the fibre and the matrix along the length of the fibre. This mode of shearing in a composite is referred to as in-plane shear and is a function of the in-plane shear modulus G_{12}.

If the fibres ran normal to the plane of the plate, i.e. out of the paper, the shear stress between fibre and matrix would be very small and most of the stress would be used in distorting the matrix. This mode of shearing is termed transverse shear and is a function of the transverse shear modulus G_{23}. Thus in a homogeneous orthotropic composite there are two shear moduli whether the fibres are isotropic or cylindrically isotropic.

Plate twisting test
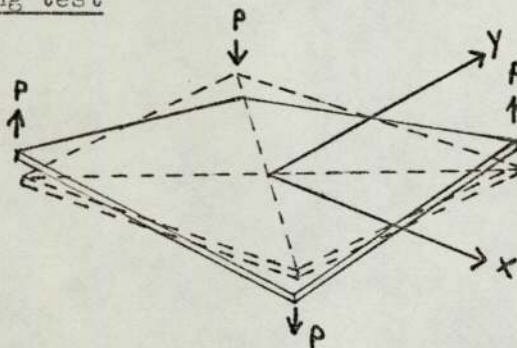
Timoshenko has shown that by applying a torque of P to the corners of a square plate, a moment M_{xy} is produced along the sides of the plate. The moment deforms the plate in the manner shown in the sketch, where it can be seen that there is a shear stress induced between the fibres and the matrix along the length of the fibre.

Torsional pendulum

The torsional pendulum is similar to the plate twisting test in the type of deflection, but is treated differently because of the sample shape and the manner of loading.

On a circular sample in torsion the sections normal to the axis remain plane, but for other cross-sections warping can occur. However for long samples with a small deflection the torque of the pendulum can induce reasonably predictable shear stresses and strains and can thus be used to measure the shear or torsional modulus.

In neither of these tests is there any attempt of the fibre to rotate in the matrix and the strain in the composite is shear strain parallel to the fibres. The two methods are used for measuring the shear modulus of a variety of materials because they are fairly easy to use, but should only be used at low strains, and in the case of non-circular sections in the pendulum, a correction factor for the sample shape must be used.

In this thesis the expressions torsional modulus and shear modulus have been taken to be identical although in a general sense this is not correct.

REFERENCES

1 Bacon R Jnl. Applied Physics 31 p283 1960

2. Brenner S S Jnl. Applied Physics 27 p1484 1956

3. Von Polayni M Z.Phys. 7 p323 1921

4. Bacon R Applied Polymer Symposia 9 p214 1969

5. Phillips L N Chem.Indust. p526 1968

6. Watt W Phillips L Johnson W Engineer May 27 p815 1966

7. Kumura K Jenkins G M Jnl Mat. Science 7 p1099 1972

8. Hawthorne H M Baker C Bentall R H Linger K R Nature 227 p946 1970

9 Watt W Johnson W Appl.Poly. Symposia 9 p215 1969

10 Bacon R Tang M M Carbon 2 p221 1964

11 Moreton R Proc. Int. Conf.Carbon Fibre London 1971

12 Statton W O Jnl.Polm.Science 58 p205 1962

13 Moreton R Watt W Johnson W Nature 213 p690 1967

14 Hawthorne H M Proc. Int. Conf. Carbon Fibre London 1971

15 Watt W Johnson W New Scientist 20 Feb 1969

16. Allen S Cooper A Mayer R M Nature 224 p684 1969

17 Kelly B T Phil Mag 9 p721 1964

18 Bacon G E Jnl. Applied Chemistry 6 p477 1956

19 Ruland W Jnl. Applied Physics 38 p3585 1967

20 Ruland W Jnl.Polm.Science 28 p143 1969

21 Statton W O Jnl.Polm.Science 58 p205 1962

22 Sharp J V Burnay S G Proc. Int. Conf.Carbon Fibre London 1971

23 Bacon R Schalamon W A Appl. Polym. Symposia 9 1964

24. Johnson J W Marjoram J R Rose P G Nature 221 p3571 1969

25. Johnson W Watt W Nature 215 p384 1967

26. Johnson D J Tyson C N Jnl. Applied Physics (Phys D) 2 p787 1969

27. Johnson D J Tyson C N Jnl. Applied Physics (Phys D) 3 p526 1970

28. Ruland W Perret R Fourdeux A Proc. Int. Conf. Carbon Fibre London 1971

29 Hill R Proc. Phys. Soc. A65 p349 1952

30 Ward I M Proc. Phys. Soc. 80 p1176 1962

31 Price R J Phil. Mag. $\underline{12}$ p561 1965

32 Spence G B Proc. 5th Carbon Conf. 1961 Pergamon

33 Goggin P R Reynolds W N Phil. Mag. $\underline{16}$ p317 1967

34 Ruland W Appl. Polym. Symposia $\underline{9}$ p293 1969

35 Brydges W T Badami D V Joiner J C Jones G A Appl. Polym. Symposia $\underline{9}$ 1969

36 Butler B L Diefendorf R J 9th Biennial Carbon Conf. Boston 1969

37 Griffith A A Trans. Roy. Soc. A $\underline{221}$ p163 1924

38 Brenner S S A.S.M.Seminar on fibre composites Oct 1964

39 Lubin G Handbook of fibreglass and reinforced plastics Van Nostrand 1969

40 Otto W H Jnl. Am. Ceramic Soc. $\underline{44}$ p68 1961

41. Bartenev G M Izmailova L K Sov.Phys. Sol. Stat. $\underline{6}$ p920 1964

42 Metcalfe A G Schmitz G K ASTM proc. p1075 1964

43 Cameron N M Am.Ceramic Soc. $\underline{49}$ p124 1966

44 Otto W H Jnl. Am Ceramic Soc. $\underline{38}$ p122 1955

45 Thomas W F Phys. and Chem. of glasses $\underline{1}$ p4 1960

46 Warren B E Jnl.Am. Ceramic Soc. $\underline{24}$ p256 1941

47 Statton W O Hoffman L C Jnl. Applied Physics $\underline{31}$ p290 1939

48 Brannan R T Jnl Am Ceramic Soc. $\underline{36}$ 230 1953

49 Kroenke W J Glass Ind. $\underline{47}$ p262 1966

50 De Wys E Min. Mag. $\underline{32}$ 1966

51 Kroenke W J Jnl.Am. Ceramic Soc. $\underline{49}$ p508 1966

52 Kroenke W J Jnl.poly.science $\underline{19}$ p151 1967

53 Galasso F kuehl D Tice W Jnl Applied Physics $\underline{38}$ p414 1967

54 Otte H M Lipsitt H A Phys.Stat.Sol. $\underline{13}$ p439 1966

55 Eakins W J SPE Trans. $\underline{1}$ p234 Oct 1961

56 Ekvall J C AIAA 6th Struct.and mat.conf. California April 1965

57 Greszczuk L B SPI 21st Conf. Chicago 1966

58 Shaffer B W Jnl AIAA $\underline{2}$ p286 1953

59 Rabinovich A L Sov.Phys. $\underline{8}$ p1233 1964

60 Abolinish D S Polym Mechs. $\underline{1}$ No48 p28 1965

61 Hashin Z Rosen B W Jnl.Appl. Mechs. $\underline{31}$ p223 1964

62 Nosarev A V Mekhanika Polimerov No 5 p858 1967

63 Hill R Jnl.Mech.Phys.Solids 13 p189 1965

64 Hershey A V Jnl.Appl.Mech. 21 p236 1954

65 Kilchinski A A Naukova Dumka,Kiev p123 1966

66 Fröhlich H Sach B Proc.Roy.Soc. Series A 185 p415 1946

67 Whitney J M Riley M B Jnl.AIAA 4 p1537 1966

68 Whitney J M Jnl.Comp.Materials 1 p189 1967

69 Whitney J M AFML TR-65-411 Jan 1966

70 Paul B Trans. Metal.Soc. AIME 218 p36 1960

71 Hashin Z Jnl.Mech.Phys.Solids 13 p119 1965

72 Hill R Jnl.Mech.Phys.Solids 12 p199 1964

73 Filshtinski L A Jnl Appl.Math.Mechs. 28 p430 1964

74 Van Fo Fy G A Prikladnaia Mekhanika 1 p110 1965

75 Chen C H Cheng S Jnl.Comp.Materials 1 p30 1967

76 Adams D F Doner D R Thomas R L AFML-TR-67-96 May 1967

77 Sendeckyj G P Jnl.Comp.Materials 4 p500 1970

78 Tsai S W NASA CR 71 July 1964

79 Bishop P H H RAE Report 66245 1966

80 Halpin J C Tsai S W AFML TR-67-423 1967

81 Foye R L Jnl. SAMPE 10 G-31 1966

82 Adams D F Tsai S W Jnl.Comp.Materials 3 p368 1969

83 Rosen B W Composites Jan p16 1973

84 Hewitt R L de Malherbe M C Jnl.Comp.Materials 1 p280 1970

85 Lekhnitskii S G Anisotropic plates.Gordon and Breach 1968

86 Calcote L R Analysis of laminated composite structures. Van Nostrand 1969

87 Ashton J E Halpin J C Petit P H Primer on composite materials. Technomic 1969

88 Greszezuk L B AFML-TR-66-274 Sept 1966

89 Hearmon R F S Brit Jnl.Appl.Phys. 3 p150 1952

90 Tsai S W Jnl.Eng.Indust. 83 p315 1965

91 Timoshenko S P Woinowsky-Krieger S Theory of plates and shells McGraw-Hill 1959

92 Tsai S W Pagano N J Composite materials workshop. Technomic 1968

ACKNOWLEDGEMENTS

I would like to express my sincere thanks to Dr.J.T.Barnby and to Dr.H.D.Williams for their advice and encouragement throughout this project.

I would also like to thank Mr.L.Mascia for his valuable consultation on matters regarding the chemical nature of the research.

Finally I am indebted to Imperial Metal Industries Limited for their sponsorship, without which this work would not have been possible.